Alma Mater Studiorum – Università di Bologna

DOTTORATO DI RICERCA IN GEOFISICA

Ciclo XXXII

Settore Concorsuale: 04/A4

Settore Scientifico Disciplinare: GEO/12

Numerical modelling and analysis of riverine influences in the Mediterranean Sea

Presentata da: Damiano Delrosso

Coordinatore Dottorato

Prof. Nadia Pinardi

Supervisore

Dr. Emanuela Clementi

Co-Supervisore

Prof. Nadia Pinardi

Esame finale anno 2020

Acknowledgements

I would like to express my sincere gratitude to my advisor Dr. Emanuela Clementi, who continuously guided and supported me during my Ph.D study with endless patience.

I would like to acknowledge my co-advisor Prof. Nadia Pinardi for her precious advices and for sharing her huge knowledge of Oceanography.

I would like to thank Dr. Giorgia Verri for providing me with the CMCC EBM code and for the fruitful discussions about estuarine modelling.

I'm really grateful to Dr. Gerasimos Korres, who supervised my research during my visiting period at HCMR, and to the HCMR Oceanography group: it was a wonderful experience for me, both on a personal and scientific level. Many thanks to Dr. Giannis Mamoutos for the interesting and fruitful discussions about Dardanelles Strait modelling.

A huge thanks to the colleagues of INGV Oceanography group in Bologna: their priceless support and encouragement in my moments of distress have been absolutely fundamental. A special thought for my office mate Dr. Gelsomina Mattia, always by my side in moments of difficulty.

I would like to acknowledge the CMCC OPA and ODA divisions staff for their kind and helpful technical support.

Finally, I really want to thank Carolina and my parents, who constantly supported me day by day. Heartfelt thanks.

Abstract

Riverine influences in the Mediterranean Sea are investigated by means of numerical experiments performed with an ocean general circulation model implemented in the basin, along with the model capability to correctly reproduce the thermohaline properties of the basin through an improved representation of the riverine inputs.

As a first step, an improved implementation of the Dardanelles Strait inflow into the Mediterranean Sea is performed, moving from a river-like parameterization to a lateral open boundary condition implementation.

The river runoff impacts on the Mediterranean Sea are then evaluated by means of sensitivity experiments considering an increased number of river runoff sources, different riverine outflow salinity values, a modified mixing at river mouths and a different vertical mixing scheme adopted in the ocean model.

With the purpose of further improving the representation of the estuarine processes affecting the riverine outflow salinity and volume flux, which cannot be resolved by the current resolution of the Mediterranean Sea ocean model, an Estuary Box Model simulating the estuaries dynamics is implemented at each river and 1-way offline coupled with the Mediterranean Sea ocean

model.

The results of the performed numerical experiments are validated with respect to in situ and satellite observations to evaluate the capability of the model to correctly represent the thermohaline properties of the Mediterranean Sea.

In addition, the riverine influences are evaluated assessing the impacts of the tested river runoff forcings on the mixed layer depth, the circulation pattern, the sea surface height and the water volume transport through the major straits of the Mediterranean Sea, comparing the numerical results with available climatological data sets and reference literature.

Contents

Chapter 1

Introduction

1.1 Overview

River runoff into the oceans, as a source of momentum and buoyancy, drives direct and strong modifications of the physical properties of the water masses close to the river outlets, but it can also impact regions of the ocean very far from the river mouth in case of large estuaries discharging into the ocean a great amount of brackish water; this is the case, for example, of the Amazon river, whose plume width can exceed 200 km from its outlet (Lentz et al., 1995 [1]).

The term Regions of Freshwater Influence (ROFIs) is introduced in Simpson et al. (1993) [2] with the purpose of defining the peculiar characteristics of the water masses off the Rhine river outlet, clearly affected by its freshwater discharge and it has become of common use in order to identify ocean areas whose physical properties are modified by riverine input.

On the climate time scales river runoff is shown to change the meridional

overturning circulation of the Adriatic Sea (Verri et al., 2018 [3]), as well as in all other ocean basins (Huang and Mehta, 2010 [4]).

The buoyant river plume of less dense water discharged by the river impacts directly also the vertical structure of the water column, leading to an increased stratification that affects the vertical mixing of the interested area (Sauvage et al., 2018 [5]).

It is also demonstrated by several studies that changes in the freshwater input from rivers can affect intermediate/deep water characteristics, as for example in Skliris et al. (2007) [6], where the impact of Ebro and Nile damming on Western and Eastern basin of the Mediterranean Sea respectively was investigated.

It should be stressed that the freshwater input from rivers does not affect only shelf sea areas (Kourafalou et al., 1996 [7], Yankovsky and Chapman, 1997 [8], Kourafalou, 1999 [9], Garvine, 1999 [10], Schiller and Kourafalou, 2010 [11]), but can have also impacts at basin scale (Rahmstorf, 1995 [12], Tseng et al., 2016 [13], Sun et al., 2017 [14]).

Moreover, it is demonstrated in several numerical studies (Sun et al., 2017 [14], Sauvage et al., 2018 [5]) how a correct implementation of riverine input in ocean models, both in terms of outflow salinity and volume flux, is of great importance in order to improve the representation of ocean properties and dynamics.

Concerning the Mediterranean Sea, riverine outflow is of paramount importance, due to the presence of rivers with very high discharge values, the Rhone and the Po, the latter one discharging in the Adriatic Sea, a semi-enclosed basin, whose dynamics and properties are strongly affected by its

freshwater input (Kourafalou, 2001 [15], Oddo and Guarnieri, 2011 [16]) as well as in other semi-enclosed Mediterranean Sea regions, like the Aegean Sea (Kourafalou, 2001 [15]).

1.2 Estuaries

Rivers represent a direct connection between the land and the sea, trough a transition zone, the estuary (Savenije, 2012 [17]).

The approaches used to describe and classify estuaries are generally broad and based on different characteristics. In Savenije (2012) [17] five categories are identified, on the basis of shape, tidal influence, river influence, geology an salinity.

Classification by shape distinguishes five classes of estuaries (Savenije, 2012 [17]):

1. Prismatic: where the banks of the estuary are parallel, this occurs when the river banks are artificially fixed by anthropogenic intervention.

2. Delta: where the tidal range is relatively small and river flow carries a large amount of sediments.

3. Funnel or trumpet shape: where the banks converge in the upstream direction, typical of alluvial estuaries.

4. Rias, fjords and sounds: mainly created by glaciers erosion and then drowned by sea level rise.

5. Bays: semi-enclosed bodies without significant input from rivers.

Classification by tidal influence is firstly proposed by Davies (1964) [18] and includes:

1. Micro-tidal estuaries: tidal range is less than 2 m, estuarine processes are dominated by waves and river flow, whose sediment transport triggers the delta formation, while waves produce spits and barrier islands.

2. Meso-tidal estuaries: tidal range is between 2 and 4 m, tidal action is strong enough to shape the delta geometry by creating flood-tide and the ebb-tide deltas.

3. Macro-tidal estuaries: tidal range is larger than 4 m, tidal action is so strong that instead of flood-tide and the ebb-tide deltas creation a funnel shaped delta is generated.

Classification by river influence (Savenije, 2012 [17]) defines:

1. Riverine estuary: estuary is dominated by river flow, in terms of discharge, sediment supply and salinity.

2. Marine estuary: estuary is dominated by the sea, without significant discharge and sediment supply by river.

Classification by geology (Savenije, 2012 [17]) distinguishes:

1. Fixed bed estuary: the estuary is a remnant of a different geological era, created by different phenomena, like in the case of fjords and rias.

2. 'Short' alluvial estuary: in this kind of estuary the sediment transport have not yet reached an equilibrium, resulting in a short coastal plain estuary with an almost linear bottom slope.

3. 'Long' alluvial or coastal plain estuary: in this kind of estuary the sediment transport have reached an equilibrium and the sediment have been deposited both by river and sea, resulting in a long coastal plain estuary with almost no bottom slope.

From the oceanographic point of view, the classification of estuaries based on salinity is surely the most useful to identify the impact that river discharge can have on ocean properties and dynamics.

On the basis of the salinity profile mainly two kind of estuaries can be distinguished (Savenije, 2012 [17]):

- Positive or normal estuaries: estuaries where the salinity decreases gradually in the upstream direction, due to a significant river discharge and to a small evaporation/rainfall ratio. This is the typical estuary in temperate and wet tropical climates.

- Negative or hypersaline estuaries: estuaries where the salinity increases gradually in the upstream direction, due to a small river discharge and to a large evaporation/rainfall ratio. This is the typical estuary in arid and semi-arid climates.

From the numerical modelling perspective (in particular for high resolution modelling) a correct geometrical representation of the estuaries is crucial; this is why the classification scheme proposed by Galloway (1975) [19] should be also mentioned, since it summarizes the main types of estuaries depending on the most important driving factors that shape their morphology. The classification scheme is shown in Figure 1.1, which well summarizes the com-

ponents that play a major role in estuarine dynamics: river discharge, waves and tides.

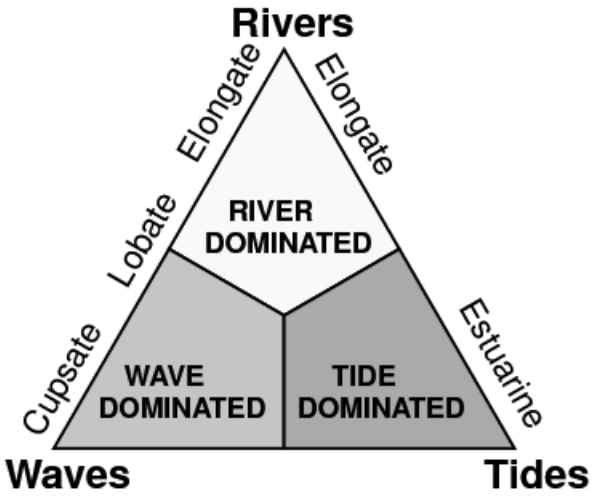

Figure 1.1: Classification scheme after Galloway, 1975 [19] (modified after Seybold et al., 2007 [20]).

Estuarine dynamics is strongly dominated by mixing and dispersion as described in Fischer (1976) [21], who defines the turbulent mixing in estuaries as *the effect of random velocity variations having length scales on the order of*

the width of the estuary or less, and time scales much less than the duration of a tidal cycle.

The author decomposes the turbulent mixing in estuaries into two components: the vertical mixing and the transverse mixing. Vertical mixing is due to the shear stress between water bodies at different density (riverine water and seawater) or to the interaction of water masses with the bottom (bottom friction). Transverse mixing is mainly due to cross-section density gradients or to different flow velocities between the center of the estuary and its sides, due to the interactions of water masses with river banks.

Longitudinal dispersion in estuaries can be defined as the ability of rivers to disperse tracers in longitudinal direction (Deng et al., 2001 [22]). Different driving mechanisms contribute to generate longitudinal dispersion in estuaries, with temporal and spatial scales which are larger than the turbulent mixing ones:

- Wind: a constant wind blowing over an estuarine area generates wind stress that produces a horizontal circulation, with shallower water masses following the wind direction and deeper water masses moving in the opposite direction: this circulation determines both mixing due to the interactions of water masses at different densities and in addition a water piling in the wind direction that drives an upwelling of saltier water from the bottom.

- River: river freshwater acts as a source of buoyancy and momentum, generating a residual internal circulation, called gravitational circulation (Fischer, 1976 [21]), forced by longitudinal salinity gradient; this

mechanism competes with tides as the most important contributor to mixing, depending on estuary geometry.

- Tide: tidal inflow into estuary acts as a source of kinetic energy, which leads to different kind of mixing (Fischer, 1976 [21] and Savenije, 2012 [17]). It contributes to turbulent mixing, which is anyway of smaller importance with respect to other mixing mechanisms.

  Other mixing processes generated by tidal inflow into estuaries are tidal trapping and tidal pumping.

  The first one has been introduced by Schijf and Schonfeld (1953) [23], considering the effect due to tidal phase difference between the main estuary branch and secondary branches: the phenomenon at the basis of the tidal trapping theory is that, because of the above mentioned tidal phase difference, the secondary branches can feed the main branch with fresher water while the main branch is still advecting saltier ocean water upstream along the estuary.

  Tidal pumping is a very important mechanism for mixing in estuaries, in particular at the mouth of wide estuaries: it results from differences in salt advection during flood and ebb tides (Sun et al., 2017 [14]). According to Fischer (1976) [21] residual circulations are produced due to the interactions between the tidal inflow and the bathymetry and to the existence of separated ebb and flood channels (Savenije, 2012 [17]).

  Significant mixing is generated also during the transition from neap to spring tide, due to the different estuary stratification occurring during the two phases (Uncles and Stephens, 1996 [24]).

Given this wide range of processes that contributes to mixing in estuaries, a quantitative classification of estuaries on the basis of their mixing structure is proposed in Fischer et al. (1979) [25], where a *flow ratio* parameter is defined as:

$$F = \overline{u_{tide_f}}/\overline{u_{river}} \tag{1.1}$$

where $\overline{u_{tide_f}}$ (m/s) is the average flood tide velocity and $\overline{u_{river}}$ (m/s) is the average river flow velocity.

On the basis of the *flow ratio* parameter, estuaries can be classified into three categories:

- Sharply stratified estuaries, with $F < 0.1$
- Partially stratified estuaries, with $0.1 < F < 10$
- Well mixed estuaries, with $F > 10$

In sharply stratified estuaries (Figure 1.2) the less dense river water flows over an underlying denser water mass intruding into the estuary from the ocean: the lower the river discharges, the larger the intrusion length of sea-water.

The sharp salinity and density gradients lead to the formation of a stable halocline and of a consequent pycnocline which inhibits the mixing between the overlying freshwater from the river and the underlying salt water from the ocean.

Anyway mixing is not null, since it is triggered by the shear stress of the two water masses flowing in opposite directions: this leads the salt water

moving from the bottom towards the upper layer, where it mixes with water from the river, becoming brackish water. Sharply stratified estuaries are typical of low tidal range seas.

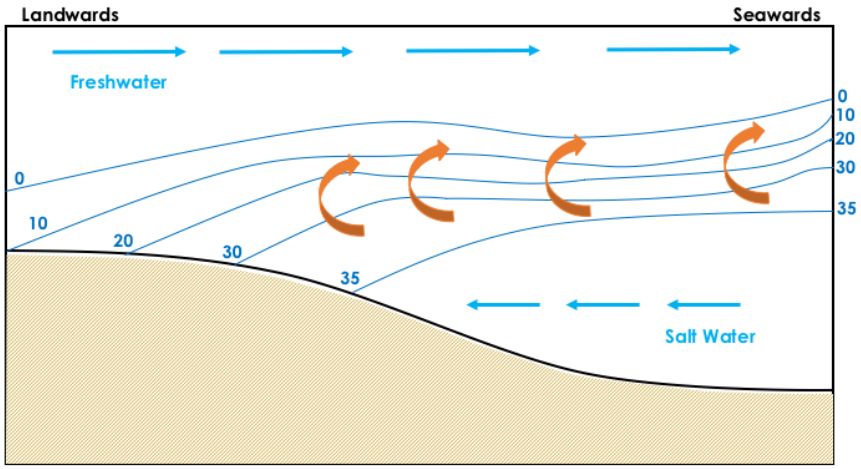

Figure 1.2: Diagrammatic representation of water circulation in a sharply stratified estuary: blue lines represent isohalines, orange arrows represent mixing (based on Wright, J., Colling, A., Park, D. (Eds.), (1999) [26]).

In case of moderate tidal range seas, mixing processes in estuary are influenced by tidal motion during flood and ebb tides. The interaction between the tidal flow and the estuary bottom produces a larger mixing with respect to sharply stratified estuaries: this results in a less defined halocline and in a weaker stratification. The estuary can be defined partially stratified (Figure 1.3).

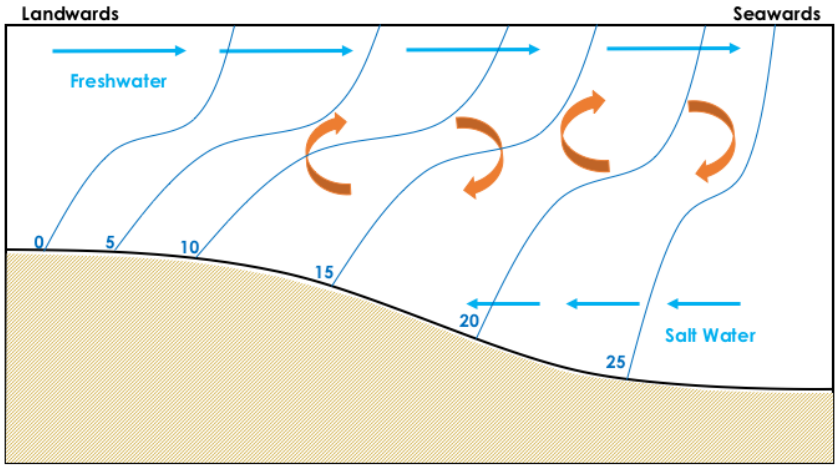

Figure 1.3: Diagrammatic representation of water circulation in a partially stratified estuary: blue lines represent isohalines, orange arrows represent mixing (based on Wright, J., Colling, A., Park, D. (Eds.), (1999) [26]).

In case of large tidal range seas, estuarine dynamics is driven by tidal flow, which is dominating with respect to river flow: the entire water column is well mixed and salinity (and density) gradients from the surface to the estuary bottom are small. The smaller is the distance from the estuary outlet, the more the water column is homogenized. This kind of estuary can be defined well mixed (Figure 1.4).

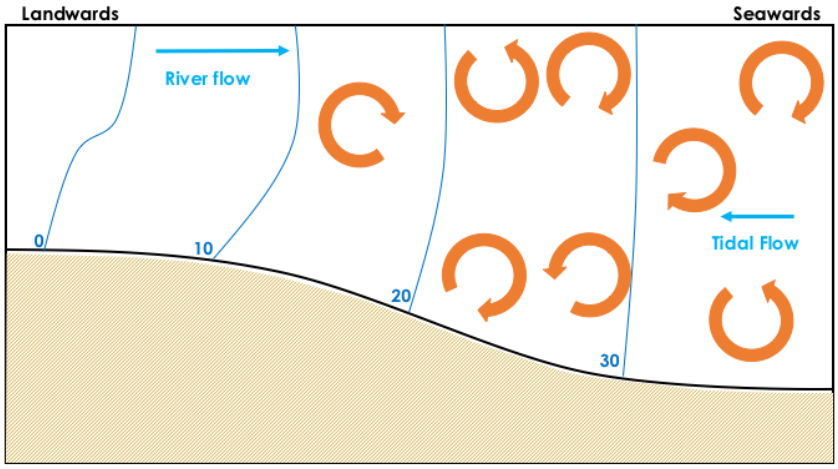

Figure 1.4: Diagrammatic representation of water circulation in a well mixed estuary: blue lines represent isohalines, orange arrows represent mixing (based on Wright, J., Colling, A., Park, D. (Eds.), (1999) [26]).

1.3 Regions Of Freshwater Influence

As already mentioned, the Regions of Freshwater Influence (ROFIs) has been introduced in Simpson et al., 1993 [2] to define the area of the ocean that is affected by the river outflow and its properties.

As soon as river water is discharged into the ocean a buoyant plume of brackish water is formed, whose initial extension is controlled by river discharge and tidal regime of the area. As an example, the plume of the world's largest river, the Amazon river, can exceed 200 km from its outlet (Lentz et al., 1995 [1]), while in case of small river discharge and large tidal range the river plume can also be pushed back into the estuary by tidal flow during flood tide.

The main processes driving the spreading of the river water buoyant plume, as reported in Kourafalou et al. (1996) [7], are essentially the following:

- The acceleration due to the balance between inertia and buoyancy forces.
- The mixing due to plume interaction with bottom and with seawater at different density.
- The geostrophy, in terms of the balance between the Coriolis force and the horizontal pressure gradient which develops as a consequence of the differences in density between the water discharged by the river close to the coast and the offshore seawater. This mechanism is extremely important in determining the shape and the extension of the buoyant plume, since it generates alongshore coastal currents which propagate leaving the coast to the right in the Northern hemisphere, or to the left in the Southern hemisphere. This is extremely evident for the Po river plume, which propagates from its outlet in the Northern Adriatic Sea down to the Southern Adriatic Sea in the Gargano Promontory area.
- The wind and its variability contributes significantly to the extension and the shape of the buoyant plume, since a favourable wind regime (in the offshore direction) can intensify southward currents due to the combination with southward Ekman transport, while onshore wind regime can slow down the currents velocity and confine the buoyant plume closer to the river outlet.

The complex system of ROFIs is also characterized by several mechanisms

that affect the vertical structure of the water column, as described in Verspecht et al. (2009) [27].

ROFIs represent dynamic systems whose vertical structure is driven by concurring processes of stratification and mixing, which produce their typical residual circulation: the heating of the sea surface and the increased buoyancy due to freshwater input generate stratification, while wind stress and tidal flow generate mixing.

It is worth mentioning the concept of *straining*, developed in several studies both for tides and for wind.

A tidal straining (whose diagrammatic representation is shown in Figure 1.5), can be defined as a periodic oscillation of the water column vertical structure between a condition of stratification during ebb tide and a condition of mixing during flood tide (Verspecht et al., 2009 [27], Simpson et al., 1990 [28], Rippeth et al., 2001 [29]).

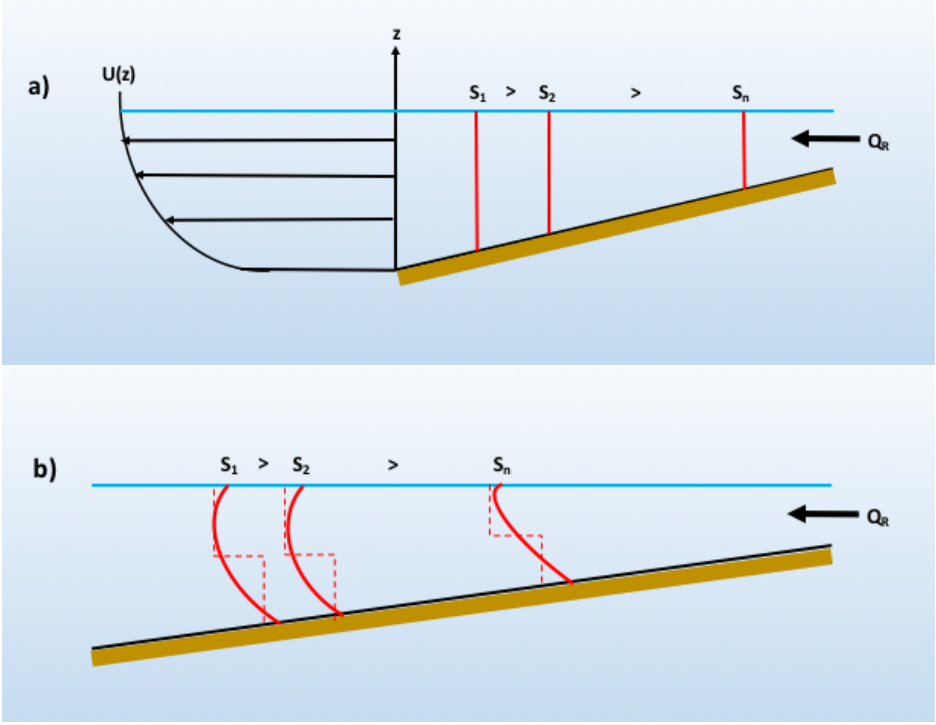

Figure 1.5: Diagrammatic representation of the tidal straining mechanism (based on MacCready and Geyer, 2010 [30]). *a*) shows the vertical structure after flood tide, while *b*) shows the vertical structure after ebb tide. Red solid lines represent salinity contours, while red dashed lines represent the influence of mixing.

In particular, as described in Simpson et al. (1990) [28], vertical shear in tidal flow plays a crucial role in this mechanism: during ebb tide, less dense water moves faster seaward at the surface, driving the entrainment of more dense water from the ocean in the lower layer and thus producing a stratified structure, which is strengthened by the vertical mixing induced by the wind stress at the surface and by the stress of the tidal flow at the bottom. During

the flood tide the mechanism is reversed, and the pumping of more saline water landward breaks down the stratification introduced during the ebb tide.

According to Linden and Simpson (1986) [31], the salt flux difference between the stratified and the mixed situation can be of one order of magnitude.

Concerning wind straining, the basic mechanism is similar to the tidal straining, since when the wind stress is directed in the same direction of the residual current, stratification is generated, while when wind stress is in the opposite direction with respect to the residual current a suppression of the residual flow can occur (Verspecht et al., 2009 [27]).

Scully et al. (2005) [32] highlights the connection between wind straining, vertical stratification and consequently vertical eddy viscosity, the latter strongly influencing the exchange flow in estuarine areas and thus affecting the most part of the ROFI.

1.4 The Mediterranean Sea

The Mediterranean Sea is a semi-enclosed sea located at mid-latitude between Europe, Asia and Africa. It is connected to the Atlantic Ocean to the west through the Gibraltar Strait, while it is connected to the Black Sea to the east through the Marmara Sea, which together with the Dardanelles Strait and the Bosphorus Strait represents the Turkish Straits System.

The Mediterranean Sea can be subdivided into two main sub-basins, the western Mediterranean and the eastern Mediterranean, interconnected by the Sicily Strait. They can be, in turn, splitted into major seas and areas, as

shown in Figure 1.6.

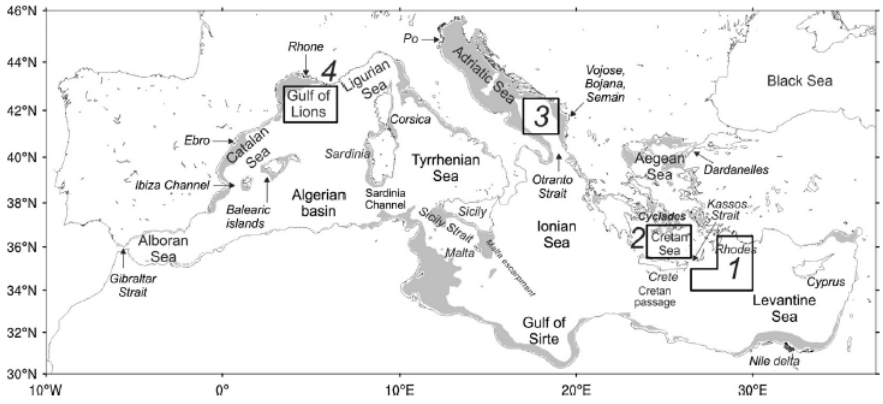

Figure 1.6: Mediterranean basin geometry and nomenclature for major seas and areas. The shaded areas indicate depths less than 200 m. The four boxes (1–4) represent water mass formation areas (reproduced from Pinardi et al., 2015 [33])

The main forcings of the Mediterranean Sea are the atmospheric forcing and the buoyancy fluxes (Pinardi et al., 2015 [33]).

The atmospheric forcing shows a high complexity and a high seasonal variability. The atmosphere transfers momentum, heat and water to the ocean through its surface showing a high seasonal and interannual variability (Pinardi and Navarra, 1993 [34]).

Another major forcing for the Mediterranean Sea circulation is the Atlantic water inflow from Gibraltar Strait, which is one of the terms contributing to the hydrological balance of the Mediterranean Sea, as shown in Equation 1.2:

$$F = E - P - R - G - B \tag{1.2}$$

where E $(mm/year)$ is the evaporation term , P $(mm/year)$ is the precipitation term, R $(mm/year)$ is the river discharge, G $(mm/year)$ is the net flux from Gibraltar Strait and B $(mm/year)$ is the net flux from Black Sea through the Dardanelles Strait.

Despite the significant amount of water introduced into the basin through the Gibraltar Strait and the Dardanelles Strait, the Mediterranean Sea has a negative water balance, which means that the evaporation term E in Equation 1.2 is not completely balanced by the other terms (Pinardi et al., 2006 [35]).

This results in an antiestuarine circulation, with bottom saltier and denser water leaving the Mediterranean Sea and surface less salty and less dense water entering into the basin through the Gibraltar Strait, with an interface between the two water masses at about 150 m depth.

Wüst (1961) [36] proposes the following classification of the Mediterranean Sea water masses based on the vertical distribution of salinity, oxygen and temperature:

- The near-surface water of Atlantic origin, between 0 and 75 m depth
- The intermediate water, between 200 and 600 m
- The deep water, between 1500 and 3000 m
- The bottom water, at depths to 4200 m

The Mediterranean Sea water masses vertical distribution is shown in Figure 1.7, and described in detail in Zavatarelli and Mellor (1995) [37].

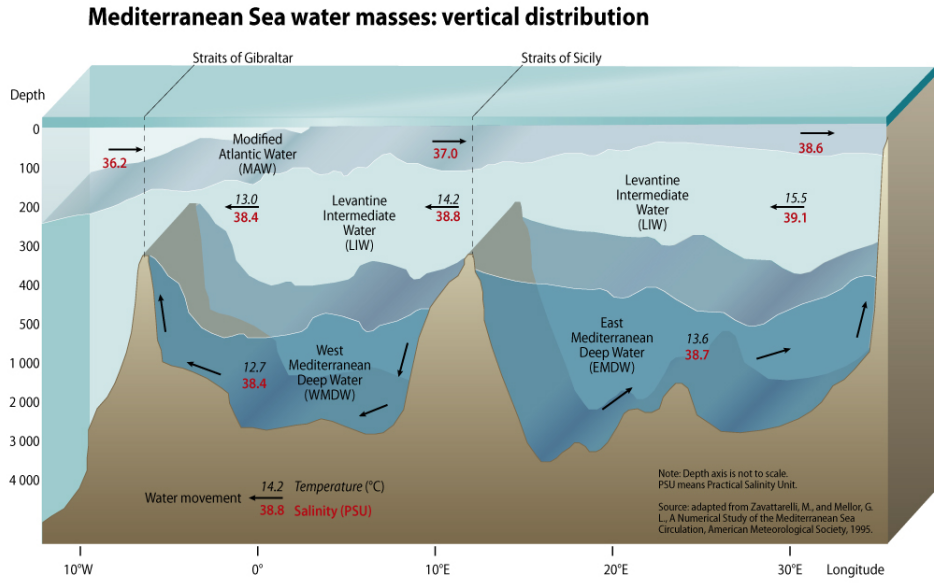

Figure 1.7: Diagrammatic representation of the Mediterranean Sea water masses vertical distribution. Image credit: GRID-Arendal, `http://www.grida.no/resources/5885`

1.4.1 The Mediterranean Sea Circulation

The Mediterranean Sea circulation at basin-scale is described in Pinardi et al. (2015) [33], where the circulation structures (Figure 1.8) are deduced from the 1987-2007 numerical reanalysis mean flow field computed in Adani et al. (2011) [38].

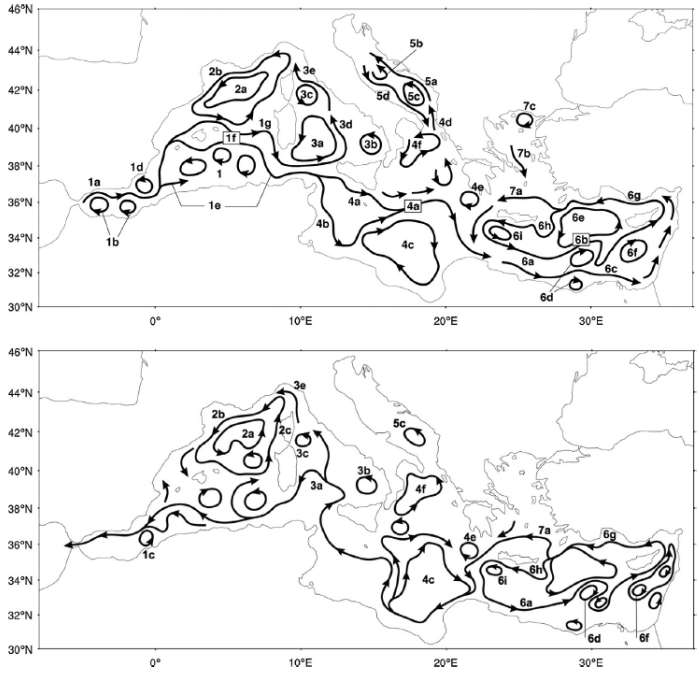

Figure 1.8: The schematic of the mean surface circulation structures as deduced from the 1987–2007 Mediterranean Sea reanalysis mean flow field. Upper panel: surface circulation. Lower panel: 200–300 m average circulation. The names of the structures are reported in Figure 1.9 (reproduced from Pinardi et al., 2015 [33])

Current systems	Components
System 1	1a: Atlantic Water Current (AWC) 1b: Western and Eastern Alboran Gyres 1c: Almera-Oran front 1d: Almera-Oran cyclonic eddy 1e: Algerian Current segments 1f: Western Mid-Mediterranean Current (WMMC) 1g: Southern Sardinia Current (SCC)
System 2	2a: Gulf of Lion Gyre (GLG) 2b: Liguro-Provenal-Catalan Current (LPCC) 2c: Western Corsica Current (WCC)
System 3	3a: South-Western Tyrrhenian Gyre (SWTG) 3b: South-Eastern Tyrrhenian Gyre (SETG) 3c: Northern Tyrrhenian Gyre (NTG) 3d: Middle Tyrrhenian Current 3e: Eastern Corsica Current (ECC)
System 4	4a: Atlantic-Ionian Stream (AIS) 4b: Sicily Strait Tunisian Current (SSTC) 4c: Syrte Gyre (SG) 4d: Eastern Ionian Current (EIC) 4e: Pelops Gyre (PG) 4f: Northern Ionian Cyclonic Gyre
System 5	5a: Eastern South-Adriatic Current (ESAC) 5b: Middle Adriatic Gyre 5c: South Adriatic Gyre 5d: Western Adriatic Coastal Current (WACC)
System 6	6a: Cretan Passage Southern Current (CPSC) 6b: Mid-Mediterranean Jet 6c: Southern Levantine Current (SLC) 6d: Mersa Matruh Gyre System (MMGS) 6e: Rhodes Gyre (RG) 6f: Shikmona Gyre System (SGS) 6g: Asia Minor Current 6h: Ierapetra Gyre (IPG) 6i: Western Cretan Cyclonic Gyre
System 7	7a: Cretan Sea Westward Current (CSWC) 7b: Southward Cyclades Current (SWCC) 7c: North Aegean Anticyclone

Figure 1.9: Nomenclature for the surface and intermediate depth circulation structures identified in Figure 1.8. (reproduced from Pinardi et al., 2015 [33])

The main features of the Mediterranean Sea surface circulation are described in the following, using as a reference Figure 1.8 (upper panel) and Figure 1.9.

The Alboran Sea is characterized by the intrusion into the Mediterranean Sea of surface fresh and relatively cold waters from the Atlantic Ocean: the

Atlantic Water Current (AWC, Figure 1.8 1a) enters into the basin through the Gibraltar Strait and propagates towards the eastern part of basin, sinking while it travels from West to East due to the modification of its thermohaline characteristics.

In the Alboran Sea the AWC generates two semi-permanent anticyclonic gyres, which together with the Almera-Oran cyclonic eddy generate an area of intense mesoscale activity (Figure 1.8 1b and 1d respectively, Vélez-Belchı et al., 2005 [39], Snaith et al., 2002 [40], Pinardi et al., 2015 [33]).

Exiting from the Alboran Sea, the AWC bifurcates into two branches, the first one is confined along the Algerian coast (Algerian Current segments, Figure 1.8 1e), while the second one flows towards the Ibiza channel, generating the so-called Western Mid-Mediterranean Current ($WMMC$, Figure 1.8 1f, Pinardi et al., 2015 [33]). The latter connects to the Gulf of Lion Gyre (GLG, Figure 1.8 2a, Madec et al., 1991 [41] and Pinardi et al., 2006 [35]) and its outer boundary represented by the Liguro-Provencal-Catalan Current ($LPCC$, Figure 1.8 2b).

The Algerian Current splits into three branches at the Sardinia Channel: one flowing northward into the Tyrrhenian Sea, the Middle Tyrrhenian Current (MTC, Figure 1.8 3d, Pinardi et al., 2015 [33]); the other two entering the Sicily Strait forming the Sicily Strait Tunisian Current ($SSTC$, Figure 1.8 4b) and the Atlantic Ionian Stream (AIS, Figure 1.8 4a) according to Robinson et al. (1999) [42], Onken et al. (2003) [43] and Lermusieaux et al. (2001) [44].

The Tyrrhenian Sea circulation, according to Artale et al. (1994) [45], is characterized by three cyclonic gyres: the South-Western Tyrrhenian Gyre

($SWTG$), the South-Eastern Tyrrhenian Gyre ($SETG$) and the Northern Tyrrhenian Gyre (NTG), identified as $3a$, $3b$ and $3c$ respectively in Figure 1.8.

Moving eastward, the Cretan Passage Southern Current ($CPSC$, Figure 1.8 $6a$, Pinardi et al., 2015 [33]) can be identified, before it branches into the Mid-Mediterranean Jet (MMJ, Figure 1.8 $6b$, Golnaraghi and Robinson, 1994 [46]) and into the Southern Levantine Current (SLC, Figure 1.8 $6c$, Pinardi et al., 2006 [35]).

The Levantine basin is characterized by significant mesoscale systems such as the Mersa Matruh Gyre System ($MMGS$, Figure 1.8 $6d$), the Shikmona Gyre System (SGS, Figure 1.8 $6f$, Hecht et al., 1998 [47], Pinardi et al., 2006 [35] and Zodiatis et al., 2005 [48]), the Ierapetra Gyre (IPG, Figure 1.8 $6h$, Robinson et al., 1991 [49]) and the Rhodes Gyre (RG, Figure 1.8 $6e$, Milliff and Robinson, 1992 [50]).

The Southern Levantine Current (SLC) flows along the coasts of Egypt, Israel, Lebanon, Syria and then, reaching the southeastern coast of Turkey, it joins the Asia Minor Current (Figure 1.8 $6g$), which propagates westward.

The Adriatic Sea, according to Artegiani et al. (1997) [51], is characterized by: the intrusion through the Otranto Strait of the Eastern Ionian Current (EIC, Figure 1.8 $4d$), by the Eastern South-Adriatic Current ($ESAC$, Figure 1.8 $5a$), which flows northward leaving the Balkan coast to the right and by the Western Adriatic Coastal Current ($WACC$, Figure 1.8 $5d$), which flows southward along the Italian coast. Two cyclonic structures are clearly identifiable in the Adriatic Sea, the Middle Adriatic Gyre and the South Adriatic Gyre (Figure 1.8 $5b$, $5c$).

The main driver of the Aegean Sea circulation (see Figure 1.10) is the inflow of low-salinity and low-temperature waters, namely Black Sea Waters (BSW), from the Marmara Sea through the Dardanelles Strait (Politikos et al., 2017 [52]). The BSW bifurcate just after the Dardanelles Strait outlet (Nittis and Perivoliotis, 2002 [53]): one branch flowing northward towards the Samothraki plateau, where the North Aegean Anticyclone ($NASA$, Figure 1.8 7c, Kourafalou and Barbopoulos, 2003 [54]) is well identifiable; the second branch flowing towards the Thermaikos gulf and the Evia island.

The North-East Aegean Sea circulation (South of the Dardanelles Strait) is influenced by the branch of the Asia Minor Current which intrudes into the Aegean Sea warm and saline waters from the Levantine basin (Nittis and Perivoliotis, 2002 [53]).

The water outflow from the Aegean Sea towards the Cretan Sea is mainly represented by the Southward Cyclades Current (SCC, Figure 1.8 7b, Pinardi et al., 2015 [33]), which pushes BSW from the North to the South Aegean Sea.

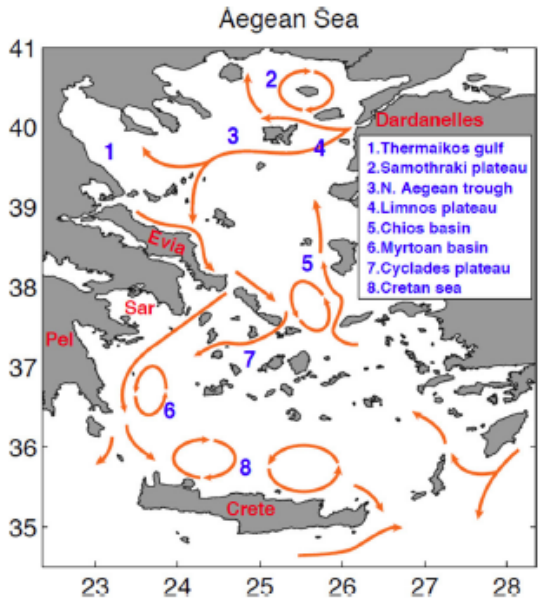

Figure 1.10: Diagrammatic representation of the surface circulation in the Aegean Sea (reproduced from Politikos et al., 2017 [52]).

The intermediate depth circulation shown in Figure 1.8 (bottom panel) is characterized in the eastern basin by the Levantine Intermediate Water (LIW), formed in the Levantine basin (Lascaratos et al., 1993 [55]). As indicated in Zavatarelli and Mellor (1995) [37], the LIW moves westward at depth ranging from 200 and 700 m and, travelling towards the western part of the basin, its temperature and salinity values decrease from about 15.5 ^oC and 39.1 PSU in the Levantine basin to about 13.0 ^oC and 38.4 PSU at Gibraltar Strait, where it exits from the Mediterranean Sea at depth, under the inflowing Atlantic Water.

The intermediate depth circulation in the eastern basin mirrors the surface circulation of the area, with the main surface structures which can be

identified also at depth.

The surface Cretan Sea Westward Current ($CSWC$, Figure 1.8 $7a$) branches into three main streams in the Gulf of Syrte: the first one generates the Syrte Gyre (SG, Figure 1.8 $4c$), which is also present at surface; the second branch flows towards the Southern Ionian Sea, while the third one propagates towards the western basin through the Sicily Strait.

The Northern Ionian Cyclonic Gyre and the South Adriatic Gyre (Figure 1.8 $4f$ and $5c$ respectively) are clearly identified in the Northern Ionian and in the Southern Adriatic Seas in the considered range of depth.

Another LIW bifurcation appears in the South Tyrrhenian Sea, East of the Sardinia coast, where one branch flows northward leaving the Italian coast to the right and then reaching the Gulf of Lion Gyre (GLG, Figure 1.8 $2a$), while the other branch flows towards the Gibraltar Strait, crossing an area of significant mesoscale activity, and finally exiting from the Mediterranean Sea basin.

The overturning circulation of the Mediterranean Sea is represented by all the vertical and horizontal water masses displacements due to density gradients. The major *conveyor belts* of the overturning circulation are represented in Figure 1.11.

- The Atlantic Water (AW, also called Modified Atlantic Water, MAW, yellow dashed line in Figure 1.11), flowing from the Gibraltar Strait is characterized by low salinity and low temperature values. It spreads from the Alboran Sea to the Levantine basin at a depth ranging between surface and 200 m, modifying its characteristics (Zavatarelli and Mellor (1995) [37]) due to an increase in salinity and temperature, with a

subsequent gradual sinking.

- The Levantine Intermediate Water flowing between 300 and 700 m in the Eastern Mediterranean, and between 200 and 400 m in the Western Mediterranean, is the result of winter convection processes in the Rhodes-Cyprus area and then it spreads towards the western basin (red dashed line Figure 1.11) with a decrease of its temperature and salinity (Zavatarelli and Mellor (1995) [37]).

- Two meridional overturning thermohaline cells form in the Western and Eastern Mediterranean basins, which are driven directly by deep convection in the Gulf of Lion and in the Adriatic Sea respectively (Demirov and Pinardi, 2007 [56]). Moreover a recent contribution to the Eastern Mediterranean meridional cell provided by the Cretan Sea Deep Waters (CDW) is observed from 1986 to 1996 (Pinardi et al., 2015 [33]).

The connection between the meridional and the zonal conveyor belts is represented by the Levantine Intermediate Water bifurcation in the Sardinia Channel (Pinardi and Masetti, 2000 [57]).

The deep water formation sites which feed the overturning circulation and the corresponding water masses are the following:

- The Rhodes Gyre for the Levantine Intermediate Water
- The Adriatic Sea for the Eastern Mediterranean Deep Water
- The Gulf of Lion for the Western Mediterranean Deep Water

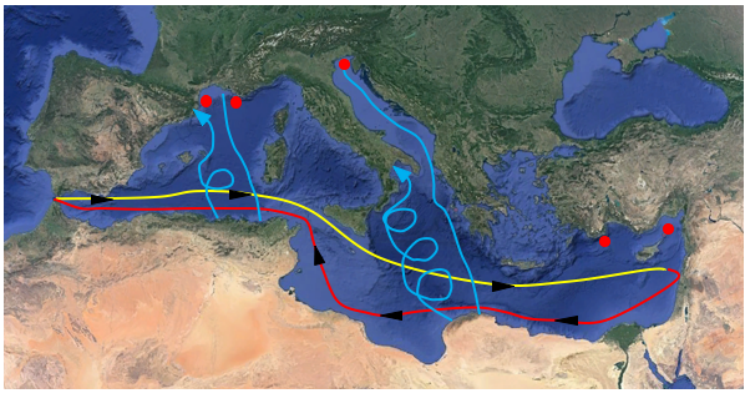

Figure 1.11: Representation of the overturning circulation in the basin with the major conveyor belt systems indicated by dashed lines with different colours. The yellow line indicates the AW stream which is the surface manifestation of the zonal conveyor belt of the Mediterranean Sea. The red line indicates the mid-depth LIW recirculation branch of the zonal thermohaline circulation. The light blue lines indicate the meridional cells induced by deep waters. The red dots indicate intermediate and deep water formation areas (based on Demirov and Pinardi, 2007 [56]).

Starting from the western part of the basin, the Western Mediterranean Deep Water formation takes place during wintertime in the Gulf of Lion, due to the cyclonic dynamics of the area (Millot, 1999 [58] and Schott et al., 1996 [59]) and to the cold and dry winds blowing during wintertime, the Mistral from the Rhone Valley and the Tramontana from the Pyrenees (Zavatarelli and Mellor, 1995 [37] and Millot and Taupier-Letage, 2005 [60]), which generate a sinking of dense waters in the area (Grignon et al., 2010

[61]).

The second site of deep water formation is the Southern Adriatic Sea, where the Eastern Mediterranean Deep Water is formed and then spreads out from the Adriatic Sea through the Otranto Strait. In addition, the Northern Adriatic Sea plays an important role in deep water formation, driven by the cooling and evaporative processes affecting the Northern Adriatic water masses during wintertime (Zavatarelli and Mellor, 1995 [37]), giving rise to the so-called shelf water formation.

The formation of the Levantine Intermediate Water is mainly caused by the presence of a surface layer of warm and salt water in the Levantine basin, the so-called Levantine Surface Water (LSW), during summer and autumn. The formation of LIW occurs in February and March, when LSW mixes with the Atlantic Water and the previously mixed LIW (Castellari et al., 2000 [62]).

1.4.2 Hydrology and riverine influences on the Mediterranean Sea basin

The hydrographic basin of the Mediterranean Sea has an extension of more than 5 millions km^2, including also the Nile river reservoir and internal areas of the Lybian coast which are not active components of the drainage basin.

Excluding these areas, that provide a quite small riverine inflow, the extension of the Mediterranean Sea drainage basin is reduced to less than 1.5 millions km^2 (Ludwig et al., 2009 [63]).

The Mediterranean Sea drainage basin there is characterized by an evident gradient of the mean annual precipitation rate decreasing in the southward

direction (Ludwig et al., 2003 [64]). Moreover the orographic characteristics of the different areas affect the precipitation rate, with maximum values (between 1500 and 2000 $mm/year$) occurring in the Alps and Pyrenees areas that feed the Po, the Rhone and the Ebro rivers, as well as along the mountain ranges of the Dalmatian coast (Ludwig et al., 2009 [63]).

One of the most important characteristics of the hydrographic basin of the Mediterranean Sea is the strong contrast in the precipitation rate between Summer and Autumn seasons, and its decrease from North to South and from West to East (Ludwig et al., 2009 [63]).

The highest precipitation rate occurs during Autumn in Spain, France, Italy and in the Balkan Peninsula, and during Winter in Turkey and Lebanon, being Summer a very dry season all over the entire drainage basin. During Spring the contribution to the total annual precipitation is nearly homogeneous in the whole basin (Ludwig et al., 2003 [64]).

The precipitation pattern and distribution play a crucial role on the riverine discharge into the Mediterranean Sea, but also the morphological configuration of the drainage basin affects the hydrologic characteristics of the area.

The most part of the rivers discharging into the Mediterranean Sea is characterized indeed by a relatively small length and volume flux, mainly due to the dry climate in the Southern part of the drainage basin and to the large number of mountain areas close to the coasts in the Northern part of the basin, that reduces the extension of river drainage basins as well as the distance between the source and the outlet.

Literature estimates of total riverine freshwater flux into the Mediterranean

Sea vary a lot among the different studies: Anati and Gat (1989) [65] propose a value of about 440 $km^3/year$, Vörösmarty et al. (1998) [66] indicate a very high value of 737 $km^3/year$, a value of about 347 $km^3/year$ is provided in Boukthir and Barnier (2000) [67] and 430 $km^3/year$ is the estimate proposed in Margat et Treyer (2004) [68]).

In Struglia et al. (2004) [69] a total freshwater value ranging from about 255 $km^3/year$ to about 328 $km^3/year$ is proposed by considering possible underestimates in river discharge values.

This is the same value proposed in Ludwig et al. (2009) [63] over the period 1991-2000, where the authors argue that the higher values suggested in Vörösmarty et al. (1998) [66] and Margat et Treyer (2004) [68] can be the results of an overestimation of the freshwater fluxes in the South Levantine Sea, since classical mapping and modelling approaches cannot take into account the particular processes that characterize the Nile river, like infiltration in swamps, river evaporation and anthropogenic water use (Nixon, 2003 [70]).

Ludwig et al. (2009) [63] also provide a very detailed description of the average freshwater fluxes in the Mediterranean Sea considering different sub-basins: during the period 1991-2000 the rivers discharging into the Adriatic Sea sub-basin provide a mean annual discharge of 118 $km^3/year$ (about the 36% of the total discharge), being the main freshwater source in the whole Mediterranean Sea, thanks to the Po river and to the large number of rivers that have their own outlets in the Adriatic Sea.

The second sub-basin in terms of mean annual river discharge is the North Western area, where the Rhone river provides around 85 $km^3/year$ of fresh-

water, representing about the 26% of the toal mean annual river inflow.

Finally a very important contribution is provided by the rivers outflowing into the Aegean Sea sub-basin: even though none of the ten largest rivers (according to Ludwig et al., 2009 [63]) of the Mediterranean Sea has its own outlet in this sub-basin, the total discharge amounts to 48 $km^3/year$, equal to about the 15%.

As already mentioned in section 1.1, anthropogenic pressures on water resources through rivers damming provide important effects on the thermohaline properties and the circulation of the Mediterranean Sea.

In Skliris et al. (2007) [6] numerical studies are performed in order to assess the impact onto the Mediterranean Sea properties of the damming that Nile, Ebro and Russian rivers (the latter discharging into the Black Sea) have undergone in the last 50 years (in addition to a large precipitation decreasing trend between the mid-eighties and the early nineties).

After the construction of the Aswan Dam in 1964, the Nile river runoff drastically reduced by more than 90%, while the damming of the Ebro river in the early sixties reduced its discharge by more than the 60%. Moreover the volume flux control of the Russian rivers discharging into the Black Sea (that affect the Dardanelles Strait outflow in the Aegean Sea), started in the fifties and provided a decrease of about 60 $km^3/year$ in the mid-nineties (Bethoux and Gentili, 1996 [71]).

Literature results show that the river damming induced a large salinity increase in the Levantine surface layer enhancing the Levantine Intermediate Water production rates and salinity. This in turn affects the production of the Levantine Deep Water, in terms of larger water mass formation rates

characterized by higher salinity.

According to Skliris et al. (2007) [6] the 50% of the changes observed in the Western Mediterranean Deep Water can be due to the higher salinity values in the Levantine Intermediate Water as a result of the damming of the Russian and Nile rivers, while the remaining 50% can be explained by the local surface salinity increase, due both to the decreased Ebro discharge and to the precipitation decrease.

An assessment of riverine influences on the thermohaline and dynamical properties of the Mediterranean Sea is described in Verri et al. (2018) [3], where the impact of river runoff on the Central Mediterranean Overturning Circulation (CMOC) is described.

The authors highlight the primary role of the river runoff (along with wind work and heat flux) in determining the characteristics of the CMOC, by modifying both its intensity and extension. Another conclusion provided by the authors is that rivers impact the dense water formation in the Adriatic Sea by affecting the stratification in the Southern Adriatic Sea due to a modified vertical mixing, thus in turn decreasing the volume of dense waters formed.

1.5 Limitations for river runoff implementation in global and regional ocean models

River runoff representation in global (in particular) and regional ocean models is a challenging issue, since their current horizontal resolution is usually not adequate to correctly reproduce the complex processes and dynamics

occurring in the estuaries and in the transition zone between the estuary and the shelf areas.

The only exception could be represented by local implementation of ultra-high resolution finite differences or finite elements numerical models, whose resolution can realistically represent river runoff and estuarine processes, but basin scale unstructured grid models with resolved river inlets are still at their infancy and there is a need to identify intermediate solutions.

Another strong limitation for a correct river runoff representation is provided by the scarcity of river volume flux, salinity and temperature data at the interface between rivers and the ocean, in particular for smallest rivers.

Salinity and temperature close to river mouths are usually monitored through dedicated campaigns, but they cannot ensure a regular temporal and spatial coverage (as moored instruments could instead provide). This leads to significant uncertainties in the river thermohaline properties that can be prescribed in numerical models.

Another source of uncertainty concerns the river discharge, since gauging stations are usually located quite upstream with respect to river outlet, so that many estuarine processes (described in section 1.2) are not taken into account, such as: the seawater entrainment into the estuary and the barotropic transport due to tides, which increase the water volume that will be then discharged to sea, as well as the water exploitation derived from anthropic activities that reduce the river volume flux.

Due to the difficulty in retrieving exhaustive riverine data sets, river discharge is usually quite simply parameterized in global and regional ocean models as a surface (often climatological) volume flux, with a prescribed

constant salinity (usually 0 PSU), while the river temperature is usually considered equal to the sea surface temperature of the grid point where the freshwater source is implemented (rarely it is prescribed by the modeller).

It is clear that such a kind of simplified implementation could lead to big errors in both coastal areas and offshore thermohaline properties and circulation, due to the complex processes and mechanisms triggered by riverine inflow into the ocean.

Choices in river runoff numerical implementation are thus of large importance for ocean models skills (Sauvage et al., 2018 [5] and Tonani et al., 2019 [72]) and definitely represent a crucial and challenging issue for numerical ocean modelling developments.

This is well described in Tseng et al. (2016) ([13]), where the authors highlight how numerical river implementation choices and constraints may potentially alter the coastal mixing of freshwater and consequently the thermohaline (in particular salinity) properties at basin scale, since riverine influences can be advected from coastal areas to open ocean.

A crucial aspect in the numerical representation of the riverine outflow in ocean models mainly include the implementation of its horizontal and vertical distribution, in addition to the choice of surface freshwater boundary condition, that can lead to difficulties in correctly reproducing the coastal ocean stratification and thus the available potential energy flux Tseng et al. (2016) [13].

In particular the choice of freshwater boundary conditions is of basic importance for river runoff implementation in ocean models: the two main approaches are represented by the so-called "natural boundary condition -

NBC" (Huang, 1993 [73] and Roullet and Madec, 2000 [74]) and the so-called "virtual salt flux boundary condition - VSF" (Bryan, 1986 [75]). The formulation of both the approaches is well described in Tseng et al. (2016) [13].

The surface boundary conditions at $z = \eta$ (Beron-Vera et al., 1999 [76] and Warren, 2009 [77]) for vertical velocity and salt conservation read respectively as follows:

$$w - \vec{u} \cdot \nabla\eta - \frac{\partial \eta}{\partial t} = -q_w \tag{1.3}$$

where w (m/s) is the vertical velocity, η (m) is the sea surface height, $\vec{u}$ (m/s) is the horizontal component of velocity and q_w (m/s) is the freshwater exchange rate.

$$S\left(w - \vec{u} \cdot \nabla\eta - \frac{\partial \eta}{\partial t}\right) + F_S^V - \vec{F}_S^H \cdot \nabla\eta = -q_w S_w + Q_s \tag{1.4}$$

where $\vec{F}_S = (\vec{F}_S^H, F_S^V)$ is the diffusive salt flux $(kg\ m^{-2}\ s^{-1})$, S_w (g/kg) is the concentration of salt in the freshwater flux and Q_s $(kg\ m^{-2}\ s^{-1})$ is the net flux of salt carried to the ocean by processes different from the freshwater exchange.

The surface boundary condition for diffusive salt flux is obtained combining Equation 1.3 and Equation 1.4:

$$F_S^V - \vec{F}_S^H \cdot \nabla\eta = -q_w \left[S_w - S\left(\eta\right)\right] + Q_s \tag{1.5}$$

In the NBC case there is no salt flux through the ocean surface boundary associated to evaporation, precipitation and runoff, consequently Q_s and S_w

in Equation 1.4 are considered equal to 0. Only the mass or volume flux through the boundary is considered, so that the surface boundary condition for vertical velocity remains as in Equation 1.3, while the equation for salt conservation reads as follows:

$$S(\eta)\left(w(\eta)-\vec{u}(\eta)\cdot\nabla\eta-\frac{\partial\eta}{\partial t}\right)+F_S^V(\eta)-\vec{F}_S^H(\eta)\cdot\nabla\eta=0 \tag{1.6}$$

thus the surface boundary condition for the diffusive salt flux is given by:

$$F_S^V(\eta)-\vec{F}_S^H(\eta)\cdot\nabla\eta=q_wS(\eta) \tag{1.7}$$

In the VSF case the dilution effect of freshwater on ocean salinity is represented as a salt flux through the ocean surface boundary, while the mass or volume flux through the boundary is imposed equal to 0. This leads to a surface boundary condition for vertical velocity that reads as follows:

$$w(\eta)-\vec{u}(\eta)\cdot\nabla\eta-\frac{\partial\eta}{\partial t}=0 \tag{1.8}$$

while the equation for salt conservation is given by:

$$S(\eta)\left(w(\eta)-\vec{u}(\eta)\cdot\nabla\eta-\frac{\partial\eta}{\partial t}\right)+F_S^V(\eta)-\vec{F}_S^H(\eta)\cdot\nabla\eta=Q_s \tag{1.9}$$

The combination of Equation 1.8 and Equation 1.9 gives the surface boundary condition for the diffusive salt flux in the VSF case:

$$F_S^V(\eta)-\vec{F}_S^H(\eta)\cdot\nabla\eta=Q_s=q_wS(\eta) \tag{1.10}$$

It is thus clear that the dilution effect due freshwater is achieved in both cases, but through totally different approaches.

The choice of one approach with respect to the other implies both numerical and physical consequences, e.g. in the VSF approach the model surface layer thickness is not directly affected by the freshwater flux, since it is not included in the salinity conservation equation (Tseng et al., 2016) [13].

1.6 Aims and structure of the thesis

The aim of this study is to analyze the impact of river runoff on the thermohaline properties and on the circulation of the Mediterranean Sea at local scale, namely in the Regions Of Freshwater Influence (ROFIs) and at basin scale, by means of numerical model experiments.

Considering the ocean general circulation models' limitations in representing the flux exchange at the interface between rivers and ocean, this work aims to improve the capability of a Mediterranean Sea numerical model in reproducing the thermohaline properties of the basin through an improved representation of the riverine outflow.

The specific objectives are:

- To improve the representation of the Mediterranean Sea dynamics by means of a realistic numerical representation of the Dardanelles Strait inflow in the Mediterranean Sea model
- To design and implement a series of numerical experiments forced by different riverine inputs in the Mediterranean Sea

- To identify realistic salinity values at the river-sea interface by means of an Estuary Box Model
- To analyze the results of the numerical experiments through a comparison with available observations in order to evaluate the model skill and to highlight possible limiting factors
- To assess how the thermohaline properties and the circulation of the Mediterranean Sea are affected by different representations of the riverine input

The thesis is organized as follows:

in Chapter 2 the modelling tools used to perform the numerical experiments are presented, along with the observations used to validate and evaluate the model results. In particular the governing equations of the ocean general circulation model implemented in the Mediterranean Sea (the NEMO model) are illustrated, together with the model surface boundary conditions formulation. The setup of the Mediterranean Sea model is then described, in terms of forcings and parameterizations. Subsequently, the CMCC Estuary Box Model principles and formulations are illustrated. Finally, a description of the observational data sets used is provided.

In Chapter 3 an improved numerical implementation of the Dardanelles Strait by means of Lateral Open Boundary Conditions is described, along with the illustration of the numerical experiments performed and their evaluation with respect to in situ observations, climatological data sets and satellite data is shown, as well as the differences with respect to a river-like Dardanelles Strait implementation.

In Chapter 4 the sensitivity of the thermohaline properties and of the circulation of the Mediterranean Sea to different riverine input forcings is investigated by means of numerical experiments finalized in particular to assess the impact of:

- An increased number of river runoff sources
- A modified riverine outflow salinity and an increased mixing at the river mouths
- Different vertical mixing schemes

The results of the numerical experiments are then validated and evaluated by means of a comparison with the observational data sets available.

In Chapter 5 the CMCC Estuary Box Model implementation for the Mediterranean Sea rivers is described, along with the coupling strategy with the Mediterranean Sea circulation model. Subsequently, the results of numerical experiments performed with the coupled system are compared with respect to observations, in order to evaluate the impact on the thermohaline and dynamical properties of the Mediterranean Sea.

A summary of the performed work and the conclusions are presented in Chapter 6.

Chapter 2

Materials and methods

2.1 The NEMO ocean general circulation model

The Nucleus for European Modelling of the Ocean (NEMO) is a state-of-the-art modelling framework for research activities and forecasting services in ocean and climate sciences, developed in a sustainable way by a European consortium (`https://www.nemo-ocean.eu/`).

The ocean physical core is represented by the NEMO-OCE component (Madec et al., 2017 [78]). It is an ocean general circulation model which solves the ocean primitive equations, thus the Navier-Stokes equations along with a nonlinear equation of state which couples the two active tracers (temperature and salinity) to the fluid velocity (Madec et al., 2017 [78]) considering the following assumptions:

- The spherical earth approximation
- The thin-shell approximation

- The turbulent closure hypothesis
- The Boussinesq hypothesis
- The hydrostatic hypothesis
- The incompressibility hypothesis

The equations solved by the model are:

$$\begin{aligned}&\frac{\partial u}{\partial t} + u\frac{\partial u}{\partial x} + v\frac{\partial u}{\partial y} + w\frac{\partial u}{\partial z} = \\ &-\frac{1}{\rho_0}\frac{\partial p}{\partial x} + \frac{\partial}{\partial x}\left(A_m\frac{\partial u}{\partial x}\right) + \frac{\partial}{\partial y}\left(A_m\frac{\partial u}{\partial y}\right) + \frac{\partial}{\partial z}\left(K_m\frac{\partial u}{\partial z}\right) + fv\end{aligned} \tag{2.1}$$

$$\begin{aligned}&\frac{\partial v}{\partial t} + u\frac{\partial v}{\partial x} + v\frac{\partial v}{\partial y} + w\frac{\partial v}{\partial z} = \\ &-\frac{1}{\rho_0}\frac{\partial p}{\partial y} + \frac{\partial}{\partial x}\left(A_m\frac{\partial v}{\partial x}\right) + \frac{\partial}{\partial y}\left(A_m\frac{\partial v}{\partial y}\right) + \frac{\partial}{\partial z}\left(K_m\frac{\partial v}{\partial z}\right) - fu\end{aligned} \tag{2.2}$$

$$\frac{\partial p}{\partial z} = -\rho g \tag{2.3}$$

$$\nabla \cdot \vec{u} = 0 \tag{2.4}$$

$$\frac{\partial S}{\partial t} + \nabla \cdot (\vec{u}S) = \frac{\partial}{\partial x}\left(A_t\frac{\partial S}{\partial x}\right) + \frac{\partial}{\partial y}\left(A_t\frac{\partial S}{\partial y}\right) + \frac{\partial}{\partial z}\left(K_t\frac{\partial S}{\partial z}\right) \tag{2.5}$$

$$\frac{\partial \theta}{\partial t} + \nabla \cdot (\vec{u}\theta) = \frac{\partial}{\partial x}\left(A_t\frac{\partial \theta}{\partial x}\right) + \frac{\partial}{\partial y}\left(A_t\frac{\partial \theta}{\partial y}\right) + \frac{\partial}{\partial z}\left(K_t\frac{\partial \theta}{\partial z}\right) \tag{2.6}$$

$$\rho = \rho\,(\theta, S, p) \tag{2.7}$$

Equations 2.1 and 2.2 show the horizontal component of momentum equation, where u (m/s) and v (m/s) are the horizontal components of the velocity vector $\vec{u} = (u, v, w)$, A_m (m^2/s) and K_m (m^2/s) are the momentum eddy coefficients for horizontal and vertical mixing respectively, while fv and $-fu$ are the horizontal components of Coriolis term, being $f = 2\omega \sin\phi$ the Coriolis parameter. Lastly p (N/m^2) is pressure and ρ_0 (kg/m^3) is the reference density.

Equation 2.3 reports the vertical momentum equation under hydrostatic hypothesis, where ρ (kg/m^3) is the in situ density.

Equation 2.4 is the continuity equation under Boussinesq and incompressibility hypotheses

Equations 2.5 and 2.6 show the advection/diffusion equations for salinity (S) and potential temperature (θ) respectively (with salinity expressed in PSU and potential temperature expressed in °C), where A_t (m^2/s) and K_t (m^2/s) are the tracers' horizontal and vertical mixing coefficients respectively, $\nabla \cdot (\vec{u}S)$ and $\nabla \cdot (\vec{u}\theta)$ represent the advection terms and the LHS of the equations represents the diffusion term.

Lastly, Equation 2.7 defines the in situ density as a function of the potential temperature relative to the surface, salinity and pressure, according to Jackett and McDougall (1995) [79].

2.1.1 Surface boundary conditions

Here an introduction to the concept and the formulation of the surface boundary conditions (SBCs) is provided, since in the present study the numerical implementation of the river runoff is achieved by means of a SBC and it directly affects the surface boundary conditions for salinity and vertical velocity.

Surface boundary conditions describe the air-sea interactions (and also the interaction of sea-ice with ocean, which will not be taken into account in the present work), in terms of momentum, heat and salt fluxes and vertical velocity.

The ocean numerical component thus needs to receive external information in order to compute the surface fluxes, such as: the wind stress, the incoming solar and non solar heat fluxes, the surface freshwater budget and in case of sea-ice presence also the salt flux associated with freezing/melting of seawater (Madec et al., 2017 [78]).

An additional information that can be provided to the ocean numerical component is the atmospheric pressure at the ocean surface, which is shown to have significant effects on the sea level structure and on the circulation for the Mediterranean Sea (Oddo et al., 2014 [80]).

Surface forcings can be provided to the NEMO ocean component through one of the following options:

- An analytical formulation
- A flux formulation
- A bulk formulae formulation

- A coupled formulation
- A mixed forced/coupled formulation

Specific bulk formulae for the Mediterranean Sea setup (Castellari et al., 1998 [81], Oddo et al., 2009 [82] and Pettenuzzo et al., 2010 [83]), are adopted in the numerical model of the Mediterranean Sea used in the present work (described in details in the next section).

The wind stress (N/m^2) components are computed as:

$$\tau_x = \rho_{air} C_d |U_r|\, u_r \qquad \tau_y = \rho_{air} C_d |U_r|\, v_r \tag{2.8}$$

where ρ_{air} (kg/m^3) is the density of the moist air, u_r (m/s) and v_r (m/s) are the x and y components of the relative wind velocity, computed as the difference between wind velocity at 10 m and sea surface currents velocity in both x and y direction, $|U_r|$ (m/s) is the relative wind speed computed as $|U_r| = \sqrt{u_r^2 + v_r^2}$. C_d is the drag coefficient and it is computed following Hellerman and Rosenstein (1983) [84].

The momentum boundary condition at the surface η is given by:

$$\rho_0 K_m \frac{\partial\,(u,v)}{\partial z}|_{z=\eta} = \left(\tau_x, \tau_y\right) \tag{2.9}$$

The heat flux boundary condition at the surface is given by:

$$K_t \frac{\partial \theta}{\partial z}|_{z=\eta} = \frac{Q}{C_p \rho_0} + \theta_{pw} P + \theta_{rw} R \tag{2.10}$$

where θ_{pw} (°C) is the precipitation P temperature (equal to the sea surface temperature), and θ_{rw} (°C) is the temperature of the river runoff R (that can be equal to the sea surface temperature or prescribed); C_p ($J/(Kkg)$) is

the specific heat capacity and Q (W/m^2) is the heat exchanged with the atmosphere and is given by:

$$Q = Q_s - Q_l - Q_h - Q_e \tag{2.11}$$

where Q_s is the solar short-wave radiation computed following Reed (1977) [85], Q_l is the long-wave radiation computed following Bignami et al., (1995) [86], Q_h and Q_e are the sensible and the latent heat fluxes, computed following Kondo (1975) [87].

The salinity boundary condition at the surface can be expressed in the following form:

$$K_t \frac{\partial S}{\partial z} \Big|_{z=\eta} = (E - P - \frac{R}{A})S(\eta) + \frac{R}{A}S_{river} \tag{2.12}$$

where $S(\eta)$ (PSU) is the ocean surface salinity, S_{river} (PSU) is the prescribed salinity associated at the river runoff, E (m/s) is the evaporation rate (whose salinity is assumed to be equal to 0 PSU), P (m/s) is the precipitation rate (whose salinity is assumed to be equal to 0 PSU) and $\frac{R}{A}$ (m/s) is the river discharge divided by the area of the ocean model cell where the river runoff source is implemented.

Finally, the surface boundary condition for the vertical velocity is given by:

$$w \Big|_{z=\eta} = \frac{\partial \eta}{\partial t} + \vec{u}_h \Big|_{z=\eta} \cdot \nabla_h \eta + (E - P - \frac{R}{A}) \tag{2.13}$$

where η (m) is the sea surface elevation and $\vec{u}_h$ (m/s) is the horizontal velocity.

2.1.2 Numerical options for river runoff implementation

The freshwater sources numerical implementation requires information on the volume flux of the riverine source, as well as its salinity and temperature. If salinity and temperature values are not specified, a constant 0 PSU salinity and the Sea Surface Temperature (SST) of the grid point (or points) where the riverine source is implemented are associated to the river inflow.

River's temperature and salinity variables are then multiplied by the amount of runoff (converted into m/s) in order to retrieve the heat and salt content of the river inflow.

The river runoff can be also implemented through a non-zero depth along the vertical direction from the surface to a maximum depth which represents the lower bound of the river runoff.

The mass/volume addition due to the river runoff is added to the horizontal divergence of the currents and this induces a water mass transfer, equal to the amount of runoff, into the grid cell above (Madec et al., 2017 [78]).

At this stage, this water mass transfer does not include the heat and salt content of runoff and thus a dilution effect is generated, since ocean water at a certain temperature and salinity is replaced by the same volume of river water, without a corresponding contribution of heat and salt (Madec et al., 2017 [78]).

The dilution effect due to runoff water addition into the system is achieved in two different ways depending on the free surface formulation adopted (Roullet and Madec, 2000 [74] and Madec et al., 2017 [78]):

1. In the linear free surface case in order to balance the amount of water added through the river runoff ensuring the volume conservation, a flux of water with the same volume of the runoff is conveyed out of the domain through the sea surface, along with the associated salt and heat flux, generating a dilution effect.

2. In the non-linear free surface case (used in the present work) there is no flux of water, heat and salt through the sea surface out of the domain: water mass due to runoff is added in the top cell without any associated addition of heat and salt, determining a dilution effect in the top cell and in the cells below, through the movement of water from the cells below towards the top cell.

In both linear and non-linear free surface cases, heat and salt content associated to river runoff are then added in the form of temperature and salinity increase.

It should be stressed that in the non-linear free surface case, near the end of the computational time step, the variation of sea surface height due to the additional water introduced through river runoff is distributed along the water column.

2.1.3 The Mediterranean Sea numerical model

A regional configuration of the NEMO model is used in this study to analyze the riverine influences in the Mediterranean Sea.

The model horizontal grid resolution is 1/24° (4.5 km, approximately) and it is resolved over 141 unevenly spaced z vertical levels with partial steps

(Clementi et al., 2017 [89]).

The computational domain covers the entire Mediterranean Sea, extending also into the Atlantic Ocean in order to better resolve the exchanges through the Strait of Gibraltar.

The model bathymetry is created starting from the GEBCO_2014 Grid (version 20150318, `www.gebco.net`) with a horizontal resolution of 30 arc-seconds. A smoothing is performed using a Shapiro filter (Shapiro, 1975 [90]) several times and then the obtained bathymetry is interpolated to the model grid.

The time-splitting technique is used to solve the primitive equations, in order to solve the free surface equation and the associated barotropic velocity equations with time step smaller than the internal mode time step, equivalent to the model time step (Madec et al., 2017 [78]). The model time step is set equal to 240 s, while the number of iterations of the barotropic mode during one model time step is set equal to 100.

A non-linear free surface formulation is adopted, with time-varying vertical z-star coordinates.

The vector form formulation for the momentum advection is used, while for tracers a mixed upstream-MUSCL (Monotonic Upwind Scheme for Conservation Laws, Van Leer, 1979 [91]) is adopted. The more diffusive upstream scheme is adopted near the lateral open boundaries in the Atlantic Ocean and in correspondence of the river mouths.

The vertical eddy diffusivity and viscosity coefficients are computed through a local Richardson number dependent formulation (Pacanowski and Philander, 1981 [92]).

The value of the vertical background diffusivity and viscosity coefficients are set equal to $10^{-7}\ m^2/s$ and $1.2 \cdot 10^{-6}\ m^2/s$ respectively, while the horizontal bilaplacian eddy diffusivity and viscosity are set equal to $-1.2 \cdot 10^8\ m^4/s$ and $-2 \cdot 10^8\ m^4/s$ respectively.

The temperature and salinity fields used to initialize the numerical experiments are derived from the World Ocean Atlas 2013 version 2 (WOA13 V2) winter climatologies at 1/4°, with time span 2005-2012 and vertical coverage 0-5500 m (Locarnini et al., 2013 [93] for temperature, Zweng et al., 2013 [94] for salinity).

As already mentioned, the air-sea fluxes of momentum, mass, and heat are computed through bulk formulae specifically designed for the Mediterranean Sea.

The atmospheric forcings used in the experiments described in Chapter 3 are the 6-hours 1/8° operational analyses from the European Centre for Medium-Range Weather Forecasts (ECMWF), while for the further experiments described in Chapters 4 and 5 the 6-hours ERA5 reanalysis fields at 1/4° are used (ERA5: Fifth generation of ECMWF atmospheric reanalyses of the global climate, Copernicus Climate Change Service Climate Data Store (CDS), `https://cds.climate.copernicus.eu/cdsapp#!/home`).

The Mediterranean Sea model is nested into the CMEMS global system GLO-MFC (Global Monitoring and Forecasting Centre - CMEMS Copernicus Marine Environment Monitoring Service) which has a 1/12° horizontal resolution and 50 vertical levels, and provides daily temperature, salinity, sea surface height and velocity fields to the Mediterranean Sea model through two different products: for the set of experiments described in Chapter 3 the

analysis product is used (GLOBAL_ANALYSIS_FORECAST_PHY_001_024 , E.U. Copernicus Marine Service Information), while for the further experiments described in Chapters 4 and 5 the reanalysis product is used (GLOBAL_REANALYSIS_PHY_001_030 , E.U. Copernicus Marine Service Information).

2.2 The CMCC Estuary Box Model

2.2.1 Estuary box modelling: an overview

The resolution of the Mediterranean Sea ocean model does not allow to properly reproduce the complex estuarine dynamics which generate at the interface between the river outlets and the ocean.

In nature estuaries strongly modify the river freshwater before it is discharged into the ocean (Sun et al., 2017 [14]), through several different mechanisms, such as tides and winds that generate a shear-driven mixing and internal wave breaking that convey salt ocean water into the estuary (Dyer, 1997 [95]). The mixing and the entrainment of ocean salty water triggers an estuarine exchange circulation that cannot be resolved by the current resolution of the regional (and even less global) ocean circulation models.

Thus, due to the mechanisms widely described in Section 1.2 and summarized here, the riverine discharge into the ocean should be characterized by a salinity larger than 0 PSU, even though prescribing zero salinity for riverine outflow is still a quite common practice, in particular in Earth system models (Sun et al., 2017 [14]).

This is the reason why the estuary box modelling approach, consisting in

creating an additional numerical interface between the river inputs and the ocean models, is showing a growing interest and has been subject of several studies in the recent past.

A first implementation of an estuary box model is performed by Garvine and Whitney (2006) [96], who based their formulation on the potential anomaly concept theorized by Simpson et al. (1990) [28], using the Delaware Bay as a test case. The two-layers formulation, adopted in several further studies, is introduced by Rice et al. (2008) [97] in the box model proposed by Garvine and Whitney (2006) [96].

Hordoir et al. (2008) [98] have implemented into the NEMO model a shelf box model based on the Simpson et al. (1990) [28] concept, that reproduced the coastal overturning on the Mekong river shelf in different wind regimes.

Herzfeld (2015) [99] has introduced a numerical method targeted to highly stratified estuaries with weak tides and/or strong river discharge, that considers salt wedge adjustment in the estuarine gravitational circulation.

A very recent study by Sun et al. (2017) [14], describes the development of an estuary box model which parameterizes the mixing processes in estuaries, adopting the Columbia river as test case and, in addition, implementing the developed estuary box model for representing the river runoff input into the Community Earth System Model (CESM) in order to assess its impact on a general circulation model.

Here we use the recent formulation of the Estuary Box Model by Verri et al. (2019) [88], thereafter called the CMCC EBM.

2.2.2 CMCC EBM: description and governing equations

A new Estuary Box Model (CMCC EBM) is described in Verri et al. (2019) [88] and here a brief illustration of its formulation and governing equations is provided.

In the model the river estuary is geometrically represented as a two-layers (denoted as upper layer and lower layer) rectangular box with constant length L_x, width L_y and depth H (see Figure 2.1). The two layers have the same thickness, being the upper layer associated to the river inflowing toward the ocean and the lower layer representing the ocean contribution to the estuary. The x-axis originates at the mouth of the EBM and it is positive towards the ocean while the z-axis is defined positive upward from the bottom.

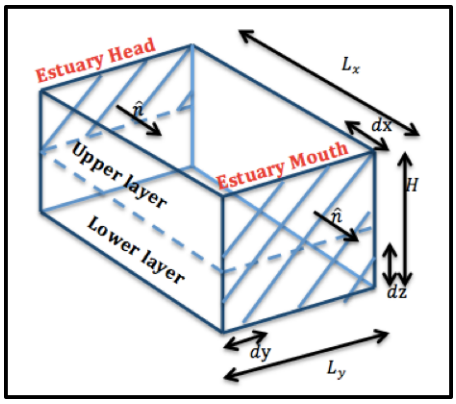

Figure 2.1: Diagrammatic representation of the CMCC EBM geometry. Reproduced from Verri et al. (2019) [88].

L_x (m) represents the estuary length, i.e. the distance between the estuary head where the salinity has a value of 0 PSU and the river outlet. L_y (m)

represents the width of the river estuary or of the river delta, depending on the river outlet geometry. H (m) represents the depth of the river at its outlet.

The tidal contribution is added to both volume and salt flux equations: the entire tidal cycle (flood and ebb phases) is considered and approximated to the solar day. Heat flux, precipitation and wind stress are not considered in the CMCC EBM formulation, as well as the temperature effects.

The model governing equations are thus the following:

$$Q_{ul}^{ebm} = Q_{river} + Q_{ll}^{ocean} + HL_y u_{tidef} \tag{2.14}$$

$$S_{ul}^{ebm} Q_{ul}^{ebm} = S_{ll}^{ocean} Q_{ll}^{ocean} + \overline{S}_{ocean} HL_y u_{tidef} + K_{S_H} HL_y \frac{\overline{S}_{ocean}}{L_x} \tag{2.15}$$

where Q_{ul}^{ebm} (m^3/s) and S_{ul}^{ebm} (PSU) represent the output variables computed by the CMCC EBM, i.e. the volume flux and the associated salinity outflowing from the upper layer of the box.

The input variables provided to the CMCC EBM are: Q_{river} (m^3/s), which is the river volume flux at the estuary head, Q_{ll}^{ocean} (m^3/s) and S_{ll}^{ocean} (PSU), respectively the volume flux and the salinity inflow from the box lower layer, while $\overline{S}_{ocean}$ (PSU) is the depth averaged ocean salinity at the estuary mouth: normal velocities landward oriented are provided by daily outputs of an ocean model in order to compute Q_{ll}^{ocean}, as well as S_{ll}^{ocean} and $\overline{S}_{ocean}$.

The tidal velocity during the flood phase u_{tidef} (m/s), is provided to the CMCC EBM by daily averaged landward oriented velocities computed by a tidal model.

Given that the x-axis is positive towards the ocean, as indicated in the geometrical description of the EBM, it has to be noticed that in Equation 2.14 the volume flux inflow from the box lower layer Q_{ll}^{ocean} directed from the estuary-ocean interface towards the estuary head has opposite direction with respect to Q_{ul}^{ebm}.

The tidal velocity during the flood phase u_{tidef} (m/s), is provided to the CMCC EBM by daily averaged landward oriented velocities computed by a tidal model.

The ebb tidal flow is included in the estuarine outflowing volume flux through the upper layer of the box Q_{ul}^{ebm}. Finally, K_{S_H} (m^2/s) represents the horizontal mixing coefficient and it is computed as $K_{S_H} = 0.035\, L_y\, u_{tidef}$, according to Banas et al. (2004) [100].

In conclusion, once Q_{ul}^{ebm} and S_{ul}^{ebm} are evaluated by the CMCC EBM, they are provided to the ocean model and used in the salinity and in the vertical velocity surface boundary conditions.

2.3 Data sets for validation

In order to validate and evaluate the numerical results provided in this study, different observational data sets are considered, including in situ data, satellite data and temperature and salinity climatologies.

The specifics for the different data sets, along with the ocean parameters provided by each of them are listed in Table 2.1.

The in situ data from Argo floats (free-drifting profiling floats, `http://www.argo.ucsd.edu/`), gliders (underwater vehicles used for measuring

oceanographic parameters which move through the water column by changing their buoyancy) and XBTs (Expendable BathyThermographs, probes that are launched from a ship falling down through the water column at a known rate) are derived from the CMEMS In Situ Thematic Assembly Centre (INS-TAC), which integrates near real-time in situ observational data, quality controlled using automated procedures, distributed in a standard format (E.U. Copernicus Marine Service Information, `http://marine.copernicus.eu/`).

The corresponding product is INSITU_MED_NRT_OBSERVATIONS_013_035.

The Sea Surface Temperature (SST) data set consists of daily (night-time) optimally interpolated satellite gridded estimates of the foundation SST over the Mediterranean Sea, provided with a spatial resolution of 1/24° corresponding approximately to 4.5 km by the CMEMS SST-TAC (Nardelli et al., 2013 [101] and Pisano et al., 2016 [102]).

The corresponding product is SST_MED_SST_L4_REP_OBSERVATIONS_010_021.

The Sea Level Anomaly (SLA) L3 data are derived from the CMEMS Sea Level Thematic Assembly Centre (SL-TAC) and consist of Sea Level Anomaly along-track observations from altimeters with respect to a reference ellipsoid. The SLA is then computed as the sea surface height over a mean dynamic topography, estimated over the period 1993-2012.

The corresponding product is SEALEVEL_MED_PHY_L3_REP_OBSERVATIONS_008_049.

The horizontal resolution of the observations is 14 km and the filtered product has been used. Data from several satellites covering different periods are retrieved, such as Altika, Cryosat-2, ENVISAT Extension Phase, Envisat, Geosat Follow On, Haiyang-2A, Jason-1 Geodetic Phase, Jason-1 Interleaved, Jason-1 and OSTM/Jason-2.

In addition to along-track observations, also SLA gridded satellite L4 data have been used (SEALEVEL_MED_PHY_L4_REP_OBSERVATIONS_008_051), obtained merging the measurement from the different altimeter missions available and using optimal interpolation techniques to obtain the final product, which has an horizontal resolution of 1/8°.

Temperature and salinity climatologies are derived from two different products: SEADATANET_MedSea_climatology_V1.1_public (SeaDataNet Pan-European infrastructure for ocean and marine data management: `https://www.seadatanet.org`) and World Ocean Atlas 2013 version 2 (WOA13 V2, Locarnini et al., 2013) [93] for temperature, Zweng et al., 2013 [94] for salinity).

The SEADATANET_MedSea_climatology_V1.1_public product (hereafter SDN) is built on the basis of SeaDataNet V1.1 aggregated data set, a quality-checked collection of all temperature and salinity measurements contained within the SeaDataNet database.

SDN climatologies are monthly climatological fields of temperature and salinity with an horizontal resolution of 1/8° and 33 vertical levels from the sea surface down to 5500 m depth. The temporal extent covers the period 1900-2013.

The data retrieved from World Ocean Atlas 2013 version 2 (WOA13 V2) product, hereafter WOA, are a set of objectively analyzed climatological fields of in situ temperature and salinity.

WOA climatologies are available as monthly fields, seasonal fields or decadal fields: in order to be as closest as possible to the period chosen for the numerical experiments described in the next sections, the available 2005-2012 period is extracted from the data set (woa13_A5B2 product).

The horizontal resolution of the chosen data set is 1/4°, standard depth levels are 102 for decadal and seasonal climatologies, with a vertical extension from the surface down to 5500 m, while vertical levels are 57 for monthly climatologies, from sea surface down to 1500 m depth.

The Houpert et al. (2015) [103] Mixed Layer Depth (MLD) monthly gridded climatologies at 1/4° horizontal resolution for the Mediterranean Sea are also used. The MLD climatologies are produced using data collected over the period 1969-2013 from XBTs, MBTs (Mechanical BathyThermographs), profiling floats, gliders and CTD (Conductivity, Temperature, and Depth probes).

Table 2.1: Data sets used for the validation and the evaluation of numerical experiments results.

Ocean parameter	**Instrument**	**Reference data set**	**Description**
Salinity	Argo floats	INSITU_MED_NRT_OBSERVATIONS_013_035	vertical profiles of salinity
Salinity	Gliders	INSITU_MED_NRT_OBSERVATIONS_013_035	vertical profiles of salinity
Salinity	SDN climatology	SEADATANET_MedSea_climatology_V1.1_public	salinity gridded climatology
Salinity	WOA climatology	woa13_A5B2	salinity gridded climatology
Temperature	Argo floats	INSITU_MED_NRT_OBSERVATIONS_013_035	vertical profiles of temperature
Temperature	Gliders	INSITU_MED_NRT_OBSERVATIONS_013_035	vertical profiles of temperature
Temperature	XBTs	INSITU_MED_NRT_OBSERVATIONS_013_035	vertical profiles of temperature
Temperature	SDN climatology	SEADATANET_MedSea_climatology_V1.1_public	temperature gridded climatology
Temperature	WOA climatology	woa13_A5B2	temperature gridded climatology
Sea Surface Temperature	Satellite	SST_MED_SST_L4_REP_OBSERVATIONS_010_021	satellite SST data
Sea Level Anomaly	Satellite	SEALEVEL_MED_PHY_L3_REP_OBSERVATIONS_008_049	satellite SLA along track data
Sea Level Anomaly	Satellite	SEALEVEL_MED_PHY_L4_REP_OBSERVATIONS_008_051	satellite SLA gridded data
Mixed Layer Depth	Climatology	Houpert et al. (2015)	MLD gridded climatology

Chapter 3

Influence of the Dardanelles Strait inflow on the Mediterranean Sea

This chapter presents a novel implementation of the Dardanelles Strait, a narrow strait connecting the Mediterranean Sea and the Black Sea through the Marmara Sea.

Low-salinity waters flow from the Black Sea to the Aegean Sea through the Marmara Sea, while high-salinity water originated in the Mediterranean Sea flow in the opposite direction.

A two-layer flow driven mainly by density differences is generated, with Black Sea waters flowing in the upper layer of the strait and Mediterranean Sea waters in the lower layer (Jarosz et al., 2012 [104]).

The improvement brought the implementation of the Dardanelles Strait from a Surface Boundary Condition (SBC), whose concept and formulation

has been discussed in the previous chapter, to a Lateral Open Boundary Condition (LOBC).

As already mentioned, surface boundary conditions describe the air-sea interactions and the interactions of sea-ice with ocean, in terms of momentum, heat and salt fluxes and vertical velocity.

The main purpose of Lateral Open Boundary Conditions, according to Røed and Cooper (1986) [105], is to allow the perturbations generated inside the computational domain to leave it without deterioration of the inner model solution, however it is in some cases of equivalent importance to let the external information to be conveyed inwards in order to improve the inner solution of the computational domain (Marchesiello et al., 2001 [106]).

This is a typical issue of regional modelling both for the atmosphere and the ocean, that need an adequate representation of the influence of the dynamical processes occurring outside the modelled domain in order to improve the inner domain numerical solution and better resolve the regional dynamics (Oddo and Pinardi, 2008 [107]).

3.1 Experimental design

In the Dardanelles Strait SBC implementation, monthly climatological values of salinity and volume flux derived from Kourafalou and Barbopoulos (2003, Table 2)[54] are prescribed for three NEMO grid points at the outlet of Dardanelles Strait, while in the LOBC implementation salinity, temperature, volume flux and sea surface height are provided through numerical models solving the Marmara Sea dynamics.

In the present study two models are selected to force the Mediterranean Sea modelling system at the Dardanelles Strait: the CMEMS GLO-MFC system (Global Ocean Monitoring and Forecasting Center, GLO-MFC, in the framework of the Copernicus Marine Service, CMEMS, `http://marine.copernicus.eu/`, Copernicus Marine Product: GLOBAL ANALYSIS FORECAST PHY 001 024) and a Turkish Straits System (TSS) box model (Maderich et al., 2015 [108]).

It should be noticed that the land/sea mask in the area of the Dardanelles Strait is slightly modified in order to better represent the geometrical shape of the strait: in the LOBC implementation the strait outlet is represented by three NEMO grid points, as well as in the SBC implementation, but eastward shifted of one grid point. Additionally the northern grid point is converted from sea to land in order to better mimic the channel-shaped geometry of the Dardanelles Strait outlet (see Figure).

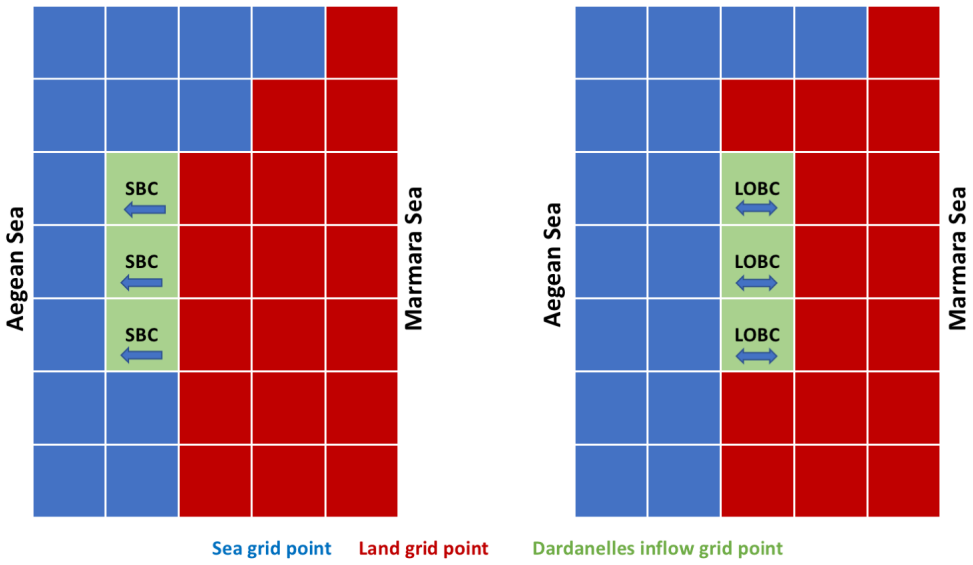

Figure 3.1: Schematic representation of the Dardanelles Strait geometrical implementation: sea grid points are represented in blue, land grid points in red and grid points for boundary conditions implementation in green.

Two different bathymetries are assigned and tested in the Dardanelles Strait section:

1. One derived from the CMEMS GLO-MFC system section used as data source, hereafter Bathy_DRD_v1

2. A flat bathymetry is created using the deepest value in Bathy_DRD_v1, hereafter Bathy_DRD_v2

A 2-year control experiment (hereafter simu_ctrl) is performed using the SBC implementation of the Dardanelles Strait, with a numerical integration covering the period 2016-2017.

Several numerical experiments are then performed in order to find the optimal setup for the LOBC implementation of the Dardanelles Strait, in terms of both representation of the thermohaline properties in the Aegean Sea and representation of the water volume flux components through the strait.

A summary of the experimental design for the LOBC implementation of the Dardanelles Strait is available in Table 3.1.

As summarized in Table 3.1, in experiment simdd_v1 the bathymetry used is Bathy_DRD_v2, previously described, while the barotropic and baroclinic components of the velocity are derived from the water volume flux daily climatologies computed by the Turkish Straits System (TSS) box model described in Maderich et al. (2015) [108], for both the components of the transport through the strait, i.e. from Marmara Sea to Mediterranean Sea and vice versa. Sea surface height, temperature and salinity provided to the Mediterranean Sea model as Lateral Open Boundary Conditions are retrieved from the CMEMS GLO-MFC system section included in the yellow box in Figure 3.2 and temperature and salinity fields are vertically interpolated from the vertical GLO-MFC system grid onto the Mediterranean Sea model vertical grid. It has to be highlighted that, as noticeable from Figure 3.2, the GLO-MFC system horizontal resolution (1/12°) does not allow to clearly geographically identify the Dardanelles Strait outlet in its domain. For this reason, the dynamical and thermohaline properties of different sections from the GLO-MFC system domain have been investigated and compared with literature, choosing the one that better represents the physical properties of the Dardanelles Strait outlet. The numerical schemes applied at the Dard-

anelles Strait LOBC are the Flather (1976) [109] radiation scheme for the barotropic component of the velocity and the Orlanski radiation condition with adaptative nudging (Marchesiello et al., 2001 [106]) for the baroclinic component of the velocity and the tracers.

The Flather (1976) lateral boundary condition equation gives the normal barotropic velocity component at the open boundary V^n_{BTm} (m/s):

$$V^n_{BTm} = V^n_{BTe} - \frac{\sqrt{gH}}{H}(\eta_e - \eta_m) \tag{3.1}$$

where V^n_{BTe} (m/s) is the normal barotropic velocity component of the external model (the TSS box model for this experiment) provided to the Mediterranean Sea model, η_e (m) is the external model (the CMEMS GLO-MFC system for this experiment) surface elevation provided to the Mediterranean Sea model and η_m (m) is the Mediterranean Sea model surface elevation at the boundary. $\sqrt{gH}$ (m/s) is the speed of external gravity waves, while H (m) denotes the water depth.

The radiation condition scheme developed in Orlanski (1976) [110] reads as follows:

$$C = -\frac{\partial \phi}{\partial t}\left(\frac{\partial \phi}{\partial n}\right)^{-1} \tag{3.2}$$

where C (m/s) is the phase speed of the waves that represent the propagation through the open boundary of the interior solutions, ϕ is a generic prognostic model variable and $\frac{\partial}{\partial n}$ denotes the normal derivative to the open boundary.

This scheme has been subsequently modified in Marchesiello et al. (2001) [106] in order to take into account a selective treatment of inward and outward

fluxes varying in time, so that the scheme proposed reads as follows:

$$\frac{\partial \phi}{\partial t} + C_x \frac{\partial \phi}{\partial x} + C_y \frac{\partial \phi}{\partial y} = -\frac{1}{\tau}\left(\phi - \phi_e\right) \tag{3.3}$$

where C_x (m/s) is the phase speed normal to the boundary, C_y (m/s) is the phase speed tangential to the boundary, ϕ is a prognostic variable for the interior solution and ϕ_e denotes external information provided at the open boundary. Finally, τ (s) represents the time scale of the nudging term, which defines the radiation/relaxation frequency for the inflow/outflow regimes. For experiment simdd_v1, and for all the further performed experiments, the nudging time scale is set equal to one day, both for inflow and outflow regime.

The phase speeds C_x and C_y at the boundary can be computed as follows:

$$C_x = -\frac{\partial \phi}{\partial t} \frac{\partial \phi / \partial x}{\left(\partial \phi / \partial x\right)^2 + \left(\partial \phi / \partial y\right)^2} \tag{3.4}$$

$$C_y = -\frac{\partial \phi}{\partial t} \frac{\partial \phi / \partial y}{\left(\partial \phi / \partial x\right)^2 + \left(\partial \phi / \partial y\right)^2} \tag{3.5}$$

In experiment simdd_v1, as well as for the all the further experiments performed, the Normal Projection of Oblique radiation case (NPO) has been chosen for the Orlanski radiation condition with adaptative nudging (referred to as Orlanski_npo in Table 3.1): in this case the normal phase speed is calculated as the normal projection of the oblique phase speed, while the tangential phase speed is neglected (Marchesiello et al., 2001 [106]).

In simdd_v2 experiment the bathymetry used is Bathy_DRD_v1, and all the fields provided to the Mediterranean Sea model are derived from the CMEMS GLO-MFC. The net volume flux through the strait is corrected to

Tuğrul et al. (2002) [111] seasonal net fluxes. The numerical schemes applied to the Dadanelles Strait LOBC are the same applied in simdd_v1.

For all the further experiments performed the Bathy_DRD_v2 batyhmetry has been used.

In simdd_v3 experiment temperature and salinity are provided to the Mediterranean Sea model from the CMEMS GLO-MFC system, while the barotropic and baroclinic components of the velocity are derived from the water volume flux daily climatologies computed by the TSS box model. In order to better fit the observational results in Jarosz et al. (2012)[104] the total zonal velocity in the upper layer of the Dardanelles Strait is unevenly distributed among the three Dardanelles Strait model grid points, with the 60% of the total velocity assigned to the central and the remaining 40% equally subdivided between the two external grid points.

In addition to this, in order to better reproduce the outflow velocity profile from the Dardanelles Strait shown in Jarosz et al. (2012) [104] the zonal velocity profile in the upper layer has been opportunely modulated in the upper layer, but conserving the volume transport provided by the TSS box model daily climatologies.

According to Jarosz et al. (2012) [104] the Dardanelles Strait upper layer thickness is set equal to 13 m. The numerical scheme applied at the Dardanelles Strait LOBC is the Orlanski radiation condition with adaptative nudging both for velocity (barotropic and baroclinic components) and tracers.

simdd_v4 follows simdd_v3 but using a novel setup for salinity fields: in the upper layer (from surface down to 13 m) daily salinity climatologies com-

puted by the TSS box model are provided to the Mediterranean Sea model as outflow salinity from the Dardanelles Strait while, since the salinity of the lower layer is not computed by the TSS model, a constant value of 38.6 PSU is set in order to represent the salinity of the outflow from the Mediterranean Sea towards the Marmara Sea, taking into account the mixing between the upper layer and the lower layer (Beşiktepe et al., 1994 [112] and Özsoy and Ünlüata, 1997 [113]). For the barotropic and baroclinic components of the velocity the numerical scheme used for the Dardanelles Strait LOBC is Orlanski radiation condition with adaptative nudging, while temperature and salinity are directly specified.

The setup for experiment simdd_v5 is the same as for simdd_v4, with an additional enhanced vertical diffusivity for tracers in a 3x3 grid points box in front of Dardanelles Strait outlet. The multiplicative factor for enhanced vertical diffusivity coefficient is set equal to 5000, from the surface level down to the level 15 (corresponding to about 46 m depth) of the vertical NEMO model grid.

The numerical experiments performed cover the period 2016-2017.

To better analyze the salinity skill differences, a check on the two input salinity data sets used in this study is provided. Figure 3.3 shows the daily mean salinity time series evaluated from the upper layer of the GLO-MFC selected section.

The depth of the upper layer is evaluated considering the average zonal velocity over the period 2016-2017 at the GLO-MFC section that provides daily fields to the Mediterranean Sea in simdd_v2 experiment (Figure 3.4), the interface depth between the upper layer (flow from the Marmara Sea to

the Mediterranean Sea) and the lower layer (flow from the Mediterranean Sea to the Marmara Sea) is noticeable at level 11 of the GLO-MFC system corresponding to 18.5 m.

It can be noticed that the TSS box model daily mean salinity values are much lower with respect to the daily mean outflow salinity from the GLO-MFC section, and in better agreement with literature values (29.29 PSU reported in Beşiktepe et al., 1994 [112] and 28.96 PSU in Özsoy and Ünlüata, 1997 [113]), with an average annual value of 29.07 PSU.

The average annual value of outflow salinity from the Aegean end of the Dardanelles Strait for the considered GLO-MFC section has instead a higher value of 30.90 PSU, which is too high with respect to the above-mentioned literature values.

Table 3.1: Summary of experimental design for the LOBC implementation of the Dardanelles Strait. T denotes temperature, S denotes salinity, BT denotes the barotropic component of velocity, BC denotes the baroclinic component of velocity, TR denotes the tracers, UL denotes upper layer, LL denotes lower layer.

EXP NAME	**BATHYMETRY**	**VELOCITIES SOURCE**	**SSH SOURCE**	**TRACERS SOURCE**	**NUMERICAL SCHEMES**
simdd_v1	Bathy_DRD_v2	TSS box	GLO-MFC	GLO-MFC for T and S	BT: Flather BC: Orlanski_npo TR: Orlanski_npo
simdd_v2	Bathy_DRD_v1	GLO-MFC	GLO-MFC	GLO-MFC for T and S	BT: Flather BC: Orlanski_npo TR: Orlanski_npo
simdd_v3	Bathy_DRD_v2	TSS box	-	GLO-MFC for T and S	BT: Orlanski_npo BC: Orlanski_npo TR: Orlanski_npo
simdd_v4	Bathy_DRD_v2	TSS box	-	GLO-MFC for T for S: UL: TSS box LL: 38.6 PSU	BT: Orlanski_npo BC: Orlanski_npo TR: Specified
simdd_v5	Bathy_DRD_v2	TSS box	-	GLO-MFC for T for S: UL: TSS box LL: 38.6 PSU	BT: Orlanski_npo BC: Orlanski_npo TR: Specified Enhanced vert. diff.

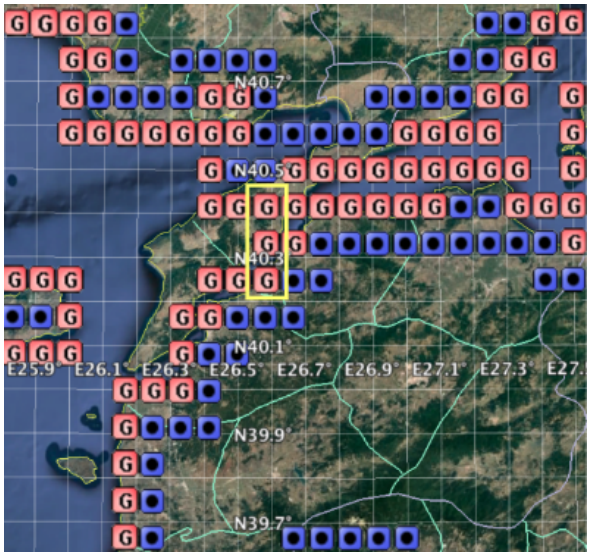

Figure 3.2: Horizontal representation of the CMEMS GLO-MFC coastline (blue squares) and closest sea grid points (red squares) in the Dardanelles area. The selected section providing the open boundary fields is represented by the yellow box.

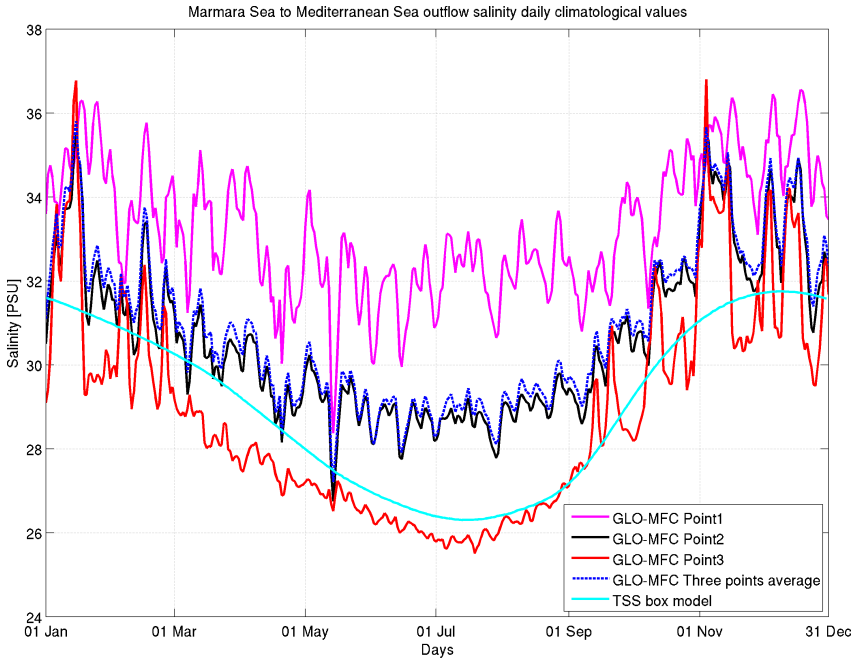

Figure 3.3: Marmara Sea to Mediterranean Sea outflow salinity daily climatological values.

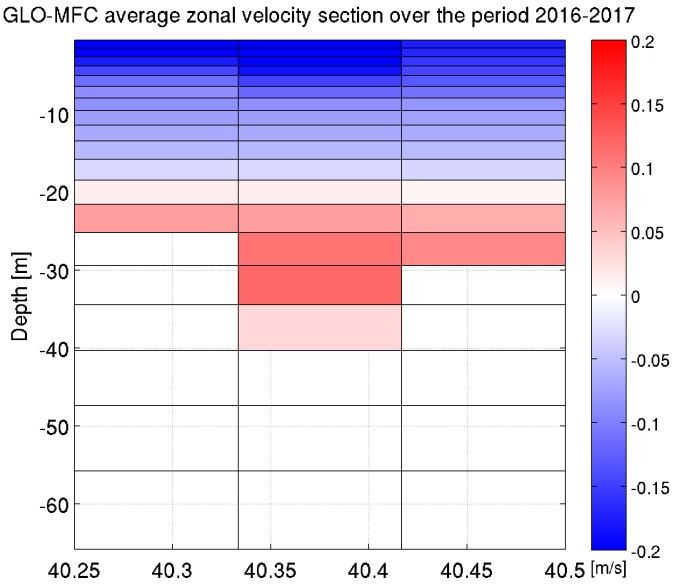

Figure 3.4: GLO-MFC average zonal velocity section over the period 2016-2017.

3.2 Evaluation and validation of experimental results

3.2.1 Water volume transport

A crucial aspect in the dynamics of the Dardanelles Strait in the novel LOBC implementation is to correctly represent the water volume transport at the interface between the strait outlet and the Aegean Sea in its three components, i.e. the Marmara Sea to Mediterranean Sea transport, the Mediterranean Sea to Marmara Sea transport and the net transport be-

tween the aforementioned two components, computed as the sum of the two components.

The annual averaged transport components computed over the simulation period are compared to literature values (Table 3.2).

The experiment showing the farthest transport values with respect to the considered literature sources is simdd_v1, where the transport from the Marmara Sea towards the Mediterranean Sea shows higher values with respect to the transport from the Mediterranean Sea to the Marmara Sea, thus resulting in a positive net transport that is in disagreement with all the considered studies.

The experiment simdd_v2 strongly underestimates both the components of the transport trough the strait, with a net transport largely smaller with respect to literature estimates.

The net transport in experiment simdd_v3 is in very good agreement with the considered literature values, but the other two components of the transport are underestimated.

Finally, simdd_v5 shows the best performances in reproducing the water volume transport through the strait for all its components with respect to the other performed experiments, with a very good agreement with the considered studies.

The temporal variability of the three components of the water volume transport through the Dardanelles Strait LOBC is shown in Figure 3.5.

Table 3.2: Annual means of water volume transport (m^3/s) through the Aegean end of the Dardanelles Strait estimated by different studies and computed from numerical experiments results. A negative value indicates a volume transport directed from the Marmara Sea towards the Mediterranean Sea.

Modeled and observed annual mean transport	**Marmara to Med transport**	**Med to Marmara transport**	**Net transport**
simdd_v1	-25879	29010	3131
simdd_v2	-19313	18088	-1224
simdd_v3	-32005	24471	-7533
simdd_v5	-38070	30529	-7540
Ünlülata et al. (1990) [114]	-39832	30627	-9205
Latif et al. (1991) [115]	-37392	27886	-9506
Beşiktepe et al. (1994) [112]	-38584	2908	-9503
Özsoy and Ünlüata (1997) [113]	-37383	27879	-9503
Tuğrul et al. (2002) [111]	-42161	31996	-10165
Jarosz et al. (2013) [116]	-36680	31670	-5010

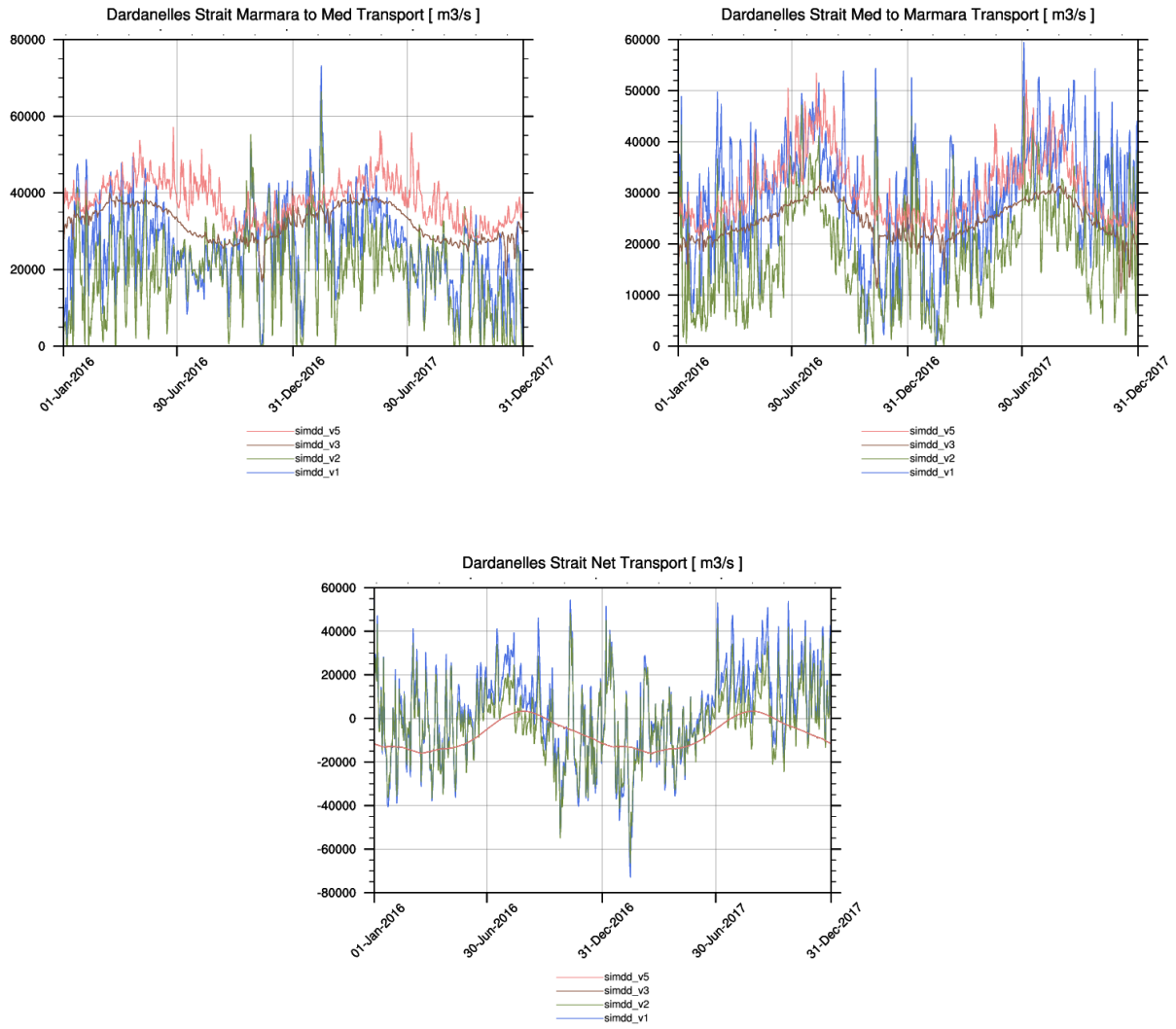

Figure 3.5: Dardanelles Strait water volume transport timeseries for experiments simdd_v1, simdd_v2, simdd_v3 and simdd_v5. Top-left panel: Marmara Sea to Mediterranean Sea transport; top-right panel: Mediterranean Sea to Marmara Sea transport; bottom panel: net transport.

3.2.2 Temperature and salinity comparison with in situ observations

The skill assessment of the different experiments in terms of temperature and salinity in the Aegean Sea is shown, through the comparison of model results with Argo floats, XBTs and gliders data available for the simulation period.

It should be noticed that experiment simdd_v4 is excluded from the comparison, since it provided the worst results after few months of integration.

It is clear from the comparison between the numerical results and the available observations for salinity and temperature in the Aegean Sea (Figures 3.6 and 3.7) that the implementation of Dardanelles Strait as LOBC represents an improvement with respect to the SBC implementation, with the exception of simdd_v3, which shows a much larger salinity RMSE with respect to the control run especially in the first 60 meters and a large negative bias along the entire the water column.

Considering the other performed experiments (simdd_v1, simdd_v2 and simdd_v5), the largest improvement in salinity representation (Figure 3.6) can be observed in the range between the surface and 10 m depth, with a significant error decrease with respect to simu_ctrl for all the considered experiments.

The experiment showing the lowest salinity RMSE for all the considered depth ranges is simdd_v2, in particular between the surface and 60 m depth. Considering the temperature metrics in the Aegean Sea, the new implementation provides almost always a slightly improved skill especially in the depth ranges between 30 and 60 m and between 100 and 150 m.

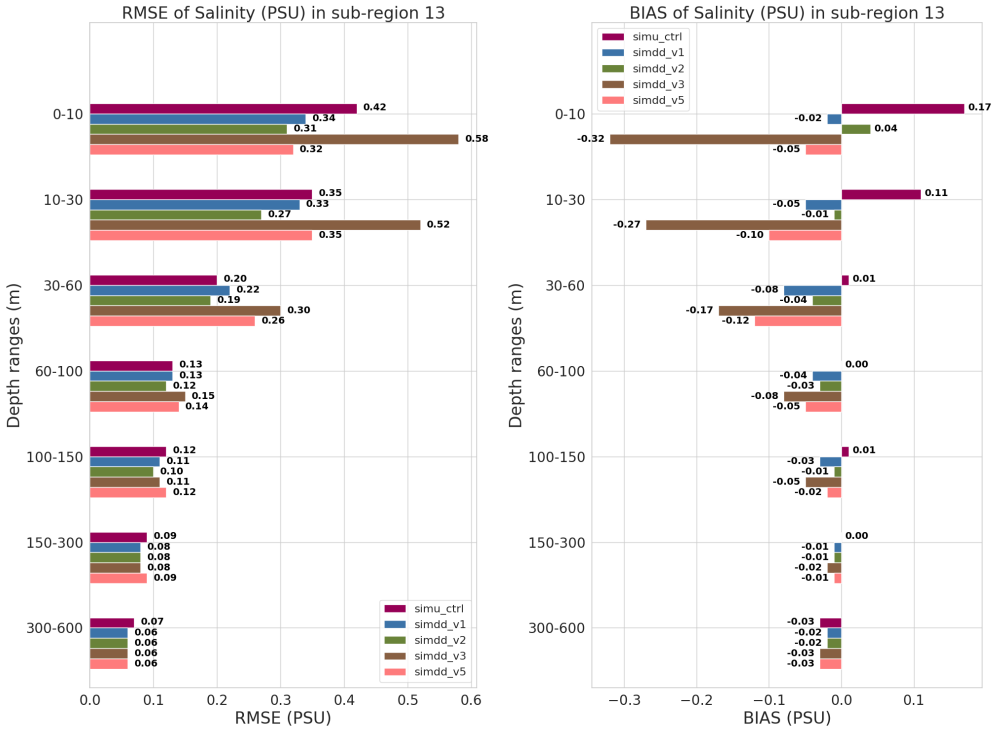

Figure 3.6: RMSE and BIAS of salinity (PSU) for experiments simu_ctrl, simdd_v1, simdd_v2, simdd_v3 and simdd_v5. Statistics consider sub-region 13.

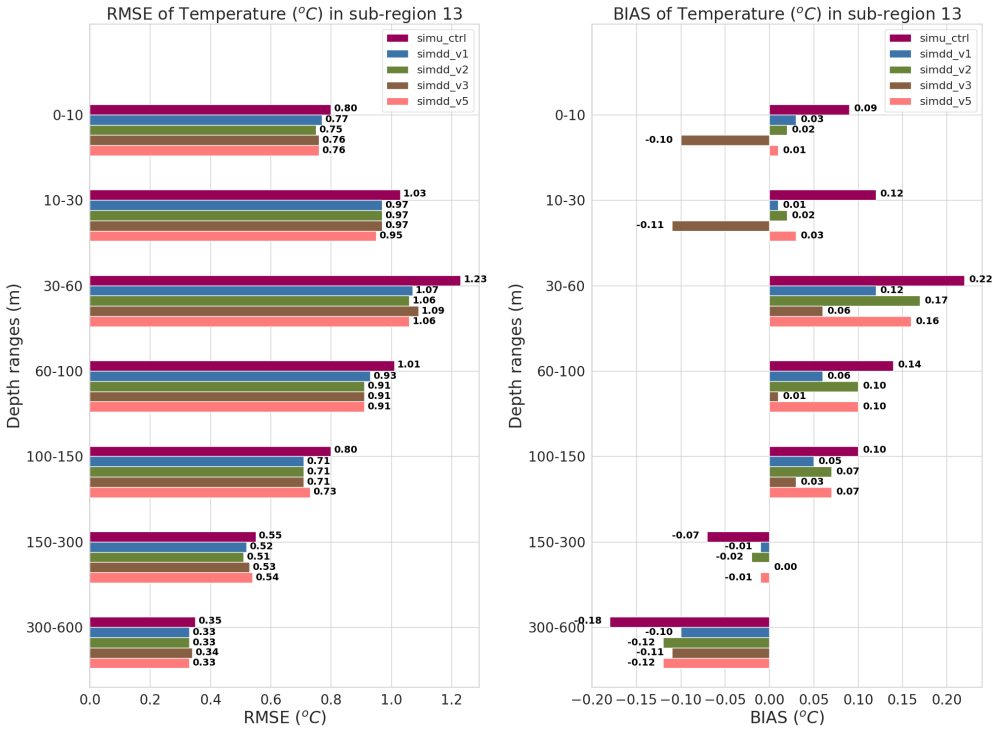

Figure 3.7: RMSE and BIAS of temperature (°C) for experiments simu_ctrl, simdd_v1, simdd_v2, simdd_v3 and simdd_v5. Statistics consider sub-region 13.

It is thus reasonable to assume that the good salinity skill achieved in simdd_v2 is provided by the strong underestimation of the Marmara Sea to Mediterranean Sea volume flux (see Table 3.2), which mitigates the large positive bias of the GLO-MFC daily climatological salinity values with respect to literature values.

In conclusion, since simdd_v5 showed an improvement in both salinity and temperature representation with respect to simu_ctrl and the best capability in reproducing the water volume transport through the Dardanelles Strait

Aegean outlet, it is chosen as final set up for the further experiments described in the next chapters, as well as for the following analyses of the present chapter.

3.2.3 Temperature and salinity vertical profiles comparison with climatological data sets

Temperature and salinity averages from experiments simu_ctrl and simdd_v5 are compared between each other in order to assess the changes in the thermohaline properties due to the new implementation of the Dardanelles Strait in the Mediterranenea Sea model, along with a comparison with SDN and WOA climatological data sets. A particular focus is dedicated to the Aegean Sea.

Temperature and salinity profiles for experiments simu_ctrl and simdd_v5 show evident differences between each other in the Aegean Sea. Focusing on the first 100 m of the water column (Figure 3.8) it can be observed that simdd_v5 shows lower values both in salinity and temperature with respect to simu_ctrl, with maximum differences at surface, gradually decreasing at depth.

Moreover for both temperature and salinity (in particular), simdd_v5 is in better agreement with SDN and WOA climatological profiles with respect to simu_ctrl.

For salinity this is due to the larger amount of water inflowing from the Marmara Sea in experiment simdd_v5 (see Table 3.2) with respect to the values prescribed in simu_ctrl derived from Korafalou and Barbopoulos (2003) [54], even though the salinity values prescribed in simu_ctrl derived from Ko-

rafalou and Barbopoulos (2003) [54] are constantly lower with respect to the ones used at the Dardanelles Strait LOBC derived from the TSS box model (Figure 3.3).

For what concern temperature, the decreasing in simdd_v5 with respect to simu_ctrl can be reasonably due to the fact that in simdd_v5 more realistic temperature values are imposed at the Dardanelles Strait LOBC inflow, while in simu_ctrl temperature was not prescribed for SBC, assuming the values of Sea Surface Temperature in the SBC implementation grid points.

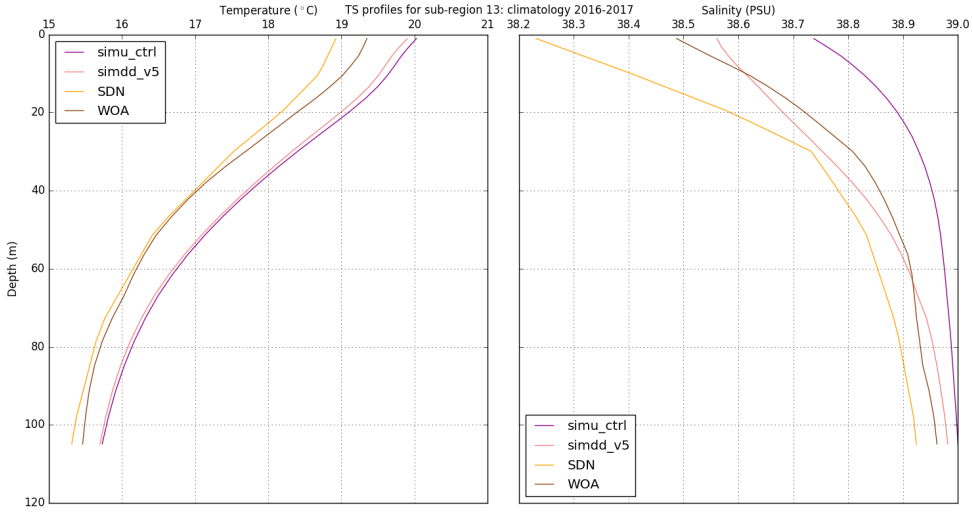

Figure 3.8: Temperature and salinity climatological profiles in sub-region 13 over the period 2016-2017 for experiments simu_ctrl, simdd_v5 and SDN and WOA climatological data sets.

3.2.4 Analysis of surface fields in the Aegean Sea

This section shows an analysis of surface fields evaluated in the Aegean Sea as seasonal mean maps derived from the numerical experiments and

climatological data sets (when available).

The seasons showing the largest differences are Spring (April-June) and Summer (July-September), reasonably due to the fact that the water inflow from the Marmara Sea shows its maximum values during Spring, with Summer still affected by the great amount of water flowing during the previous season, as shown in Figure 3.5 (pink line).

The circulation of the Aegean Sea is mainly driven by the buoyant plume generated by the low-salinity waters input of Black Sea Waters (BSW) from the Marmara Sea. The BSW then spread towards the interior of the basin bifurcating around the Limnos Island, partially flowing towards the northeastern part of the basin and the Saros Gulf and partially flowing towards the western part of the basin, in front of the Chalkidiki Peninsula and in the Thermaikos Gulf; a southward coastal current is then generated, spreading along Evia Island (Politikos et al., 2017 [52], Skliris et al., 2010 [117] and Olson et al., 2007 [118]).

In Figure 3.9, it can be observed that the northern branch of the Dardanelles Strait outflow is better defined and has higher velocity amplitude values in simdd_v5 with respect to simu_ctrl, and appears to be in better agreement in its structure with literature (Politikos et al., 2017 [52], Skliris et al., 2010 [117] and Olson et al., 2007 [118]). On the contrary, a lowering in velocity amplitude can be observed in the northeastern part of the basin in simdd_v5 with respect to simu_ctrl.

The new implementation of the Dardanelles Strait outflow increases also the velocity amplitude of the boundary current flowing from the southern edge of the Thermaikos Gulf along the Evia Island (Figure 3.9), being this

circulation structure better defined in simdd_v5 with respect to simu_ctrl.

The permanent cyclonic gyre in Chios basin (Olson et al., 2007 [118]) is observable in both the experiments, with similar velocity amplitude values.

A comparison between Spring surface salinity between the two experiments, along with the SDN and WOA climatological fields in shown in Figure 3.10. In the southern part of the Aegean Sea the two experiments show very similar results. The largest differences are indeed concentrated in the northernmost part of the basin, where the BSW low salinity plume is much more evident in simdd_v5 with respect to simu_ctrl due to a better representation of the outflow from the Dardanelles Strait.

Despite the larger amount of BSW outflow in simdd_v5, the lower salinity values prescribed in simu_ctrl at Dardanelles Strait SBC generates a large area of low salinity (about 2 PSU fresher with respect to simdd_v5) in the Saros Gulf and along the coast of Thrace and East Macedonia. This effect could be enhanced by the weaker control run circulation in the area with respect to simdd_v5 that could trap the BSW in the Saros Gulf, while in simdd_v5 the fresher BSW are spread towards the interior of the basin mixing with saltier water.

A wide area of lower surface salinity values in simdd_v5 with respect to simu_ctrl can be identified in front of the Chalkidiki Peninsula and in the Thermaikos Gulf, extending southward along Thessaly and Central Greece, affecting also the Myrtoan Sea: this is due to the circulation pattern generated by the buoyant plume of BSW from the Dardanelles Strait, whose northern branch reaches the northwestern part of the basin with a largest intensity in simdd_v5 with respect to simu_ctrl (Figure 3.9).

The lower surface salinity values shown in the area by simdd_v5 with respect to simu_ctrl appear to be in better agreement with SDN and WOA climatological data sets.

During Spring large differences in Sea Surface Temperature (SST) between the two experiments can be also noticed (Figure 3.11), the whole northwestern part of the Aegean Sea showing strongly lower values in simdd_v5 with respect to simu_ctrl.

This can be clearly attributed to the different Dardanelles Strait implementation between the two experiments: a larger amount of BSW enter into the Aegean Sea in simdd_v5 with respect to simu_ctrl, with a more realistic lower temperature with respect to simu_ctrl.

From a comparison with SDN and WOA climatological data sets it can be observed that both the experiments overestimate the SST in the Aegean Sea, in particular in the southern part of the basin.

The comparison of model SST with respect to satellite SST shows a decreasing in RMSE in simdd_v5 with respect to simu_ctrl from April to June in the northern part of the Aegean Sea, due to a cooling of the northernmost part of the basin, in particular in May (Figure 3.12).

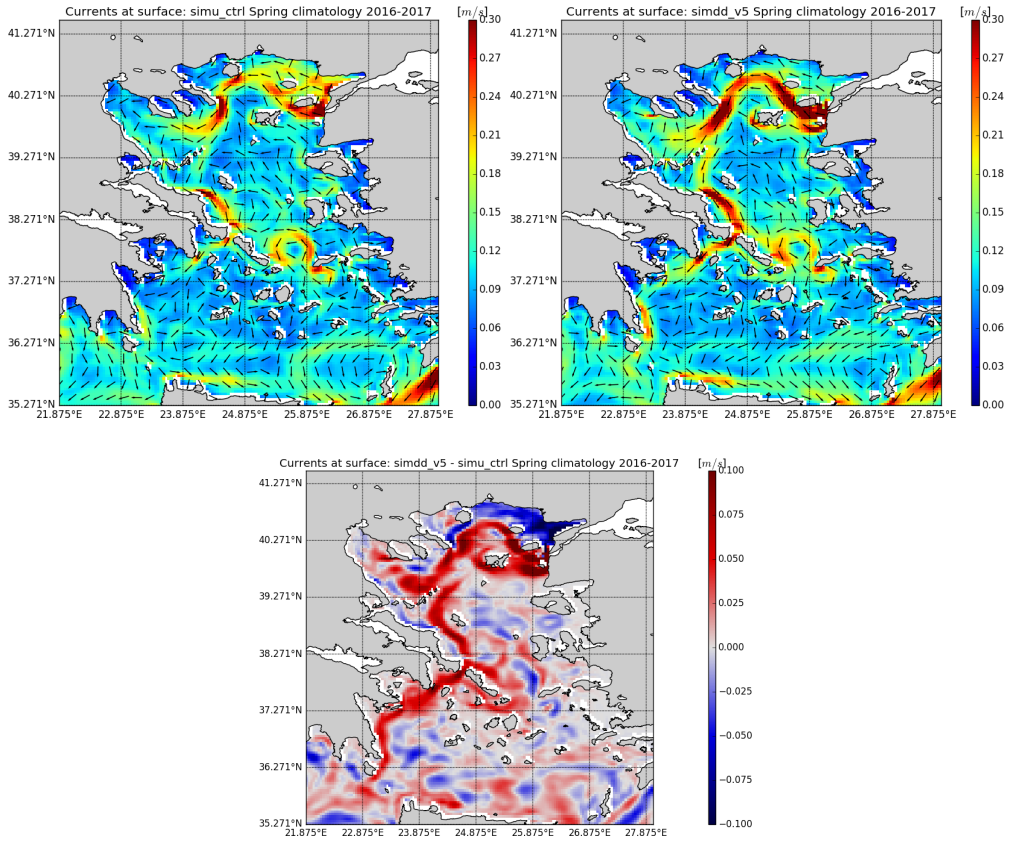

Figure 3.9: Surface currents Spring (Apr - Jun) climatologies over the period 2016-2017 for simu_ctrl (top-left panel), simdd_v5 (top-right panel), simdd_v5 - simu_ctrl (bottom panel).

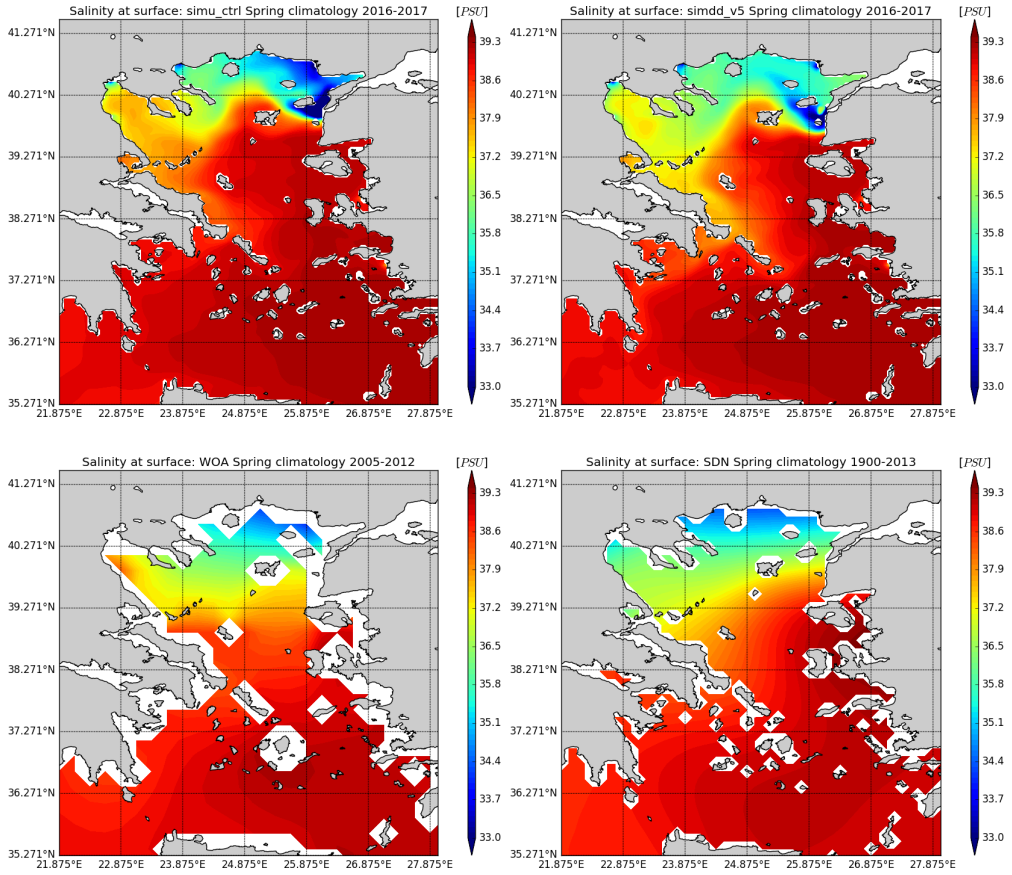

Figure 3.10: Salinity Spring (Apr - Jun) climatologies over the period 2016-2017 at surface for simu_ctrl (top-left panel), simdd_v5 (top-right panel), WOA (bottom-left panel) and SDN (bottom-right panel).

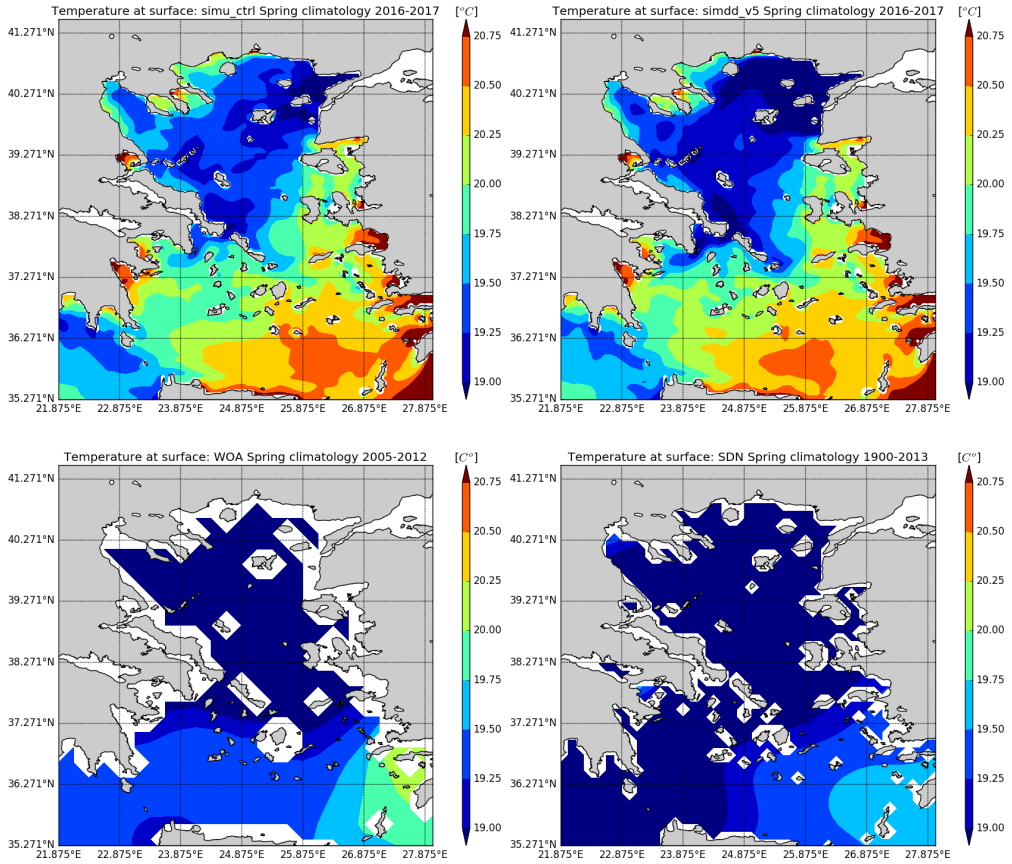

Figure 3.11: Temperature Spring (Apr - Jun) climatologies over the period 2016-2017 at surface for simu_ctrl (top-left panel), simdd_v5 (top-right panel), WOA (bottom-left panel) and SDN (bottom-right panel).

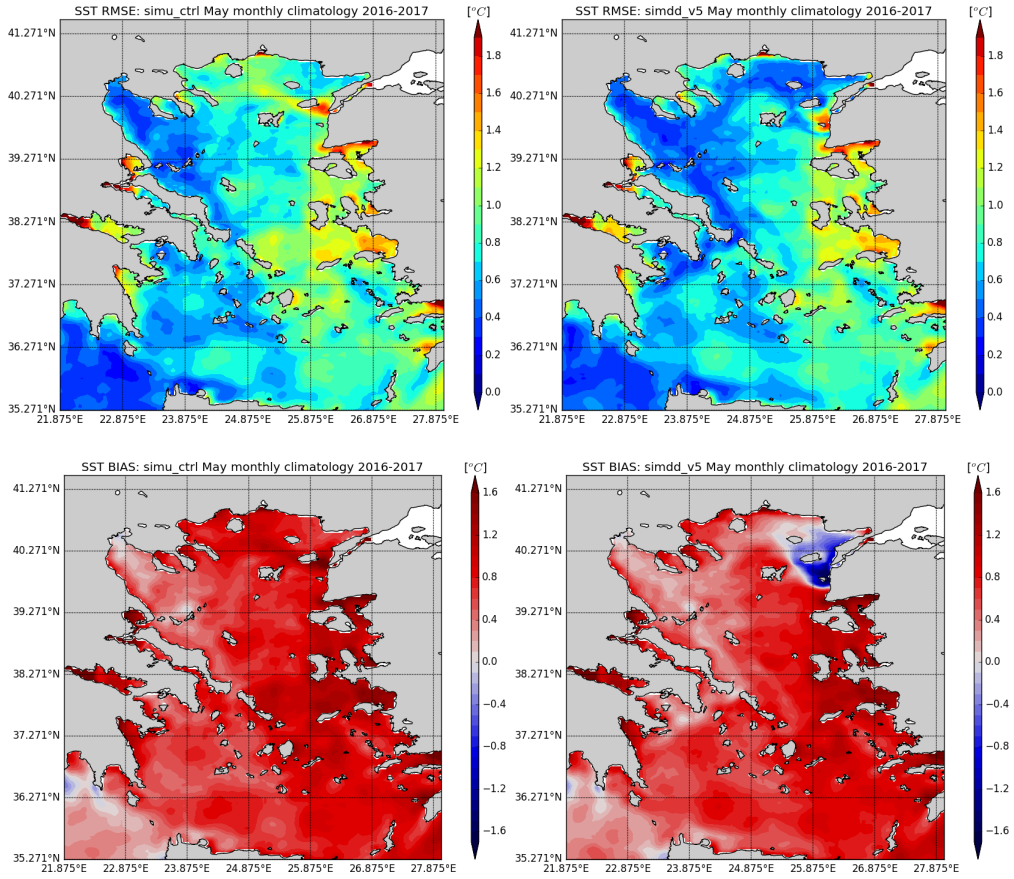

Figure 3.12: May sea surface temperature climatological RMSE (top panels) and BIAS (bottom panels) over the period 2016-2017 for simu_ctrl (left column) and simdd_v5 (right column).

The lowering in salinity introduced in the Aegean Sea by the new Dardanelles Strait implementation is very large and affects the entire Aegean basin, so that also the Mediterranean Sea basin-averaged salinity is clearly impacted, as observable in Figure 3.13, which presents the daily mean model time series of salinity at different model layers with respect to climatological data sets.

Starting from the second year of integration, the mean volume salinity difference starts to be evident, with simdd_v5 constantly showing lower values with respect to simu_ctrl.

In surface salinity a clear seasonal cycle is observable, with the two experiments showing the largest differences (about 0.02 PSU) in Summer (July-September), in correspondence of the minimum in salinity associated to the Dardanelles Strait inflow into the Mediterranean Sea.

Evident and gradually increasing differences (up to 0.02 PSU) in the 0-100 m depth range can be observed between the two experiments, indicating that Dardanelles Strait inflow affects also the mixed layer depth range in the area.

Both at surface and in the 0-100 m depth layer simdd_v5 appears to be closer to SDN and WOA climatological data sets with respect to simu_ctrl.

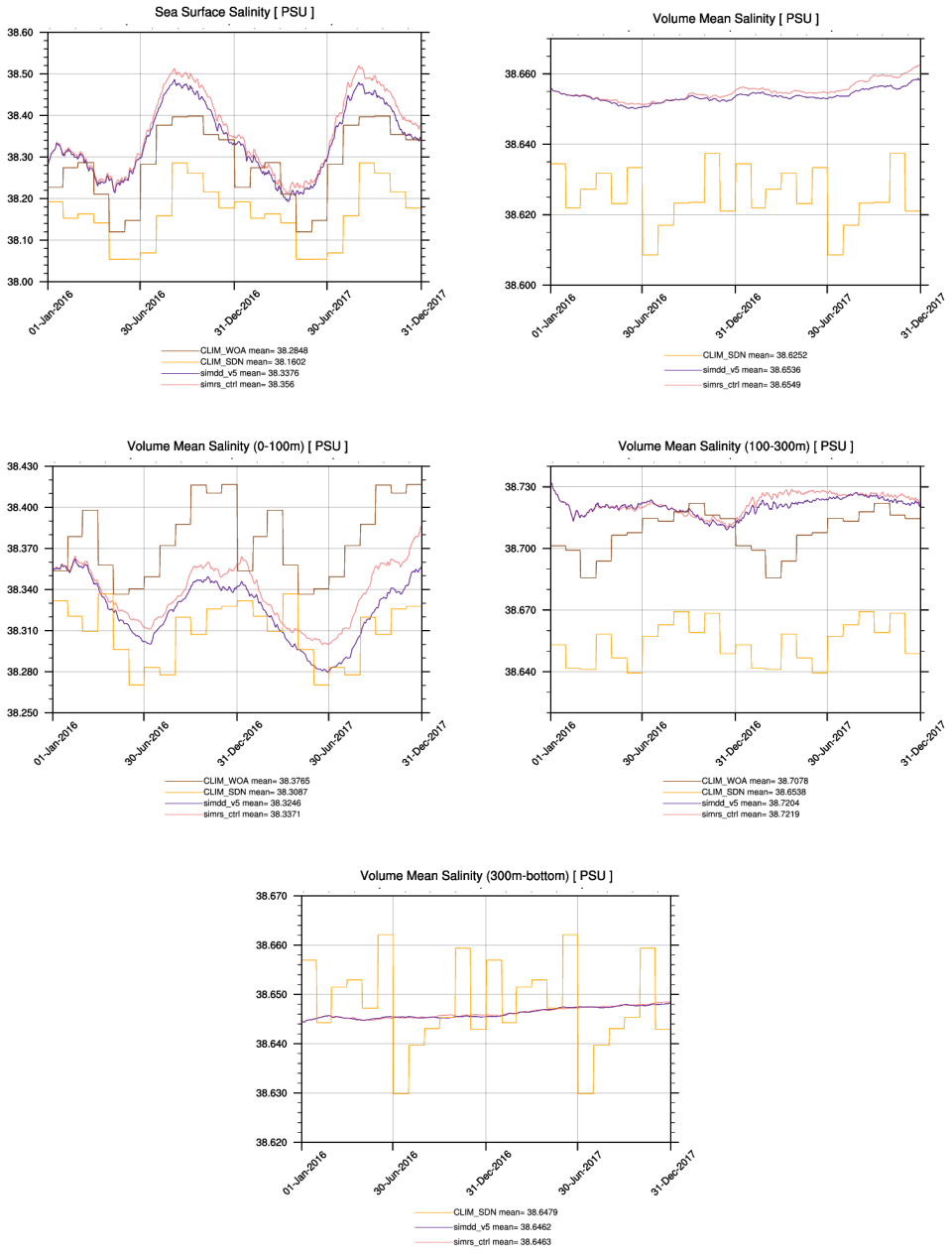

Figure 3.13: Mediterranean Sea salinity daily mean computed from numerical experiments and climatological data sets at different layers.

3.2.5 Mixed Layer Depth comparison with climatologies

The main differences in Mixed Layer Depth (MLD) between the two experiments can be observed between the end of Autumn and the beginning of Winter, in particular in January, which is shown in Figure 3.14.

Strong differences (more than 50 m) can be noticed in the northern and in the western part of the Aegean Sea: the larger amount of Black Sea Waters inflow into the sub-basin in simdd_v5 generates a large negative anomaly (thus shallower MLD) in front of the Dardanelles Strait outlet, which is in turn spread towards the western and southward part of the basin by the circulation pattern, finally reaching the Myrtoan Sea.

The eastern part of the basin shows instead a positive MLD anomaly (thus deeper MLD values) in simdd_v5 with respect to simu_ctrl, which let suppose an increased inflow of denser water into the Aegean Sea from the Levantine basin.

A comparison with the Houpert et al. (2015) [103] climatological data set is quite difficult for such a limited area, due to the difference in resolution, anyway on the basis of the available data set both the experiments seem to overestimate the MLD, which in the climatological data set appears to be more affected by the fresher water input from the Dardanelles Strait, being better represented when the inflow is implemented as an open boundary condition.

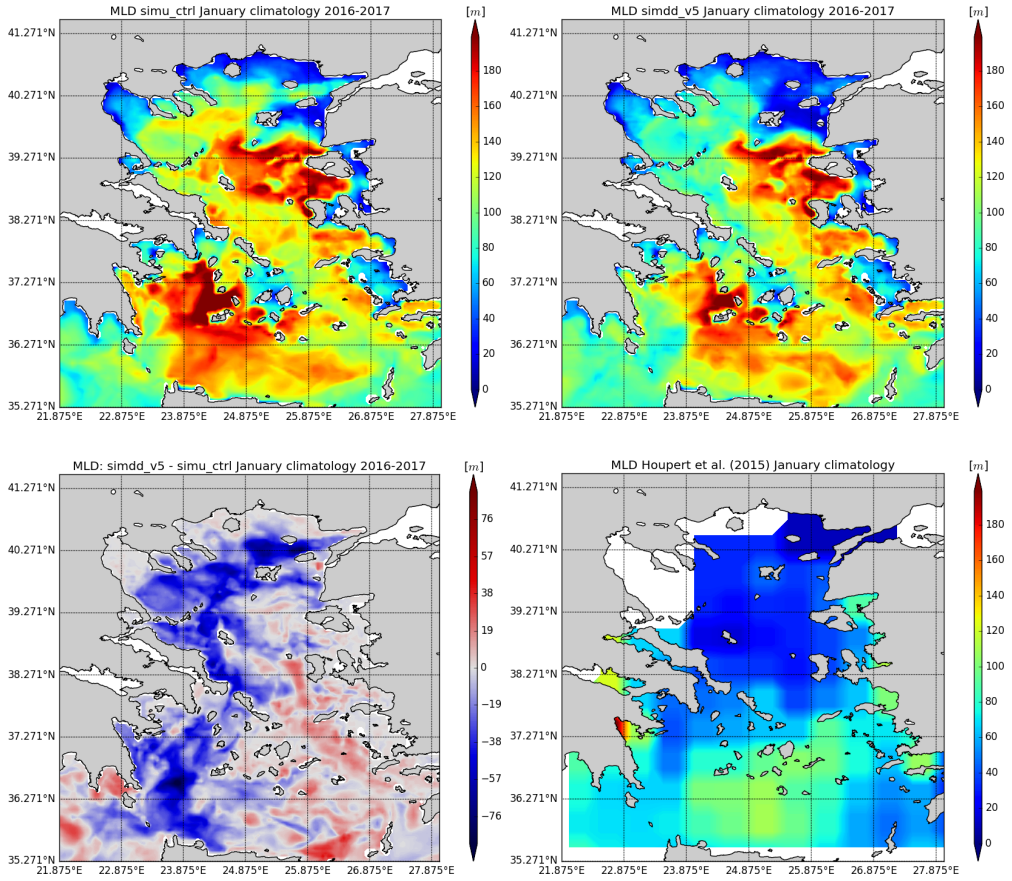

Figure 3.14: January climatological Mixed Layer Depth over the period 2016-2017 in the Aegean Sea. Top-left panel: simu_ctrl; top-right panel: simdd_v5; bottom-left panel: simdd_v5 - simu_ctrl; bottom-right panel: Houpert et al. (2015) climatological data set.

3.2.6 Sea Surface Height comparison with satellite data

In Figure 3.15 the seasonal differences in Sea Surface Height (SSH) between experiments simu_ctrl and simdd_v5 are shown.

The influence of the larger BSW inflow from the Dardanelles Strait in

simdd_v5 experiment is evident on the SSH over the entire Aegean Sea, and in particular in the northern and eastern areas of the basin, where the increased inflow of water at lower salinity generates a large increase in SSH; the lighter water is then spread along the eastern coast of Greece by the already described circulation pattern.

Increased SSH values in simdd_v5 are particularly evident in Spring and Summer, due to the Dardanelles Strait westward transport seasonal cycle.

It is interesting to notice, during Summer, the local SSH decrease in simdd_v5 with respect to simu_ctrl in front of the Thrace coast: this can be reasonably due to the largely lower, even though localized, SST values that simdd_v5 displays in correspondence of the BSW plume (not shown).

An intercomparison with Sea Level Anomaly (SLA) from satellite gridded data is performed on a seasonal basis, in order to assess if the Dardanelles Strait LOBC implementation in simdd_v5 leads to an improvement with respect to the SBC implementation used in experiment simu_ctrl. The results are shown in Figures from 3.16 to 3.19.

If compared with satellite data, simdd_v5 shows an improvement with respect to simdd_ctrl in SLA representation in the most part of the Aegean Sea, down to about 37°N, with a decrease in RMSE gradually less pronounced in southward direction, that seems to indicate a direct effect of the Dardanelles Strait implementation in the improvement of model SLA solution. The SLA BIAS of the two experiments indicates a general tendency of simdd_v5 towards less negative BIAS values, due to an increased SLA in this experiment. The southernmost part of the basin does not show significant differences in SLA representation skill between the two considered experiments.

The northernmost part of the basin shows the largest decrease in SLA RMSE for experiment simdd_v5 with respect to simu_ctrl, with a difference of about 2-3 cm between the two experiments.

This is particularly evident in front of the Dardanelles Strait outlet, especially during Spring and Summer: during Summer (see Figure 3.18) the main improvements in SLA representation in simdd_v5 can be observed, with a decrease in RMSE of about 4-5 cm in close proximity of the outlet.

It can be noticed that the Dardanelles Strait LOBC implementation in simdd_v5 has a positive impact also on the central part of the Aegean Sea, due to the cyclonic circulation in the basin, that brings the BSW outflowing from the Dardanelles Strait down to the area in front of the coasts of Thessaly and Central Greece.

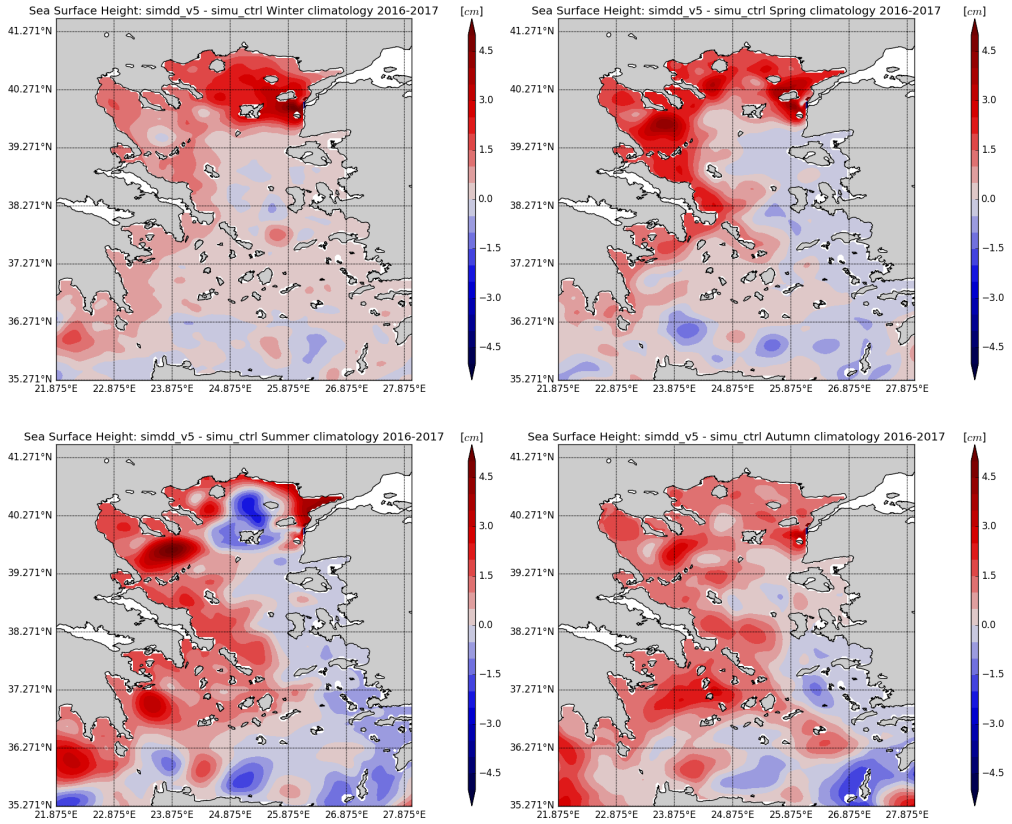

Figure 3.15: Seasonal climatological sea surface height differences between experiments simu_ctrl and simdd_v5. From top to bottom panel: Winter (Jan - Mar), Spring (Apr - Jun), Summer (Jul - Sep) and Autumn (Oct - Dec).

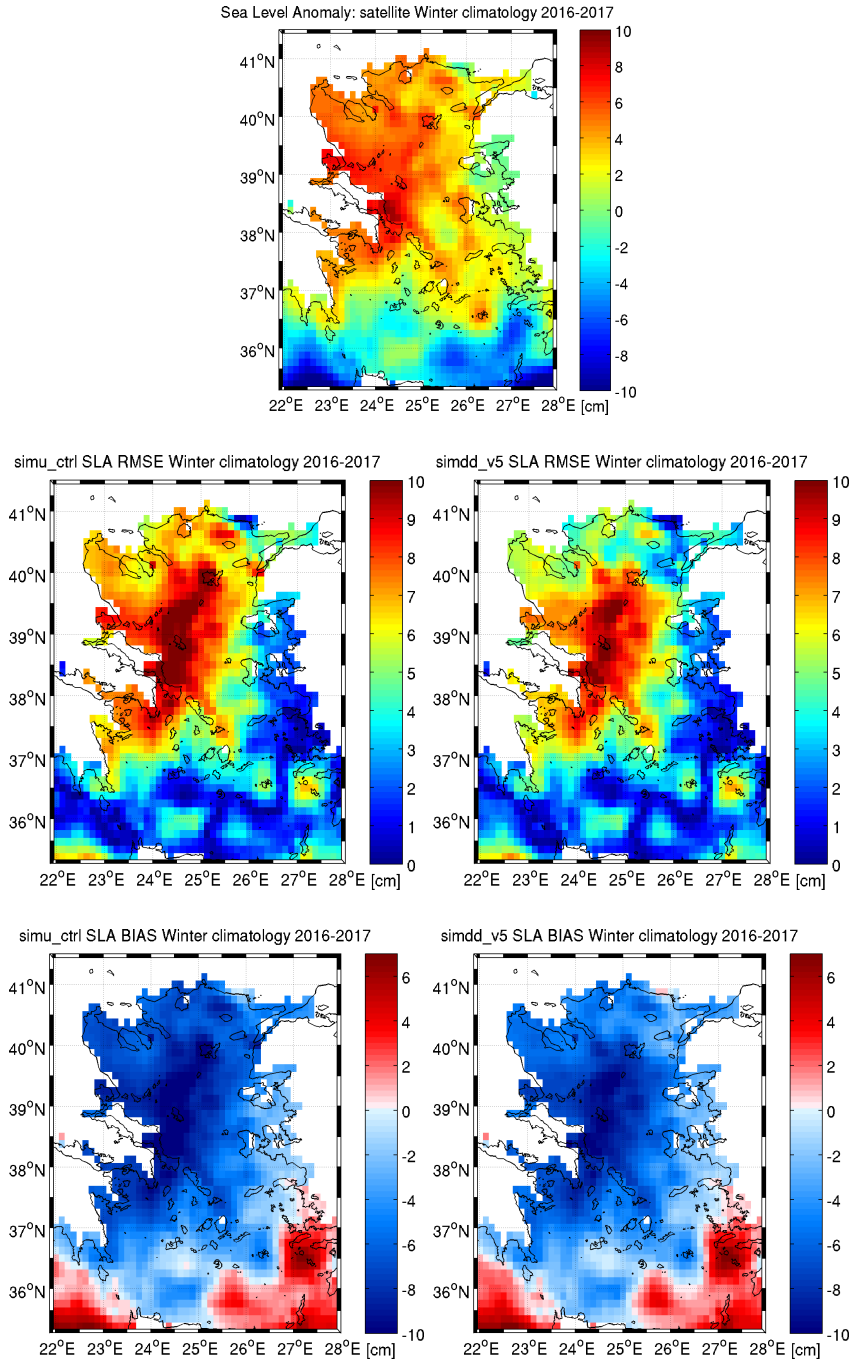

Figure 3.16: Winter Sea Level Anomaly (SLA) metrics of simu_ctrl and simdd_v5, along with SLA from satellite, computed over the period 2016-2017, generated using AVISO+ Dynamic Atmospheric Correction product. Panels on the left column: RMSE and BIAS for simu_ctrl; panels on the right column: RMSE and BIAS for simdd_v5.

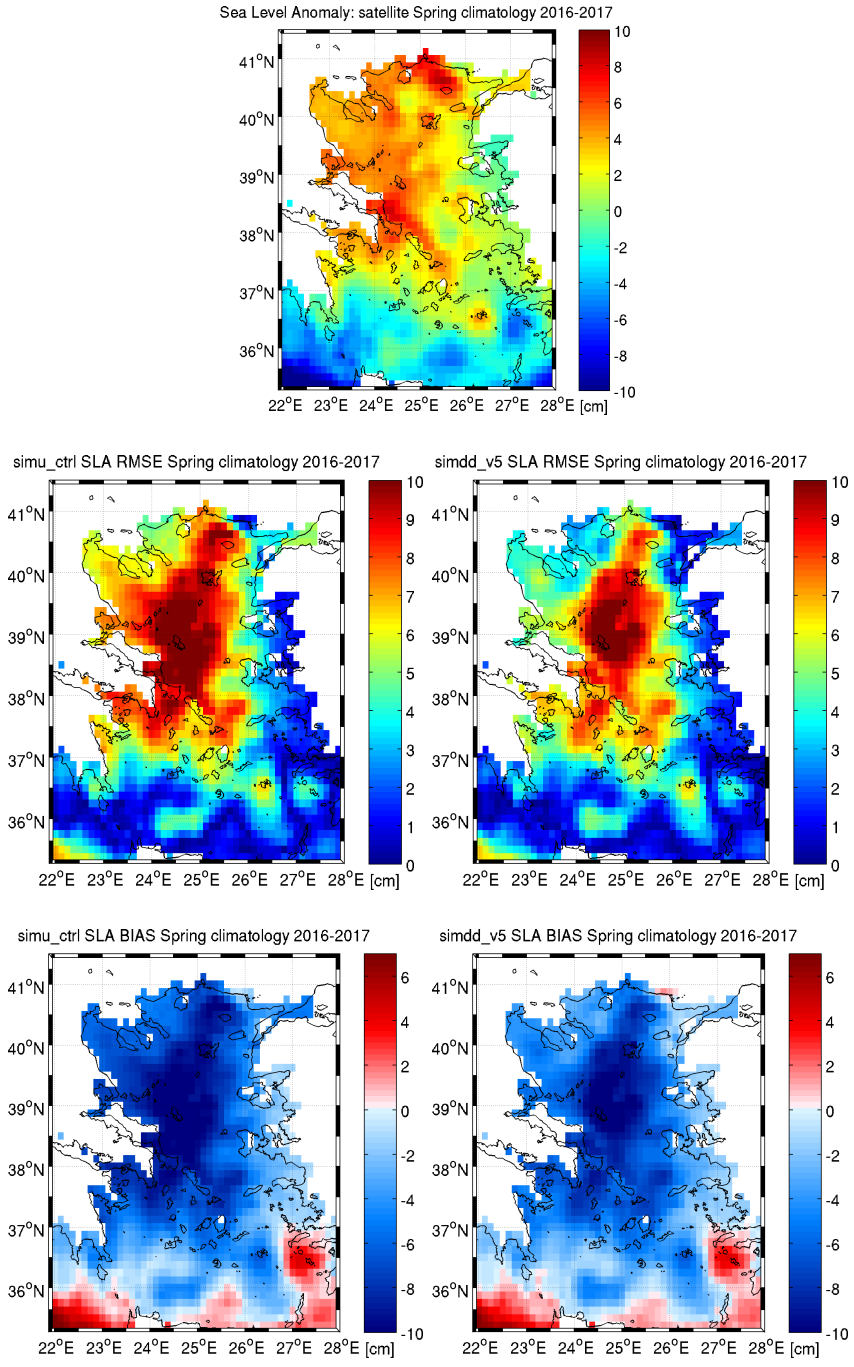

Figure 3.17: Spring Sea Level Anomaly (SLA) metrics of simu_ctrl and simdd_v5, along with SLA from satellite, computed over the period 2016-2017, generated using AVISO+ Dynamic Atmospheric Correction product. Panels on the left column: RMSE and BIAS for simu_ctrl; panels on the right column: RMSE and BIAS for simdd_v5.

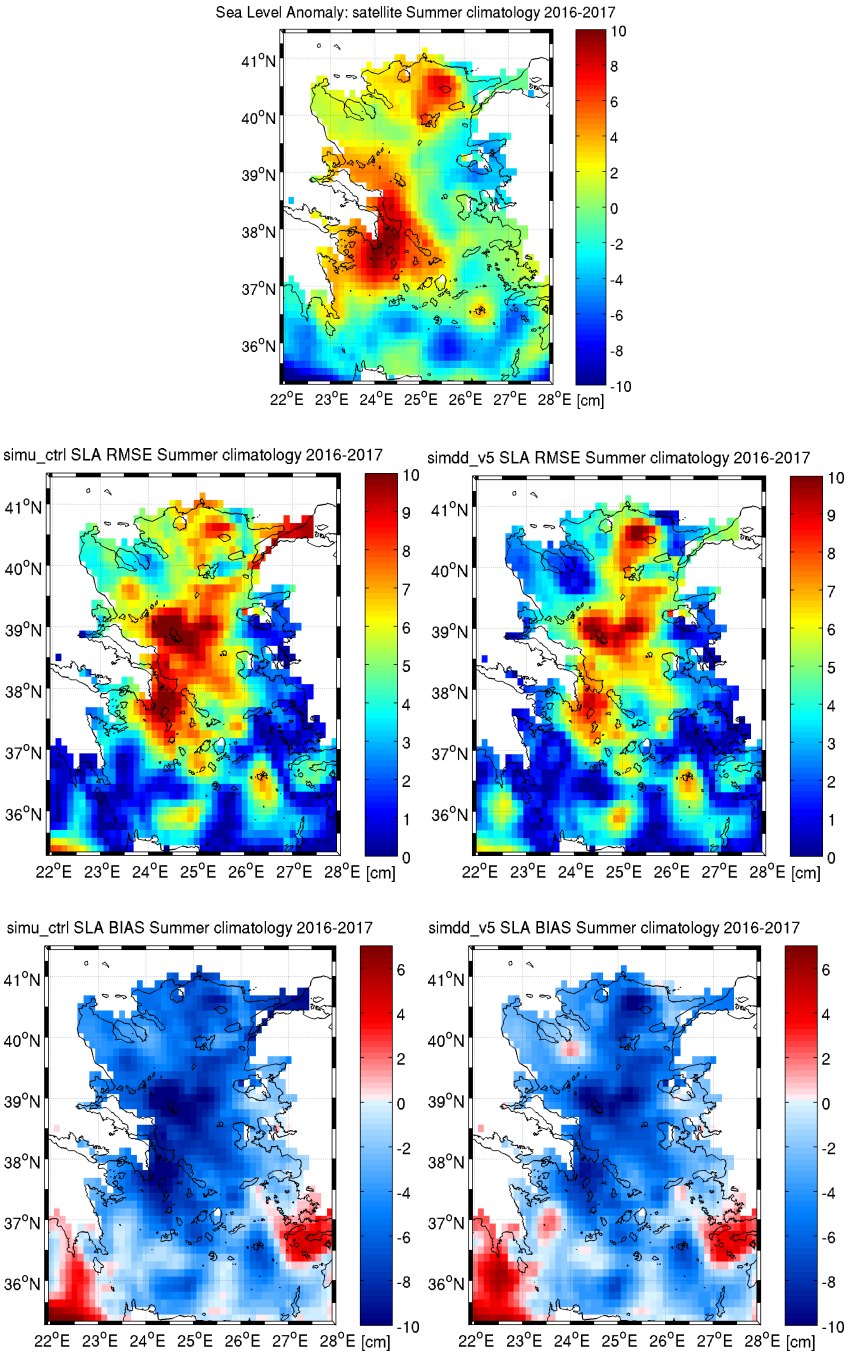

Figure 3.18: Summer Sea Level Anomaly (SLA) metrics of simu_ctrl and simdd_v5, along with SLA from satellite, computed over the period 2016-2017, generated using AVISO+ Dynamic Atmospheric Correction product. Panels on the left column: RMSE and BIAS for simu_ctrl; panels on the right column: RMSE and BIAS for simdd_v5.

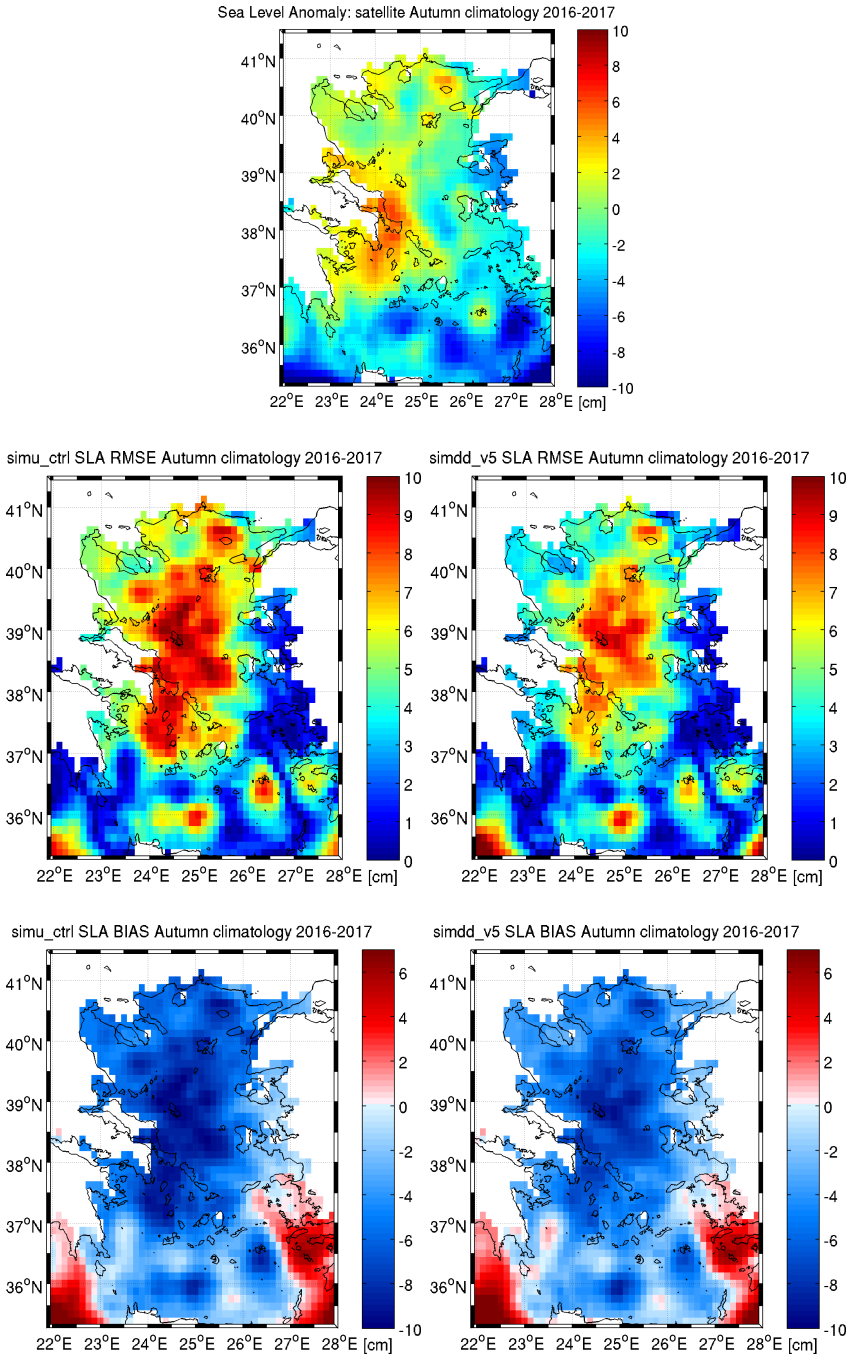

Figure 3.19: Autumn Sea Level Anomaly (SLA) metrics of simu_ctrl and simdd_v5, along with SLA from satellite, computed over the period 2016-2017, generated using AVISO+ Dynamic Atmospheric Correction product. Panels on the left column: RMSE and BIAS for simu_ctrl; panels on the right column: RMSE and BIAS for simdd_v5.

3.3 Summary of the chapter

In this chapter the implementation of the Dardanelles Strait as Lateral Open Boundary Condition (LOBC) for the Mediterranean Sea is described and evaluated with respect to a Surface Boundary Condition (SBC) implementation.

Both the setups are evaluated with respect to in situ and satellite data, in order to assess the impact of the new formulation introduced.

Among the different experiments performed in order to test the new implementation the one that gives the best results considering both temperature and salinity representation with respect to in situ observations and water volume transport through the strait is experiment simdd_v5.

simdd_v5 shows a significant improvement with respect to simu_ctrl in salinity representation in the first 10 meters of the water column, while in the depth range between 30 and 60 m an increase in salinity RMSE can be noticed in simdd_v5 with respect to simu_ctrl; in the rest of the water column the two experiments show similar skills.

Considering temperature representation skill, simdd_v5 shows a constant improvement with respect to simu_ctrl along the whole water column, in particular in the depth range between 30 and 60 m.

From a comparison with SDN and WOA climatologies of simu_ctrl and simdd_v5 it can be observed that the latter shows salinity values much closer to the climatological datasets with respect to simu_ctrl with a general freshening of the entire water column. The differences of temperature vertical structure between the two experiment are much smaller with respect to salinity, but anyway sufficient to ensure better performances of experiment simdd_v5,

as already mentioned.

The new LOBC implementation affects also the main circulation structures of the Aegean Sea, producing a surface circulation pattern in better agreement with literature in simdd_v5 with respect to simu_ctrl.

Large differences in Mixed Layer Depth (MLD) between the two experiments can be observed in particular in January in the northern and western part of the Aegean basin, with a shallower MLD in simdd_v5. An assessment of the eventual improvement due to LOBC implementation is difficult due to the low resolution of the observational dataset.

The comparison of Sea Level Anomaly (SLA) for the two considered experiment with respect to data from satellite shows a clear improvement in the experiment simdd_v5, due to an increase of SLA in particular in the northern part of the Aegean Sea.

Despite the good improvement achieved in the Dardanelles Strait LOBC implementation with respect to the SBC implementation, the former would benefit from a nesting with a numerical model specifically designed for the Turkish Straits System, since the GLO-MFC system is not designed to fully resolve all the complex dynamics that characterize the strait.

In addition, the vertical structure of the boundary, and thus the dynamics of the strait, would take advantage from the possibility to provide an outflowing salinity varying in time instead of a constant prescribed salinity as it is done in the final setup of the Dardanelles Strait LOBC.

Moreover, the possibility to retrieve velocity and sea surface height fields from the same source would be of great use in improving the performances of the tested (but finally not chosen) Flather scheme for barotropic veloci-

ties, which is instead successfully used for the Atlantic Ocean Lateral Open Boundary Condition.

The improvements achieved through the new LOBC implementation of the Dardanelles Strait suggest that the new parameterization of the Black Sea Waters input into the Mediterranean Sea could be a useful improvement in the capability of the model to reproduce well-known events such as the Eastern Mediterranean Transient (EMT, Roether et al., 1996 [119]), characterized by the contribution of the Aegean Sea outflowing waters to the Eastern Mediterranean deep waters formation during the late eighties and early nineties, due to a modified Black Sea Waters input into the Aegean Sea (Pinardi et al., 2015 [33]).

Chapter 4

Analysis of riverine influences in the Mediterranean Sea through numerical experiments

4.1 Sensitivity experiments with modified river runoff sources

Two numerical experiments are performed with the aim of evaluating the impact of an increased number of freshwater inputs on the thermohaline properties of the Mediterranean Sea and on its dynamics. In the first experiment (hereafter simrs_v1) 7 main rivers with an annual mean discharge larger than 100 m^3/s have been implemented (green dots in Figure 4.1), and 32 additional rivers (red dots in Figure 4.1) have been included in the second experiment (hereafter simrs_v2). The added rivers are characterized by a mean annual

discharge larger than 50 m^3/s over the period 2000–2010 according to the values derived from the PERSEUS project (http://www.perseus-net.eu).

The river discharge has been implemented as monthly climatology: the monthly climatological discharge values for the 7 rivers implemented both in experiment simrs_v1 and in simrs_v2 are derived from Fekete et al. (1999) [120] for Ebro, Rhone, Nile and Po (in addition to Simoncelli et al., 2011 [121] for Po di Levante and Po di Volano), from Raicich (1996) [122] for Seman and Vjiose, from Demiraj et al. (1996) [123] for Buna-Bojana. The monthly climatological discharge values for the additional 32 rivers are derived from the PERSEUS project (http://www.perseus-net.eu).

The salinity associated to river runoff is set constant in time for all the considered rivers: for the 7 rivers implemented both in experiment simrs_v1 and in simrs_v2 the used values, based on previous sensitivity experiments, are: 30 PSU for Ebro, 25 PSU for Rhone, 8 PSU for Nile, 18 PSU for Po and 15 PSU for Seman, Vjiose and Buna-Bojana.

The prescribed salinity for the additional 32 rivers implemented in experiment simrs_v2 has been set equal to 15 PSU, following Verri et al. (2018) [3].

Table 4.1 summarizes the salinity prescribed for each river, along with the mean annual discharge.

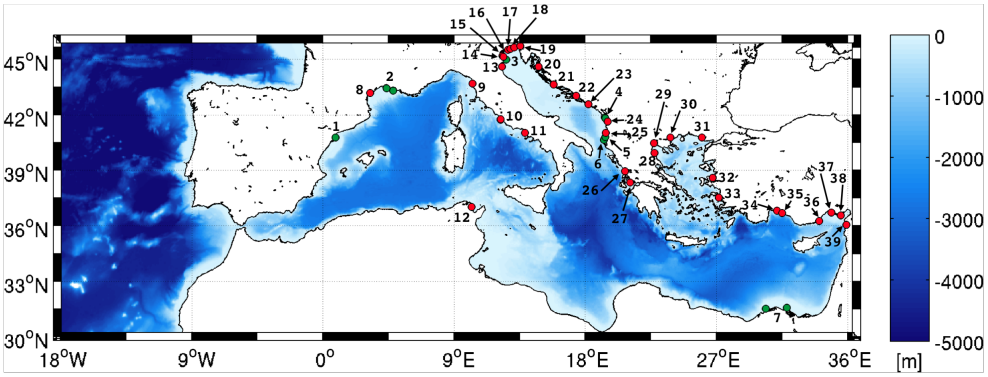

Figure 4.1: Model domain, bottom topography and location of river inputs: green dots represent the 7 river sources included in both experiment simrs_v1 and simrs_v2, red dots represent the 32 additional rivers implemented in experiment simrs_v2. The numeric labels for each river are listed in Table 4.1.

Table 4.1: Rivers labels as in Figure 4.1, prescribed salinity (S, PSU) and mean annual discharge (Q, m^3/s).

Label	**River name**	S	Q
1	Ebro	30	432
2	Rhone	25	1707
3	Po	18	1519
4	Buna-Bojana	15	675

Table 4.1 Continued: Rivers labels as in Figure 4.1, prescribed salinity (S, PSU) and mean annual discharge (Q, m^3/s).

5	Seman	15	201
6	Vjiose	15	183
7	Nile	8	475
8	Aude	15	59
9	Arno	15	88
10	Tevere	15	181
11	Volturno	15	63
12	Medjerda	15	59
13	Reno	15	67
14	Adige	15	232
15	Brenta	15	163
16	Piave	15	128
17	Livenza	15	96
18	Tagliamento	15	79
19	Isonzo	15	175
20	Lika	15	84
21	Krka	15	57

Table 4.1 Continued: Rivers labels as in Figure 4.1, prescribed salinity (S, PSU) and mean annual discharge (Q, m^3/s).

22	Neretva	15	239
23	Trebisnjica	15	93
24	Mati	15	99
25	Shkumbini	15	54
26	Arachtos	15	75
27	Acheloos	15	106
28	Pinios	15	67
29	Axios	15	97
30	Struma	15	81
31	Meric	15	166
32	Gediz	15	53
33	Buyuk Menderes	15	106
34	Kopru	15	85
35	Manavgat	15	122
36	Goksu	15	203
37	Seyhan	15	200
38	Ceyhan	15	231

Table 4.1 Continued: Rivers labels as in Figure 4.1, prescribed salinity (S, PSU) and mean annual discharge (Q, m^3/s).

39	Asi	15	94

It is worth to have here a brief overview of the seasonal variability of the riverine runoff into the Mediterranean Sea to gain insight about the minimum and maximum discharge periods, in order to identify the moments corresponding to the minimum (maximum) riverine influence on the Mediterranean Sea thermohaline properties, in particular on the ROFIs.

The minimum discharge period for all the rivers is during Summer: the only exception is represented by Nile river (Figure 4.2), which has its peak discharge in July and very high runoff values in June and August, an opposite behavior with respect to all the other rivers discharging into the Mediterranean Sea.

For the most part of the considered rivers the peak discharge occurs between November and March; in particular for Adriatic Sea rivers it is concentrated between November and December (see as an example the Buna-Bojana climatological runoff shown in Figure 4.2).

The Po river (Figure 4.2) represents an exception with respect to the other rivers discharging into the Mediterranean Sea, since it has two large discharge peaks quite far from each other, in May and November.

The Ebro and the Rhone rivers (Figure 4.2) have a similar seasonal discharge distribution, with maximum discharge in March and February respectively, with a typical low flow rate during Summer.

All the rivers discharging into the Aegean Sea show a similar behavior (see Meric in Figure 4.2 as an example), with a maximum flow rate in January or February (river Struma only); the only exception is represented by Axios river, which has its peak discharge in April.

Also the Turkish rivers discharging into the Southern Aegean Sea, Gediz and Buyuk Menderes, display the same seasonal variability observed for the rivers that have their own outlets in the northern part of the sub-basin.

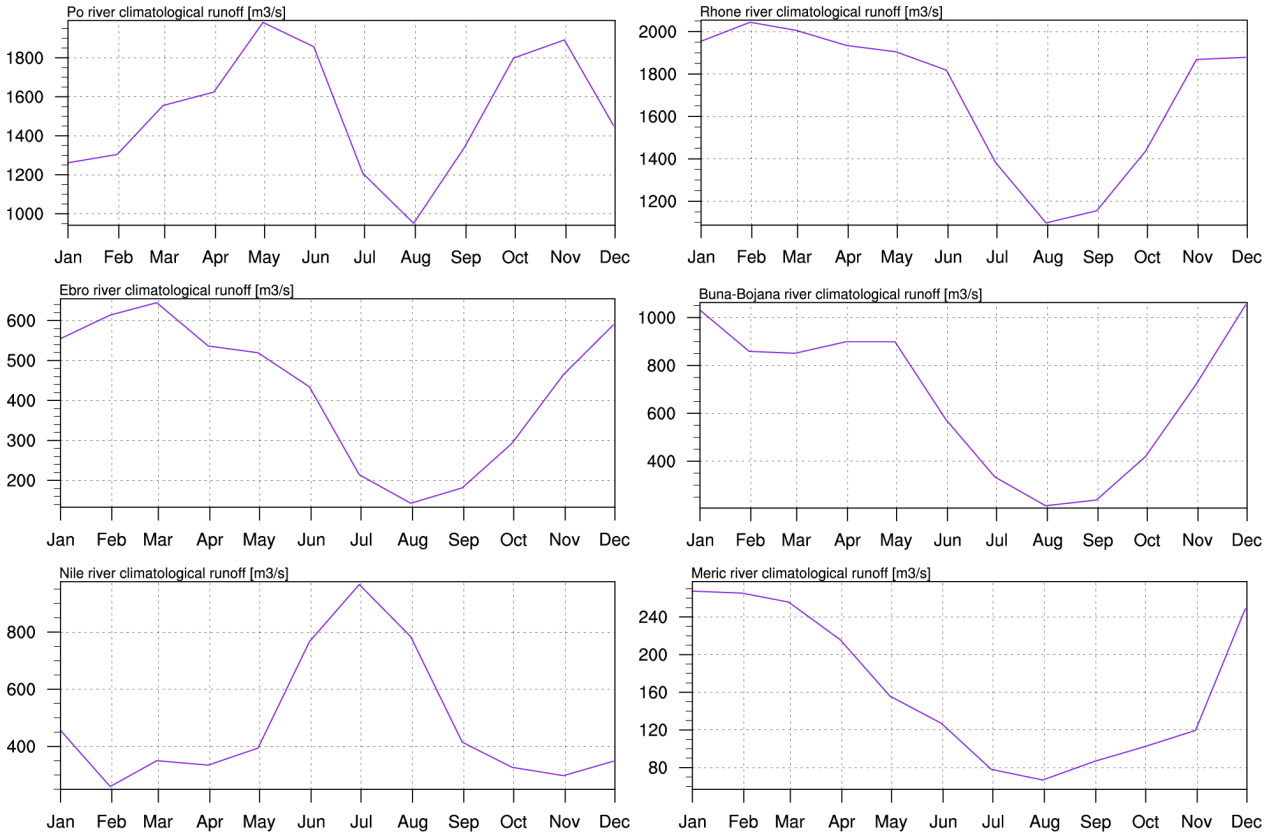

Figure 4.2: River runoff climatologies for sample rivers.

The numerical river representation in the NEMO model is achieved by

implementing the river sources in the sea grid point closest to the river outlet, or in the mid-point of the river delta, by prescribing monthly climatological discharge values along with the salinity values indicated in Table 4.1, in order to compute the salt flux and the volume flux through the ocean surface boundary associated to runoff.

It was decided not to prescribe a temperature value for freshwater discharge into the ocean, so that the Sea Surface Temperature (SST) of the grid point (or points) where each river is implemented is used by the model to compute the runoff heat content for each riverine source.

A particular treatment is chosen for the following rivers:

- The Buna-Bojana, the Tevere and the Nile rivers are implemented on the two grid points closest to their two branches, equally splitting the imposed discharge between the two grid points.

- The Rhone delta is implemented on the two model grid points better representing its two functional arms, the Petit Rhone (the westernmost one) and the Grand Rhone (the easternmost one). Moreover, according to Ibañez et al. (1997) [124], the imposed discharge is split between a 90% in the Grand Rhone and a 10% in the Petit Rhone.

- The Po discharge at its gauge station (Pontelagoscuro) is unevenly distributed into eight grid points representing the nine main branches of the delta: Po di Goro, Po di Gnocca, Po di Tolle, Po di Bastimento, Po di Scirocco, Po di Bonifazi, Po di Dritta, Po di Tramontana, Po di Maistra. Due to the horizontal resolution of the numerical model the branches of Po di Scirocco and Po di Bonifazi are represented by a

single grid point.

In addition to the above-mentioned branches, also the Po di Levante and the Po di Volano are taken into account and implemented on one grid point each.

The discharge is distributed according to the percentages provided in Provini et al. (1992) [125], proportionally decreased in order to consider also the Po di Levante branch, which diverges from the Po mainstream after the Pontelagoscuro gauge station.

The Po di Volano branch climatological discharge is instead assigned as in Simoncelli et al. (2011) [121], since it diverges from the river mainstream before the Pontelagoscuro gauge station.

It should be noticed that the monthly climatological values for Nile river derived from Fekete et al. (1999) [120] is reduced in order to fit more recent discharge estimates from Hamza et al. (2003) [126], Nixon (2003) [70] and Pinardi et al. (2006).

For both the performed experiments, the Dardanelles Strait LOBC setup implemented is the one used in experiment simdd_v5, previously described in Section 3.1 and summarized in Table 3.1.

The numerical experiments are run from January 2005 to December 2015, initialized from World Ocean Atlas 2013 version 2 (WOA13 V2) winter climatologies of temperature and salinity, considering the year 2005 as spin-up for the model integration.

A summary of the experiments configuration is provided in Table 4.2.

Table 4.2: Summary of simrs_v1 and simrs_v2 experiments configuration.

Experiment	**simrs_v1**	**simrs_v2**
Initial Conditions	WOA13 V2	WOA13 V2
Run period	2005-2015	2005-2015
Atlantic Ocean LOBC	Daily fields from CMEMS GLO-MFC	Daily fields from CMEMS GLO-MFC
Dardanelles Strait LOBC	Daily fields from CMEMS GLO-MFC and TSS box model daily climatological fields	Daily fields from CMEMS GLO-MFC and TSS box model daily climatological fields
Number of rivers	7 (from line 1 to 7 in Table 4.1, column *River name*)	39 (from line 1 to 39 in Table 4.1, column *River name*)
Rivers salinity	From line 1 to 7 in Table 4.1, column S	From line 1 to 39 in Table 4.1, column S
Rivers temperature	SST of the river grid point(s) implementation	SST of the river grid point(s) implementation

4.2 Evaluation and validation of experimental results

4.2.1 Water fluxes

As a first step, the numerical Mediterranean Sea hydrologic cycle is analyzed, as well as the differences between the freshwater components of hydrologic cycle between the two considered experiments (Figure 4.4).

The climatological hydrologic cycle is well reproduced by both experiments according to Mariotti et al. (2002) [127], see Figure 4.3, with simrs_v2 showing lower values for upward water flux (given by E - P - R), due to the increase in the runoff (R) component.

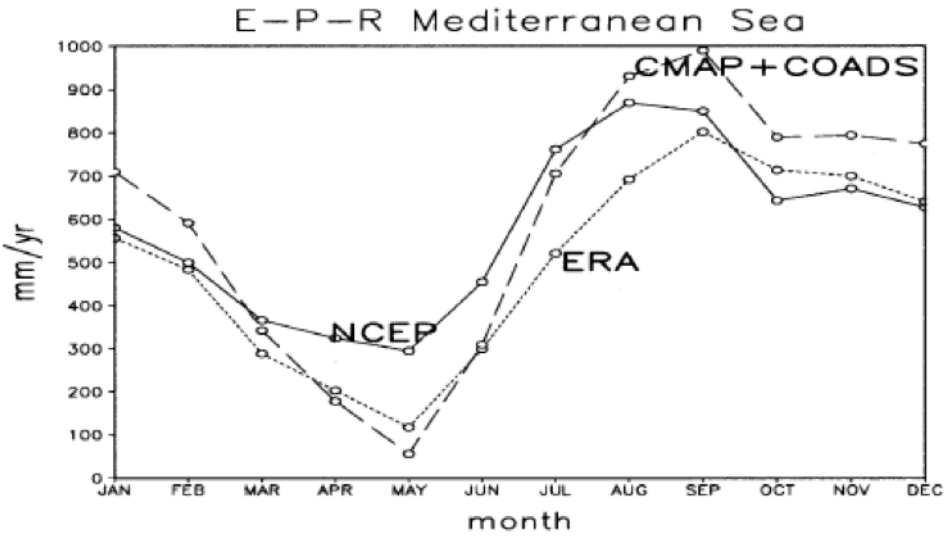

Figure 4.3: Climatological seasonal cycle of area-averaged Mediterranean freshwater flux (period 1979–93). Reproduced from Mariotti et al. (2002) [127]

The mean annual runoff discharge in experiment simrs_v2 is increased of about the 70 % with respect to simrs_v1, from about 164 $km^3/year$ to 280 $km^3/year$, still far from literature estimates described in section 1.4.2 (since it does not account for minor rivers), but much closer with respect to the riverine freshwater flux used in experiment simrs_v1.

In Figure 4.5 maps of the seasonal climatological upward water flux (E - P - R) differences between experiments simrs_v1 and simrs_v2 (simrs_v2 values - simrs_v1 values) are shown; since precipitation (P) is unchanged between the two experiments and runoff (R) has direct effects only locally (i.e. on the grid points where rivers are implemented), the differences in the upward water flux are mainly due to differences in evaporation rate (E), as can be deduced by Figure 4.6. This is due to differences in SST between the two experiments that will be shown in the following.

Both upward water flux (Figure 4.5) and evaporation (Figure 4.6) seasonal maps of differences generally show positive and negative values in the basin with a stronger negative pattern in the Adriatic Sea and a positive one in the area of the Gulf of Lion.

The main differences in upward water flux between the two experiments can be observed during Autumn and Winter, which are the two seasons characterized by both a high evaporation rate and a large riverine input, in particular in the Adriatic Sea, where the increased number of rivers included in experiment simrs_v2 has significantly lowered the upward water flux with respect to simrs_v1.

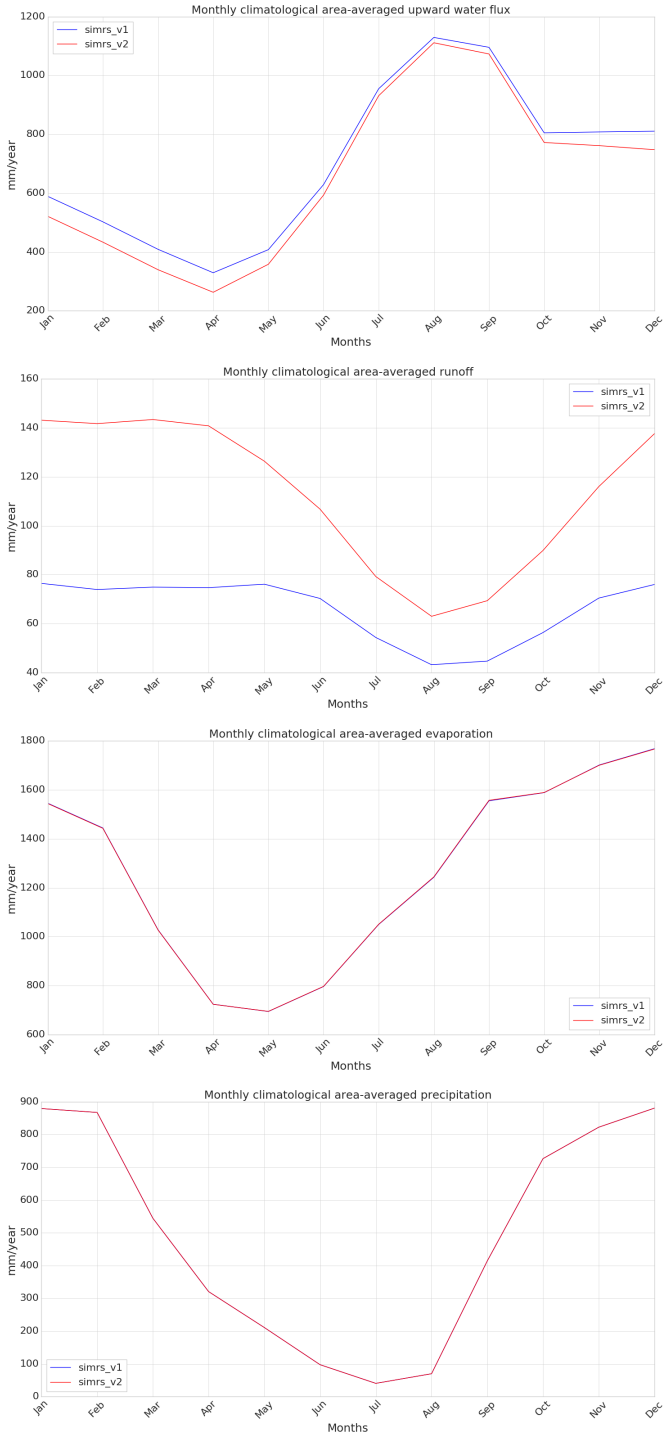

Figure 4.4: Monthly climatological area-averaged hydrologic cycle and its components for simrs_v1 and simrs_v2. From top to bottom panel: upward water flux, runoff, evaporation, precipitation.

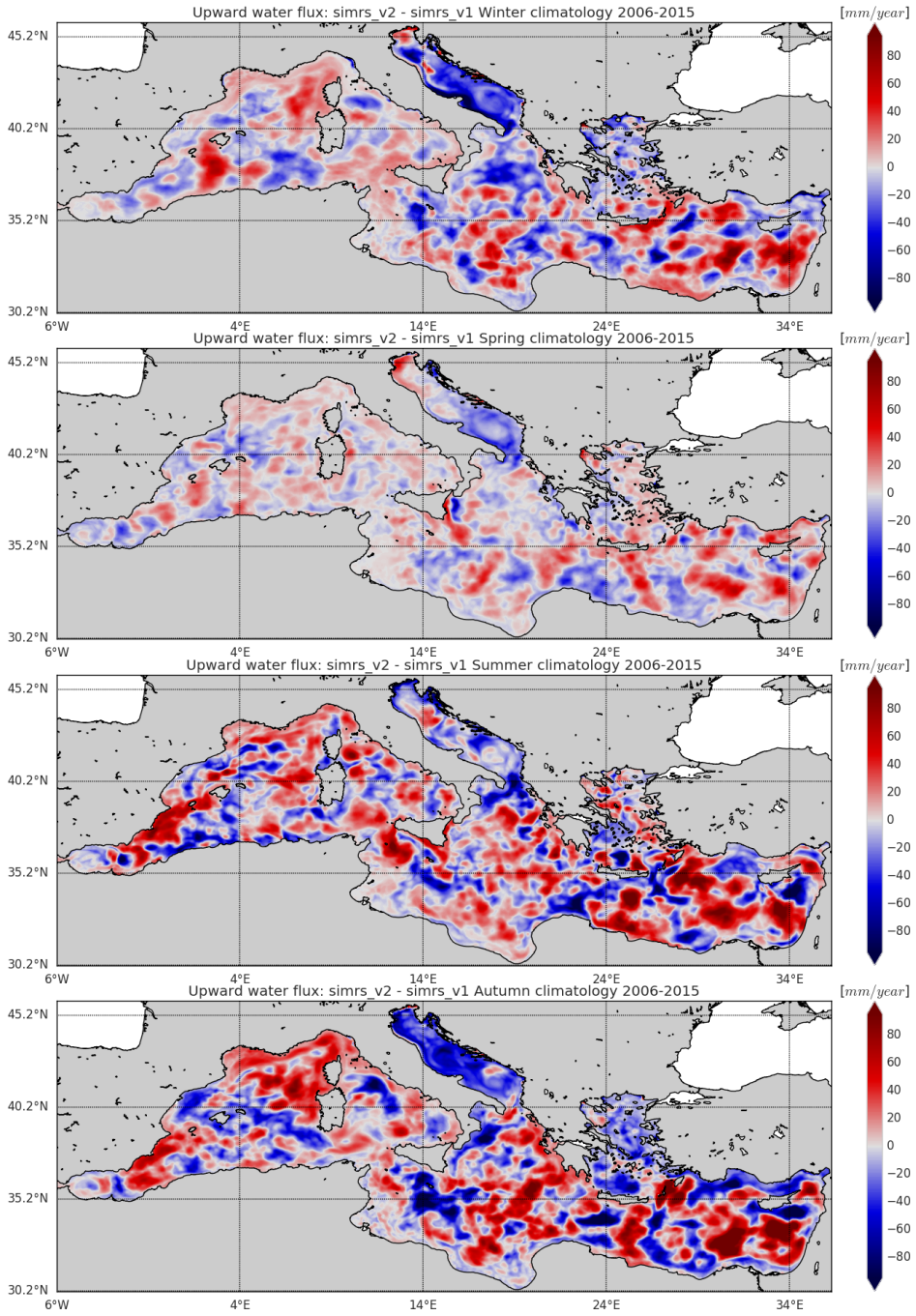

Figure 4.5: Seasonal climatological upward water flux (E - P - R) differences between experiments simrs_v1 and simrs_v2. From top to bottom panel: Winter (Jan - Mar), Spring (Apr - Jun), Summer (Jul - Sep) and Autumn (Oct - Dec).

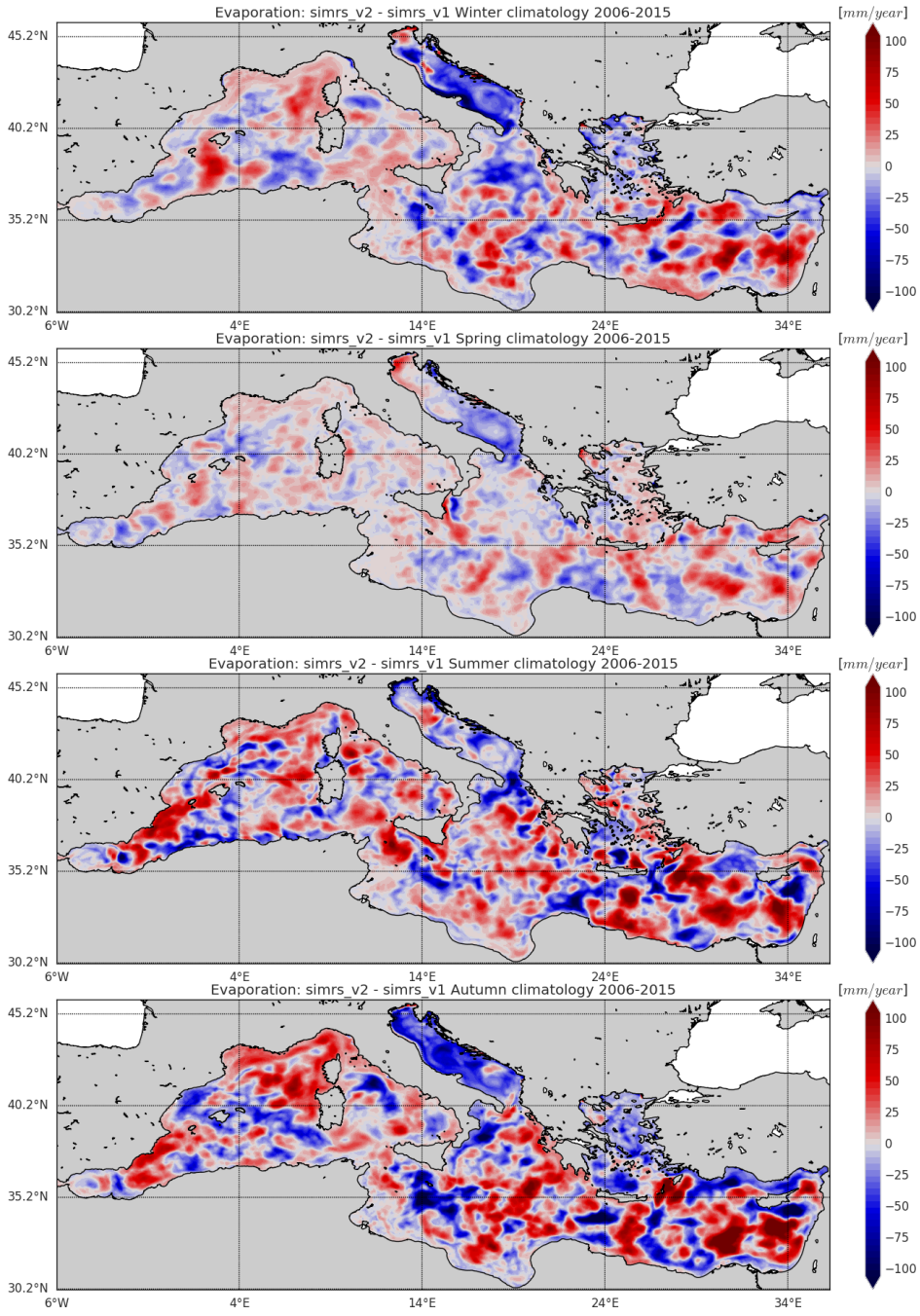

Figure 4.6: Seasonal evaporation rate differences between experiments simrs_v1 and simrs_v2. From top to bottom panel: Winter (Jan - Mar), Spring (Apr - Jun), Summer (Jul - Sep) and Autumn (Oct - Dec).

4.2.2 Temperature and salinity comparison with in situ observations

In the following, the results of the numerical experiments described in the previous sections are analyzed and compared with the available observations to evaluate the model skill and evaluate how the thermohaline properties and the dynamics of the Mediterranean Sea are affected by different riverine forcings.

First of all, an evaluation of the models skills in reproducing temperature and salinity for the whole Mediterranean Sea and for different sub-regions of the basin (see Figure 4.7) at different depths is shown, through the comparison of model results with Argo floats, XBTs, gliders and satellite data available for the simulation period (see section 2.3).

The evaluation of the Mixed Layer Depth (MLD) with respect to climatological values is then shown, in addition to an analysis of the transport at straits.

Finally, an evaluation of the climatological circulation is shown, in order to highlight the differences between the performed experiments in terms of impacts on the Mediterranean Sea dynamics, in particular for the areas where the largest number of rivers are added.

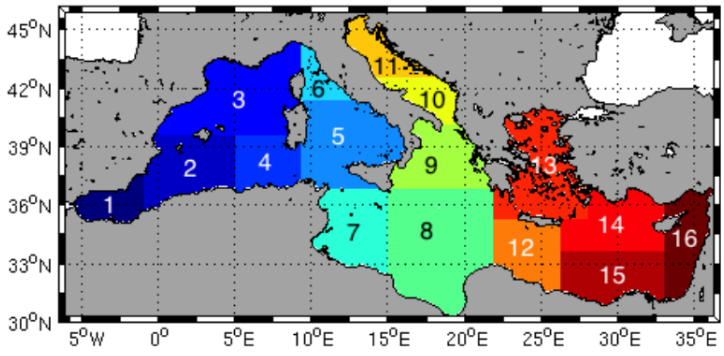

Figure 4.7: The Mediterranean Sea sub-regions subdivision for validation metrics.

Root Mean Square Error (RMSE) and BIAS metrics are used to assess the skill of the modelling results. which are defined as:

$$RMSE = \sqrt{\frac{1}{N}\sum_{i=1}^{N}(M_i - O_i)^2} \tag{4.1}$$

$$BIAS = \frac{1}{N}\sum_{i=1}^{N}(M_i - O_i) \tag{4.2}$$

where M represents the model fields, O the observations and N is the number of data.

In the following, the statistics for the entire basin and for selected sub-regions is shown.

As displayed in Figure 4.8, which shows the RMSE and BIAS for salinity in the Mediterranean Sea at different layers, experiment simrs_v2 presents a lower salinity RMSE with respect to experiment simrs_v1 from the sea surface down to 60 m depth for the considered period: the first two layers show a decreased error of about 10%.

On the contrary, a slight worsening can be noticed from 60 m down to 300 m depth, while same results are achieved below 300 m, where the impact of the modified river setup is negligible.

The salinity BIAS shows an underestimation of the model salinity with respect to observations in particular when increasing the freshwater sources.

Concerning temperature skill at Mediterranean Sea basin scale, the two experiments show very similar results as displayed in Figure 4.9, indicating that the implementation of the new 32 runoff sources in experiment simrs_v2 has no significant impact on temperature at basin scale, since the temperature associated to the river inputs is the one of the model surface.

Let's now consider the performances of the two considered experiments in reproducing salinity (Figure 4.10) and temperature (Figure 4.11) at sub-regional scale, in particular in the sub-regions where the largest number of rivers has been added in simrs_v2 with respect to simrs_v1.

The North Eastern Ionian Sea (sub-region 9 in Figure 4.7) salinity skill of the two considered experiments is very similar, even though slightly lower salinity RMSE values can be observed for simrs_v1 with respect to simrs_v2, the latter experiment showing excessively low salinity values, as can be noticed from the BIAS.

Experiment simrs_v2 shows a significant improvement both in Southern Adriatic Sea (sub-region 10 in 4.7) and in Northern Adriatic Sea (sub-region 11 in 4.7) in reproducing the observed salinity values in the first 30 m of the water column, while it shows a worsening from 60 m depth down to 600 m.

For both the sub-regions of the Adriatic Sea, experiment simrs_v1 has a large positive BIAS in the first 30 m of the water column, strongly reduced

in experiment simrs_v2; on the contrary, from 60 m depth down to 600 m simrs_v2 has a large negative BIAS, corresponding to an excessive freshening of the water column.

In the Aegean Sea (sub-region 13 in Figure 4.7) the implementation of several freshwater sources did not produce a significant impact, even though a slight worsening in salinity representation skill can be noticed in simrs_v2 with respect to simrs_v1 in the depth range between the surface and 30 m depth, due to an excessive freshening of the water column.

The implementation of the Turkish rivers in simrs_v2 produced a positive impact on salinity representation skill in the North-Central Levantine Sea (sub-region 14 in Figure 4.7) for what concern the first 60 m of the water column, due to a freshening in this depth range, while at greater depths simrs1̌ and simrs_v2 show very similar results; the positive impact in noticeable also for the Eastern Levantine Sea (sub-region 16 in Figure 4.7), but only at depths greater than 150 m, while in the upper part of the water column no changes are detected between the two considered experiments.

In the Western Levantine Sea (sub-region 12 in Figure 4.7), experiment simrs_v2 shows constantly lower salinity RMSE values along the whole water column with respect to simrs_v1, with an increased salinity from the surface down to 150 m depth.

Differences between the two considered experiments can be observed also in the Southern Tyrrhenian Sea and Northern Tyrrhenian Sea (sub-regions 5 and 6 respectively in Figure 4.7), where Arno, Tevere and Volturno rivers have been implemented in experiment simrs_v2.

In the Southern Tyrrhenian Sea the major differences between the two

experiments can be noticed from the surface down to 150 m which are characterized by a constant fresher BIAS for experiment simrs_v2 with respect to experiment simrs_v1. As well as for the Southern Tyrrhenian Sea, also for the Northern Tyrrhenian Sea sub-region the main differences between the two experiments are concentrated in the first 150 m of the water column.

A slight improvement in salinity skill can be observed in the first 30 m of the North West Mediterranean Sea (sub-region 3 in Figure 4.7), which is observable also in the upper water column of the eastern part of the South Mediterranean Sea (sub-region 3 in Figure 4.7), probably due to the connection between the two sub-regions which are linked by the Liguro-Provencal-Catalan Current.

Concerning the temperature skill, in the North Eastern Ionian Sea the considered experiments show very similar results, even though simrs_v2 shows a general, even though slight, improvement from the surface down to 100 m depth, and a worsening from 100 to 600 m depth.

Experiment simrs_v2 shows a general worsening with respect to experiment simrs_v1 along the entire water column for both sub-regions 10 and 11, more pronounced from 30 m depth down to 600 m, which is more evident in the Northern Adriatic Sea with respect to the Southern Adriatic Sea.

It has to be stressed that statistics for the Adriatic Sea (in particular for the Northern part of the sub-basin) are strongly influenced by the scarcity of data available from Argo floats, XBTs and gliders, and a careful analysis of the behavior of experiment simrs_v2 is essential in order to understand the reasons of a worsening in model performances.

In the Aegean Sea, the temperature RMSE values are very similar between

the two experiments, even though a slight improvement can be noticed in simrs_v2 from the surface down to 60 m depth, and a slight worsening with respect to simrs_v1 for the rest of the water column.

The salinity representation skill improvement in the North-Central Levantine Sea is not accompanied by an equivalent temperature representation skill improvement in simrs_v2, which has worse performances with respect to simrs_v1 along the whole water column, due to an excessive cooling with respect to simrs_v1.

Significant improvements can be instead noticed in simrs_v2 temperature skill in the Eastern Levantine Sea, with experiment simrs_v2 showing a constantly lower RMSE along the whole water column with respect to simrs_v1, due to a significant warming with respect to experiment simrs_v1, as highlighted by BIAS values.

Western Levantine Sea shows lower temperature RMSE values for the whole water column (except for the depth range 60-100 m) in experiment simrs_v2 with respect to simrs_v1, in particular from 100 to 600 m depth; in particular, BIAS indicates higher salinity values in simrs_v2 with respect to simrs_v1 from the surface down to 100 m.

In the Alboran Sea (sub-region 1 in Figure 4.7) a constantly lower temperature RMSE in experiment simrs_v1 can be noticed from the surface down to 600 m depth, due to a warming of the water column from the surface down to 60 m depth with respect to experiment simrs_v2, while a cooling of the water column from 100 to 600 m depth is shown by BIAS values.

In the Western part of the South-Western Mediterranean Sea an improvement in temperature skill for experiment simrs_v2 is evident from the surface

down to 150 m depth, due to a general cooling of the water column with respect to experiment simrs_v1, while simrs_v1 show better performances from 150 m depth down to 600 m depth.

In the Eastern part of the South-Western Mediterranean Sea (sub-region 4 in Figure 4.7) the temperature RMSE is almost constantly lower for experiment simrs_v1 with respect to simrs_v2, due to a general cooling of the water column, as noticeable from the BIAS values of the two considered experiments.

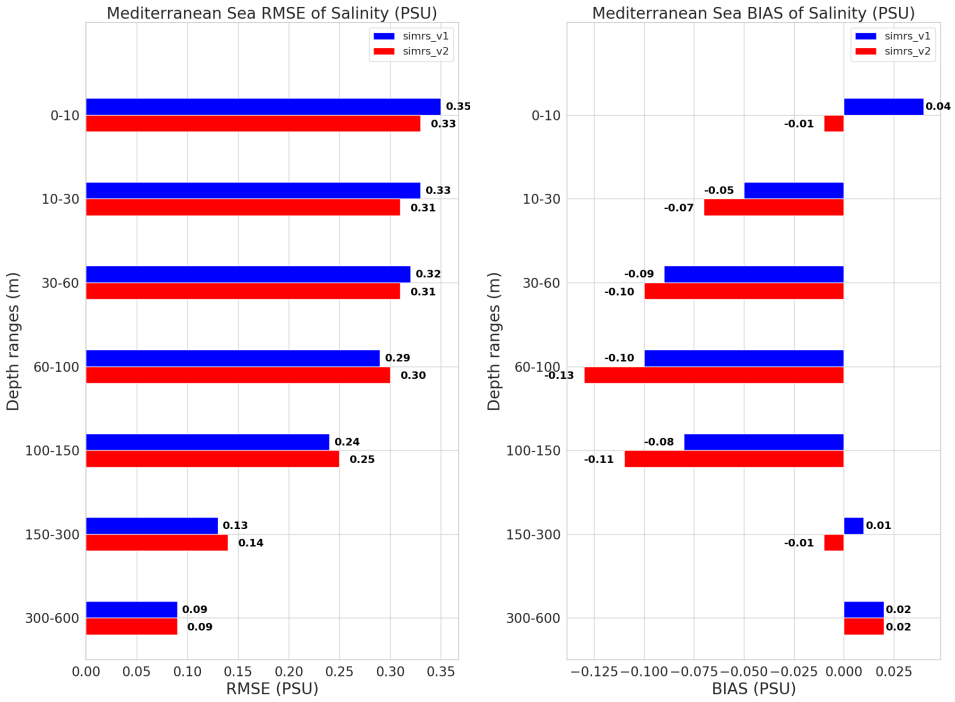

Figure 4.8: Mediterranean Sea mean RMSE and BIAS of salinity (PSU) for experiments simrs_v1 and simrs_v2.

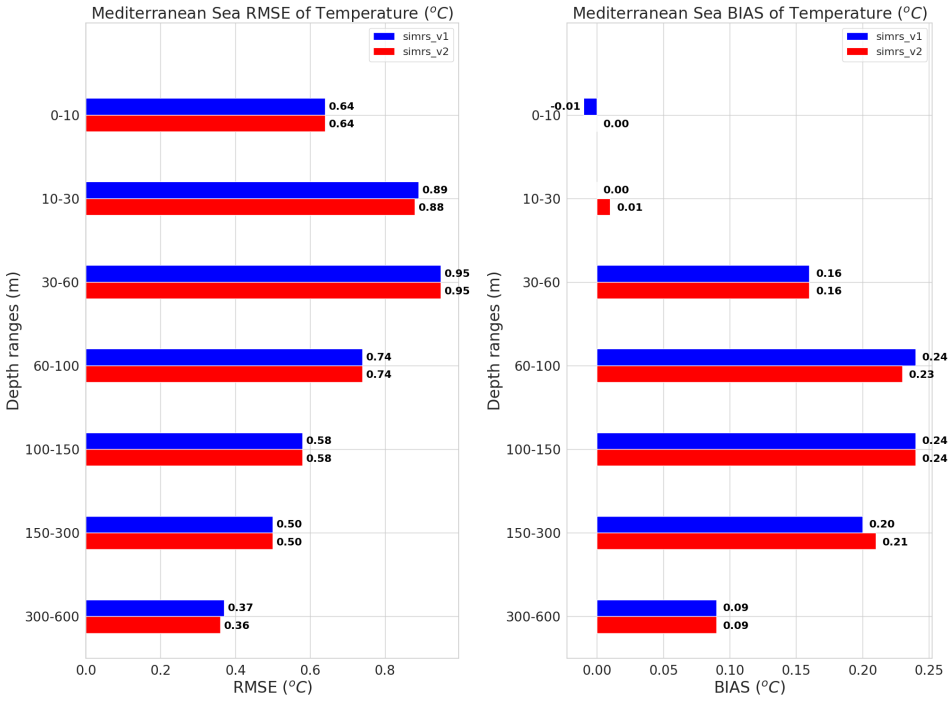

Figure 4.9: Mediterranean Sea mean RMSE and BIAS of temperature (°C) for experiments simrs_v1 and simrs_v2.

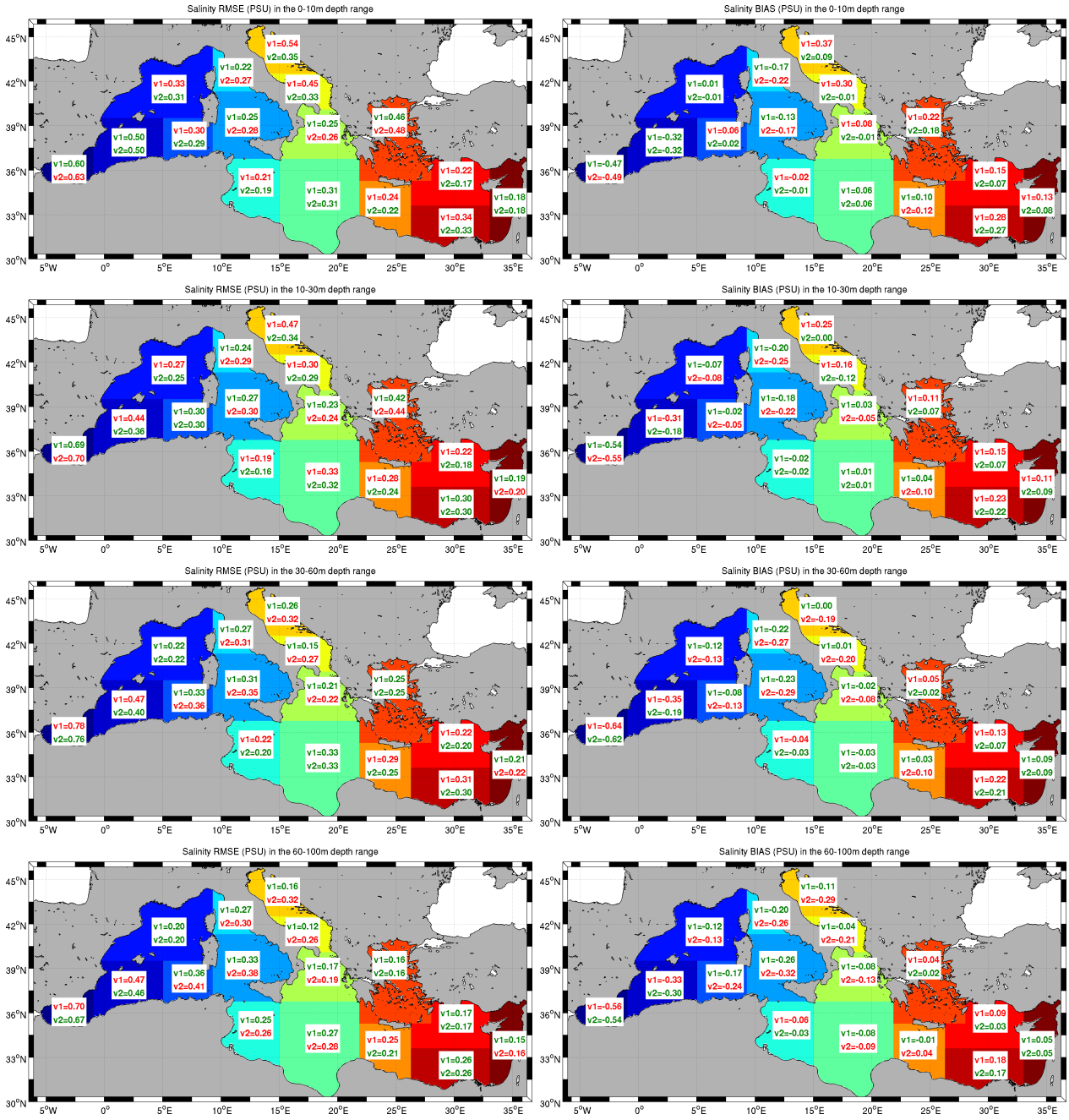

Figure 4.10: Sub-regional mean RMSE and BIAS of salinity (PSU) for experiments simrs_v1 and simrs_v2 at selected depth ranges. For each sub-region the experiment with the lowest salinity RMSE and BIAS is indicated in green, while the experiment with the highest salinity RMSE and BIAS is indicated in red.

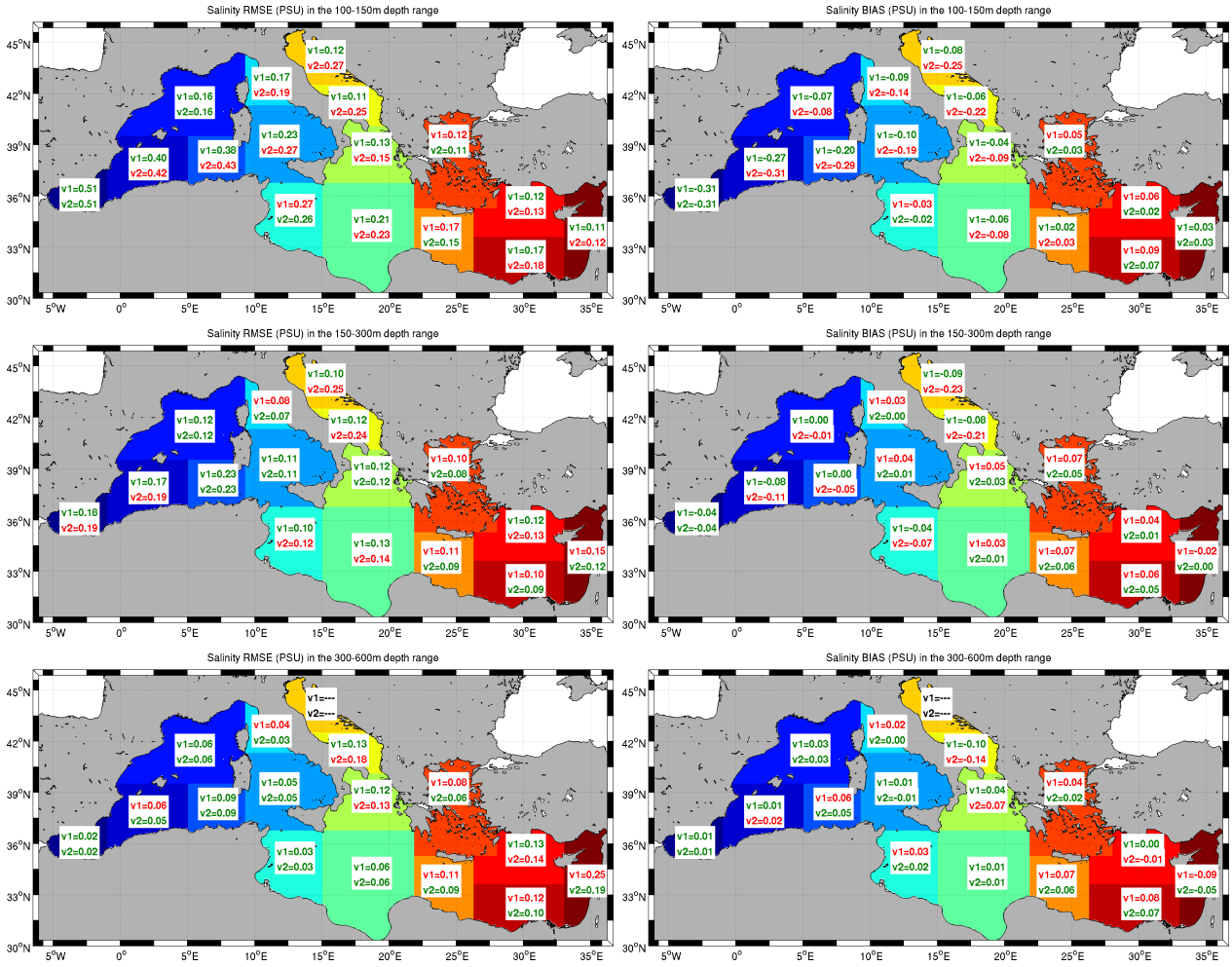

Figure 4.10: Sub-regional mean RMSE and BIAS of salinity (PSU) for experiments simrs_v1 and simrs_v2 at selected depth ranges. For each sub-region the experiment with the lowest salinity RMSE and BIAS is indicated in green, while the experiment with the highest salinity RMSE and BIAS is indicated in red (continued).

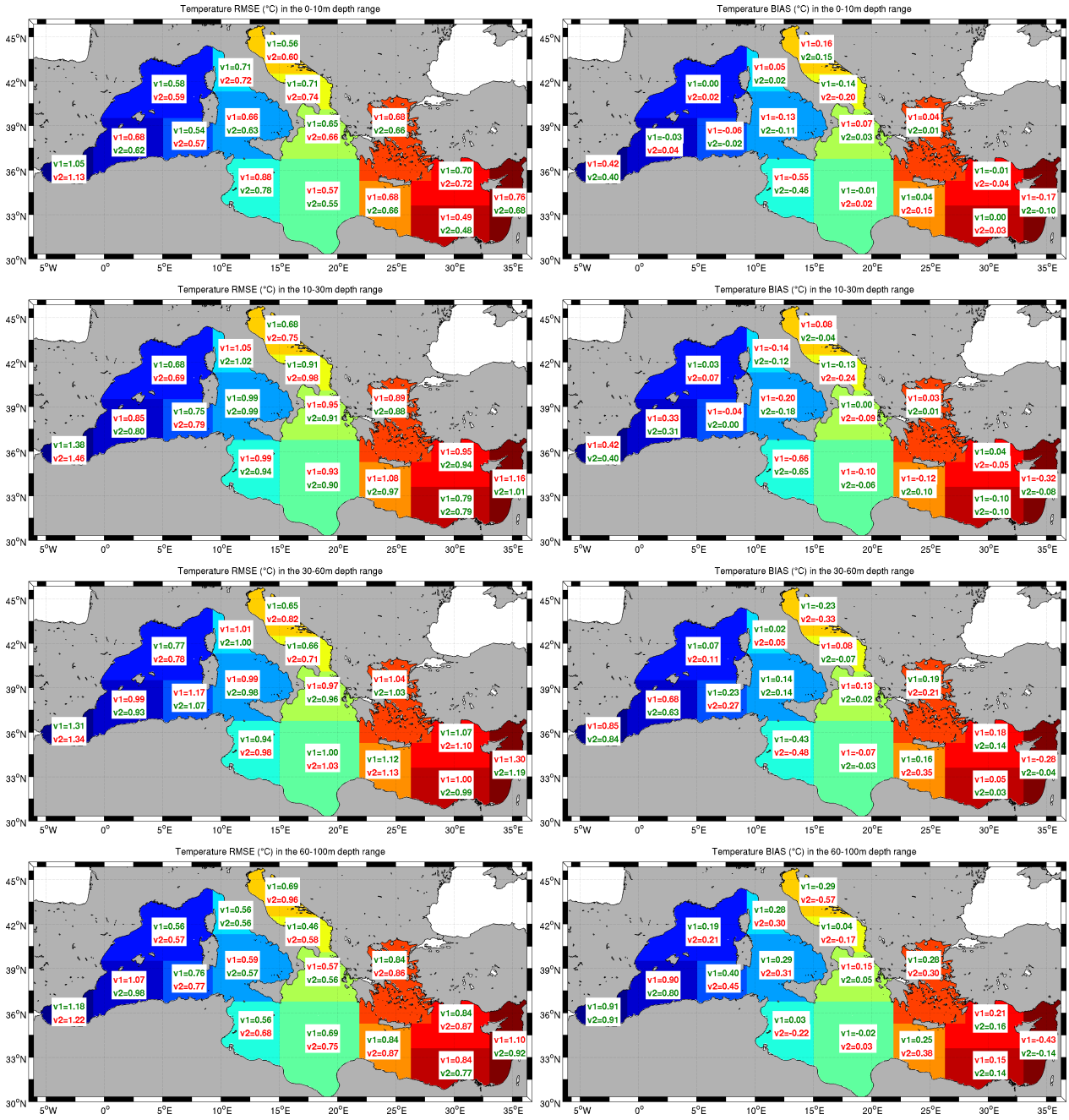

Figure 4.11: Sub-regional mean RMSE and BIAS of temperature (°C) for experiments simrs_v1 and simrs_v2 at selected depth ranges. For each sub-region the experiment with the lowest temperature RMSE and BIAS is indicated in green, while the experiment with the highest temperature RMSE and BIAS is indicated in red.

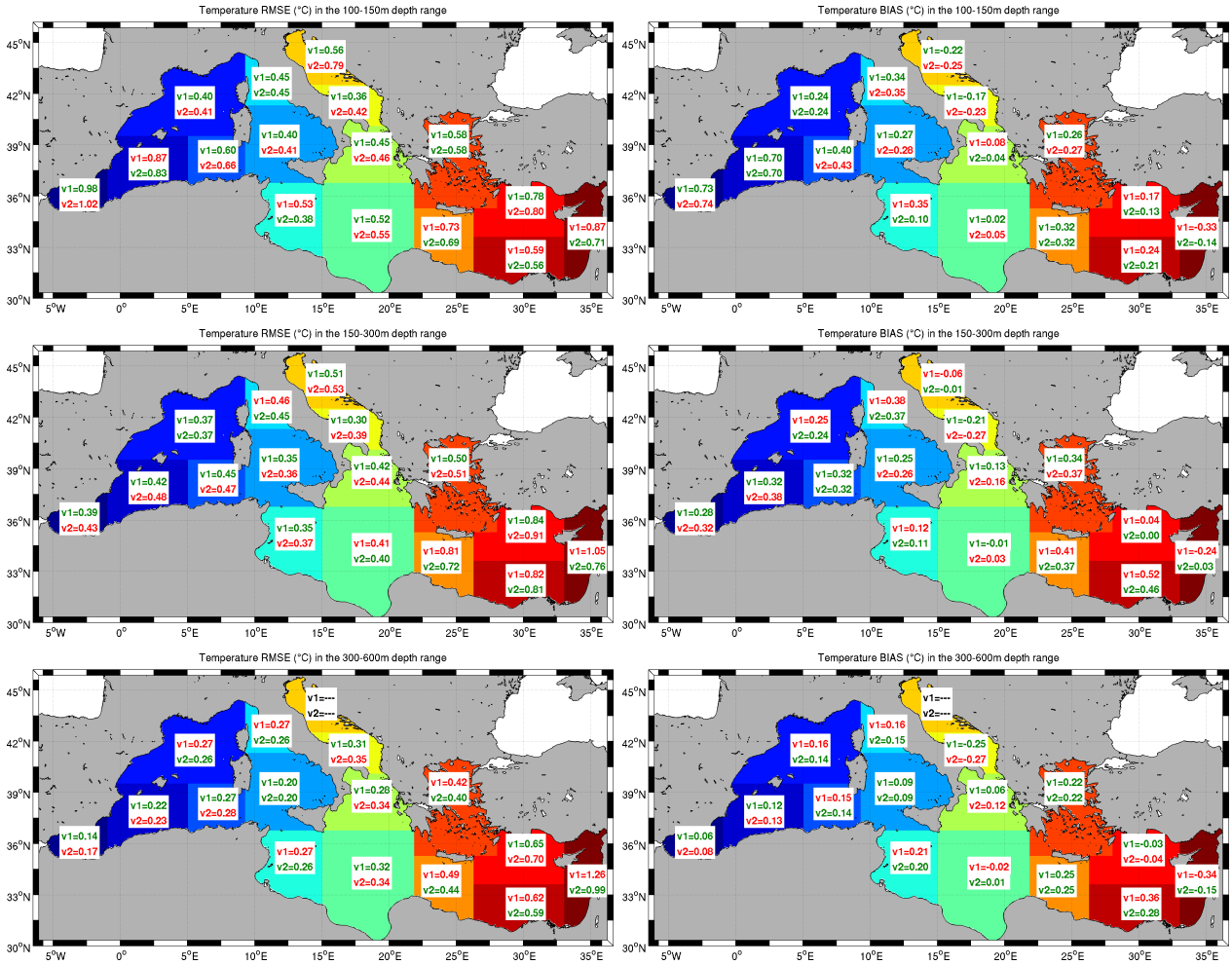

Figure 4.11: Sub-regional mean RMSE and BIAS of temperature (°C) for experiments simrs_v1 and simrs_v2 at selected depth ranges. For each sub-region the experiment with the lowest temperature RMSE and BIAS is indicated in green, while the experiment with the highest temperature RMSE and BIAS is indicated in red (continued).

4.2.3 Temperature and salinity comparison with climatological data sets and satellite data

In this section the numerical results for temperature and salinity are evaluated and compared with respect to SeaDataNet V1.1 (hereafter SDN) and World Ocean Atlas 2013 version 2 (hereafter WOA) climatology data sets, in order to get insights about the distribution patterns of the performed experiments and about the temporal evolution of tracers derived from the numerical simulations with respect to the considered observational data set.

Considering the vertical mean profiles of temperature and salinity for numerical experiments and climatological data sets for the different areas of the Mediterranean basin, the area showing the largest differences among the two considered experiments is the central Mediterranean Sea (sub-regions from 5 to 11 in Figure 4.7), with differences in salinity profiles evident from the surface (about 0.1 PSU) and gradually decreasing down to about 250 m depth. No significant differences can be observed for temperature (4.12).

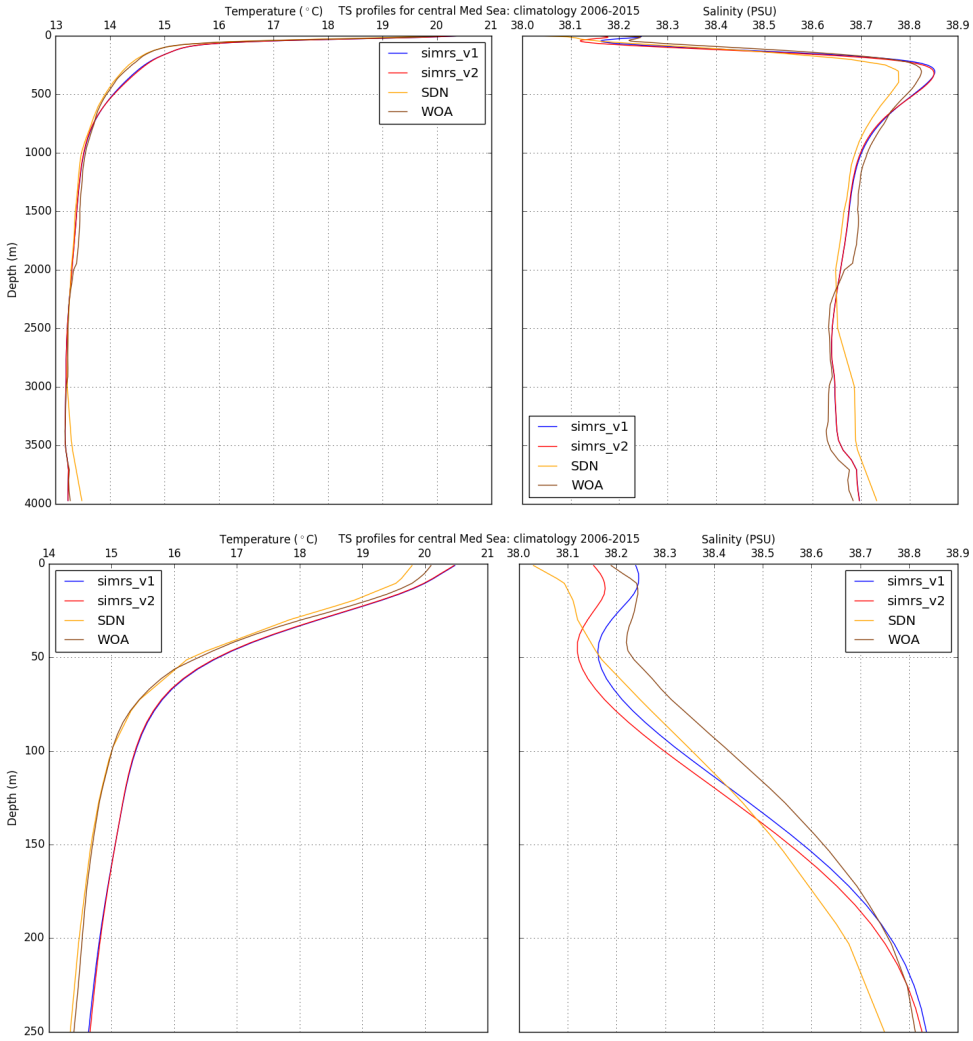

Figure 4.12: Temperature and salinity climatological profiles in central Mediterranean Sea for the whole water column (top panel) and for the depth range 0-250 m (bottom panel) over the period 2006-2015 for experiments simrs_v1, simrs_v2 and SDN and WOA climatological data sets.

Maps of climatological means of both experiments simrs_v1 and simrs_v2 are computed and compared with the climatologies from SDN and WOA

data sets (from Figure 4.13 to Figure 4.16).

Since the largest differences in salinity between experiments simrs_v1 and simrs_v2 can be noticed at surface, Figure 4.13 presents the sea surface salinity for the entire Mediterranean Sea, showing that in general the numerical experiments are in good agreement with climatological data sets, with larger salinity values in the eastern basin, decreasing westward and minimum values in the North Aegean Sea and in the Northern Adriatic Sea.

Moreover the main differences between the two experiments are located in the Adriatic Sea, where the 13 additional rivers implemented in simrs_v2 provide a general freshening of the sub-basin in line with the climatological data set.

The largest differences can be observed in the northernmost part of the Adriatic Sea (more than 1 PSU), in the coastal region spanning from the Conero Promontory to the Gulf of Trieste.

The Po river plume shows large differences between the two experiments, both in terms of surface salinity values and of zonal and meridional extension: in experiment simrs_v2 the Po river plume is more pronounced, with a southward extension larger with respect to simrs_v1 , beyond the Gargano Promontory, and with lower salinity values with respect to simrs_v1, probably thanks to the signal of the new rivers implemented in the Northern Adriatic Sea. In addition, also the offshore extension of the Po river plume seems to be larger in simrs_v2, while in experiment simrs_v1 it is more confined close to the coast.

Experiment simrs_v2 in general presents lower salinity in the North-Eastern Ionian Sea and in the Levantine Sea, in agreement with climatological data

sets, while larger salinity values can be noticed in the western part of the basin.

The remaining part of the Mediterranean Sea presents much smaller differences between the two experiments, with values generally ranging from -0.1 PSU to 0.1 PSU.

Concerning the temperature pattern, since the largest differences between the two considered experiments don't occur at surface, Figure 4.14 presents the temperature at 30 m depth.

An area of negative BIAS is evident in the Adriatic Sea, with simrs_v2 temperature values lower with respect to simrs_v1, as well as for the Aegean Sea, even though the magnitude of the differences are smaller. In addition, it can be noticed that the negative anomaly observable in the Adriatic Sea propagates into the North-Eastern Ionian Sea, spread by the Western Adriatic Coastal Current.

Positive anomalies can be generally observed on the contrary in the north western Mediterranean Sea, in particular in correspondence of the area interested by the Liguro-Provencal-Catalan Current.

For what concern the eastern part of the Mediterranean Sea basin a large positive BIAS in simrs_v2 with respect to simrs_v1 can be observed in correspondence of the Rhodes Gyre and of Shikmona Gyre, while lower temperature values occur along the Asia Minor Current path.

Both the experiments show generally higher temperature values with respect to SDN and WOA climatological data sets, in particular along the African coast from Tunisia to Egypt and then northward up to the Turkish coast. The lower temperature values in the Adriatic and Aegean Seas

achieved in simrs_v2 are closer to the climatological data sets.

Since the area affected by the largest differences between simrs_v1 and simrs_v2 both for salinity and temperature is the Adriatic Sea sub-basin, Figure 4.15 and Figure 4.16 respectively show the surface salinity and the 30 m temperature of the seasonal mean model differences.

The differences in the Adriatic surface salinity (Figure 4.15) are always negative, in particular in the northernmost part of the sub-basin, confirming the lower salinity content in simrs_v2 in all seasons.

The negative salinity anomaly spreads eastward towards the interior of the basin during Spring and Summer: this could be generated by the heat input occurring during the warmer seasons that stabilizes the water column, conveying the additional freshwater input from the added rivers towards the central part of the Northern Adriatic basin (Orlić et al. (1992) [128]).

This seems to be confirmed by the salinity anomaly distribution in Winter and Autumn, which is much more confined towards the Italian coast with respect to Spring and Summer: this can be reasonably considered as an effect of the many rivers added in the northernmost part of the Adriatic Sea, whose signal is spread along the Italian coast by the Western Adriatic Coastal Current.

The seasonal temperature differences at 30 m depth are particularly significant in the Adriatic Sea and in the North Eastern Ionian Sea, where a clear seasonal cycle in the temperature anomaly pattern is observable (Figure 4.16).

In simrs_v2 a larger riverine discharge with associated temperature equal to the SST and associated salinity lower with respect to the basin salinity

introduces modifications to the vertical mixing whose effects are observable in the 30 m depth temperature pattern.

During Winter and Spring the Po river plume is characterized by a positive temperature anomaly with respect to simrs_v1, while the inner part and the eastern part of the Adriatic Sea show a general cooling in simrs_v2, more pronounced in the southern part of the basin.

A general cooling in simrs_v2 occurs in Summer and Autumn and affects the entire Adriatic Sea, in particular during Summer.

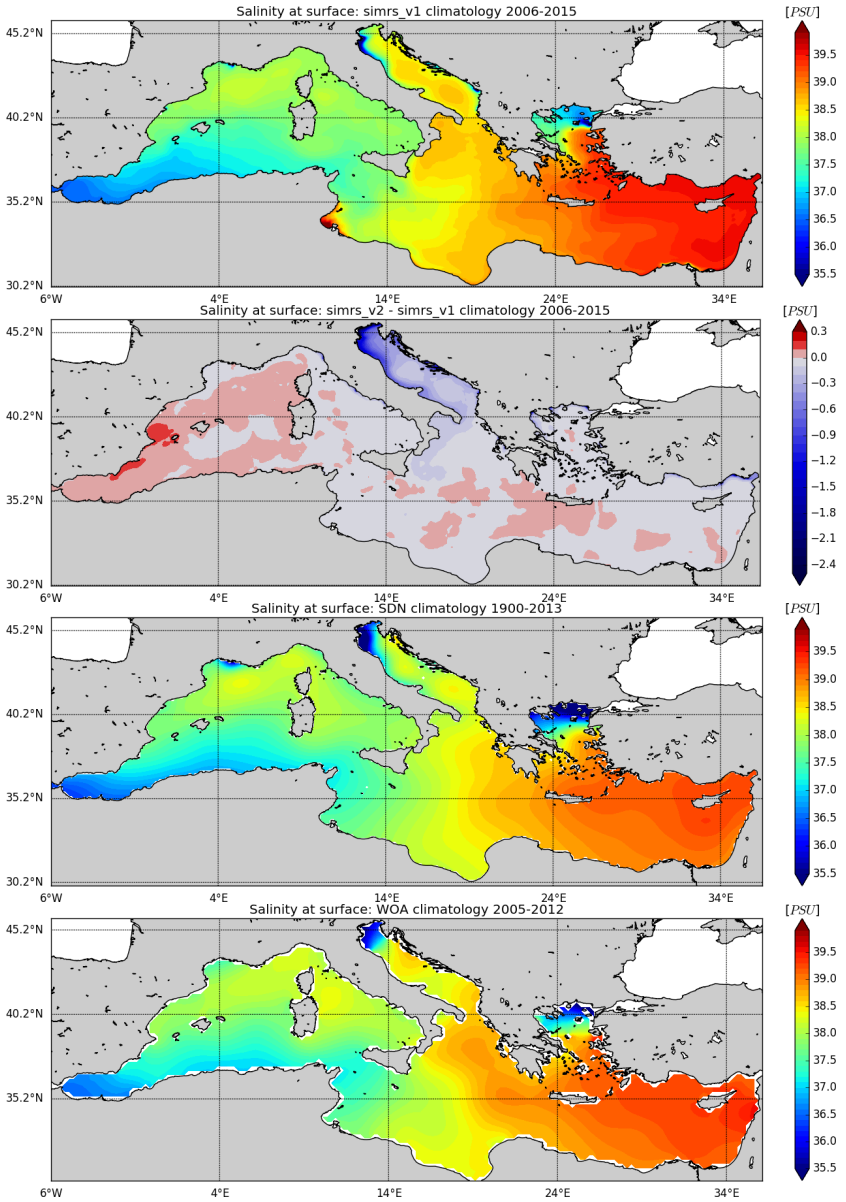

Figure 4.13: Salinity climatology at surface. From top to bottom panel: simrs_v1, simrs_v2 - simrs_v1, SDN, WOA.

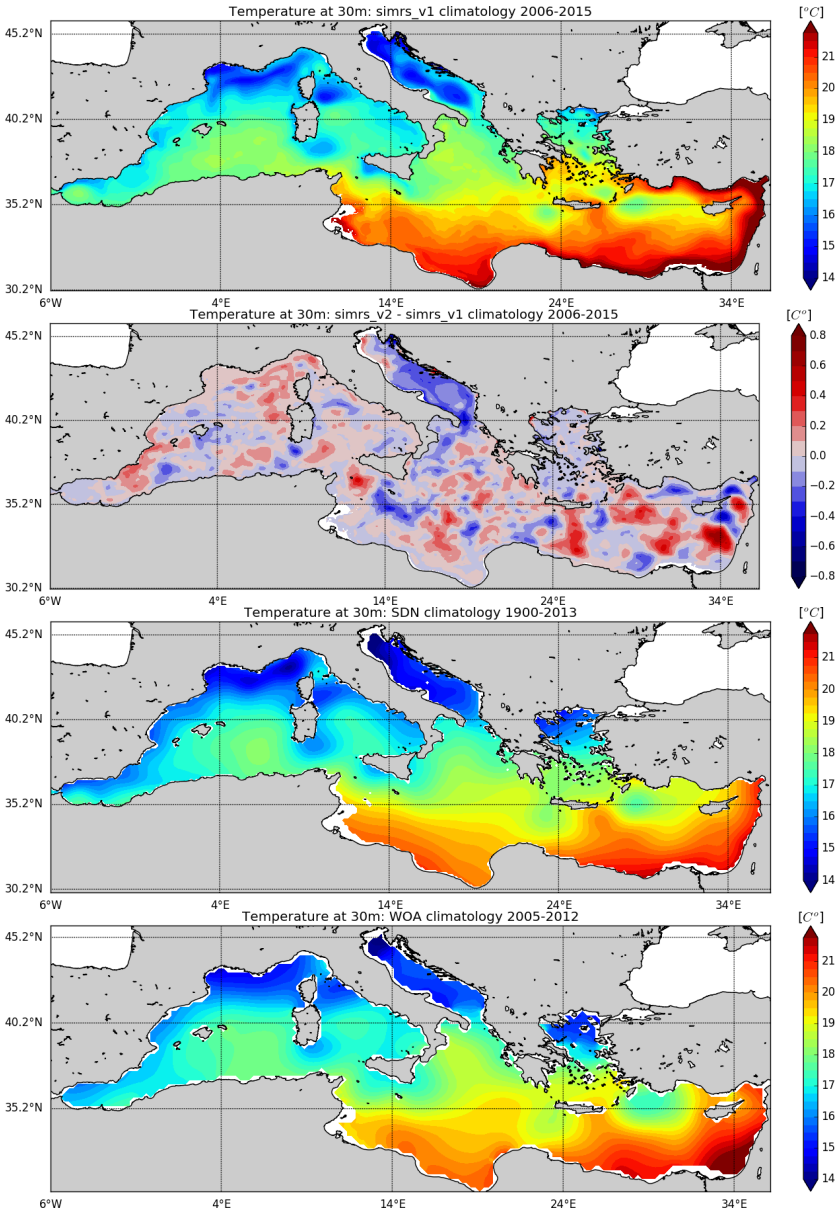

Figure 4.14: Temperature climatology at 30 m depth. From top to bottom panel: simrs_v1, simrs_v2 - simrs_v1, SDN, WOA.

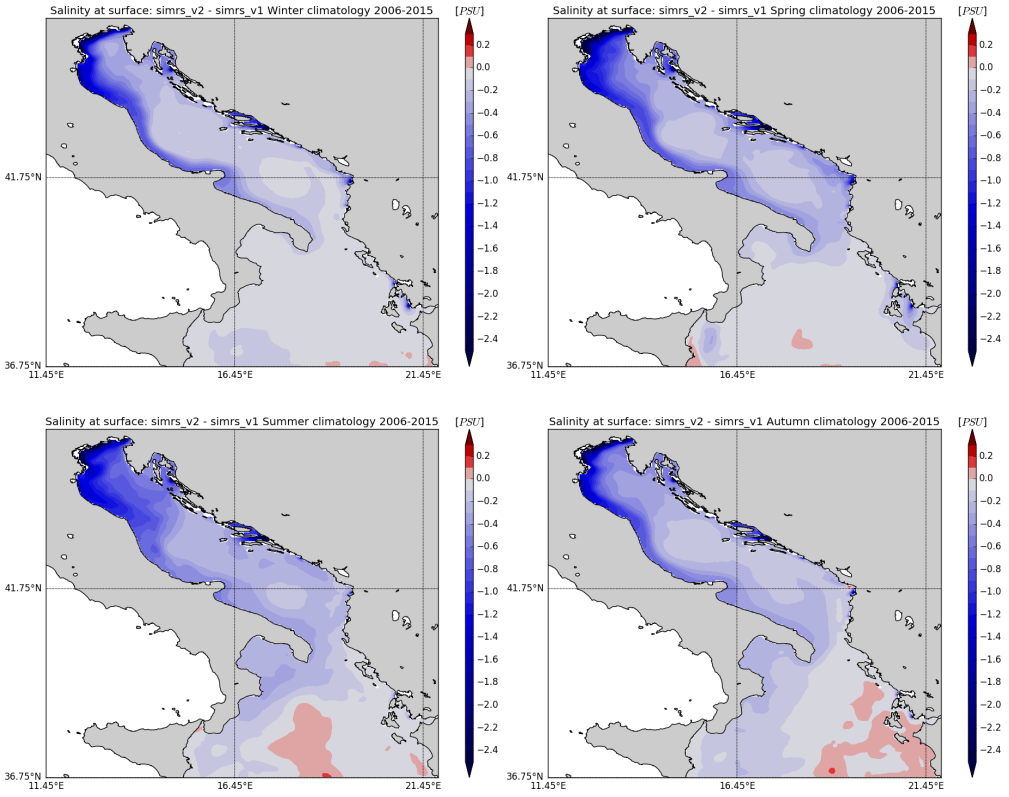

Figure 4.15: Salinity seasonal climatologies over the period 2006-2015 at surface for simrs_v2 - simrs_v1 difference. Top-left panel: Winter (Jan - Mar); top-right panel: Spring (Apr - Jun); bottom-left panel: Summer (Jul - Sep); bottom-right panel: Autumn (Oct - Dec).

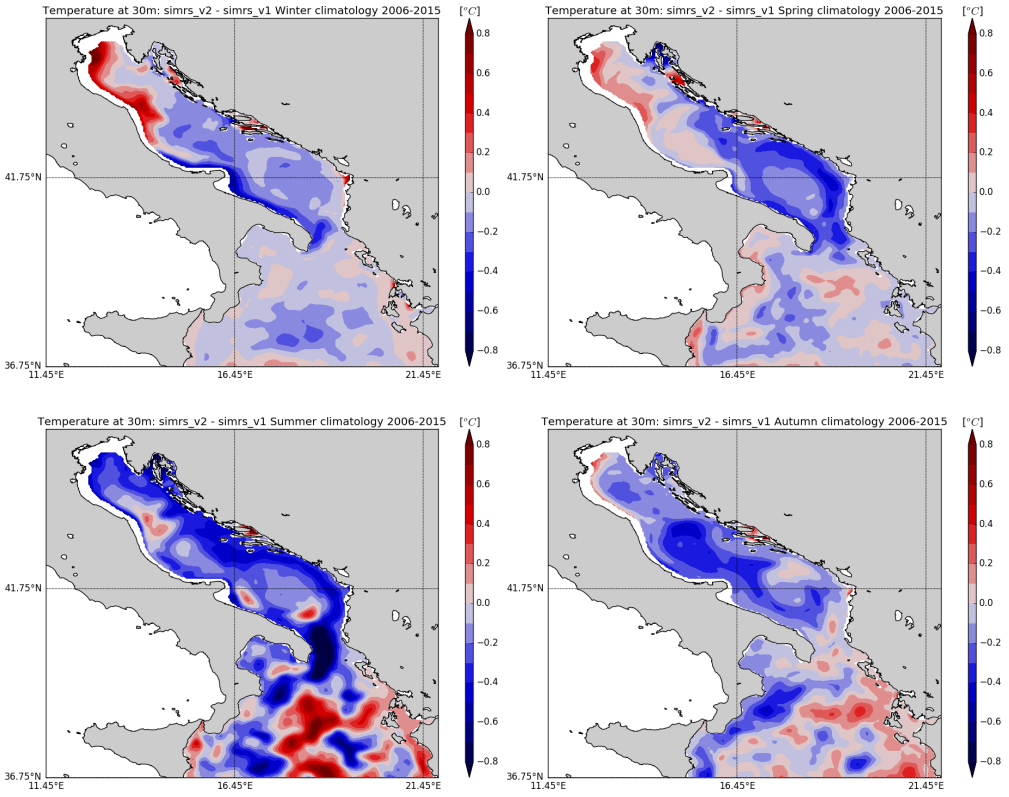

Figure 4.16: Temperature seasonal climatologies over the period 2006-2015 at 30 m depth for simrs_v2 - simrs_v1 difference. Top-left panel: Winter (Jan - Mar); top-right panel: Spring (Apr - Jun); bottom-left panel: Summer (Jul - Sep); bottom-right panel: Autumn (Oct - Dec).

In addition to the horizontal maps comparison, daily mean salinity time series from model outputs and SDN and WOA climatological data sets (Figure 4.17) are computed for sea surface and at different depth (WOA monthly climatological data set reaches the maximum depth of 1500 m, so for comparison at greater depths only SDN data set is considered).

simrs_v2 presents lower salinity values with respect to simrs_v1 for all the

considered layers. The model mean salinity presents a seasonal variability at surface with lower values during Winter and larger values during Summer. Both the experiments overestimate the climatologies, but simrs_v2 shows values closer both to SDN and WOA climatological data sets with respect to simrs_v1.

The average volume salinity of both experiments is larger than the SDN data set and shows a slightly positive trend.

In the depth range 0-100 m the two experiments well reproduce SDN climatological data sets, while they are both less saline than WOA; in particular simrs_v2 seems to better reproduce SDN values for all the periods of the year.

In the depth range 100-300 m both simrs_v1 and simrs_v2 show higher salinity values with respect to the two climatological data sets considered, even though simrs_v2 values are closer to the SDN and WOA ones. A positive trend can be noticed in the time series of both experiments, the one from simrs_v1 being more pronounced with respect to the one from simrs_v2 in particular from year 2011.

The volume mean salinity of the two experiments computed in the depth range between 300 m and the bottom is very similar and close to SDN despite a clear positive trend.

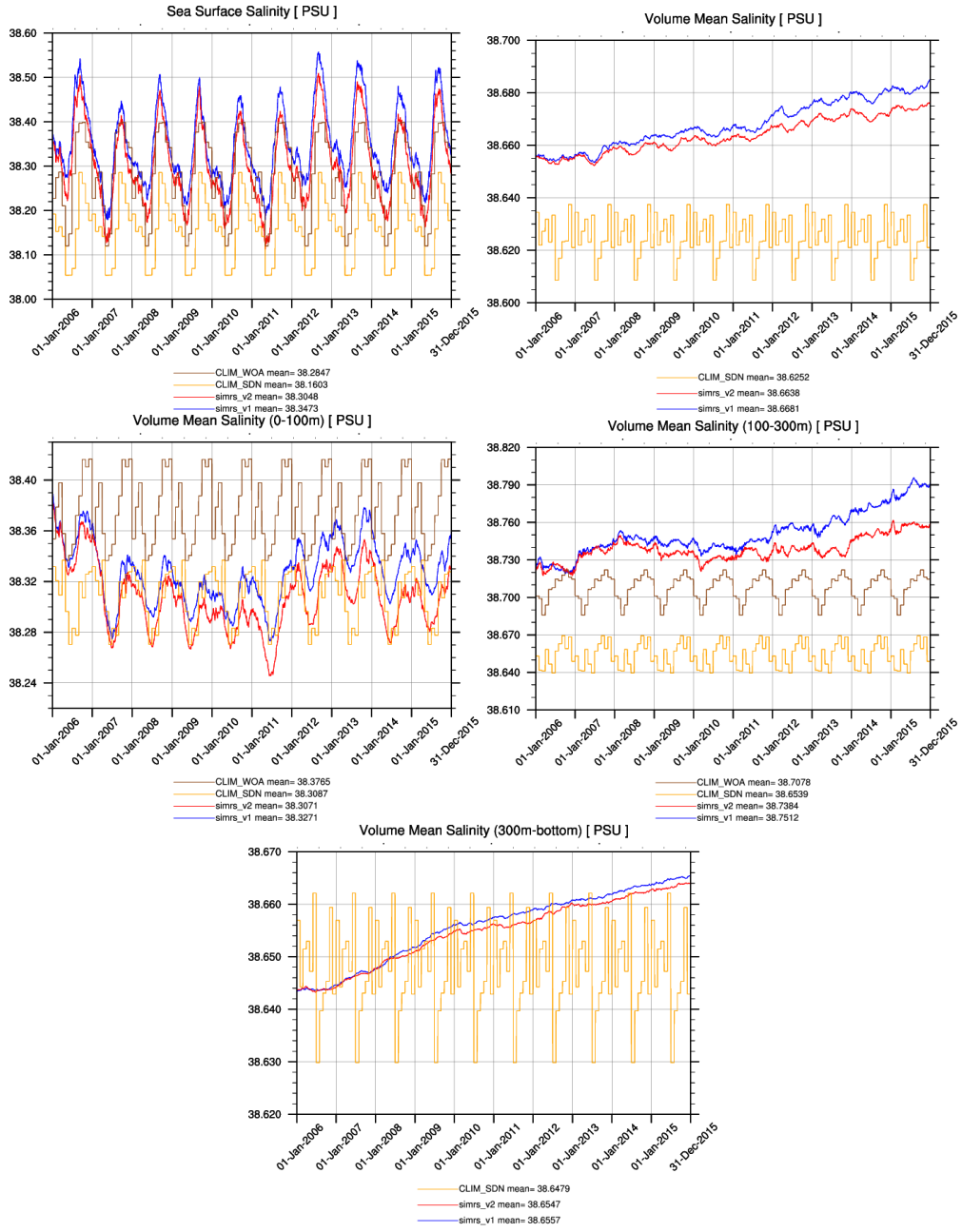

Figure 4.17: Mediterranean Sea salinity daily mean computed from numerical experiments and climatological data sets at different layers.

A comparison between Sea Surface Temperature (SST) from numerical experiments and from satellite data (see section 2.3) has been performed and the results in terms of monthly mean RMSE and BIAS are summarized in Table 4.3.

Results are almost identical between the two considered experiments at basin scale, but differences at regional scale can be observed, mainly during Winter and Autumn.

In particular in December (Figure 4.18) simrs_v2 shows a reduction of the SST RMSE mainly in the Adriatic Sea and along the Turkish coast.

In the Adriatic Sea the RMSE in simrs_v2 is reduced in particular in the final segment of the Western Adriatic Coastal Current, with a significant decrease of the error mainly in the area around the Gargano Promontory. An improvement in SST representation can be observed in the South Adriatic Gyre, where the simrs_v2 BIAS is lower with respect to simrs_v1.

On the contrary, higher SST RMSE values can be observed for simrs_v2 in correspondence of the Middle Adriatic Gyre, where a higher negative BIAS can be identified with respect to simrs_v1.

It can be noticed that the whole Adriatic Sea sub-basin has undergone a general cooling in simrs_v2 with respect to simrs_v1: this could be due to the larger amount of freshwater into the sub-basin, that triggers a general freshening of the suraface water masses, more exposed to the atmospheric forcing. Due to this it can be supposed that a surface overcooling occurs, lowering the SST of the entire Adriatic Sea.

In addiction, several rivers have been added in the Northern Adriatic Sea, so a large amount of water with a lower temperature with respect to rest of

the basin is added into the system and then spread to the entire Adriatic Sea.

Another area showing interesting differences between the two considered experiments is the southern Turkish coast, along the Asia Minor Current path, that shows lower SST RMSE values in simrs_v2 with respect to simrs_v1: this is due to a decrease in SST BIAS reasonably caused by the implementation in simrs_v2 of several rivers in the area that can induce the aforementioned overcooling effect.

Table 4.3: Monthly mean RMSE and BIAS of SST (°C) for experiments simrs_v1 and simrs_v2 with respect to satellite data. Statistics consider the whole Mediterranean Sea basin.

Month	**SST RMSE simrs_v1**	**SST RMSE simrs_v2**	**SST BIAS simrs_v1**	**SST BIAS simrs_v2**
Jan	0.54	0.55	0.27	0.26
Feb	0.50	0.50	0.26	0.25
Mar	0.48	0.48	0.26	0.25
Apr	0.47	0.47	0.23	0.23
May	0.54	0.54	0.26	0.26
Jun	0.60	0.61	0.30	0.30
Jul	0.69	0.70	0.32	0.32
Aug	0.68	0.68	0.24	0.25
Sep	0.65	0.65	0.19	0.19
Oct	0.61	0.61	0.11	0.11
Nov	0.60	0.60	0.17	0.16
Dec	0.58	0.58	0.23	0.22

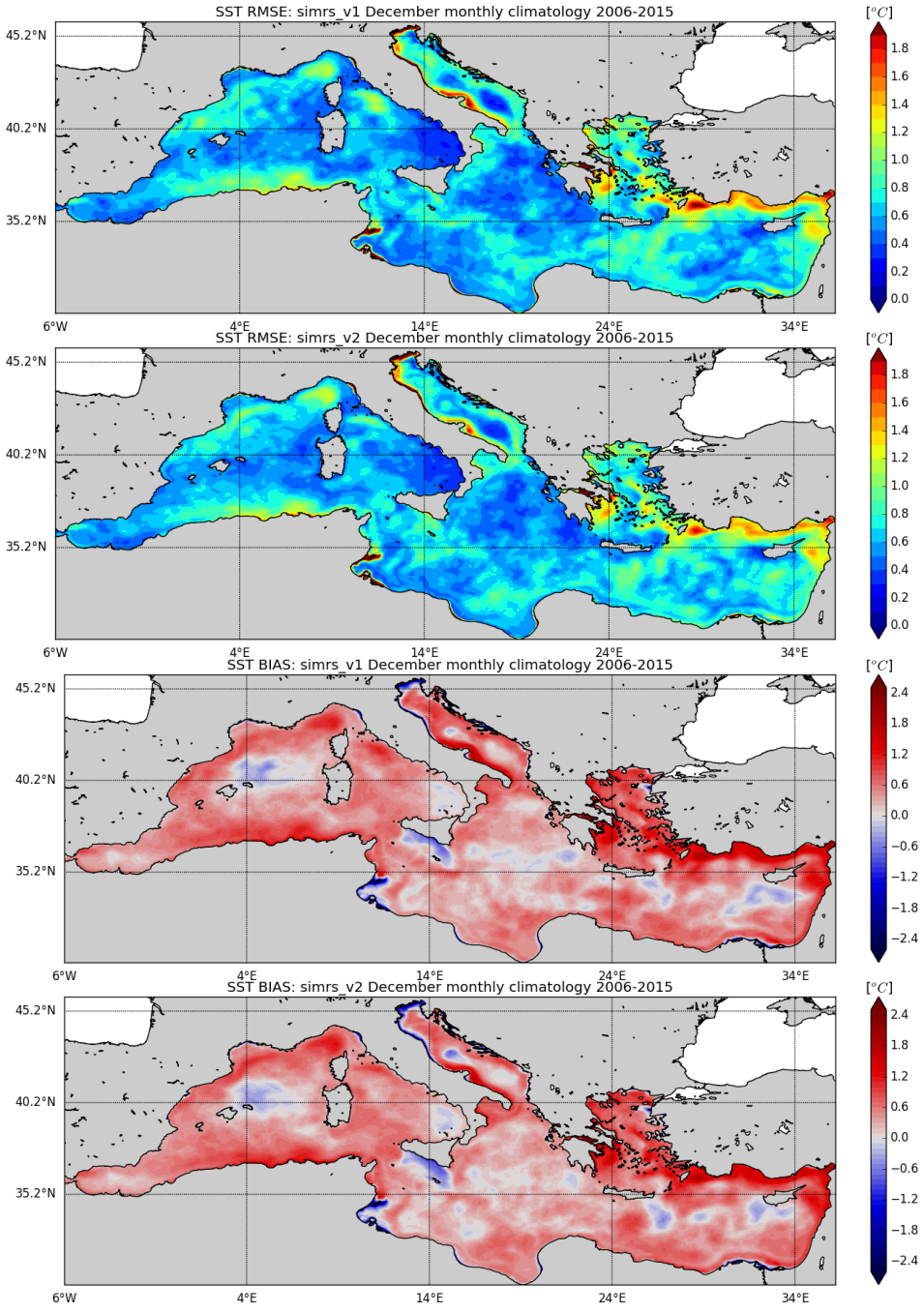

Figure 4.18: December sea surface temperature time averaged RMSE and BIAS. From top to bottom panel: simrs_v1 RMSE, simrs_v2 RMSE, simrs_v1 BIAS, simrs_v2 BIAS.

4.2.4 Mixed Layer Depth comparison with climatologies

In order to assess the differences between experiments simrs_v1 and simrs_v2 in reproducing the Mixed Layer Depth (MLD), monthly climatological averages of MLD for both the experiments have been compared with the Houpert et al. (2015) [103] climatological data set already described in section 2.3.

The main differences in MLD between the two experiments have been observed between the end of Autumn and Winter, in particular during February, when anyway both the experiments show a good agreement with the considered climatological data set, even though a general deepening in MLD can be observed in the eastern part of Mediterranean Sea and in particular in the Aegean Sea (Figure 4.19).

Observing the February MLD climatology, the most evident differences between the two experiments are located in the South Adriatic Gyre area and in the North Western Mediterranean Sea, in correspondence of the Gulf of Lion Gyre, two of the areas of deep water formation of the Mediterranean Sea (Pinardi et al., 2015 [33]).

Off the Gulf of Lion large differences, both positive and negative, can be observed between the two experiments (Figure 4.20, top panel).

This could be reasonably due to the winter variability among the considered experiments of the Liguro-Provencal-Catalan current (shown in next section) since all the water masses in the area, the Modified Atlantic Water (MAW), the Levantine Intermediate Water (LIW) and the Western Mediterranean Deep Water (WMDW), are carried by the current during its flowing (Conan and Millot, 1995 [129]).

In the Adriatic Sea (Figure 4.20, bottom panel), large differences can be noticed in correspondence of the South Adriatic Gyre, where simrs_v2 shows shallower values (about 50 m, with peaks of more than 70 m) with respect to simrs_v1, that can be reasonably attributed to the increased number of freshwater sources in the area. It can be noticed that the negtive MLD anomaly in simrs_v2 propagates southward, affecting the entire North-Eastern Ionian Sea.

Shallower values of MLD in simrs_v2 can be observed also along the first segment of the Western Adriatic Coastal Current, which conveys lighter water discharged by the rivers of Northern Adriatic Sea.

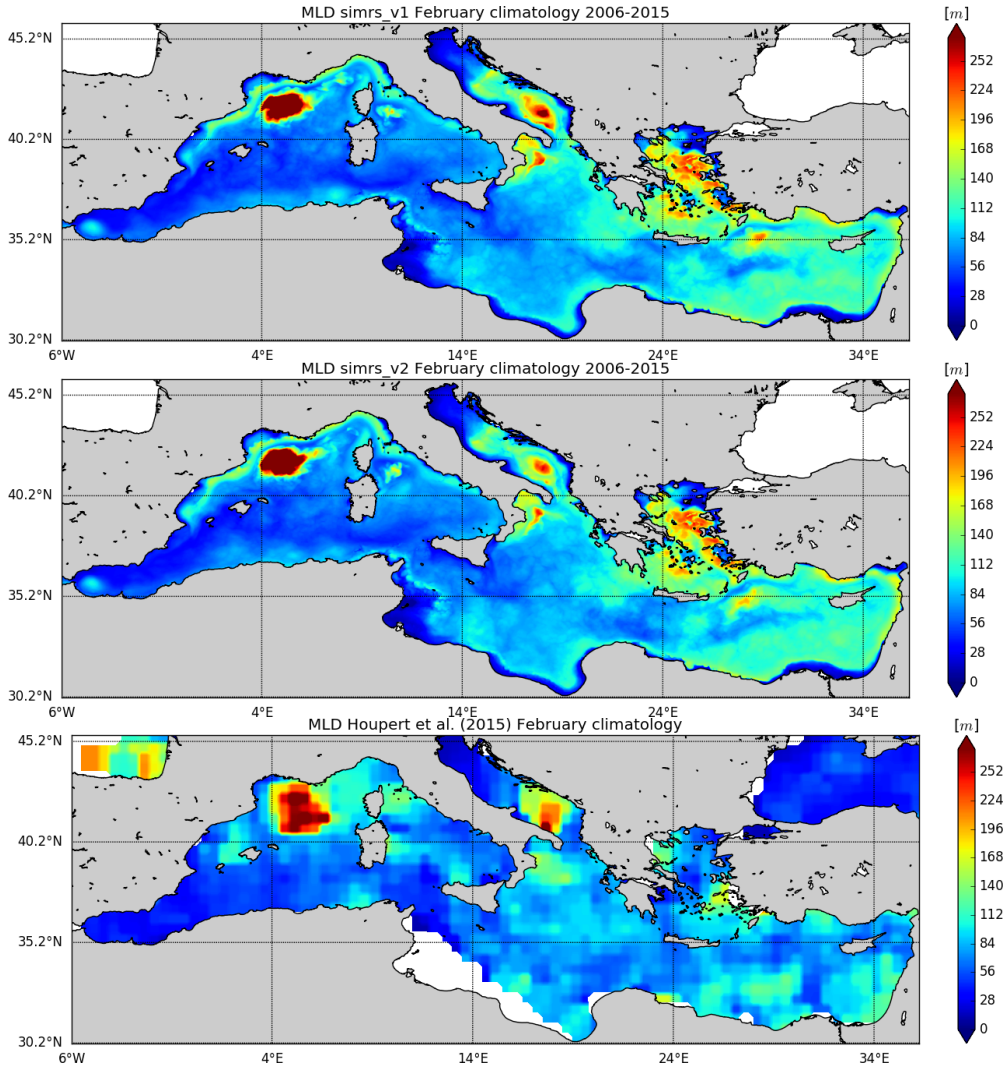

Figure 4.19: February climatological Mixed Layer Depth. From top to bottom panel: simrs_v1, simrs_v2, Houpert et al. (2015) climatological data set.

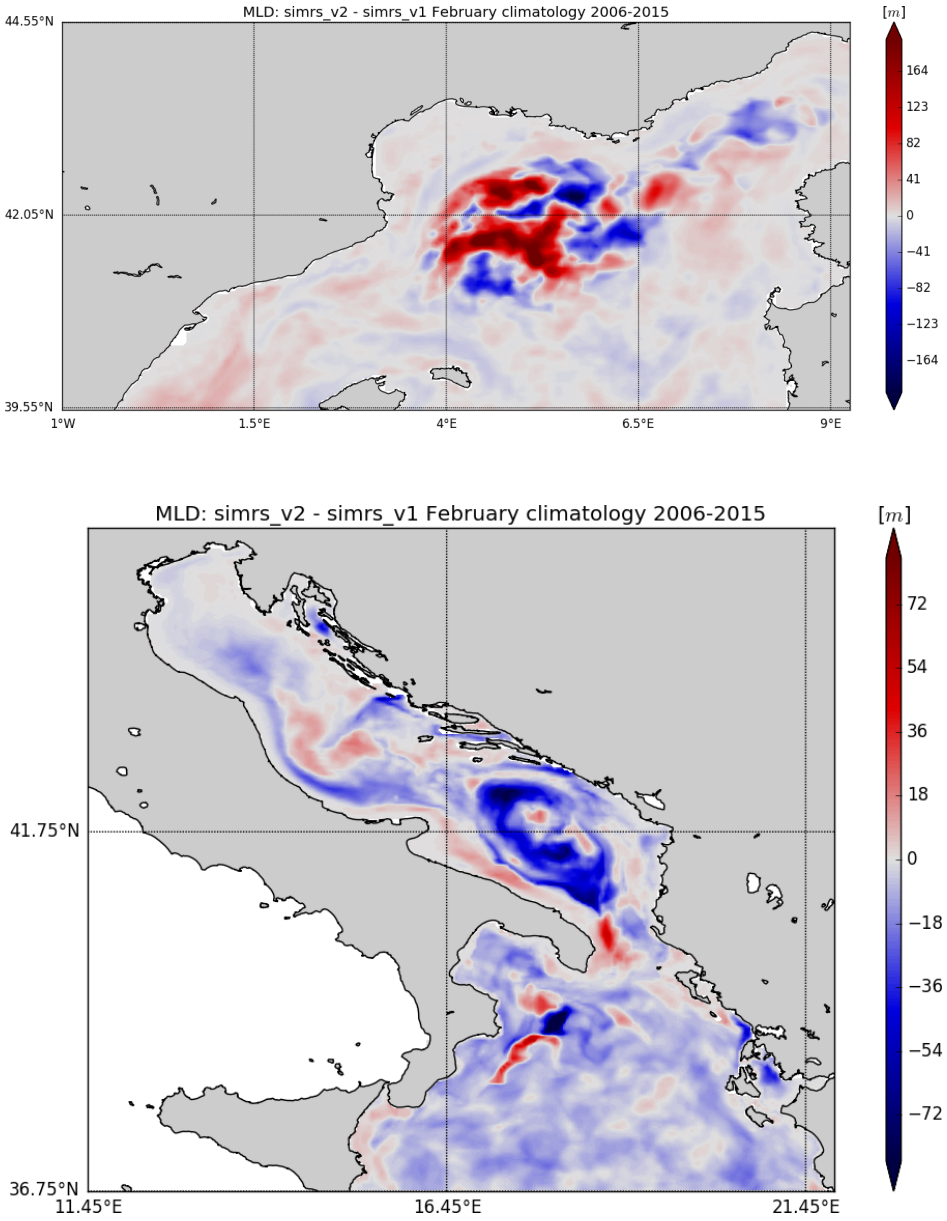

Figure 4.20: February climatological Mixed Layer Depth simrs_v2 - simrs_v1 differences over the period 2006-2015 in North Western Mediterranean Sea and Adriatic Sea.

4.2.5 Currents and water volume transport at straits

As a first step, the mean circulation for the whole considered period (2006-2015) is computed at 15 m depth for both the experiments (Figure 4.23) and compared to the Mediterranean Sea circulation structure from Pinardi et al. (2015) [33].

The circulation pattern displayed in Figure 4.21 is based on a 23-year-long reanalysis carried out by Adani et al. (2011) [38], which thus includes the assimilation of historical ocean observations into the modelling system.

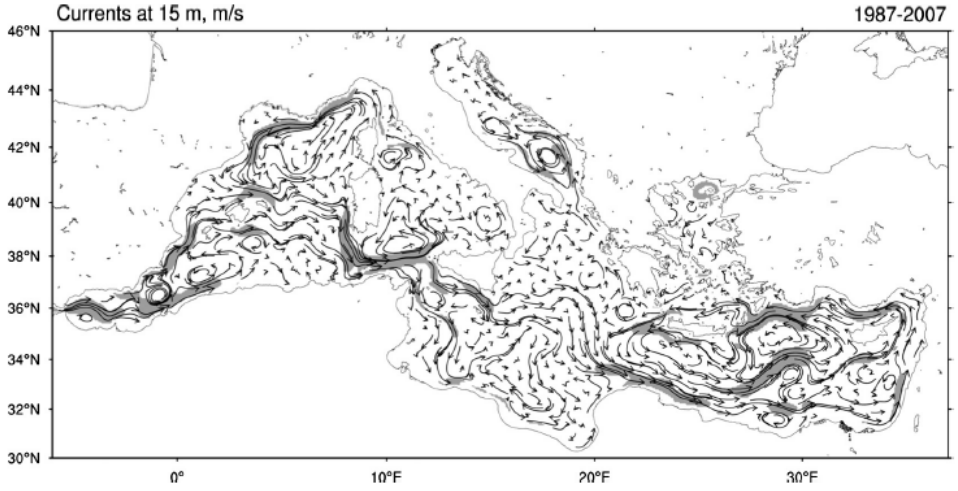

Figure 4.21: The 1987–2007 time-mean circulation at 15 m depth from the reanalysis: gray areas indicate velocity amplitudes greater than 0.1 m/s. Reproduced from Pinardi et al. (2015) [33].

Both the experiments well reproduce the mean circulation at 15 m depth shown in Pinardi et al. (2015) [33] (even though computed over different periods), presenting the major Mediterranean Sea circulation features.

The differences in velocity amplitude between the two experiments are of

the order of about 0.1 m/s with main differences along the largest circulation structures.

The average currents between 200 and 300 m depth (the intermediate circulation) for the whole considered period are shown in Figure 4.24 since this layer can be considered as representative of the Levantine Intermediate Water in the eastern part of the Mediterranean Sea basin.

Both the experiments well reproduce the mean circulation between 200 and 300 m depth shown in Pinardi et al. (2015) [33] and based on Adani et al. (2011) [38] (see Figure 4.22), even though in both experiments the main outflowing current path in the western part of the Mediterranean Sea basin seems to be more confined towards the coast in the Balearic Sea area, while in Pinardi et al. (2015) [33] the mainstream flows eastward with respect to the Balearic Islands before entering the Alboran Sea.

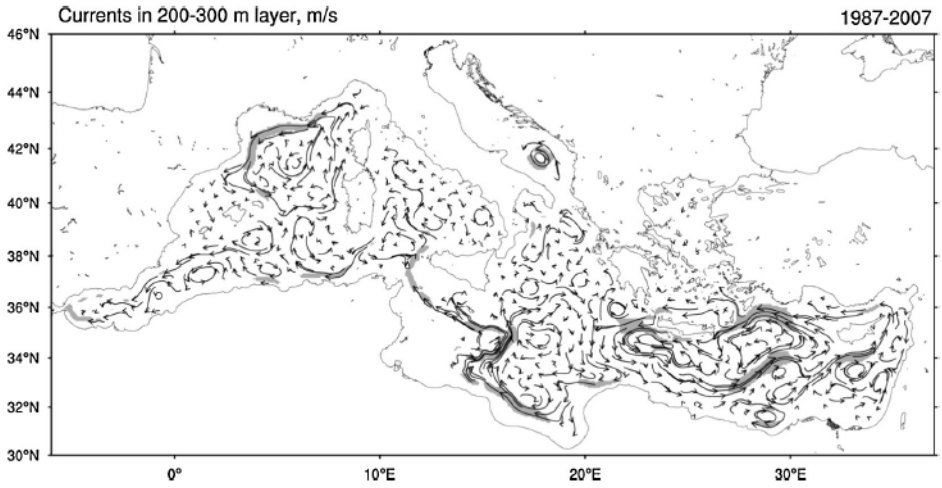

Figure 4.22: The 1987–2007 time-mean circulation, averaged in the layer between 200 and 300 m, from the reanalysis: gray areas indicate velocity amplitudes greater than 0.05 m/s. Reproduced from Pinardi et al. (2015) [33].

Focusing on the surface circulation, the main differences between the two experiments can be observed during Winter (Figure 4.25), when local effects on the velocity amplitude near the outlets of the new implemented rivers in experiment simrs_v2 can be noticed, in particular in the northernmost part of the Adriatic Sea, where the signal of the added river discharge can be observed as a positive velocity amplitude anomaly in experiment simrs_v2 with respect to simrs_v1.

Also the Po river plume shows higher velocity amplitude values in simrs_v2 with respect to simrs_v1, probably due to a strengthening triggered by the new rivers implemented in Northern Adriatic Sea.

An intensification of the Western Adriatic Coastal Current (WACC) can be

noticed in experiment simrs_v2 with respect to simrs_v1, while the southernmost portion of the Eastern South-Adriatic Current (ESAC) shows a weakening in simrs_v2 with respect to simrs_v1.

Relevant differences between the two experiments can be noticed in correspondence of the South Adriatic Gyre, where an outer core of positive velocity amplitude anomaly and an inner core of negative velocity amplitude anomaly can be observed in experiment simrs_v2 with respect to simrs_v1.

An increase of current intensity for Northern Tyrrhenian Gyre and Liguro-Provencal-Catalan Current can be noticed for experiment simrs_v2 with respect to simrs_v1, as well as the differences at the edge between the Rhodes Gyre and the Mid-Mediterranean Jet.

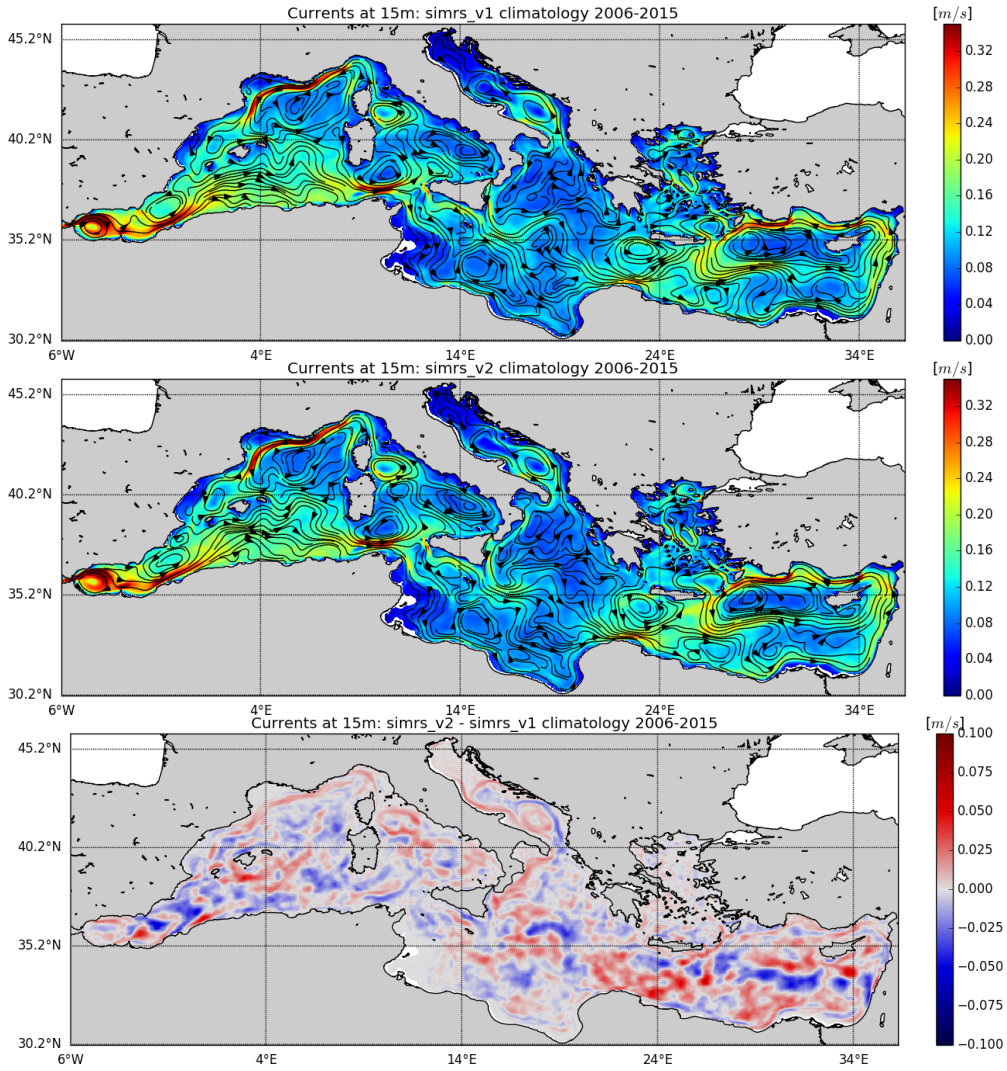

Figure 4.23: Climatological circulation at 15 m depth over the period 2006-2015. From top to bottom panel: simrs_v1, simrs_v2, simrs_v2 - simrs_v1.

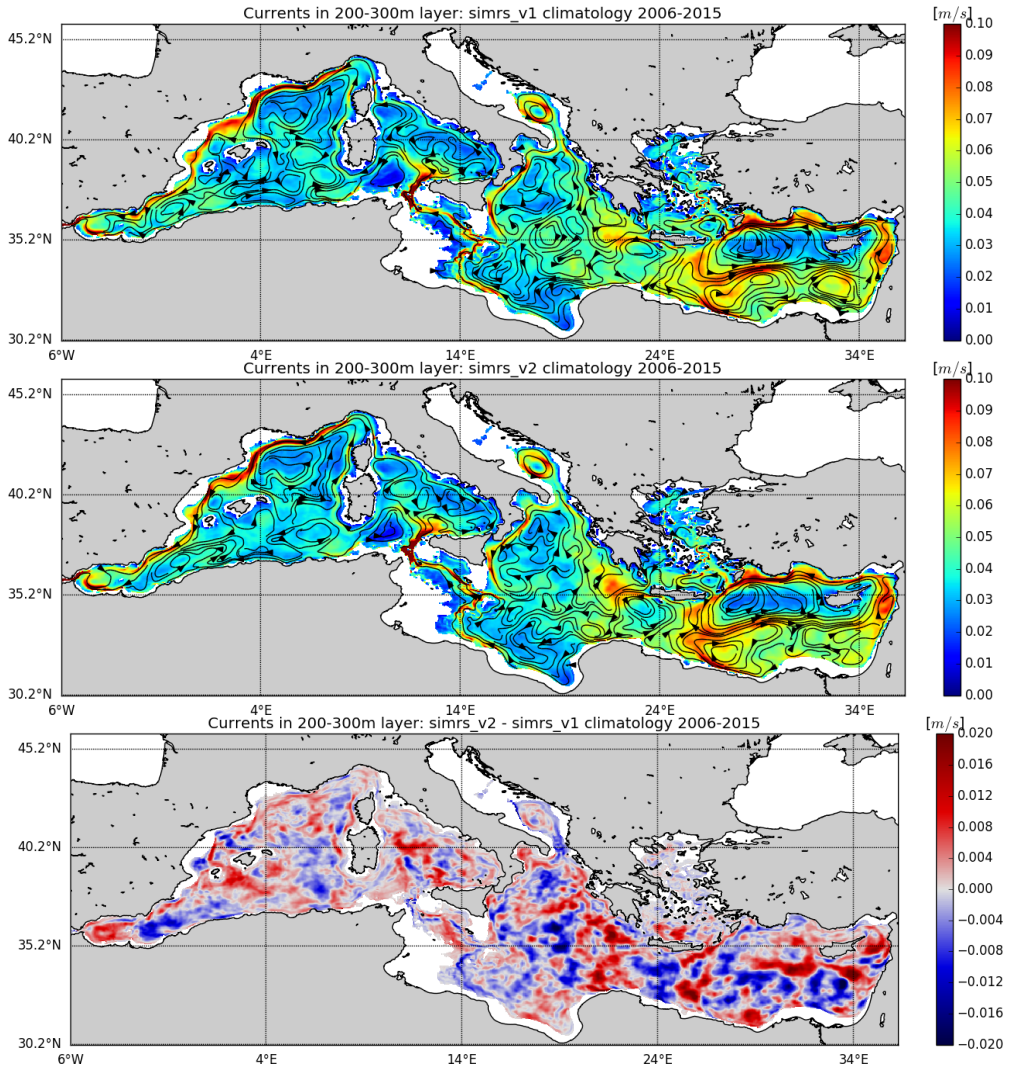

Figure 4.24: Climatological circulation average in the 200-300 m depth layer over the period 2006-2015. From top to bottom panel: simrs_v1, simrs_v2, simrs_v2 - simrs_v1.

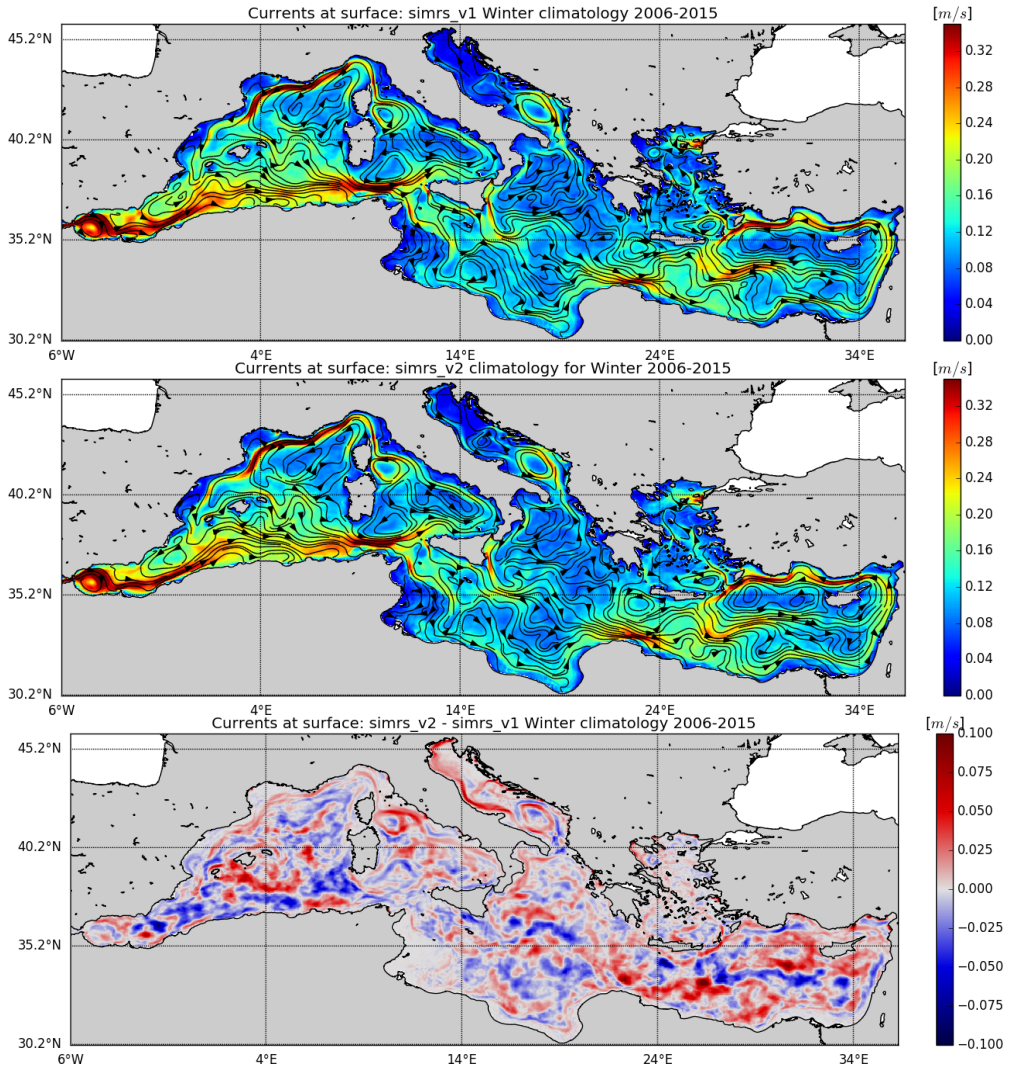

Figure 4.25: Climatological Winter surface circulation over the period 2006-2015. From top to bottom panel: simrs_v1, simrs_v2, simrs_v2 - simrs_v1.

In addition to the circulation pattern evaluation, an assessment of the water volume transport through the major straits of the Mediterranean Sea basin is provided, whose location is indicated in Figure 4.26.

Comparing the water volume transport through the Strait of Gibraltar

(Table 4.4 and transect A in Figure 4.26) it can be observed that the two experiments show very similar values and a good agreement with literature values for mean net transport (Soto-Navarro et al., 2010 [130], computed over the period 2004-2009 and Candela, 2001 [131], computed over the period 1994-1996); for eastward and westward transport both the experiment underestimate the values by Candela (2001) [131] but are very close to the values by Soto-Navarro et al. (2010) [130], in particular to the proposed observational upper limit.

Concerning the water volume transport through the Strait of Otranto (transect B in Figure 4.26), experiments simrs_v1 and simrs_v2 show very similar values for net mean transport (Table 4.5). The model net transport values are quite different with respcet to the literature values proposed in Yari et al. (2012) [132] and Astraldi et al. (1999) [133], both computed over the period 1994-1995, while the northward and southward transport values are closer to literature ones, showing in general lower values in simrs_v2 with respect to simrs_v1.

It can be noticed that a reduction of northward and southward water volume transport through the Strait of Otranto due to riverine influence has been observed also in Verri et al. (2018) [3], whose numerical findings prove that rivers reduce both the Modified Levantine Intermediate Water inflow on the Eastern shelf of the Adriatic Sea and the South Adriatic Deep Water outflow on the western side, through the Strait of Otranto.

Considering the transport through the Strait of Sicily (Table 4.6), a very similar mean net transport can be observed between experiments simrs_v1 and simrs_v2, the latter showing lower values for both northward and south-

ward water volume transport.

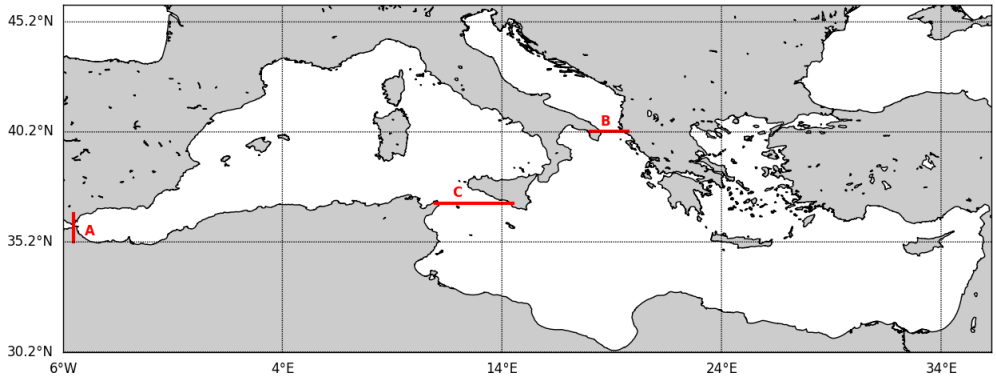

Figure 4.26: Location of sections for water volume transport computation through the major straits. A) Strait of Gibraltar; B) Strait of Otranto; C) Strait of Sicily.

Table 4.4: Strait of Gibraltar water volume transport [Sv] from simrs_v1 and simrs_v2 averaged over the period 2006-2015 compared to literature values.

Gibraltar mean transport [Sv]	**simrs_v1**	**simrs_v2**	**Soto-Navarro et al., 2010**	**Candela 2001**
Net	0.046	0.043	0.038 ±0.007	0.04
Eastward	0.883	0.878	0.81 ±0.06	1.01
Westward	0.837	0.835	0.78 ±0.05	0.97

Table 4.5: Strait of Otranto water volume transport [Sv] from simrs_v1 and simrs_v2 averaged over the period 2006-2015 compared to literature values.

Otranto mean transport [Sv]	**simrs_v1**	**simrs_v2**	**Yari et al., 2012**	**Astraldi et al., 1999**
Net	-0.003	-0.004	-0.04 ±0.28	0.01
Northward	0.923	0.844	0.90 ±0.04	1.15 ±0.53
Southward	0.926	0.848	0.94 ±0.32	1.16 ±0.53

Table 4.6: Strait of Sicily water volume transport [Sv] from simrs_v1 and simrs_v2 averaged over the period 2006-2015 compared to literature values.

Sicily mean transport [Sv]	**simrs_v1**	**simrs_v2**
Net	0.089	0.084
Northward	1.911	1.838
Southward	1.822	1.754

4.2.6 Sea Surface Height comparison with satellite data

The capability of experiments simrs_v1 and simrs_v2 to reproduce Sea Surface Height (SSH) is evaluated by comparing the numerical results with data from available satellites (along track observations) for the period considered: the RMSE and BIAS of Sea Level Anomaly (SLA) are computed for the whole Mediterranean Sea basin and for the sub-regions displayed in Figure 4.7 and the results are shown in Figure 4.27 , together with the number of observations considered for the comparison.

Both the experiments show very similar results, even though a slight improvement in simrs_v2 can be noticed with respect to simrs_v1, with several sub-regions showing differences that can be considered significant between the two experiments, like Northern Tyrrhenian Sea (sub-region 6 in 4.7), Western Levantine Sea (sub-region 12 in 4.7), Aegean Sea (sub-region 13 in 4.7) and Eastern Levantine Sea (sub-region 16 in 4.7), where experiment simrs_v2 shows lower RMSE values with respect to simrs_v1.

In addition to SLA RMSE and BIAS metrics, Figure 4.28 shows the spatial pattern of the differences in SSH between the two experiments along the four seasons.

The Adriatic Sea shows always higher SSH values in experiment simrs_v2 due to the increased riverine discharge into the basin, being the positive difference with respect to simrs_v1 more pronounced during Winter and Spring. The same situation can be observed for the Aegean Sea, which shows higher SSH values in simrs_v2 with respect to simrs_v1, even though less evident than in the Adriatic Sea.

The western part of the Mediterranean Sea basin shows generally lower

SSH values in simrs_v2 with respect to simrs_v1, in particular for Autumn and Winter, while in the Levantine Sea positive and negative SSH differences between the two experiments can be observed equally; moreover, for the coastal area comprised between the Gulf of Gabes and the Gulf of Sirte simrs_v2 show slightly higher SSH values with respect to simrs_v2.

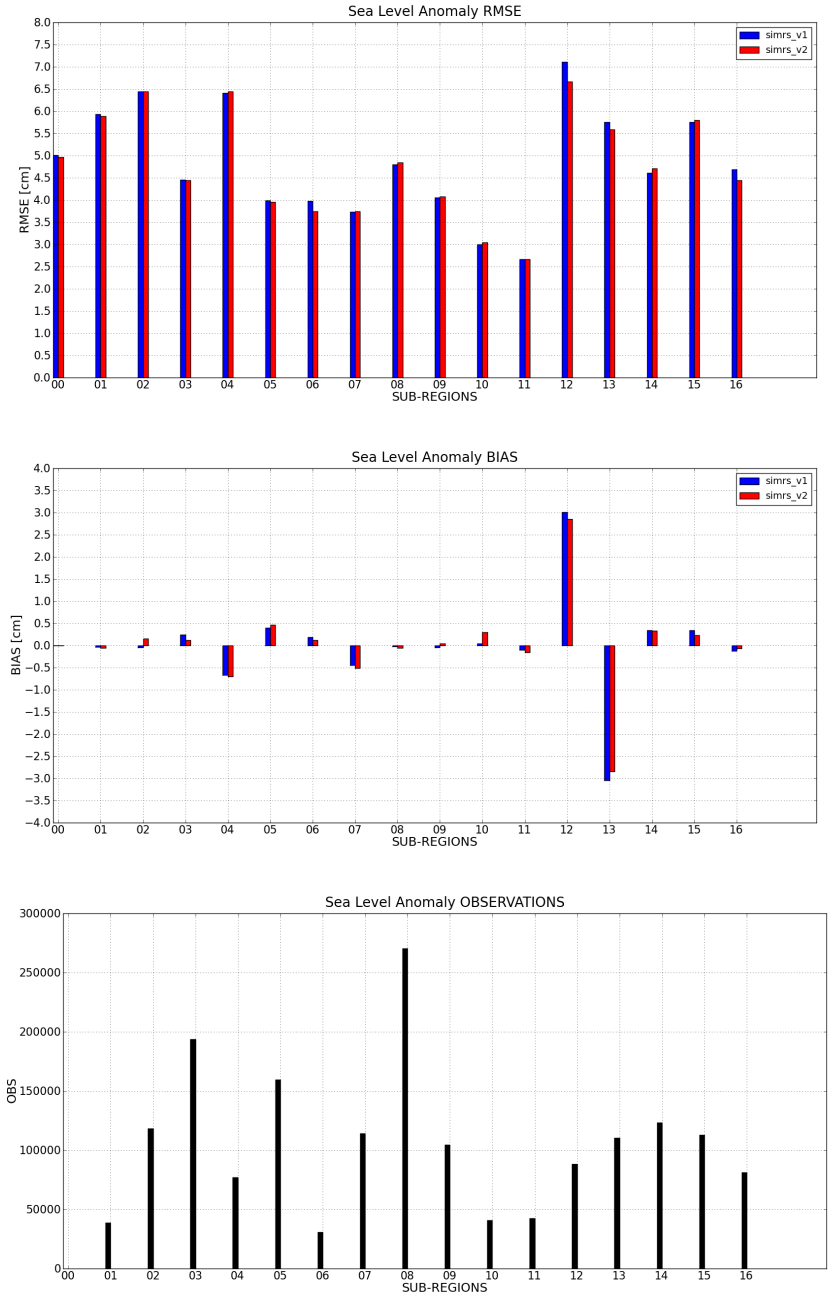

Figure 4.27: Sea Level Anomalies (cm) metrics of simrs_v1 and simrs_v2 computed over the period 2006-2015 for the Mediterranean Sea (00) and for the 16 sub-regions. From top to bottom panel: RMSE, BIAS, number of observations.

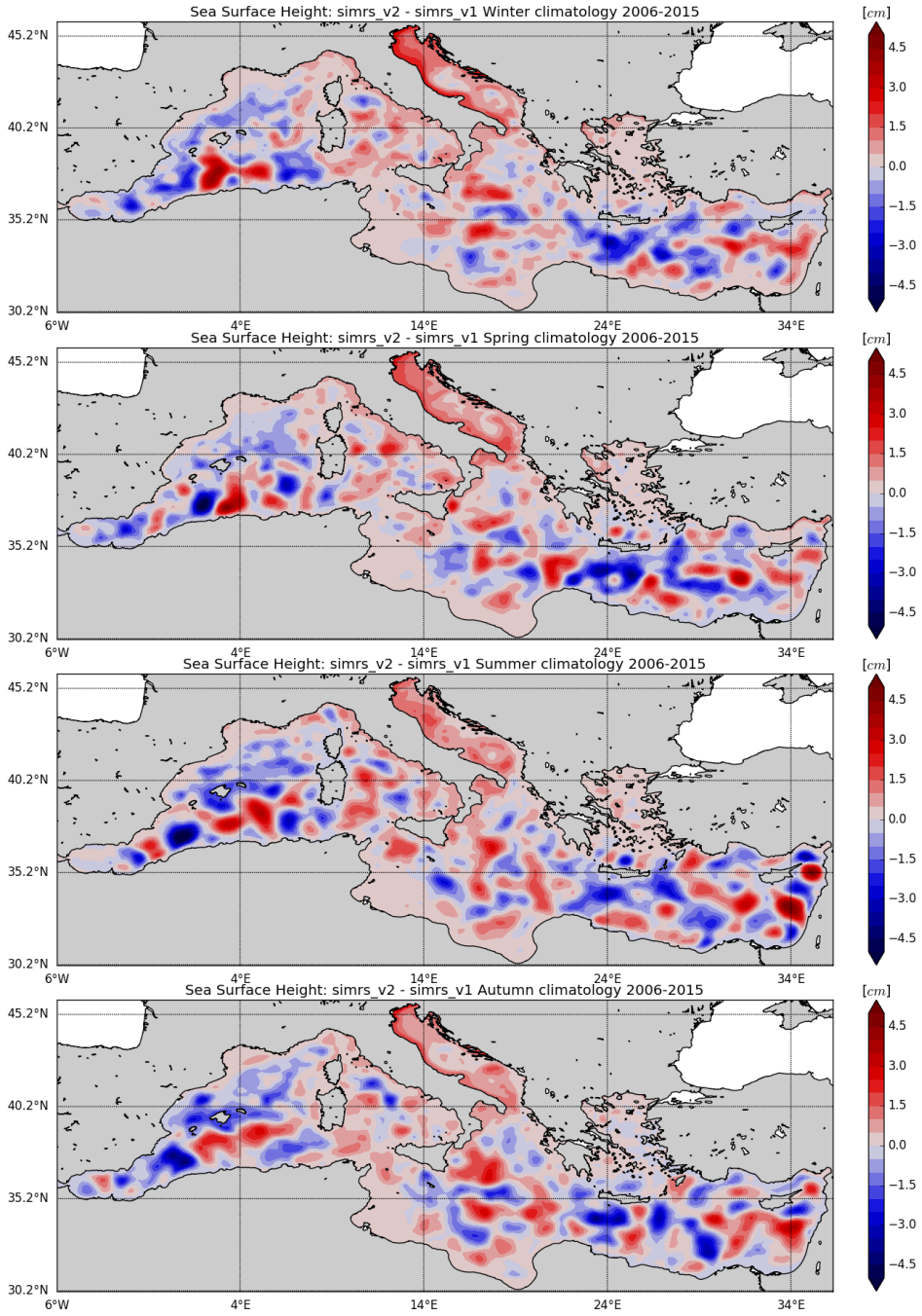

Figure 4.28: Seasonal climatological sea surface height differences between experiments simrs_v1 and simrs_v2. From top to bottom panel: Winter (Jan - Mar), Spring (Apr - Jun), Summer (Jul - Sep) and Autumn (Oct - Dec).

4.3 Sensitivity experiments on modified river runoff salinity and mixing parameterization

In order to assess the impact of the prescribed salinity at the freshwater inputs and of the mixing parameterization at river mouths on the thermohaline properties of the Mediterranean Sea and on its dynamics two numerical experiments are performed, with an integration period from 2005 to 2010 (considering the year 2005 as a spin-up year), which will be compared to simrs_v2 experiment presented in the prevous sections.

The two new experiments, simrs_v3 and simrs_v4, have the following characteristics: in experiment simrs_v3 the salinity of the 39 rivers implemented in simrs_v2 has been set equal to 0 PSU, while in experiment simrs_v4 the vertical mixing in correspondence of the river outlets has been enhanced.

The vertical mixing scheme adopted in the model configuration used to perform the numerical experiments is based on a local Richardson number dependent formulation (Pacanowski and Philander, 1981 [92]), where the vertical eddy diffusivity and viscosity coefficients are respectively computed as follows:

$$\begin{cases} A^{vT} = \dfrac{A^{vT}_{ric}}{(1 + a\ Ri)^n} + A^{vT}_b \\ A^{vm} = \dfrac{A^{vT}}{(1 + a\ Ri)} + A^{vm}_b \end{cases} \tag{4.3}$$

where $Ri = N^2 / \left(\partial_z \mathbf{U}_h\right)^2$ is the local Richardson number, N is the local Brunt-Vaisälä frequency, A^{vT}_b and A^{vm}_b are the background values set equal

to 10^{-7} m^2/s and $1.2 \cdot 10^{-6}$ m^2/s respectively, and $A^{vT}_{ric} = 10^{-4}$ m^2/s is the maximum value that can be reached by the coefficient when $Ri \leq 0$, $a = 5$ and $n = 2$ (default values).

The enhanced vertical mixing at river mouths is obtained by using the following equation:

$$A^{vT} = A^{vT} + 2 \cdot A^{vT}_{rnf} \tag{4.4}$$

where the vertical eddy diffusivity coefficient computed by using the aforementioned Richardson number dependent formulation is increased of the value defined by A_rnf^{vT} (m^2/s), from the surface down to a user-defined maximum depth.

For A^{vT}_{rnf} a value equal to $2 \cdot 10^{-3}$ m^2/s has been used in several studies (Webb, 2016 [134], Blockley et al., 2014 [135], Haid et al., 2017 [136], Megann et al., 2014 [137]), so this is the value that is used for A^{vT}_{rnf} in simrs_v4 experiment.

The maximum depth to which the enhanced mixing is applied in the present work is 12 m, which is selected considering the vertical model discretization and following the aforementioned studies proposing to use values ranging from 10 m (Webb, 2016 [134], Blockley et al., 2014 [135], Megann et al., 2014 [137]) to 15 m depth (Haid et al., 2017 [136]), while in Benshila et al. (2014) [138] a value of 12 m is used.

The setup of experiments simrs_v2, simrs_v3 and simrs_v4 is summarized in Table 4.7.

Table 4.7: Summary of simrs_v2, simrs_v3 and simrs_v4 experiments configuration.

Experiment	**simrs_v2**	**simrs_v3**	**simrs_v4**
Initial Conditions	WOA13 V2	WOA13 V2	WOA13 V2
Run period	2005-2010	2005-2010	2005-2010
Atlantic Ocean LOBC	Daily fields from CMEMS GLO-MFC	Daily fields from CMEMS GLO-MFC	Daily fields from CMEMS GLO-MFC
Dardanelles Strait LOBC	Daily fields from CMEMS GLO-MFC and TSS box model daily climatological fields	Daily fields from CMEMS GLO-MFC and TSS box model daily climatological fields	Daily fields from CMEMS GLO-MFC and TSS box model daily climatological fields
Number of rivers	39 (from line 1 to 39 in Table 4.1, column *River name*)	39 (from line 1 to 39 in Table 4.1, column *River name*)	39 (from line 1 to 39 in Table 4.1, column *River name*)
Rivers salinity	From line 1 to 39 in Table 4.1, column S	0 PSU	From line 1 to 39 in Table 4.1, column S
Rivers temperature	SST of the river grid point(s) implementation	SST of the river grid point(s) implementation	SST of the river grid point(s) implementation
Numerical scheme at river mouths	Upstream scheme	Upstream scheme	Upstream scheme and increased vertical eddy diffusivity coefficient

4.4 Evaluation and validation of experiments results

4.4.1 Water fluxes

In this section the capability of experiments simrs_v2, simrs_v3 and simrs_v4 to reproduce the Mediterranean Sea hydrologic cycle is analyzed, but since the three experiments share the same precipitation forcing and the same riverine discharge, the main focus will be dedicated to the analysis of the third component of the hydrologic cycle, namely the evaporation rate (E).

In Figure 4.29 it can be noticed that the climatological hydrologic cycle is well reproduced by both the experiments according to Mariotti et al. (2002) [127], with the three experiment showing extremely small differences among them.

From Figure 4.30 it can be noticed that experiments simrs_v3 and simrs_v4 show significant differences with respect to simrs_v2, that will be considered as the reference experiment; the differences between the experiments show a comparable amplitude along the whole basin.

During Autumn, simrs_v3 presents clear lower evaporation rates values with respect to simrs_v2 in the whole Adriatic Sea and the northernmost part of the North Eastern Ionian Sea, while simrs_v4 shows higher values with respect to simrs_v2 around the Po river delta and in correspondence of the river mouths along the Balkan coast, in addition to the area of the South Adriatic Gyre; negative differences can be instead noticed in correspondence of the Middle Adriatic Gyre.

Differences between simrs_v3 and simrs_v4 with respect to the reference

experiment simrs_v2 are much smaller during Spring but anyway evident in the Adriatic Sea, where simrs_v3 shows generally higher values of evaporation rate with respect to simrs_v2, with the only exception of the outer edge of the South Adriatic Gyre; the local effect of the enhanced vertical mixing at river mouths is clearly noticeable in experiment simrs_v4, where a negative difference in evaporation rate with respect to simrs_v2 is clearly observable around Po river delta and in front of Albanian rivers outlets.

Figure 4.29: Monthly climatological area-averaged hydrologic cycle and its components for simrs_v2, simrs_v3 and simrs_v4. Top panel: upward water flux. Bottom panel: evaporation.

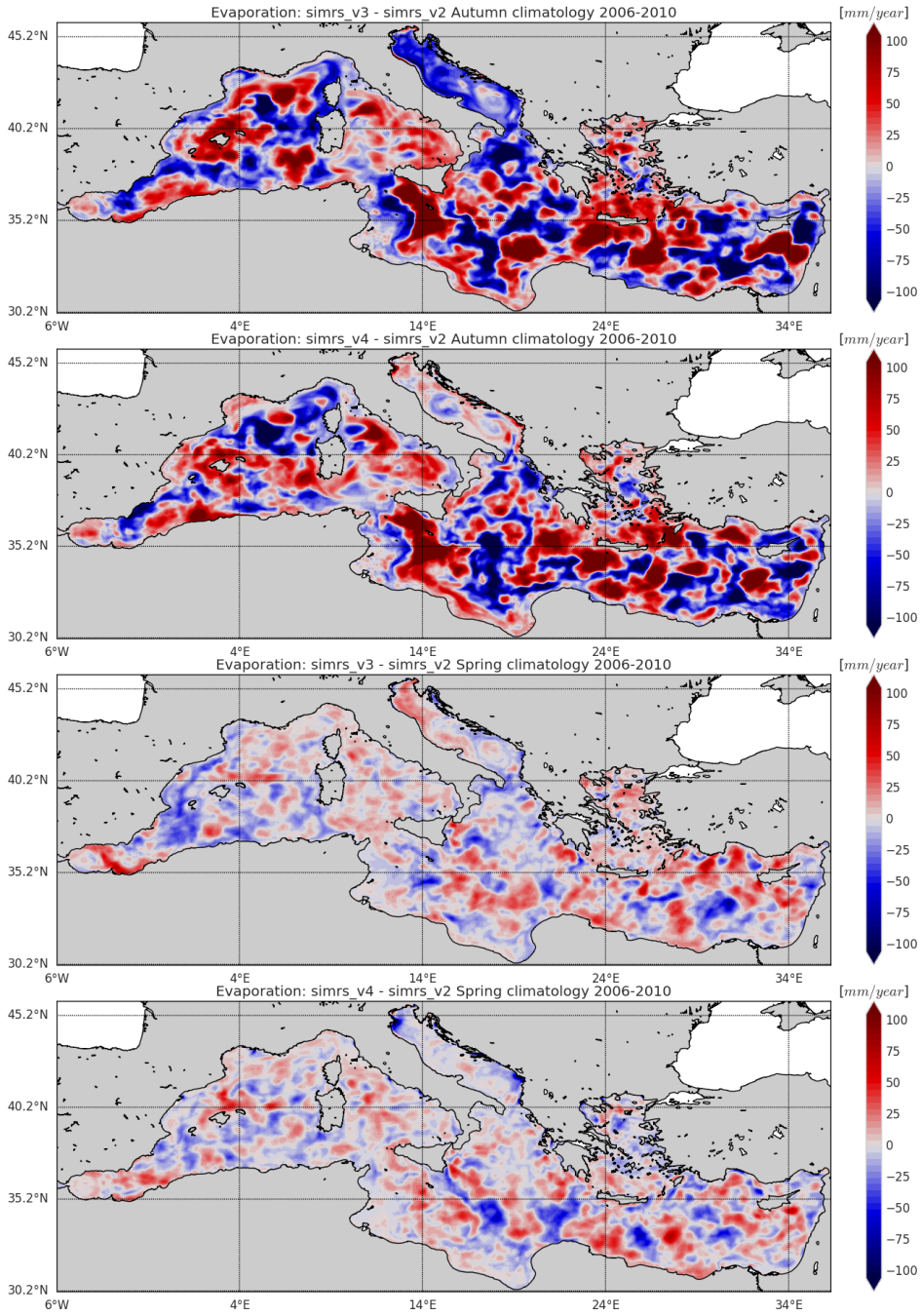

Figure 4.30: Seasonal evaporation rate differences. From top to bottom panel: Autumn (Oct - Dec) simrs_v3 - simrs_v2, Autumn (Oct - Dec) simrs_v4 - simrs_v2, Spring (Apr - Jun) simrs_v3 - simrs_v2, Spring (Apr - Jun) simrs_v4 - simrs_v2.

4.4.2 Temperature and salinity comparison with in situ observations

The experiments ability in reproducing temperature and salinity for the whole Mediterranean Sea and for different sub-regions of the basin (see Figure 4.7) at different depths is provided hereafter, through the comparison of model results with Argo floats, XBTs, gliders and satellite data available for the simulation period.

As displayed in Figure 4.31, the salinity RMSE in the Mediterranean Sea basin is similar for the three experiments, while simrs_v3 presents the largest negative BIAS values.

For what concern temperature skill (Figure 4.32), simrs_v2 shows the lowest RMSE values along the whole water column with respect to the other two considered experiments, among which simrs_v3 is the experiment showing the worst performances.

Considering the RMSE and BIAS of salinity (Figure 4.33) and temperature (Figure 4.34) at sub-regional scale and focusing on the sub-regions characterized by the largest number of river inputs, in Northern Adriatic Sea (sub-region 11 in Figure 4.7), simrs_v2 shows the best performances in salinity skill for almost the whole water column, in particular in the depth range from surface down to 100 m depth, due to lower salinity values (except in the depth range 60-100 m) as noticeable from BIAS values. Experiment simrs_v3 shows the worst performances among the three considered experiments, with extremely low salinity values, as indicated by bias values.

In Southern Adriatic Sea (sub-region 10 in Figure 4.7) simrs_v2 is the experiment showing the best performances along the whole water column,

with simrs_v3 being the worst experiments, with RMSE values more than double with respect to simrs_v2 from the surface down to 100 m depth, while under this depth the differences remain large but less pronounced with respect to the upper water column. As noticeable from BIAS values, the high RMSE values in simrs_v3 are due to an excessive freshening of the water column from the surface down to 150 m depth, while from 150 to 600 m depth salinity shows too high values.

Concerning temperature, in Northern Adriatic Sea the experiments with the lowest RMSE values are simrs_v2 and simrs_v4 from the surface to 10 m depth, while from 30 to 300 m depth the experiment showing the best performances is simrs_v3 which shows higher salinity values with respect to simrs_v2. With the exception of the depth range from the surface down to 30 m depth, the experiment simrs_v4 shows the highest RMSE values, due to excessively high values of salinity, in particular from 30 to 100 m depth.

In Southern Adriatic Sea simrs_v2 shows the lowest temperature RMSE values from the surface down to 150 m depth, due to a higher heating of the water column, while in the rest of the water column the experiment showing the best performances is simrs_v4 thanks to higher temperature values. simrs_v4 appears as the worst experiment for all the depth ranges considered.

In North Eastern Ionian Sea (sub-region 9 in Figure 4.7), simrs_v3 shows the lowest salinity RMSE in the depth range between surface and 30 m depth, while simrs_v2 has the worst performances between the three experiments, due to excessively high salinity values, as noticeable from BIAS values; in the range between 60 and 150 m simrs_v2 has the lowest RMSE, due to higher

salinity values, even though in the depth range between 100 and 150 m the three experiments show very similar performances, as well as between 150 and 600 m depth.

In the Aegean Sea (sub-region 13 in Figure 4.7) experiment simrs_v4 shows the lowest RMSE salinity values from the surface down to 60 m depth (especially in the depth range 0-10 m), with salinity values higher with respect to the other experiments, as indicated by BIAS values. From 60 to 300 m depth the experiment showing the best performances is simrs_v2, while simrs_v3 has the highest RMSE values for all the depth ranges considered.

Concerning temperature skill in North Eastern Ionian Sea, simrs_v4 shows lower RMSE values for almost the whole water column, due to higher heating as noticeable from BIAS values; simrs_v2 shows the best performances in the range between surface and 10 m depth, due to a higher heating with respect to the others experiments; simrs_v3 has the highest RMSE values, due to excessively low temperature values, except for the depth range between 300 and 600 m.

The experiment showing the best performances concerning temperature is simrs_v2 from the surface down to 100 m depth, while at greater depth simrs_v4 is the experiment with the lowest temperature RMSE.

In the North-Central Levantine Sea (sub-region 14 in Figure 4.7) is not observed an experiment performing clearly better in terms of salinity representation with respect to the others from the surface down to 100 m depth, while at greater depths simrs_v4 shows the lowest salinity RMSE.

In the Eastern Levantine Sea (sub-region 16 in Figure 4.7) simrs_v2 has the lowest salinity RMSE values along the whole water column, while simrs_v3

is the experiment showing the worst performances.

Concerning temperature, in the North-Central Levantine Sea simrs_v4 shows the best performances for the whole water column, with the exception of the depth range between 10 and 60 m, where simrs_v2 provides better results.

The capability of the different experiments to correctly reproduce temperature in the Eastern Levantine Sea is clearly evident, with simrs_v2 providing the best results among the considered experiments, while simrs_v4 shows to be constantly the experiment with the worst performances.

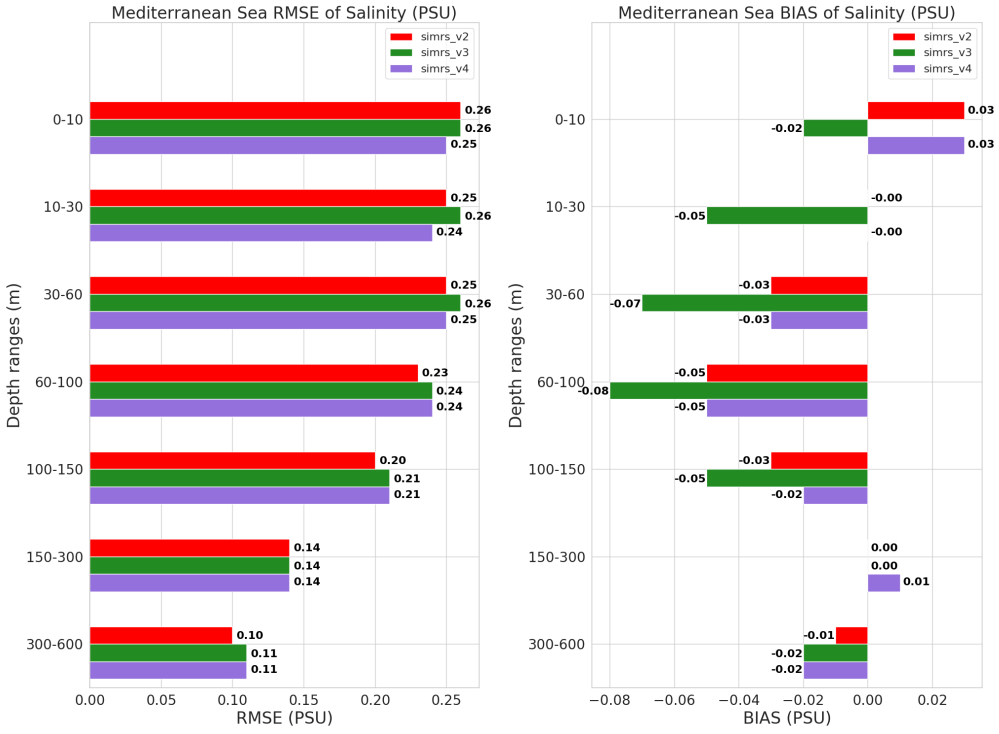

Figure 4.31: Mediterranean Sea mean RMSE and BIAS of salinity (PSU) for experiments simrs_v2, simrs_v3 and simrs_v4.

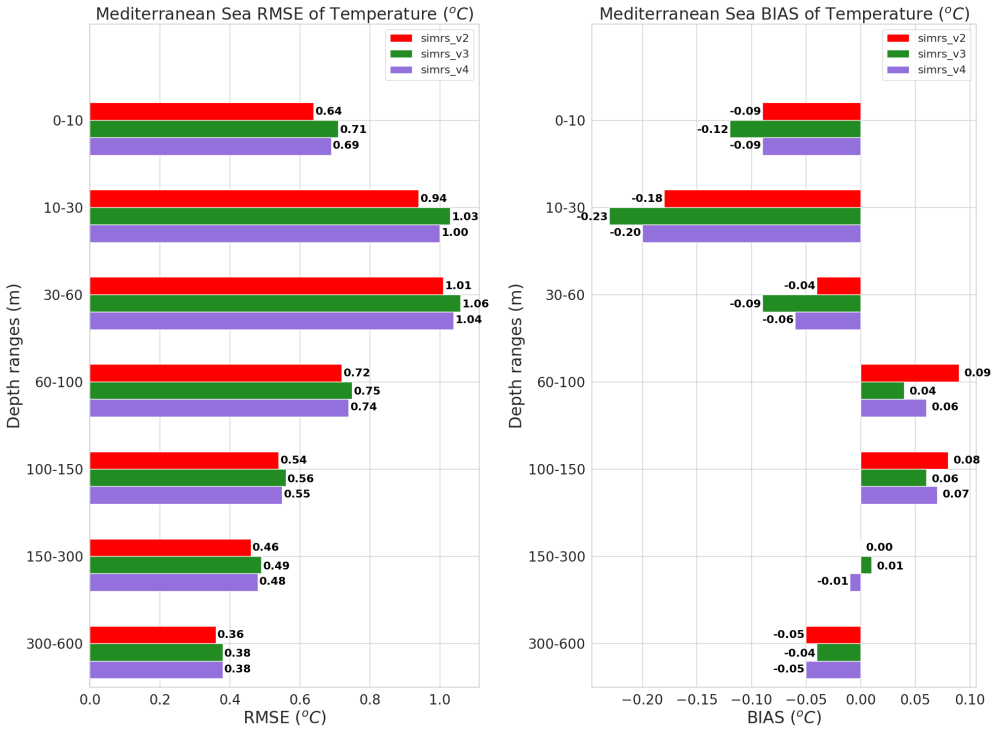

Figure 4.32: Mediterranean Sea mean RMSE and BIAS of temperature (°C) for experiments simrs_v2, simrs_v3 and simrs_v4.

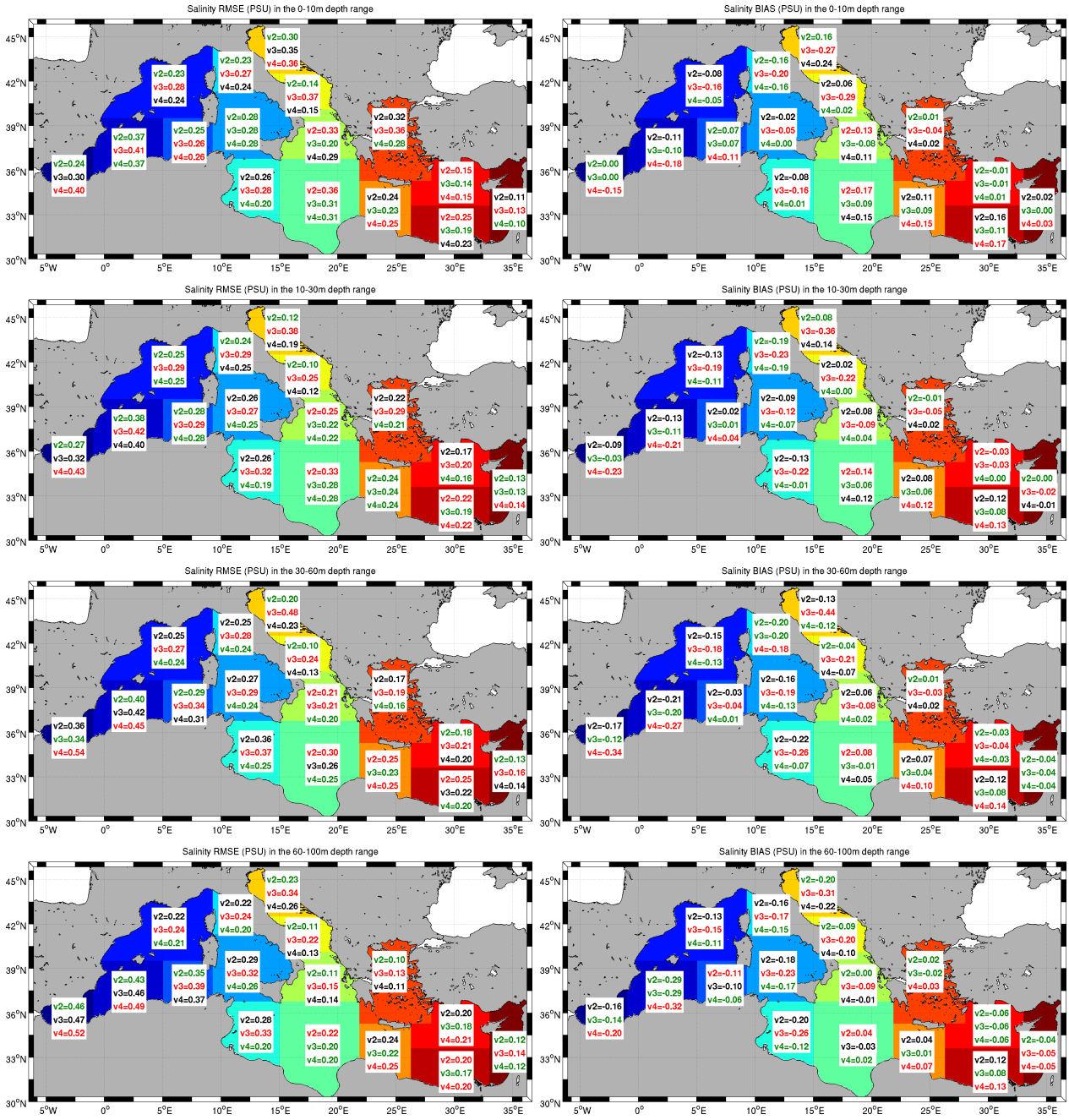

Figure 4.33: Sub-regional mean RMSE and BIAS of salinity (PSU) for experiments simrs_v2, simrs_v3 and simrs_v4 at selected depth ranges. For each sub-region the experiment with the lowest salinity RMSE and BIAS is indicated in green, while the experiment with the highest salinity RMSE and BIAS is indicated in red.

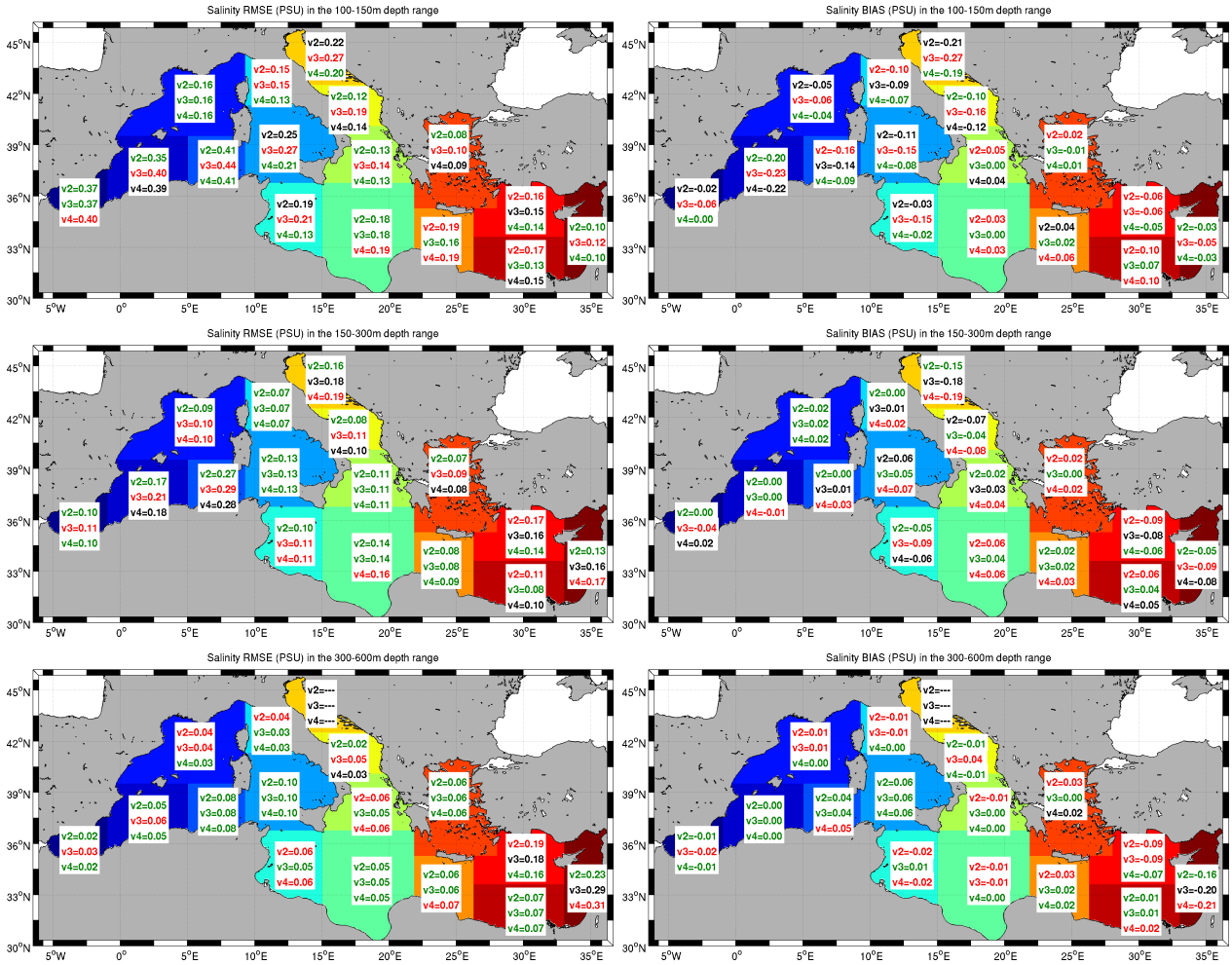

Figure 4.33: Sub-regional mean RMSE and BIAS of salinity (PSU) for experiments simrs_v2, simrs_v3 and simrs_v4 at selected depth ranges. For each sub-region the experiment with the lowest salinity RMSE and BIAS is indicated in green, while the experiment with the highest salinity RMSE and BIAS is indicated in red (continued).

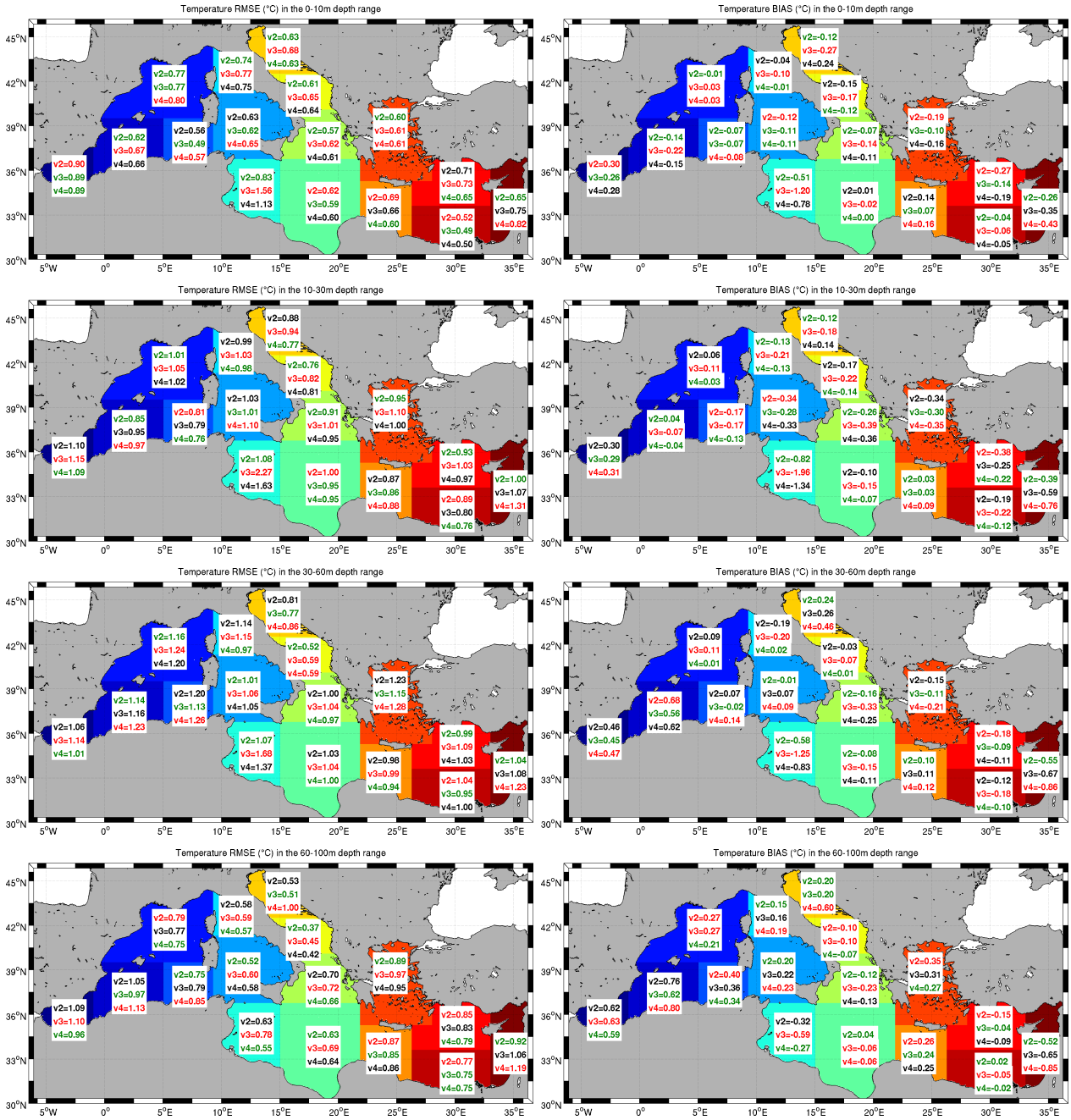

Figure 4.34: Sub-regional mean RMSE and BIAS of temperature (°C) for experiments simrs_v2, simrs_v3 and simrs_v4 at selected depth ranges. For each sub-region the experiment with the lowest temperature RMSE and BIAS is indicated in green, while the experiment with the highest temperature RMSE and BIAS is indicated in red.

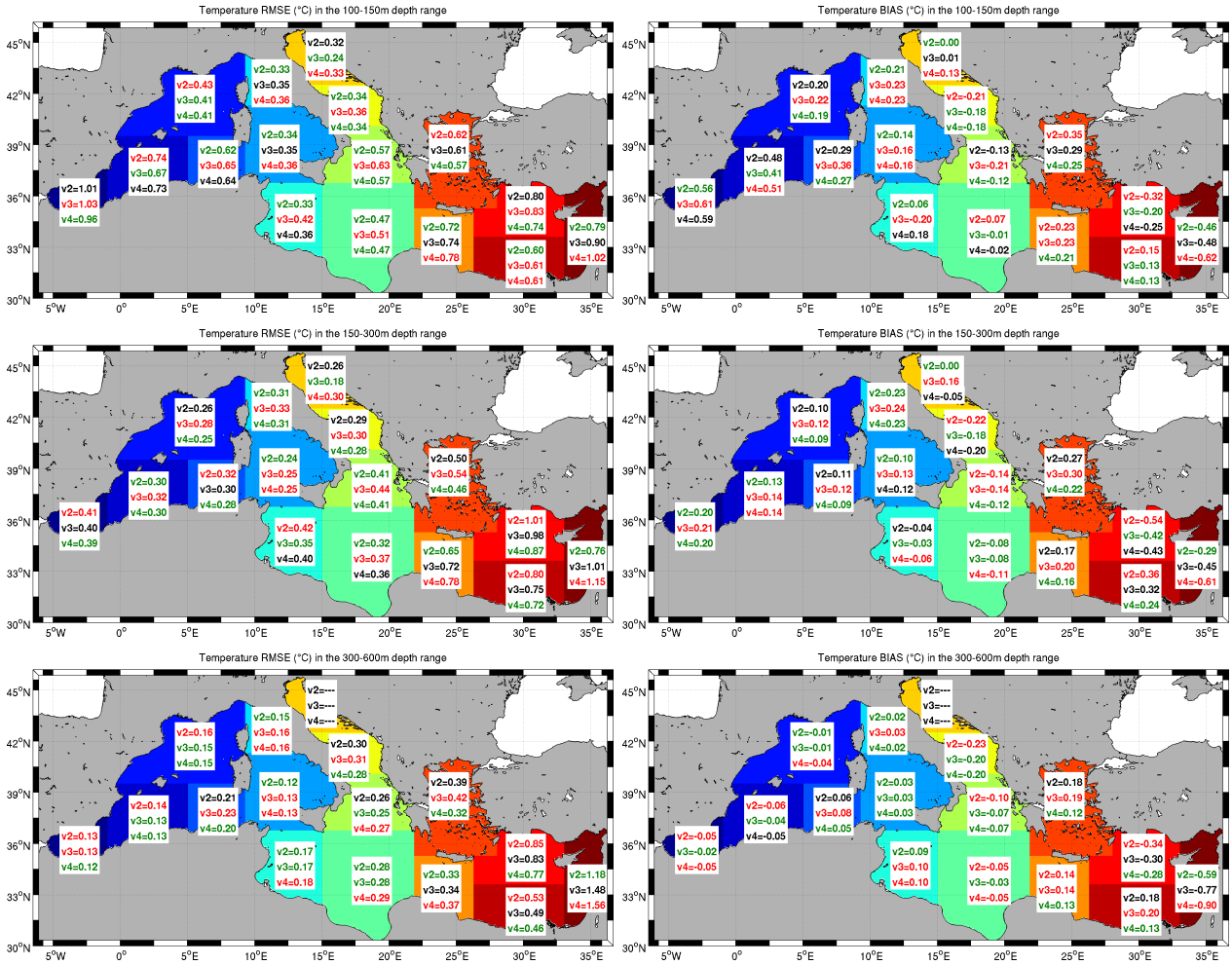

Figure 4.34: Sub-regional mean RMSE and BIAS of temperature (°C) for experiments simrs_v2, simrs_v3 and simrs_v4 at selected depth ranges. For each sub-region the experiment with the lowest temperature RMSE and BIAS is indicated in green, while the experiment with the highest temperature RMSE and BIAS is indicated in red (continued).

4.4.3 Temperature and salinity comparison with climatological data sets and satellite data

The numerical temperature and salinity are evaluated and compared with respect to SeaDataNet V1.1 (hereafter SDN) climatology data set and World Ocean Atlas 2013 version 2 (hereafter WOA) climatology data set, analyzing the tracers distribution pattern through different seasons and considering different significant depths.

By analyzing the differences between experiments simrs_v3 and simrs_v4 with respect to simrs_v2, considered the reference experiment, the impact of river runoff salinity and mixing parameterization at river mouths on the Mediterranean Sea thermohaline properties will be assessed.

Considering the mean temperature and salinity profiles for western, central and eastern Mediterranean Sea, the area showing the largest differences among the three considered experiments is the central Mediterranean Sea, and in particular the Adriatic Sea with differences in salinity profiles limited to the depth range from surface down to about 200 m depth, while temperature is not showing significant differences among the three experiments (Figure 4.35).

In general experiments simrs_v2 and simrs_v4 present very similar vertical salinity and temperature patterns, which are quite in good agreement with the climatological data sets. On the contrary imposing 0 PSU salinity at river mouths has provided a large lowering of the salinity, especially at surface layers and in particular in the areas of largest riverine discharge, as shown in Figure 4.36.

This is particularly evident in the Northern Adriatic Sea (sub-region 11),

where at surface experiment simrs_v3 shows an average salinity value of almost 1 PSU lower with respect to simrs_v2 and simrs_v4, which on the contrary show a good agreement with the climatological data sets considered, in particular the SDN data set.

The large negative differences between simrs_v3 and the other two considered experiments are significant (even though smaller) also in the Southern Adriatic Sea (sub-region 10), where the it shows an average salinity BIAS of about 0.5 PSU with respect to simrs_v2, simrs_v4 and the climatological data sets considered.

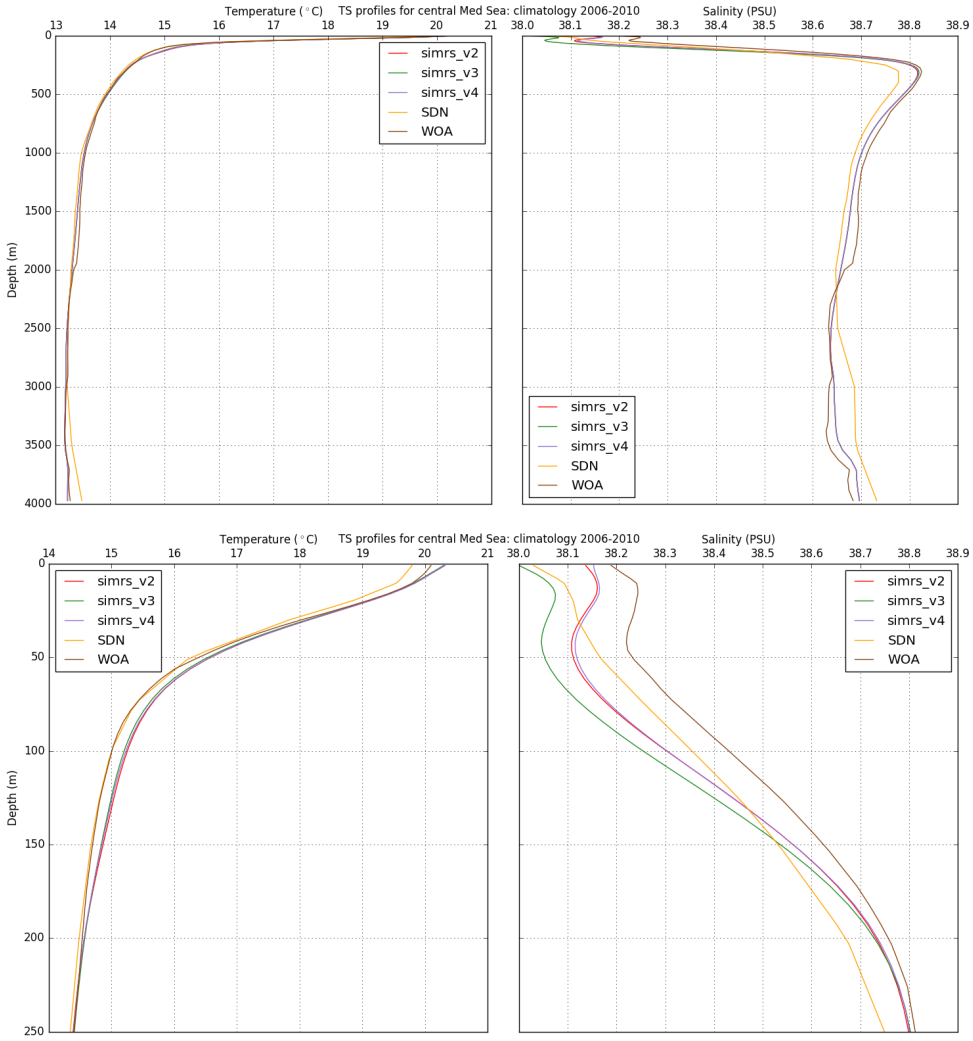

Figure 4.35: Temperature and salinity mean profiles in central Mediterranean Sea for the whole water column (top panel) and for the depth range 0-250 m (bottom panel) over the period 2006-2010 for experiments simrs_v2, simrs_v3, simrs_v4 and SDN and WOA climatological data sets.

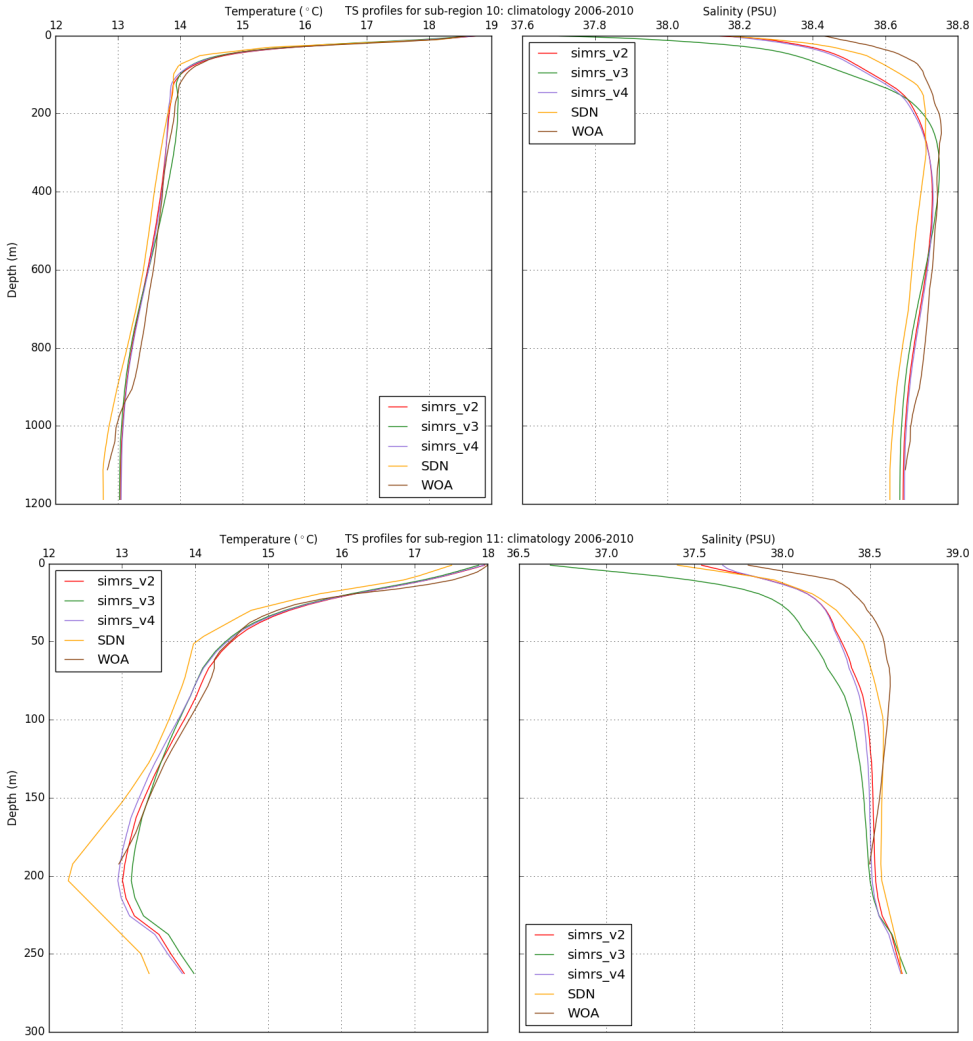

Figure 4.36: Temperature and salinity mean profiles in Southern Adriatic Sea (sub-region 10, top panel) and Northern Adriatic Sea (sub-region 11, bottom panel) over the period 2006-2010 for experiments simrs_v2, simrs_v3, simrs_v4 and SDN and WOA climatological data sets.

The surface salinity pattern and the differences between the experiments are shown in Figure 4.37.

Experiment simrs_v3 shows a general freshening with respect to simrs_v2 along the whole Mediterranean Sea basin, with large negative anomalies (that can exceed 4 PSU) in the whole Adriatic Sea and in particular in correspondence of Po, Rhone and Ebro mouths. Local smaller negative anomalies can be identified along the Balkan coast, in particular in correspondence of the Buna-Bojana river.

Also for the other rivers implemented a very local and slight negative BIAS can be observed.

The Adriatic Sea is the area showing the largest differences between experiments simrs_v2 and simrs_v3: in the northernmost part of the basin significantly lower salinity values can be observed due to the signal of Adige, Brenta, Piave, Livenza, Tagliamento and Isonzo.

The negative anomaly in salinity generated by the aforementioned rivers and by the Po discharge propagates along the Italian coast along the Western Adriatic Coastal Current, down beyond the Gargano Promontory, and offshore towards the Croatian coast, with smaller differences between the two considered experiments. The central part of the Southern Adriatic Sea shows smaller differences with respect to the coastal areas between simrs_v2 and simrs_v3.

In the western part of the Mediterranean Sea basin, the lower salinity discharge from Rhone and Ebro mouths is advected southward along the French and Spanish coast by the Liguro-Provencal-Catalan Current; in addition, the Balearic Sea shows higher salinity values in experiment simrs_v3 with respect to experiment simrs_v2.

In experiment simrs_v4 the local effect of the enhanced vertical mixing

at river mouths is clearly visible, with higher salinity values in correspondence of river outlets: this is particularly evident for Po river, where positive anomalies can exceed 2.5 PSU around the delta; along with the influence of the rivers discharging in the northernmost part of the sub-basin, the Po runoff generates higher salinity values in simrs_v4 with respect to simrs_v2 in the most part of the Northern Adriatic Sea.

For what concern temperature, the main differences between the experiments are not located at surface, but in the upper mixed layer, as can be observed in Figure 4.38.

The differences between experiments simrs_v3 and simrs_v4 with respect to simrs_v2 are comparable, except for the Adriatic Sea and the North Eastern Ionian Sea, where simrs_v3 is largely colder except in the vicinity of the Po river and its plume.

A difference between simrs_v3 and simrs_v4 experiments can be noticed in the Aegean Sea, the latter showing a generally negative temperature anomaly with respect to simrs_v2, while simrs_v3 shows generally higher temperature values with respect to simrs_v2.

Focusing on the eastern part of the Mediterranean Sea basin, in both the experiments with respect to simrs_v2 a warming can be observed in correspondence of the Asia Minor Current, and a general cooling in the area of Rhodes Gyre is displayed by both the experiments with respect to simrs_v2, more pronounced in simrs_v3.

Moving towards the eastern Italian coast, a warming in correspondence of the South-Eastern Tyrrhenian Gyre can be observed for both simrs_v3 and simrs_v4 with respect to simrs_v2, as well as between the Lazio coast and the

eastern Sardinia coast.

In the western part of the Mediterranean Sea a cooling affects the Gulf of Lion Gyre in both the experiments (in particular simrs_v3).

Surface salinity differences between simrs_v2 and simrs_v3 are largely evident in the Adriatic Sea, and in particular during Spring (Figure 4.39), mostly due to Po river peak discharge that occurs in May: in Spring the area around the Po river delta shows much lower values in experiment simrs_v3 with respect to simrs_v2, and the negative anomaly is spread along the western Italian coast by the Western Adriatic Coastal Current.

It can be noticed that during Spring the negative anomaly is much less confined towards the Italian coast with respect to Winter and Autumn. This is even more evident in Summer, when the Po river water spreads at the surface over the whole interior of the Northern Adriatic Sea: according to Orlić et al. (1992) [128], this can be due to the heat input that stabilizes the water column, enabling surface waters to spread from the Po river delta towards the interior of the Adriatic basin.

The seasonal differences in temperature with respect to simrs_v2 for the Adriatic Sea at 30 m (not shown) are smaller in simrs_v4 than in simrs_v3, the latter experiment showing a seasonal differences distribution pattern similar to the one previously described for the differences between simrs_v1 and simrs_v2.

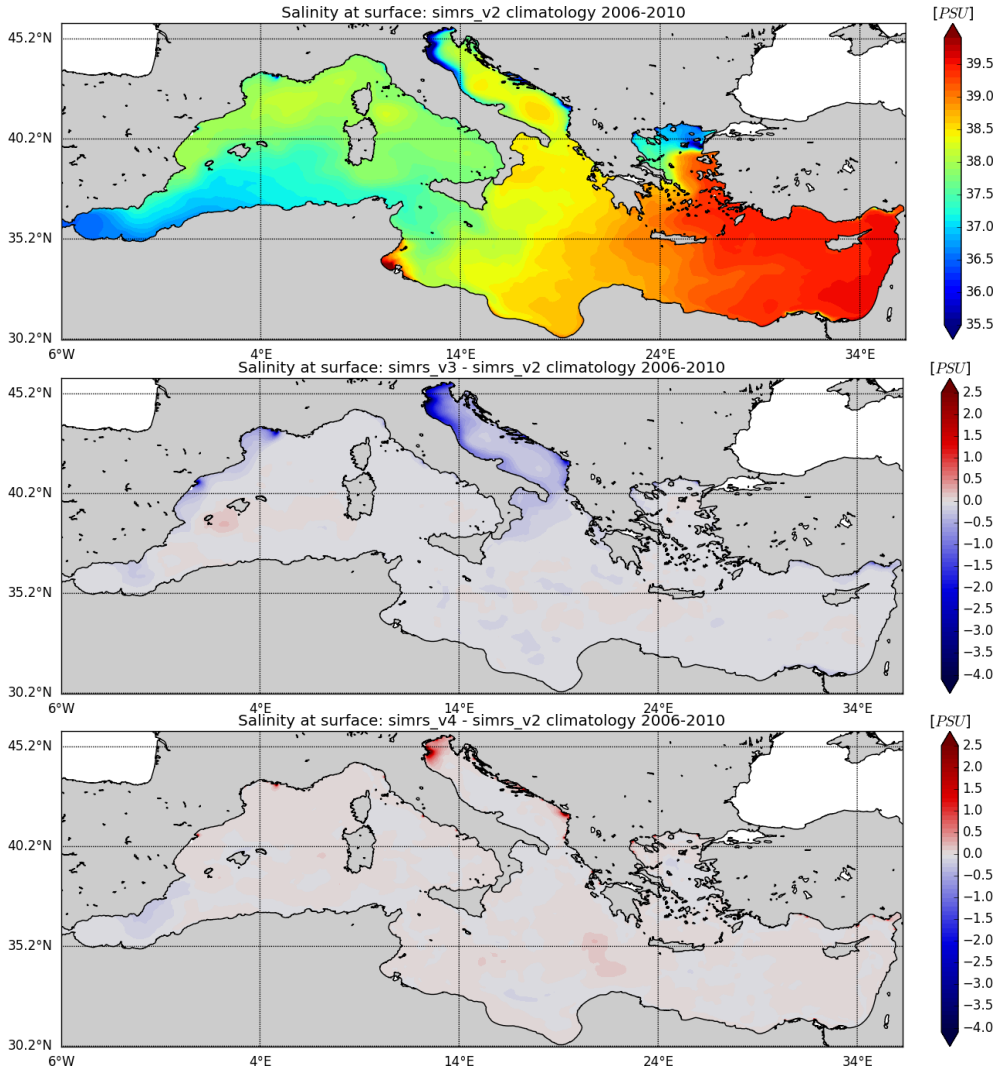

Figure 4.37: Salinity climatology and salinity climatological differences over the period 2006-2010 at surface. From top to bottom panel: simrs_v2, simrs_v3 - simrs_v2, simrs_v4 - simrs_v2.

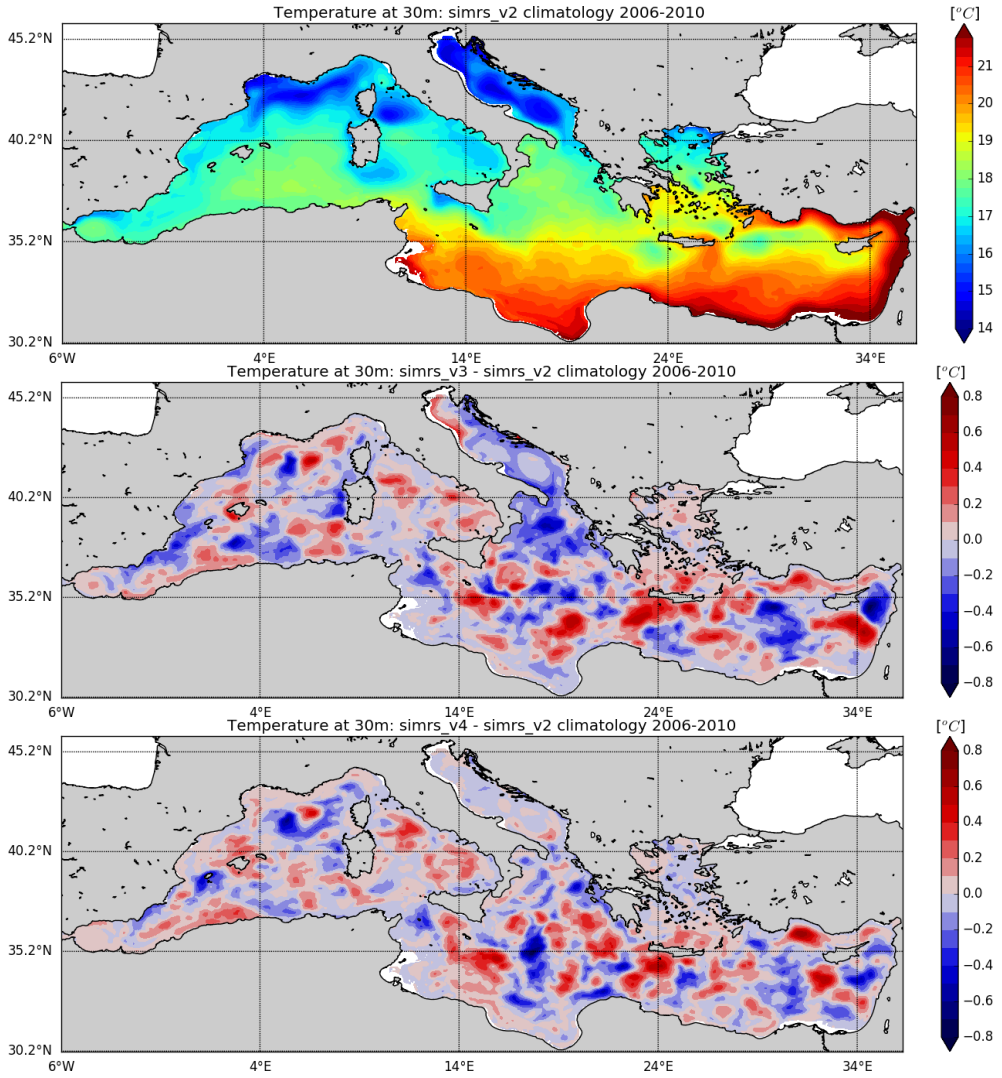

Figure 4.38: Temperature climatology and temperature climatological differences over the period 2006-2010 at 30 m depth. From top to bottom panel: simrs_v2, simrs_v3 - simrs_v2, simrs_v4 - simrs_v2.

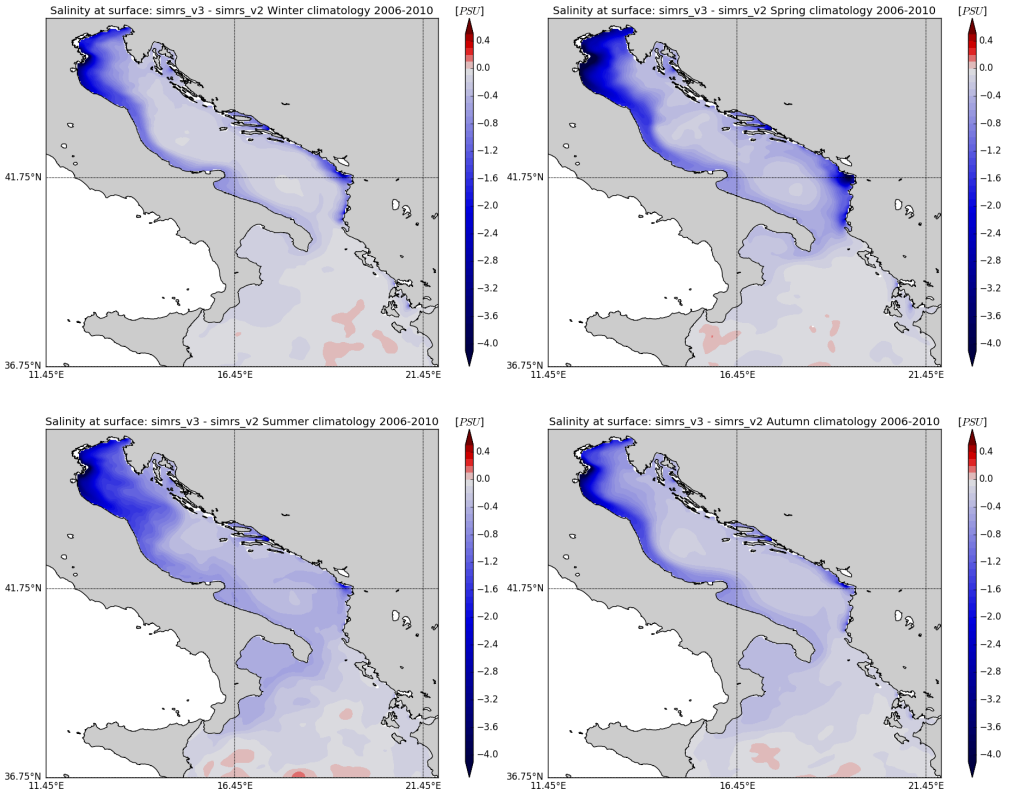

Figure 4.39: Salinity seasonal climatologies over the period 2006-2010 at surface for simrs_v3 - simrs_v2 difference. Top-left panel: Winter (Jan - Mar); top-right panel: Spring (Apr - Jun); bottom-left panel: Summer (Jul - Sep); bottom-right panel: Autumn (Oct - Dec).

The monthly Sea Surface Temperature (SST) RMSE and BIAS of the considered numerical experiments with respect to satellite data are computed and the results at basin scale are summarized in Table 4.8.

The three considered experiments show almost the same SST skill, even though slight differences can be noticed in BIAS during Winter.

Model skill differences at sub-basin scale can be noticed, in particular in

February and in the Northern Adriatic Sea (Figures 4.40 and 4.41).

All the three experiments show a positive BIAS with respect to satellite data, except for the northernmost part of the Adriatic Sea and along the Po river plume advected by the Western Adriatic Coastal Current, where a decrease in SST larger than 1.5 °C is observable.

The largest negative SST anomalies can be observed in the aforementioned areas for experiment simrs_v3, where the 0 PSU salinity prescribed for Po river and for the Northern Adriatic rivers, probably generated a fresh water barrier layer that makes the whole Northern Adriatic Sea more sensitive to the atmospheric forcing (Sauvage et al., 2018 [5]), with a consequent overcooling of the surface water masses.

The same effect can be observed also for experiments simrs_v2 and simrs_v4: it should be noticed that the impact of the increased vertical mixing at river mouths in simrs_v4 produces an attenuate overcooling with respect to the other two experiments, with a positive BIAS with respect to SST data in the area surrounding the Po river delta.

Table 4.8: RMSE and BIAS of SST (°C) for experiments simrs_v2, simrs_v3 and simrs_v4 with respect to satellite data. Statistics consider the whole Mediterranean Sea basin.

Month	**SST RMSE simrs_v2**	**SST RMSE simrs_v3**	**SST RMSE simrs_v4**	**SST BIAS simrs_v2**	**SST BIAS simrs_v3**	**SST BIAS simrs_v4**
Jan	0.54	0.53	0.53	0.22	0.19	0.21
Feb	0.49	0.48	0.49	0.21	0.19	0.21
Mar	0.48	0.47	0.48	0.24	0.22	0.24
Apr	0.51	0.51	0.51	0.29	0.28	0.29
May	0.56	0.56	0.56	0.31	0.31	0.31
Jun	0.62	0.62	0.62	0.33	0.33	0.33
Jul	0.69	0.69	0.69	0.30	0.30	0.30
Aug	0.70	0.70	0.70	0.23	0.22	0.22
Sep	0.67	0.67	0.66	0.20	0.20	0.20
Oct	0.63	0.62	0.62	0.12	0.12	0.12
Nov	0.60	0.59	0.59	0.12	0.12	0.13
Dec	0.57	0.56	0.56	0.17	0.15	0.17

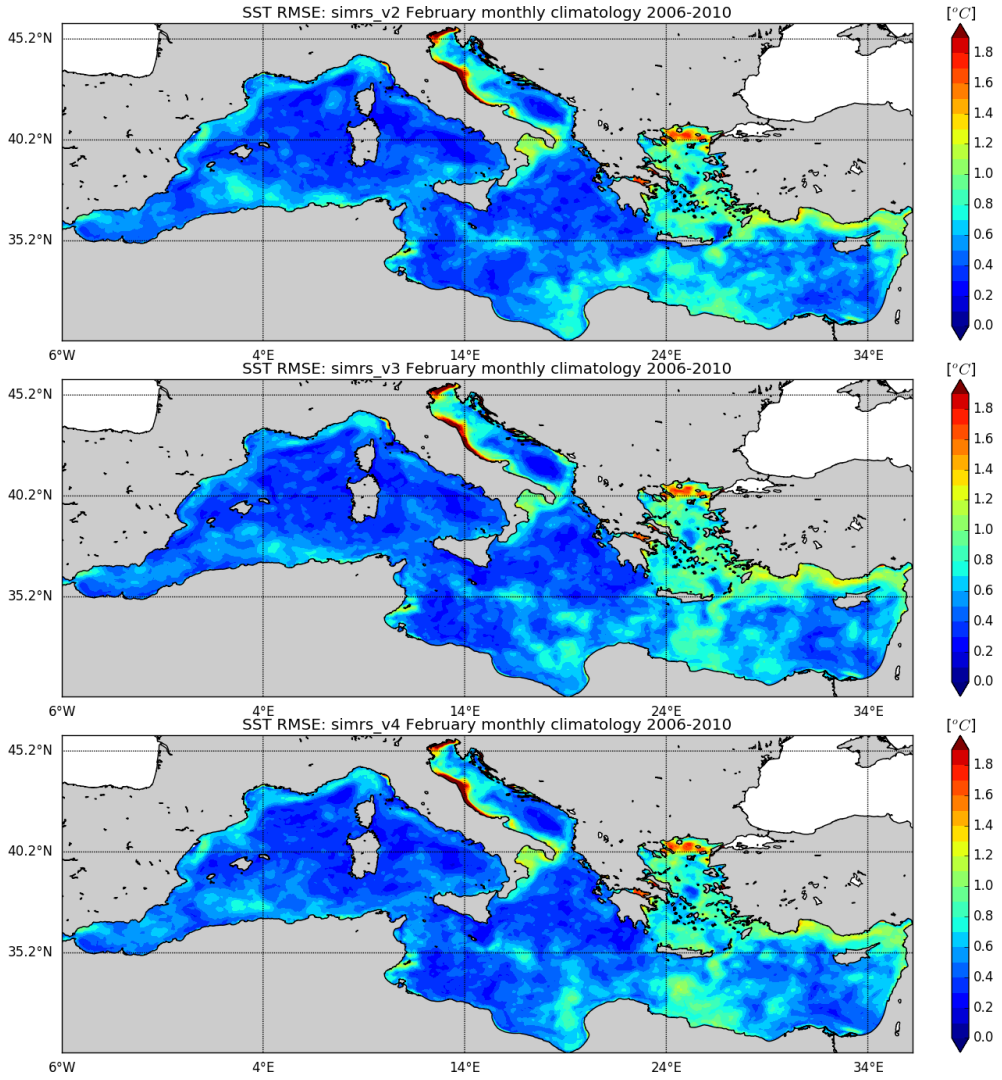

Figure 4.40: February sea surface temperature climatological RMSE. From top to bottom panel: simrs_v2 RMSE, simrs_v3 RMSE, simrs_v4 RMSE.

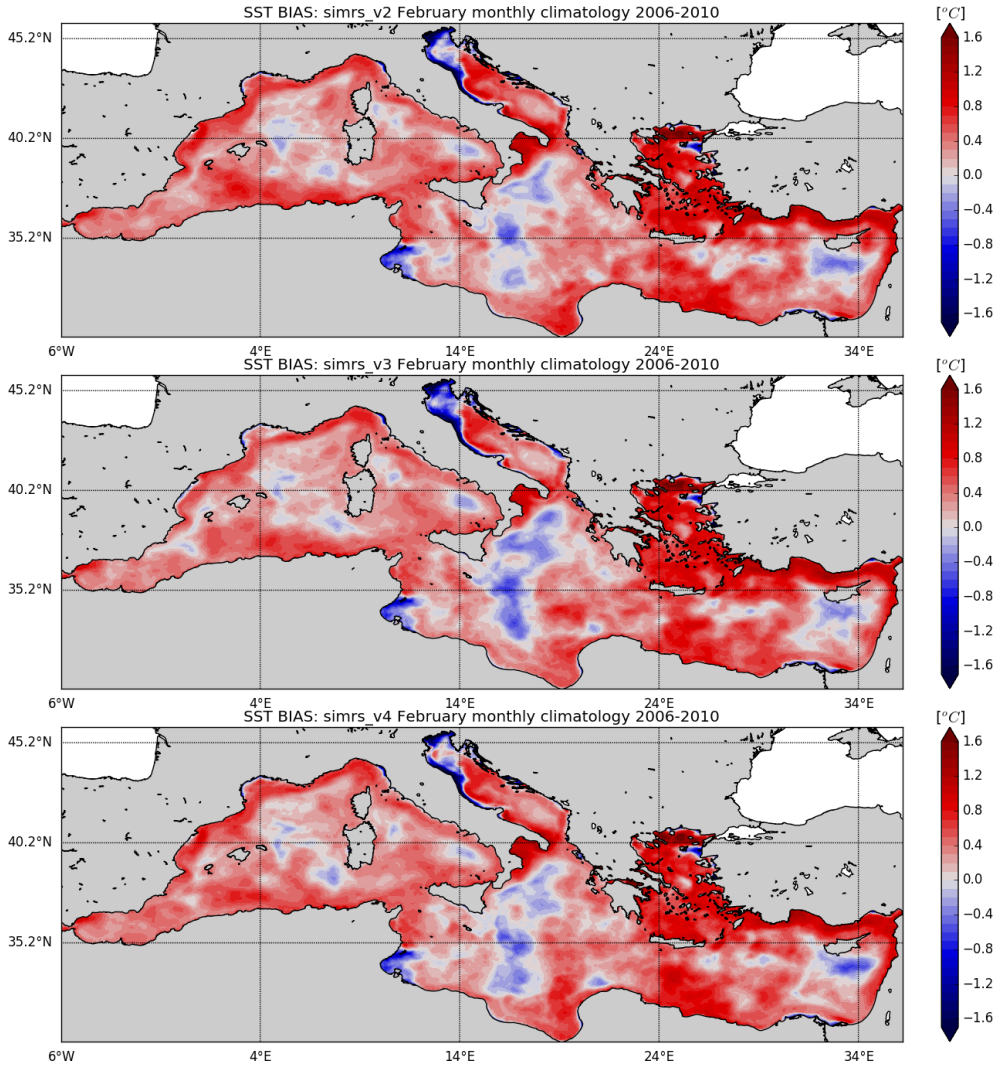

Figure 4.41: February sea surface temperature climatological BIAS. From top to bottom panel: simrs_v2 BIAS, simrs_v3 BIAS, simrs_v4 BIAS.

Time series of volume and layer-averaged salinity are presented in Figure 4.42, where simrs_v2 and simrs_v4 show similar results, while lower values are confirmed in the case of 0 PSU river salinity experiment at all layers.

Concerning sea surface salinity both simrs_v2 and simrs_v4 show a good

agreement with WOA climatological data set, while simrs_v3 is closer to SDN climatology. The volume mean salinity values for experiments simrs_v2 and simrs_v4 show a slight positive trend.

In the depth range between surface and 100 m depth, all the three experiments considered show a negative trend, which is more pronounced for simrs_v3, the latter being the experiment that more underestimate both the climatological data sets considered, that on the contrary are quite well fitted by simrs_v2 and simrs_v4.

Concerning the depth range between 100 and 300 m all the three experiments show an overestimation of salinity with respect to the considered climatological data sets.

A slightly positive trend in all the experiments is visible at the depth range between 300 m depth and the bottom, where the numerical results well fit the SDN climatological data set, even though the seasonal variability shown by SDN is not present in the considered experiments.

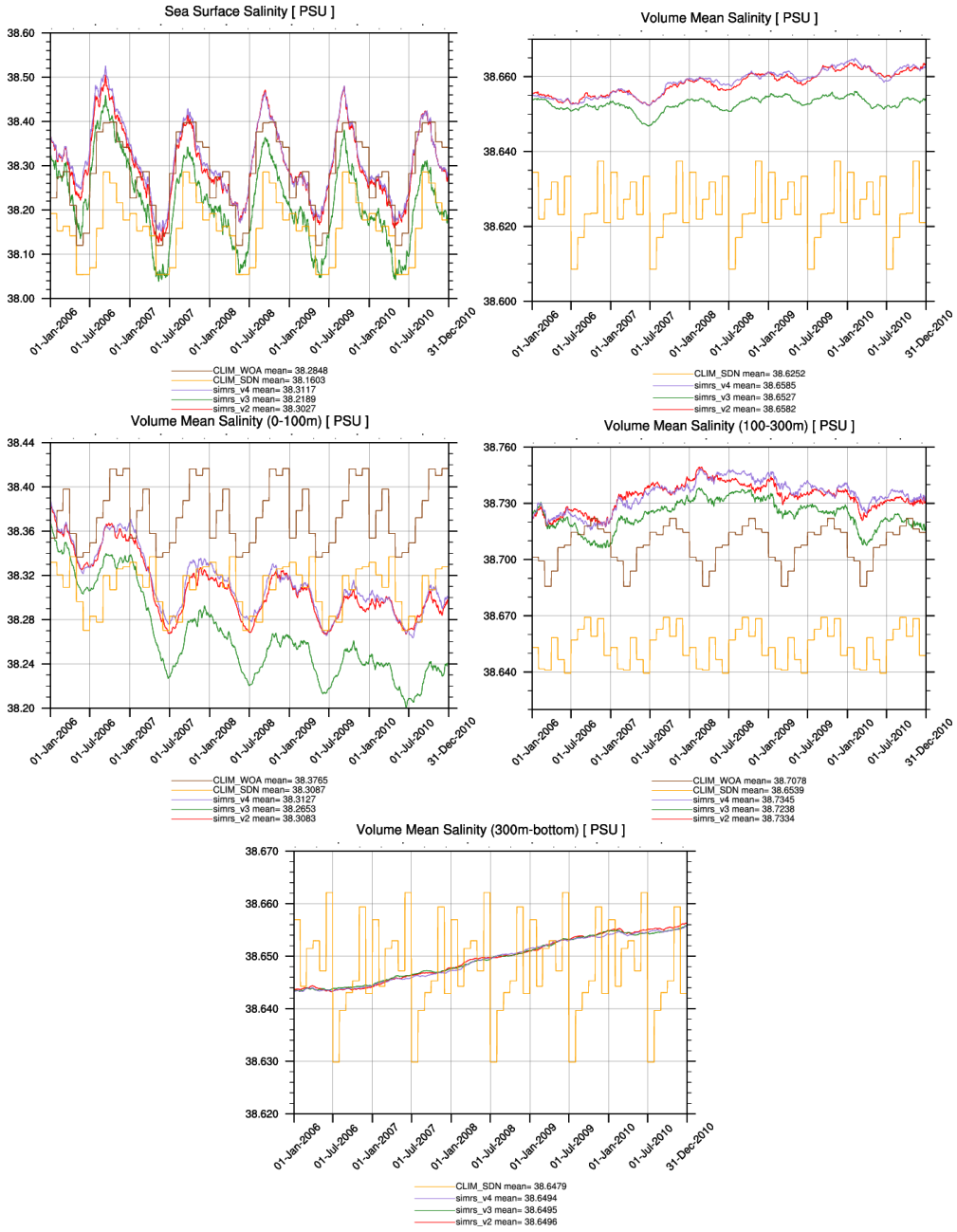

Figure 4.42: Mediterranean Sea salinity daily mean computed from numerical experiments and climatological data sets at different layers.

4.4.4 Mixed Layer Depth comparison with climatologies

Considering the Mixed Layer Depth (MLD), the major impacts provided by the tested river runoff implementations are observed during Winter season and especially in the Southern Adriatic Sea.

During February, the reference experiment simrs_v2 shows the deepest MLD at the South Adriatic Gyre and Northern Ionian Cyclonic Gyre.

In the same areas the null river salinity has provided a shallowing of the MLD, being closer to the Houpert et al. (2015) [103] climatological values.

A shallowing of MLD in the Gulf of Taranto with respect to simrs_v2 can be observed also in experiment simrs_v4, that on the contrary is not showing large differences in MLD in Southern Adriatic.

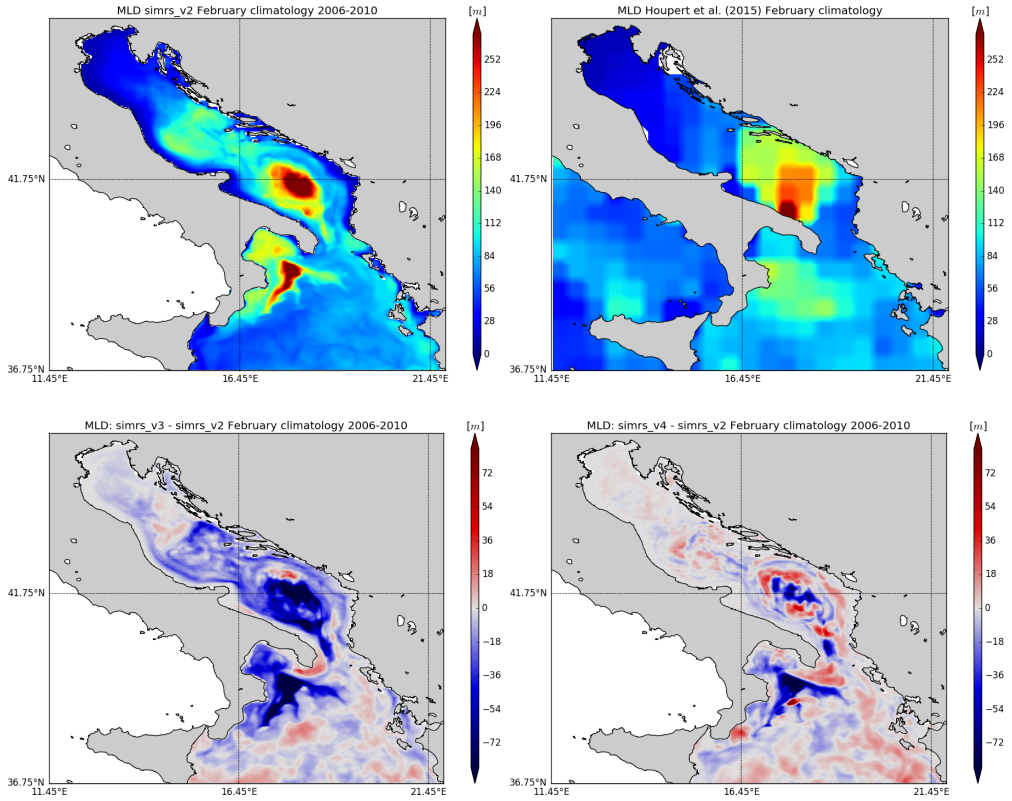

Figure 4.43: February climatological Mixed Layer Depth over the period 2006-2010 in Adriatic Sea and North Eastern Ionian Sea. Top-left panel: simrs_v2; top-right panel: Houpert et al. (2015) climatological data set; bottom-left panel: simrs_v3 - simrs_v2; bottom-right panel: simrs_v4 - simrs_v2.

4.4.5 Currents and water volume transport at straits

The circulation pattern at 15 m depth and in the 200-300 m layer are evaluated for all the experiments as an average of the experimental period and compared to Pinardi et al. (2015) [33], showing a good agreement with

literature (not shown).

Hereafter the Mediterranean Sea surface circulation during Winter period is presented for experiment simrs_v2 together with the differences with the two considered experiments (Figure 4.44), showing the largest differences between simrs_v3 and simrs_v4 with respect to simrs_v2 in the Adriatic Sea and along the Liguro-Provencal-Catalan Current.

In the Adriatic Sea simrs_v3 shows a general increase of the velocity amplitude with respect to simrs_v2, particularly evident along the Western Adriatic Coastal Current and in the segment of Northern Ionian Cyclonic Gyre close to the Italian coast, while a weakening of the eastern edge of the South Adriatic Gyre can be noticed in simrs_v3 with respect to simrs_v2.

On the contrary, simrs_v4 does not show significant differences in velocity amplitude with respect to simrs_v2 for the Adriatic Sea, with the exception of a weakening of the South Adriatic Gyre.

In the central Mediterranean Sea for both simrs_v3 and simrs_v4 a weakening of the North Tyrrhenian Gyre with respect to simrs_v2 is noticeable, while in the western Mediterranean Sea significant differences can be identified in the Liguro-Provencal-Catalan Current: this is particularly evident in simrs_v3, where the contribution of Rhone river and Ebro river is significant.

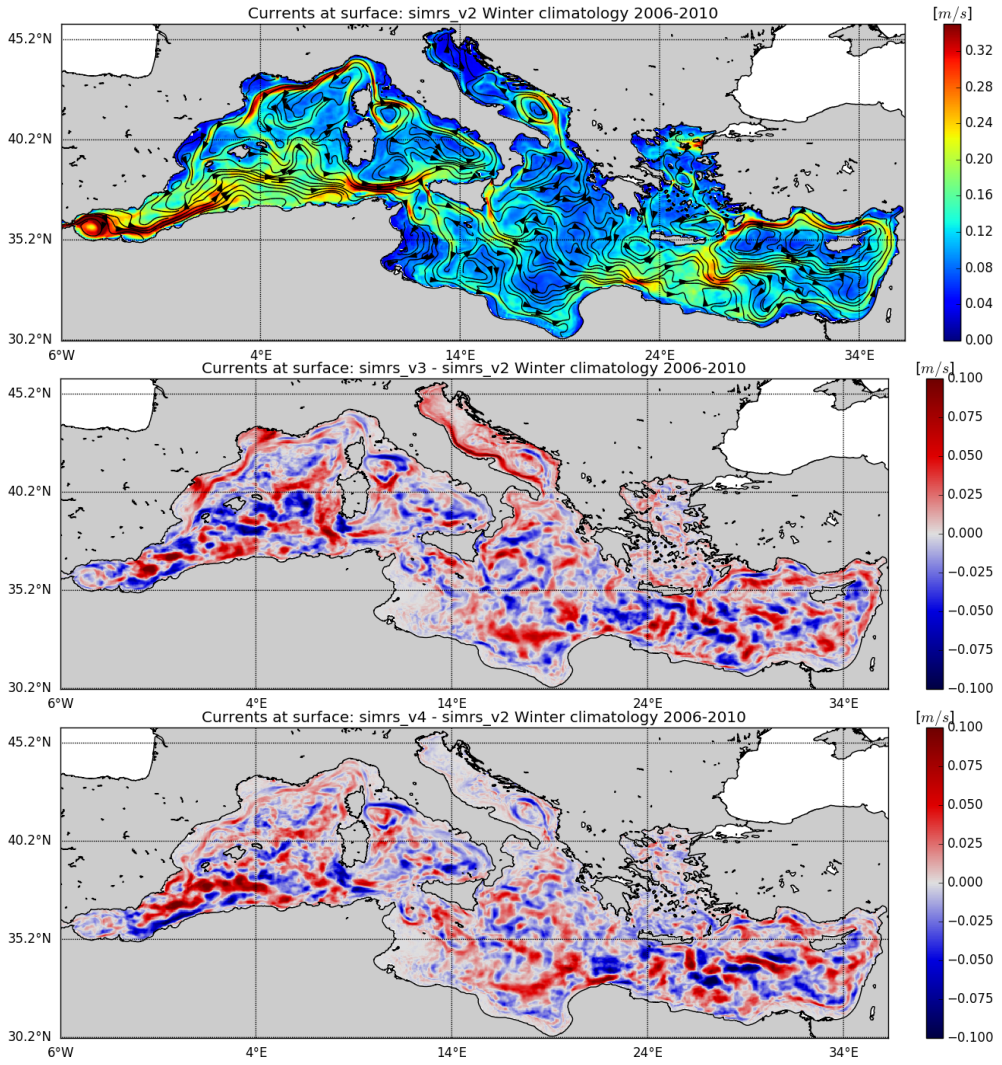

Figure 4.44: Winter average surface circulation over the period 2006-2010. From top to bottom panel: simrs_v2, simrs_v3 - simrs_v2, simrs_v4 - simrs_v2.

Comparing the water volume transport through the Strait of Gibraltar (Table 4.9) the three experiments provide similar results which are close to the literature ones, with a slightly decreased eastward and westward transport when imposing 0 PSU river salinity.

The net mean water volume transport through the Strait of Otranto (Table 4.10 is the same for the three experiments, being clearly lower with respect to the available literature, while the northward and southward transports are closer to the literature ones, presenting lower values in case of 0 PSU river salinity.

For what concern the Strait of Sicily (Table 4.11), the three experiments show very similar values, even though simrs_v3 is the experiment showing the lowest water volume transport, while simrs_v2 is the experiment showing the highest water volume transport through the Strait of Sicily.

Table 4.9: Strait of Gibraltar water volume transport [Sv] from simrs_v2, simrs_v3 and simrs_v4 averaged over the period 2006-2010 compared to literature values.

Gibraltar mean transport [Sv]	**simrs_v2**	**simrs_v3**	**simrs_v4**	**Soto-Navarro et al., 2010**	**Candela 2001**
Net	0.043	0.043	0.043	0.038 ±0.007	0.04
Eastward	0.900	0.881	0.896	0.81 ±0.06	1.01
Westward	0.857	0.839	0.853	0.78 ±0.05	0.97

Table 4.10: Strait of Otranto water volume transport [Sv] from simrs_v2, simrs_v3 and simrs_v4 averaged over the period 2006-2010 compared to literature values.

Otranto mean transport [Sv]	**simrs_v2**	**simrs_v3**	**simrs_v4**	**Yari et al., 2012**	**Astraldi et al., 1999**
Net	-0.004	-0.004	-0.004	-0.04 ±0.28	0.01
Northward	0.915	0.861	0.918	0.90 ±0.04	1.15 ±0.53
Southward	0.919	0.865	0.923	0.94 ±0.32	1.16 ±0.53

Table 4.11: Strait of Sicily water volume transport [Sv] from simrs_v2, simrs_v3 and simrs_v4 averaged over the period 2006-2010 compared to literature values.

Sicily mean transport [Sv]	**simrs_v2**	**simrs_v3**	**simrs_v4**
Net	0.105	0.091	0.100
Northward	1.940	1.911	1.926
Southward	1.835	1.820	1.825

4.4.6 Sea Surface Height comparison with satellite data

Even though the basin-average metrics (Figure 4.45) have shown a similar skill, local differences can be observed when analyzing the differences between the spatial pattern of the sea level differences among the three experiments (Figure 4.46).

As in previous analysis, the experiments present differences in the whole basin, but the areas where a direct connection between riverine inputs and SSH can be identified are the Adriatic Sea and the Liguro-Provencal zone.

This is much more evident in simrs_v3 with respect to simrs_v4, due to the 0 PSU salinity prescribed for riverine outflow.

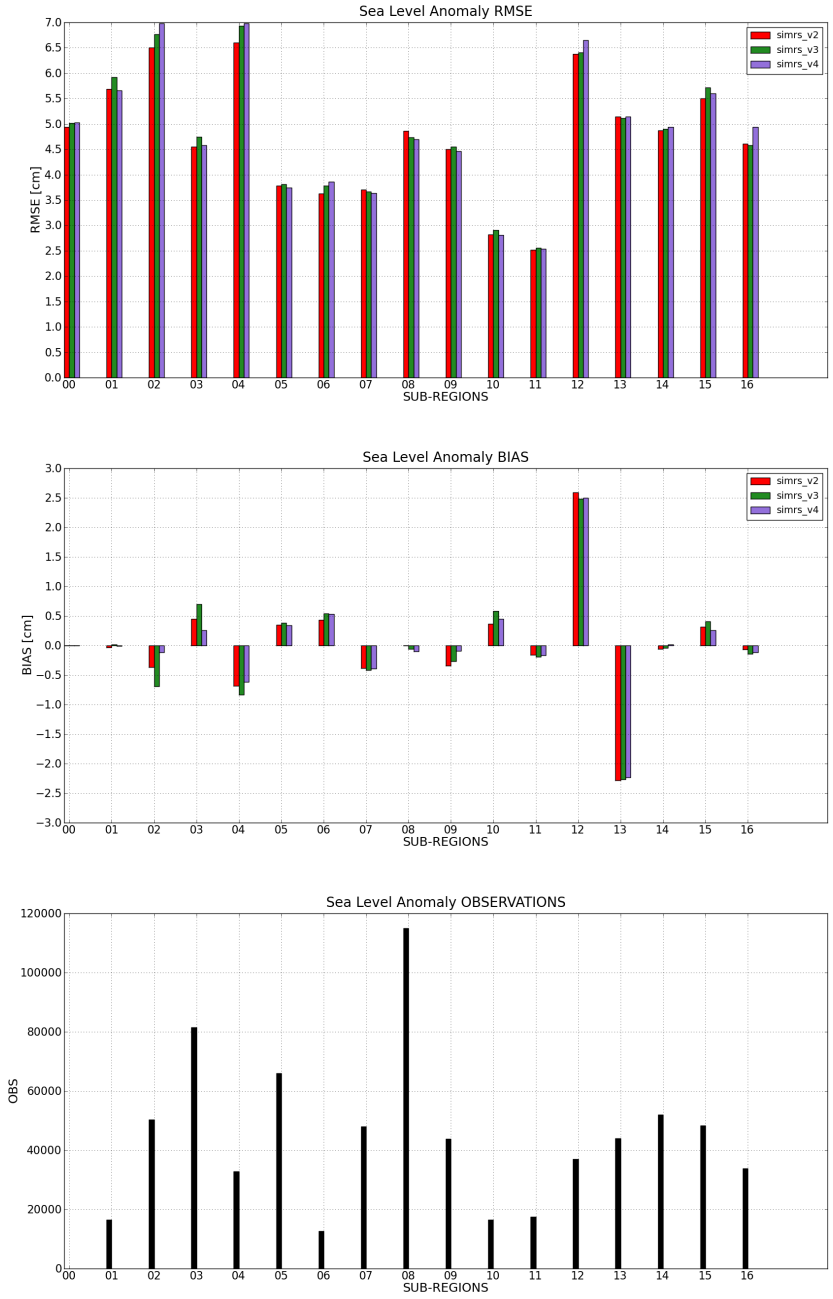

Figure 4.45: Sea Level Anomaly (cm) metrics of simrs_v2, simrs_v3 and simrs_v4 computed over the period 2006-2010 for the Mediterranean Sea (00) and for the 16 sub-regions. From top to bottom panel: RMSE, BIAS, number of observations.

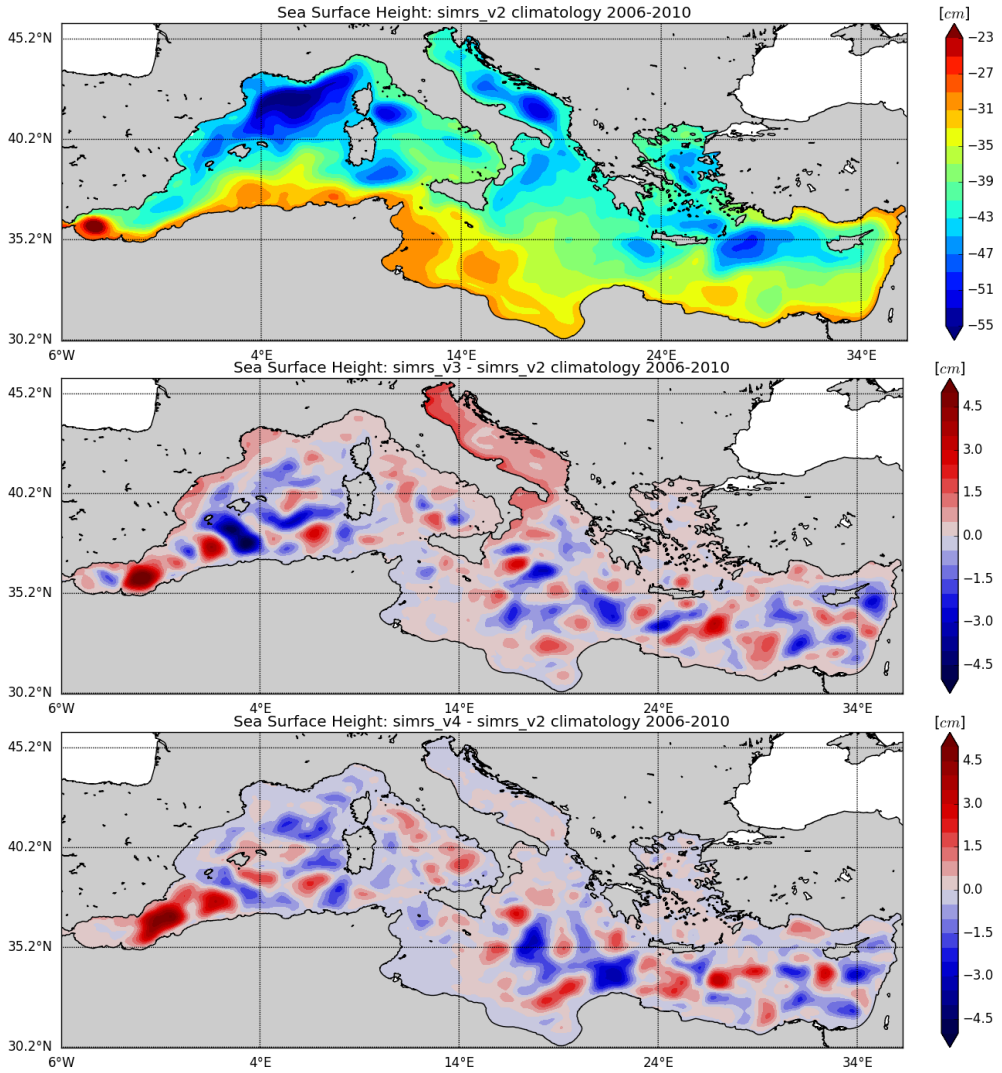

Figure 4.46: Mean simrs_v2 SSH and SSH differences between experiments over the period 2006-2010. From top to bottom panel: simrs_v2, simrs_v3 - simrs_v2, simrs_v4 - simrs_v2.

4.5 Sensitivity experiments on vertical mixing scheme

Given the significant impact of river runoff on the vertical structure of the water column in the ROFIs and the differences in the model salinity and temperature representation skills along the different depth ranges considered, the impact due to a different vertical mixing closure scheme in the Mediterranean Sea ocean model is investigated in this section.

As already described in section 2.1.3, in the experiments carried out so far the vertical eddy diffusivity and viscosity coefficients are computed through a local Richardson number dependent formulation (Pacanowski and Philander, 1981 [92]), which is shown in Equation 4.3.

The vertical mixing scheme chosen to estimate the impact of the vertical mixing parameterization is the TKE scheme, firstly adapted to the ocean (starting from the atmospheric case) by Gaspar et al. (1990) [139]: it is based on the computation of vertical eddy diffusivity and viscosity coefficients through the turbulent kinetic energy and the mixing length scale (Reffray et al., 2015 [140]).

The prognostic equation for the turbulent kinetic energy $\overline{e}$ (m^2/s^2) reads as follows (Calvert and Siddorn, 2013 [141]):

$$\frac{\partial \overline{e}}{\partial t} = K_m \left(\frac{\partial \overline{U}_h}{\partial z} \right)^2 - K_\rho N^2 + \frac{\partial}{\partial z} \left(K_e \frac{\partial \overline{e}}{\partial z} \right) - \varepsilon \tag{4.5}$$

where $\overline{U}_h$ $(m\ kg\ s^{-1})$ is the horizontal momentum and N is the local Brunt-Vaisälä frequency, K_m and K_ρ (m^2/s) are respectively the vertical eddy viscosity and the vertical eddy diffusivity coefficients, K_e (m^2/s) is an

additional eddy diffusivity coefficient, while ε is the dissipation term.

K_m and K_ρ are defined as:

$$K_m = c_k l_k \sqrt{\overline{e}} \tag{4.6}$$

$$K_\rho = \frac{K_m}{P_{rt}} \tag{4.7}$$

In Equation 4.6, c_k is a constant and denotes a stability function, while l_k (m) indicates a mixing length scale. In equation 4.7, P_{rt} is the Prandtl number (Calvert and Siddorn, 2013 [141]).

In Equation 4.5 the dissipation term ε in the Kolmogorov (1942) [142] form reads as follows:

$$\varepsilon = c_\varepsilon \frac{e^{-3/2}}{l_\varepsilon} \tag{4.8}$$

with c_ε denoting a constant, while l_ε indicating a dissipation length scale (Calvert and Siddorn, 2013 [141]).

Several processes in the TKE scheme are only partially resolved, thus additional parameterization is required, so that the accuracy of the vertical mixing scheme depends on a correct calibration of the parameters introduced (Calvert and Siddorn, 2013 [141]).

In the light of this additional needed tuning, several short tests are performed, choosing different parameterizations for the TKE scheme, and the results are evaluated with respect to insitu observations in order to define an optimal setup for the TKE scheme, with the purpose of designing a further experiment to be compared with simrs_v2 (the experiment providing at this

stage the best results using a local Richardson number dependent formulation for the vertical mixing scheme).

The calibration tests are run for the Winter period of 2014 and mainly focus on the tuning of two parameters: the coefficient of the surface input of tke due to surface breaking (α, rn_ebb parameter in NEMO model namelist) and the Langmuir turbulence coefficient (c_{LC}, rn_lc parameter in NEMO model namelist).

According to Craig and Banner (1994) [143] the boundary condition for surface TKE reads as follows:

$$\overline{e} = \frac{1}{2}\left(15.8\alpha_{CB}\right)^{2/3}\frac{|\tau|}{\rho_0} \tag{4.9}$$

where α_{CB} is the Craig and Banner (1994) [143] constant of proportionality, depending on wave age (Madec et al., 2017 [78]), τ (N/m^2) is the wind stress and ρ_0 (kg/m^3) is the reference density.

Within NEMO model the surface boundary condition for TKE is defined as:

$$\overline{e} = \alpha\frac{|\tau|}{\rho_0} \tag{4.10}$$

thus $\alpha = \frac{1}{2}\left(15.8\alpha_{CB}\right)^{2/3}$

The Langmuir turbulence coefficient c_{LC} is used in the formulation for the vertical velocity profile of the Langmuir circulations w_{LC} as follows (Madec

et al., 2017 [78]):

$$w_{LC} = \begin{cases} c_{LC} u_s \sin\left(-\pi z / H_{LC}\right), & \text{if } -z \leq H_{LC} \\ 0, & \text{otherwise} \end{cases} \tag{4.11}$$

where u_s (m/s) is the Stokes drift velocity, z (m) is depth and H_{LC} (m) is the depth of Langmuir circulations (Madec et al., 2017 [78]).

Four sensitivity experiments are performed, built on the basis of simrs_v2, whose different choices in TKE scheme parameterization among each other are summarized in Table 4.12. The run period spans from January 2014 to March 2014.

Table 4.12: TKE vertical mixing scheme parameters tuning in calibration tests.

Parameter	**simrs_v2_tkeA**	**simrs_v2_tkeB**	**simrs_v2_tkeC**	**simrs_v2_tkeD**
α (rn_ebb)	3.75	67.83	3.75	3.75
c_{LC} (rn_lc)	0.15	0.15	0.2	0.05

From a comparison with observations derived from Argo floats the four performed experiments show quite similar results, both in temperature and salinity representation skills, even though focusing on the Adriatic Sea (the area with the largest number of implemented rivers) experiment simrs_v2_tkeA provides slightly better results (not shown). According to this result, a longer experiment based on simrs_v2_tkeA parameterization is performed in the pe-

riod 2014-2015, to be compared with simrs_v2, in order to assess the impact of two different vertical mixing schemes dealing with the thermohaline modifications introduced in the water column by river runoff.

Considering the basin-averaged timeseries of salinity and temperature (Figures 4.47 and 4.48) for different depth ranges an increase in Sea Surface Salinity (SSS) values can be observed in experiment simrs_v2_tkeA for the period January-May, while for the rest of the year simrs_v2 shows slightly higher SSS values.

At depth the main differences in salinity (Figure 4.47) between the two experiments can be observed in the depth range between the surface and 100 m, where from January to August 2015 simrs_v2_tkeA shows higher salinity values with respect to simrs_v2: this is reasonably due to the fact that this is the layer most affected by vertical mixing.

Very small differences can be observed at basin-scale between the two considered experiments for what concern temperature (Figure 4.48), even thought slightly higher values between July and November for simrs_v2_tkeA can be observed in volume mean temperature and in the depth range between surface and 100 m.

Considering the spatial distribution of salinity (Figure 4.49) and temperature (Figure 4.50), the major differences between the two considered experiments are located in the Adriatic Sea and in the Aegean Sea. An increase in SSS in simrs_v2_tkeA with respect to simrs_v2 is evident in both the mentioned areas: this can be observed in particular during Summer, when the freshwater input contributes to increase the seasonal vertical stratification of the water column. The impact of the vertical mixing scheme adopted is thus

clear in regions affected by a large amount of freshwater input, such as the Italian coast along the Po river plume and the Aegean Sea, characterized by a semi-enclosed basin morphology, the high number of rivers discharging and the Black Sea Waters input.

At 30 m depth the behavior of the Aegean Sea is similar with respect to surface. In the Adriatic Sea the differences along the Po river plume are no more noticeable, while the whole sub-basin is characterized by a freshening in experiment simrs_v2_tkeA with respect to simrs_v2.

For what concern temperature differences distribution (Figure 4.50) along the considered period, it is observed that the main differences in temperature at surface occur during Spring, when the whole basin is characterized by a decrease in temperature values in experiment simrs_v2_tkeA.

At 30 m depth it can be instead noticed an increase in temperature values in simrs_v2_tkeA for the whole basin, which is particularly evident during Summer, suggesting a deepening of the thermocline in simrs_v2_tkeA.

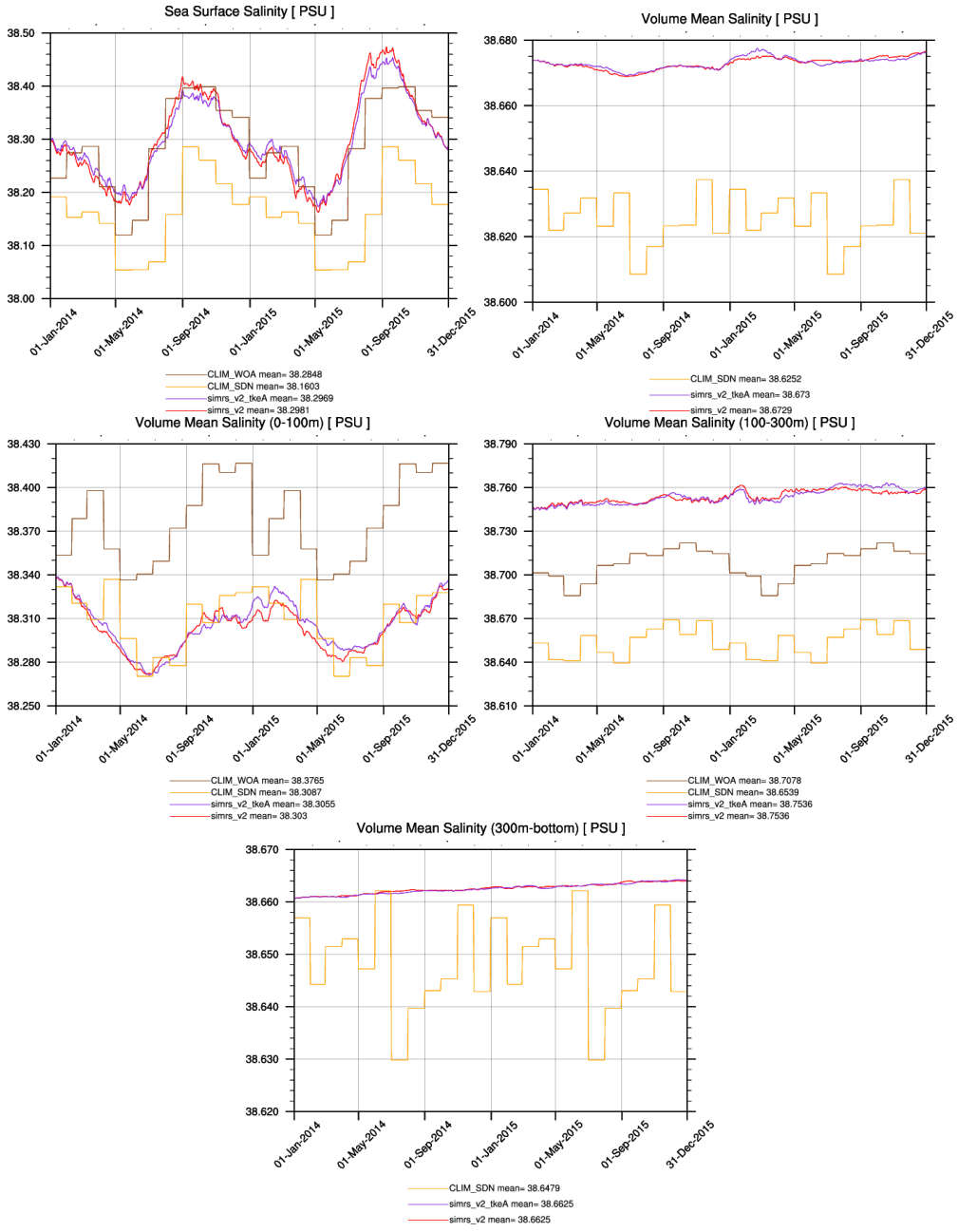

Figure 4.47: Mediterranean Sea salinity daily mean computed from numerical experiments and climatological data sets at different layers.

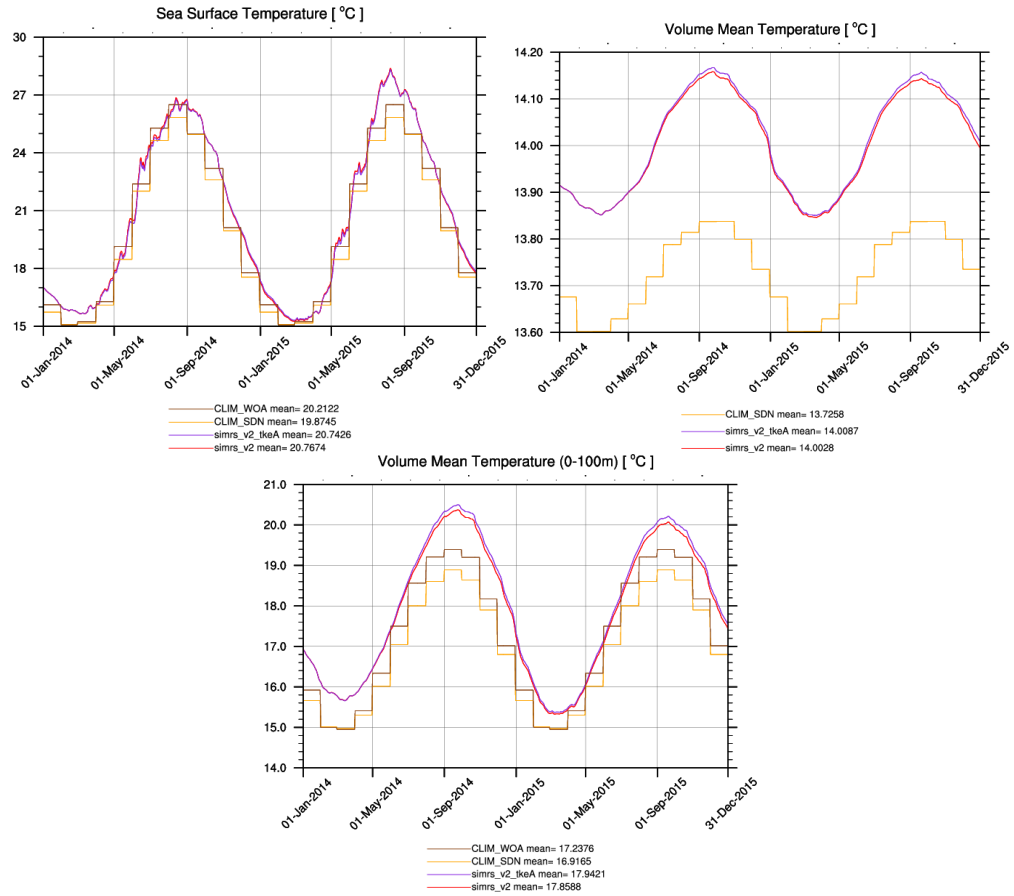

Figure 4.48: Mediterranean Sea temperature daily mean computed from numerical experiments and climatological data sets at different layers.

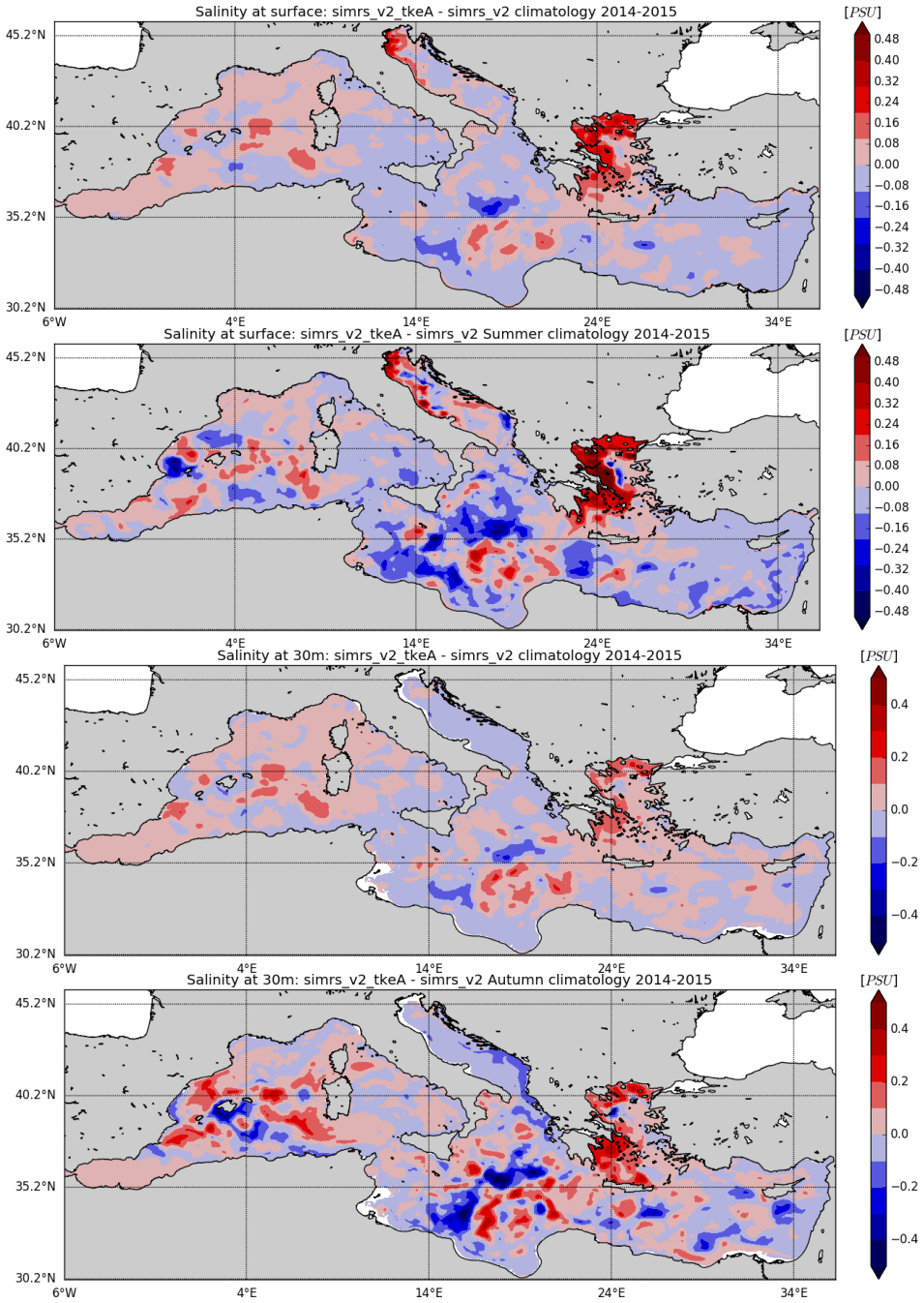

Figure 4.49: simrs_v2_tkeA - simrs_v2 salinity climatology at surface and at 30m depth. From top to bottom panel: climatology for 2014-2015 at surface, summer climatology for 2014-2015 at surface, climatology for 2014-2015 at 30 m depth, autumn climatology for 2014-2015 at 30 m depth.

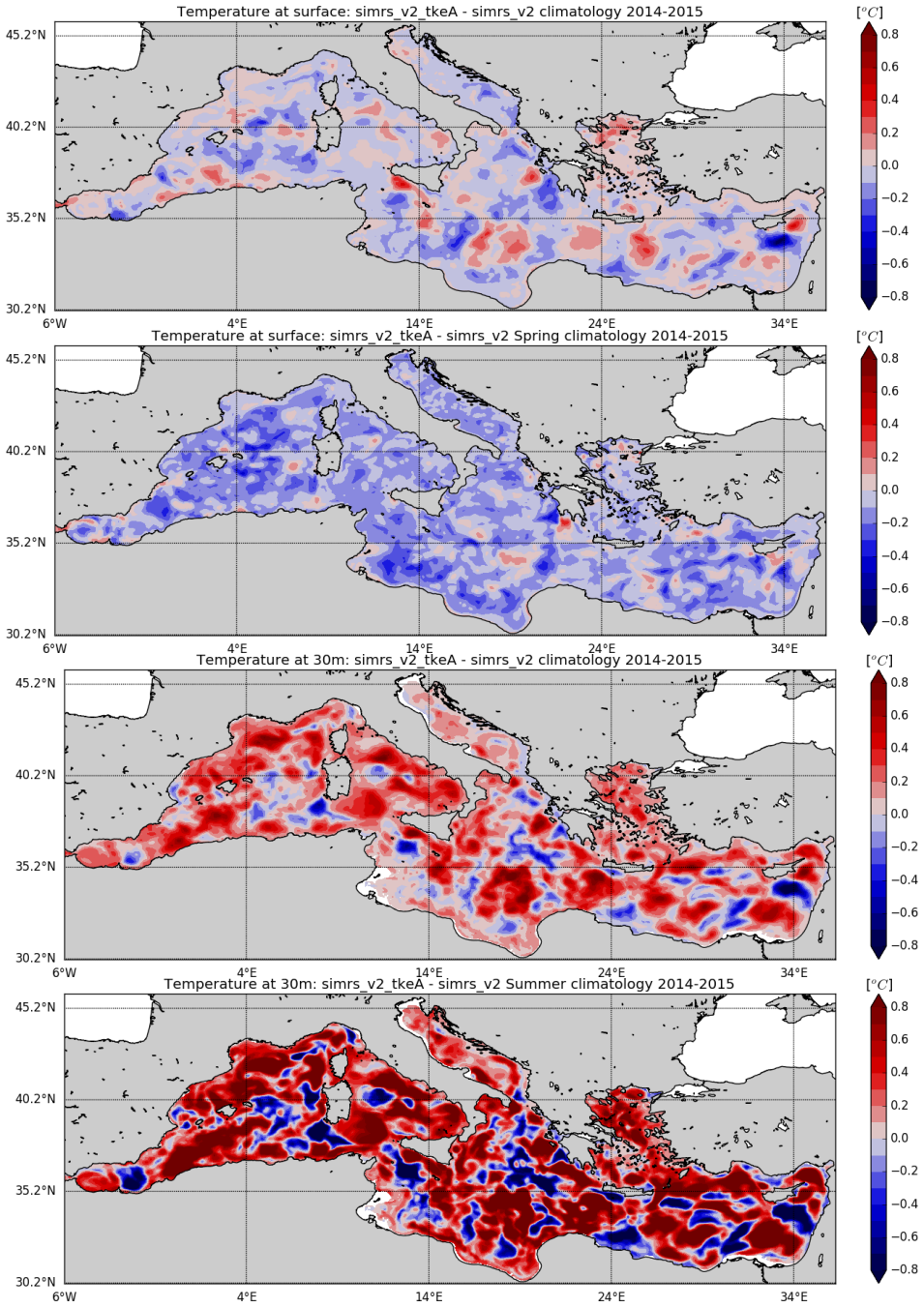

Figure 4.50: simrs_v2_tkeA - simrs_v2 temperature climatology at surface and at 30m depth. From top to bottom panel: climatology for 2014-2015 at surface, summer climatology for 2014-2015 at surface, climatology for 2014-2015 at 30 m depth, autumn climatology for 2014-2015 at 30 m depth.

The assessment of the experiments results with respect to in situ observations shows that at basin scale no particular differences in reproducing salinity skills can be observed between the two performed experiments, for all the depth ranges considered (Figure 4.51).

Concerning temperature, simrs_v2_tkeA shows a slightly higher RMSE with respect to simrs_v2 along the whole water column, due to a general increase in temperature in simrs_v2_tkeA as observable from the BIAS statistics. The main differences between the two experiments are concentrated between 10 and 100 m depth.

When considering the salinity and temperature skill at sub-regional scale (Figures 4.53 and 4.54), focusing on the sub-regions characterized by a large amount of riverine discharge, it can be noticed that in the first 30 m of the water column in the Northern Adriatic Sea (sub-region 11 in Figure 4.7) simrs_v2_tkeA provides better performances in terms of salinity representation with respect to simrs_v2, while at greater depths simrs_v2 is the experiment showing the lowest RMSE.

In the Southern Adriatic Sea (sub-region 10 in Figure 4.7) the differences between the two experiments are smaller with respect to the northern part of the sub-basin, with simrs_v2 showing slightly better skills in the first 100 m of the water column and equivalent results at greater depths.

Significant differences between the two experiments can be observed in temperature representation skill in the Northern Adriatic Sea, where simrs_v2_tkeA performs constantly better with respect to simrs_v2 in the first 150 m of the water column, while at greater depths simrs_v2 provides better results.

Differences in temperature performances are much smaller in Southern

Adriatic Sea, where simrs_v2_tkeA shows the lower RMSE between surface and 60 m, in addition to the depth range between 150 m and the bottom, while at intermediate depths simrs_v2 provides better results.

In the North Eastern Ionian Sea (sub-region 9 in Figure 4.7) simrs_v2 shows lower salinity RMSE values with respect to simrs_v2_tkeA for the entire water column, in particular from the surface down to 100 m depth.

In the Aegean Sea (sub-region 13 in Figure 4.7) simrs_v2 provides better results in the depth range between surface and 60 m depth, while at greater depths the two experiments show an equivalent salinity RMSE.

simrs_v2_tkeA has lower temperature RMSE in the first 30 m of the North Eastern Ionian Sea, while simrs_v2 shows better results at greater depths.

The temperature representation skills of the two experiments is very similar at depth (from 60 m down to the bottom) in the Aegean Sea, while in the first portion of the water column simrs_v2 shows a lower RMSE with respect to simrs_v2_tkeA (with the exception of the first 10 meters).

In the Central-South Levantine Sea (sub-region 15 in 4.7), where Nile river has its own outlet, simrs_v2_tkeA shows an improvement in terms of salinity representation, in particular between the surface and 60 m depth; the same improvement can be noticed also for temperature skill, even though less significant.

In the North Western Mediterranean Sea (sub-region 3 in 4.7), characterized by the Rhone river discharge, simrs_v2_tkeA provides better results in terms of salinity representation, while very similar values for the two experiments can be observed at greater depths.

The improvement shown by simrs_v2_tkeA in salinity skill is not confirmed

for temperature skill; simrs_v2 indeed has lower temperature RMSE values from the surface down to 150 m, while the performances are equivalent at greater depths.

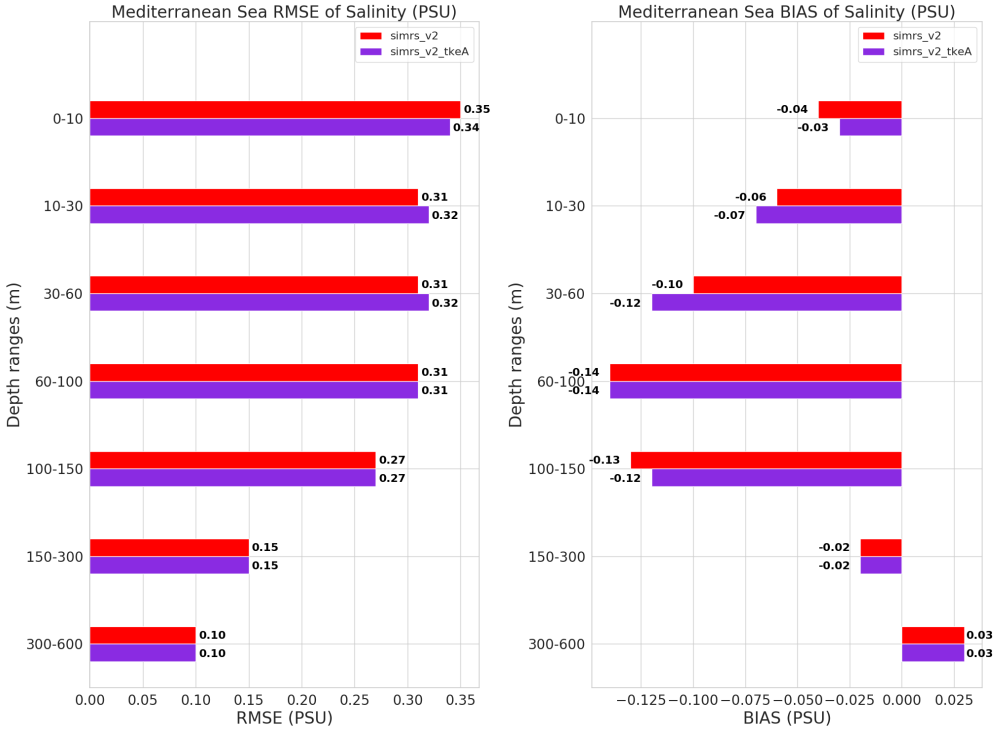

Figure 4.51: Mediterranean Sea mean RMSE and BIAS of salinity (PSU) for experiments simrs_v2 and simrs_v2_tkeA.

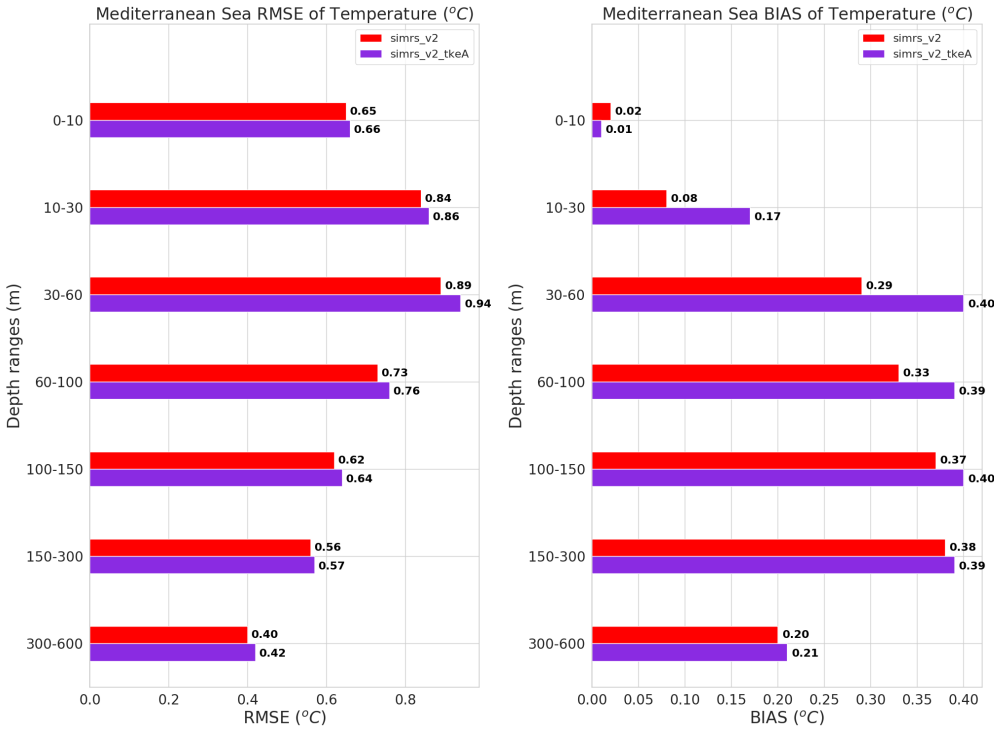

Figure 4.52: Mediterranean Sea mean RMSE and BIAS of temperature (°C) for experiments simrs_v2 and simrs_v2_tkeA.

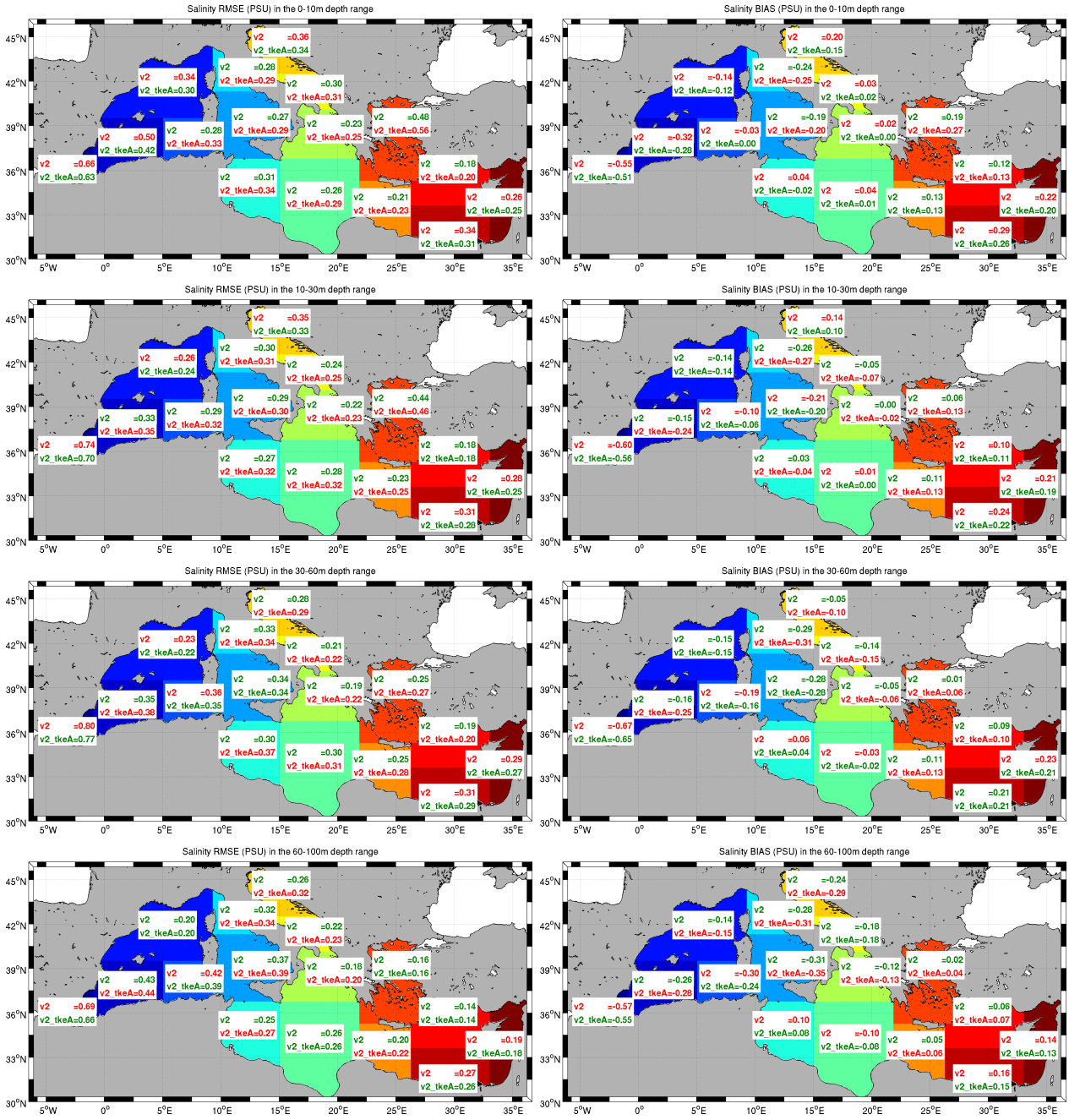

Figure 4.53: Sub-regional mean RMSE and BIAS of salinity (PSU) for experiments simrs_v2 and simrs_v2_tkeA at selected depth ranges. For each sub-region the experiment with the lowest salinity RMSE and BIAS is indicated in green, while the experiment with the highest salinity RMSE and BIAS is indicated in red.

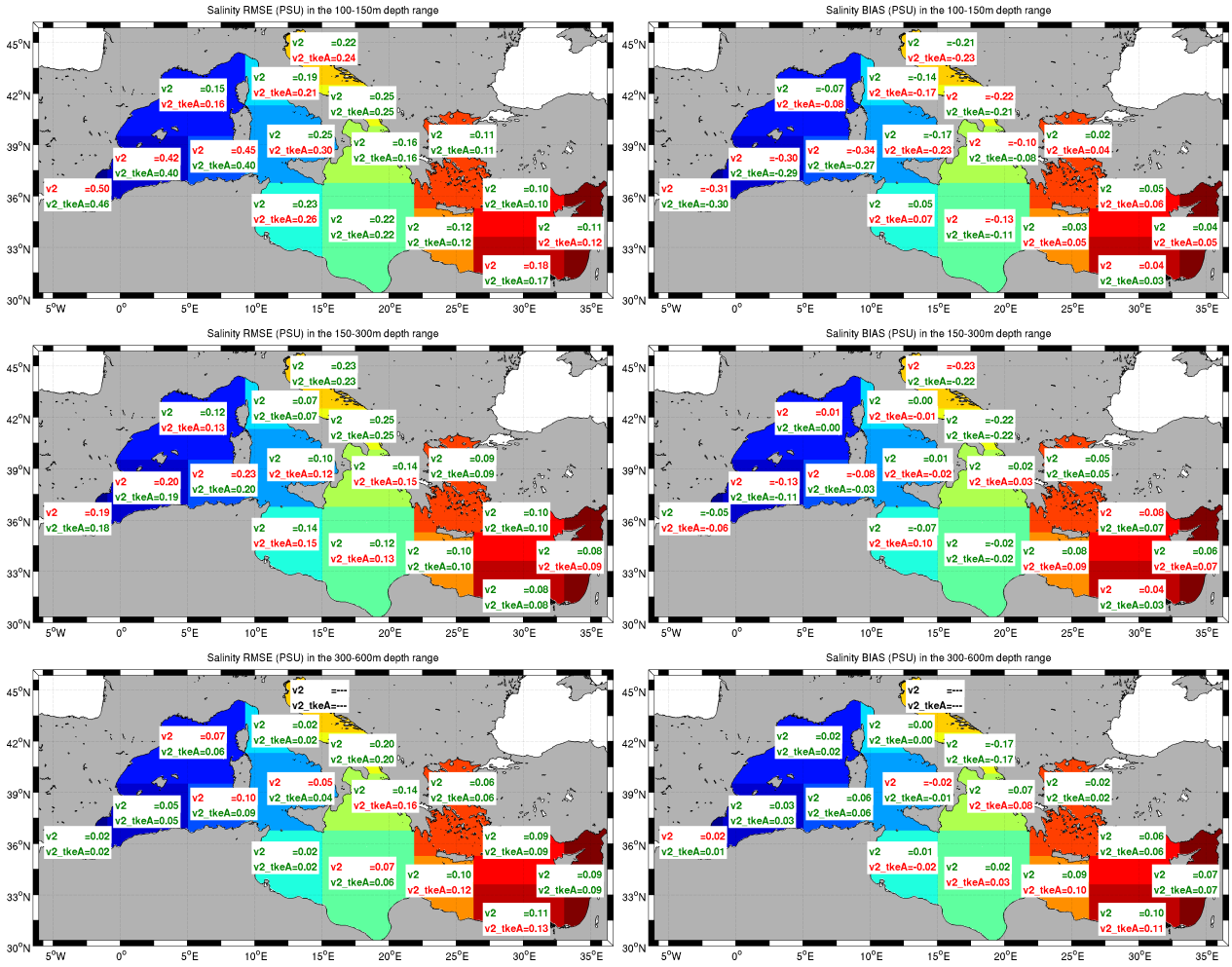

Figure 4.53: Sub-regional mean RMSE and BIAS of salinity (PSU) for experiments simrs_v2 and simrs_v2_tkeA at selected depth ranges. For each sub-region the experiment with the lowest salinity RMSE and BIAS is indicated in green, while the experiment with the highest salinity RMSE and BIAS is indicated in red (continued).

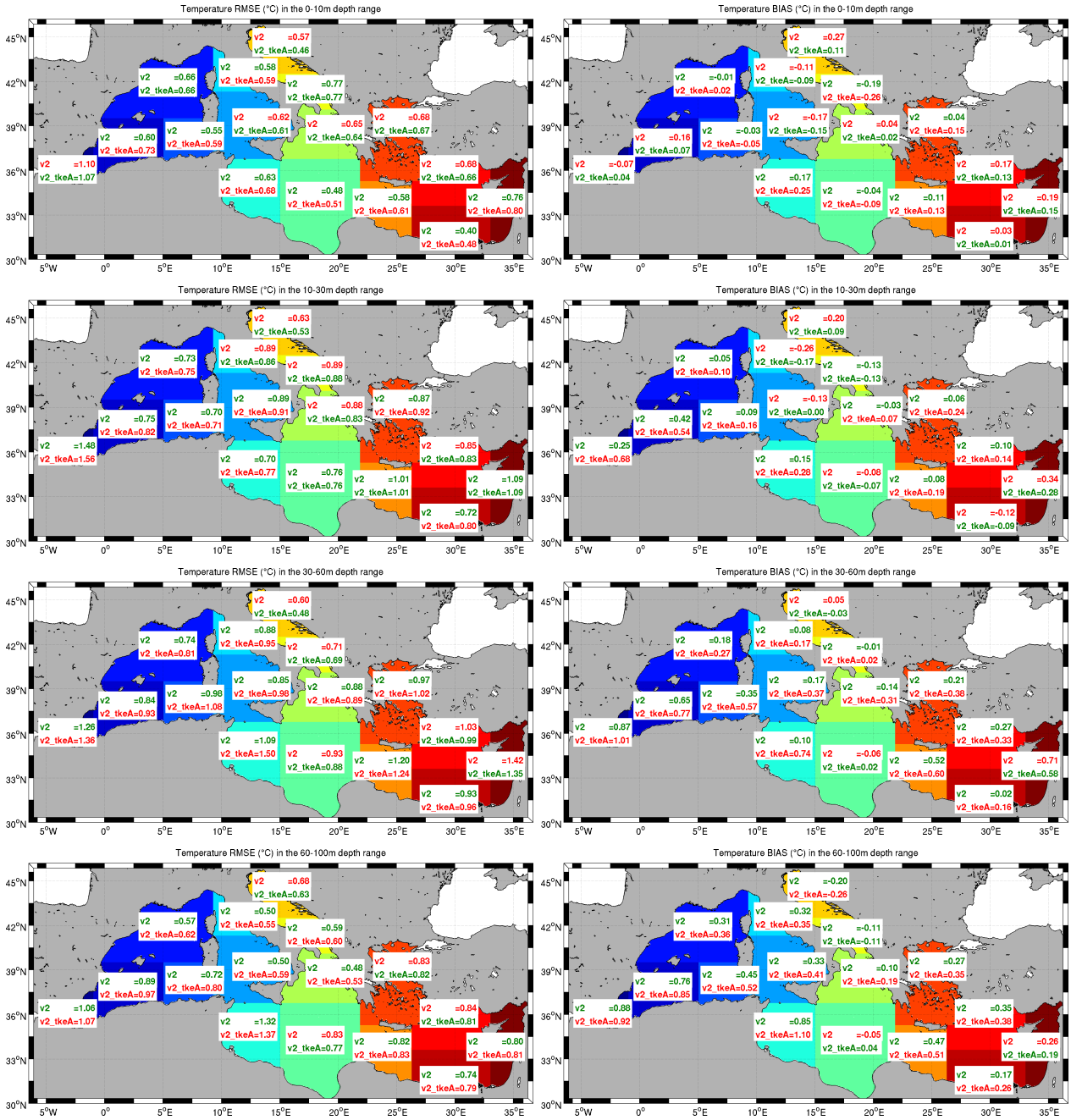

Figure 4.54: Sub-regional mean RMSE and BIAS of temperature (°C) for experiments simrs_v2 and simrs_v2_tkeA at selected depth ranges. For each sub-region the experiment with the lowest temperature RMSE and BIAS is indicated in green, while the experiment with the highest temperature RMSE and BIAS is indicated in red.

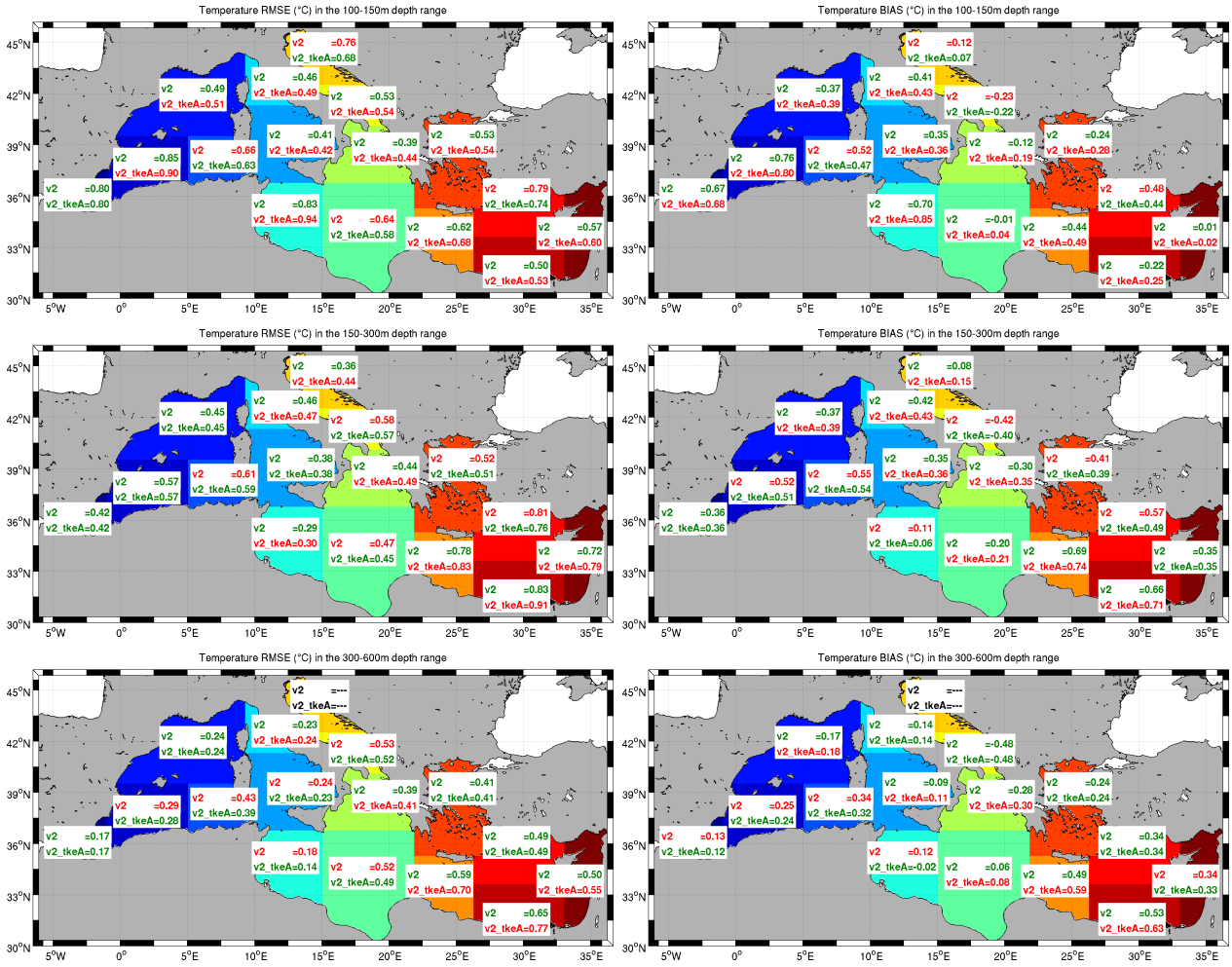

Figure 4.54: Sub-regional mean RMSE and BIAS of temperature (°C) for experiments simrs_v2 and simrs_v2_tkeA at selected depth ranges. For each sub-region the experiment with the lowest temperature RMSE and BIAS is indicated in green, while the experiment with the highest temperature RMSE and BIAS is indicated in red (continued).

4.6 Summary of the chapter

From the evaluation and validation of the results of numerical experiments simrs_v1 and simrs_v2 over the period 2006-2015 it can be concluded that the increased number of river sources in experiment simrs_v2 led, at Mediterranean Sea basin scale, to a lowering of the RMSE of salinity from the sea surface down to 60 m depth, while a worsening in the performances in simrs_v2 with respect to simrs_v1 can be observed in the depth range from 60 m to 300 m depth, both due to a freshening of the water column in simrs_v2, that can be connected to the increased amount of freshwater discharged from rivers into the basin (an increment of about the 70 % in simrs_v2 with respect to simrs_v1). The two considered experiments show very similar skill in reproducing salinity from observations at depth.

Concerning temperature, at basin scale, no significant differences can be noticed between simrs_v1 and simrs_v2 skills, along the whole water column.

It can be observed that the capability of the considered numerical experiments in reproducing the temperature and salinity data available from observations has a large variability among the different sub-regions of the Mediterranean Sea and through the different depth ranges considered.

Analyzing the RMSE for salinity and temperature for experiments simrs_v2, simrs_v3 and simrs_v4 over the period 2006-2010, it can be noticed that at basin scale the differences in skill in reproducing observations for the three considered experiments are extremely small for salinity, while are more significant for temperature, being simrs_v2 the experiment showing the best skill for the entire depth range considered.

As well as for the first set of experiments, the variability among the sub-

regions is very strong, being the Adriatic Sea and the North Eastern Ionian Sea the areas showing the largest differences in particular for simrs_v3, where the 0 PSU salinity prescribed for river runoff strongly affects both temperature and salinity, and consequently the capability of the ocean model to correctly reproduce the observations.

Both for simrs_v2 and simrs_v3 a strong decrease in evaporation can be noticed in the Adriatic Sea and in the North Eastern Ionian Sea during Winter and Autumn: these are the seasons where the many rivers implemented in the area have their own maximum peak discharge, thus an increased number of river runoff sources, as in experiment simrs_v2, or a large decrease in runoff prescribed salinity, as in experiment simrs_v3, strongly affects the evaporation rate in the area.

Comparing the time series of mean daily salinity values for simrs_v1 and simrs_v2, the effect of the increased number of river runoff sources in simrs_v2 is evident both in sea surface salinity and in volume salinity, while no particular differences can be noticed for temperature at basin scale; contrarily at sub-basin scale, significant differences can be noticed in surface salinity mostly located in the Adriatic Sea, where a freshening is evident due to the large number of new rivers implemented in experiment simrs_v2, while for temperature it can be observed that the largest differences are not at surface but mainly in the mixed layer.

The 0 PSU river runoff salinity prescribed in simrs_v3 has an evident effect on surface salinity in particular in a semi-enclosed basin like the Adriatic Sea and for major rivers, such as the Rhone river and the Ebro river, where simrs_v3 shows strong negative anomalies with respect to simrs_v2; the effect

of the enhanced vertical mixing implemented in simrs_v4 is more localized to the areas close to the river mouths where positive anomalies can be identified with respect to simrs_v2.

The increased number of river runoff in simrs_v2 determines a shallower Mixed Layer Depth in particular in the South Adriatic Gyre, the deep water mass formation area of the Adriatic Sea, where the most part of newly added rivers in simrs_v2 with respect to simrs_v1 has been implemented.

This is even more evident in simrs_v3, where the MLD in correspondence of the South Adriatic Gyre is even more shallow with respect to simrs_v2; it can be noticed in simrs_v3 that the decreased salinity of Rhone river affects the MLD in correspondence of the Gulf of Lion Gyre, while the enhancement of vertical mixing at Rhone river mouth appears to have a lower influence on the MLD in the area.

Many circulation structures are affected by the increase in number of river runoff sources introduced in simrs_v2, and circulation pattern seems to be impacted also at considerable depths. The circulation structures for which a direct effect of the new river runoff implementation can be supposed are mainly located in the Adriatic Sea, such as the Eastern South-Adriatic Current, the Western Adriatic Coastal Current, the Middle Adriatic Gyre and the South Adriatic Gyre; the influence of the newly added rivers in simrs_v2 with respect to simrs_v1 is observable also in the North Eastern Ionian Sea; this is particular evident at depth, where a weakening of the South Adriatic Gyre and of the Northern Ionian Cyclonic Gyre is evident.

Considering experiments simrs_v2, simrs_v3 and simrs_v4 the imposed 0 PSU salinity for river runoff in simrs_v3 seems to have a stronger impact on

circulation structures with respect to the different vertical mixing at river mouths implemented in simrs_v4: in particular the variations in velocity amplitude in the Adriatic Sea can be directly connected to the lowering in salinity, in agreement with Chao and Boicourt (1986) [144], due to the discharge of the many rivers implemented in the sub-basin, as well as the intensification of the Liguro-Provencal-Catalan Current can be reasonably connected to the different salinity values prescribed for the discharge of Rhone river and Ebro river.

Concerning the transport through the major straits, all the performed experiments show quite similar values among each other, even though a tendency to a reduction of the water volume flux through the considered straits (in particular Strait of Otranto) can be observed in experiments simrs_v2 and simrs_v3.

Observing the comparison with satellite data, at basin scale the Sea Level Anomaly (SLA) is slightly better reproduced in simrs_v2 than in simrs_v1, with a quite large variability among the different sub-regions, especially in the the Adriatic Sea, where an increased freshwater discharge into the sub-basin generates in simrs_v2 a positive SLA difference with respect to simrs_v1.

The better performances of simrs_v2 experiment in correctly reproduce SLA are confirmed also by the comparison with simrs_v4 and simrs_v3, the latter showing an evident positive SLA difference with respect to simrs_v2 in the Adriatic Sea, that can be reasonably due to the lower salinity prescribed for the many rivers that discharge into the sub-basin.

In view of the performed experiments, the increase of the number of rivers in experiment simrs_v2 allows to better reproduce the hydrologic cycle of the

Mediterranean Sea with respect to simrs_v1, with total river discharge into the basin much closer to literature values.

simrs_v2 setup ensures, with respect to simrs_v1, an improvement in salinity representation from the sea surface down to 60 m depth, while a slight worsening in the performances can be noticed in the depth range from 60 m to 300 m depth.

If compared with simrs_v3 and simrs_v4 experiments, simrs_v2 allows a generally better representation of the water column, both in terms of salinity and temperature.

The vertical mixing scheme chosen for experiment simrs_v2_tkeA introduced significant differences in salinity in the Adriatic Sea and above all in the Aegean Sea; in the latter area, both at surface and in the mixed layer, an increase in salinity in simrs_v2_tkeA with respect to simrs_v2 can be observed, while the behavior of the two experiments in the Adriatic Sea is different at surface with respect to greater depths (30 m depth): at surface a positive salinity anomaly can be identified along the Po river plume in simrs_v2_tkeA, while in the mixed layer the experiment is characterized by a freshening with respect to simrs_v2.

For what concern temperature, significant differences have been introduced in the mixed layer by the usage of the TKE vertical mixing scheme in simrs_v2_tkeA, which shows a large positive temperature anomaly for almost the entire basin.

From a comparison with insitu data, it can be observed that at basin scale no great differences are present between simrs_v2 and simrs_v2_tkeA for salinity representation skill, while temperature is better reproduced by

simrs_v2 along the entire water column.

It should be stressed that there is a quite large variability in the results provided by the two experiments among the different sub-regions: the most impacted sub-regions are the Northern Adriatic Sea and the Aegean Sea: for the former area simrs_v2_tkeA provides better results in salinity representation only in the first 30 m of the water column, while significant improvements in temperature representation can be observed from the surface down to 150 m depth; in the Aegean Sea the TKE vertical mixing scheme used in simrs_v2_tkeA does not provide an improvement with respect to simrs_v2 both in salinity and temperature skill, due to an overestimation observable from BIAS.

simrs_v2_tkeA provides good results in the Central-South Levantine Sea, where Nile river has its own outlet, both for temperature and salinity; in the North Western Mediterranean Sea, characterized by the discharge of Rhone river, simrs_v2_tkeA provides good results for salinity only, while for temperature the lower RMSE is shown by experiment simrs_v2.

At this stage, simrs_v2 represents the better setup for river runoff implementation in the Mediterranean Sea, even though the differences in performances among the different sub-regions of the Mediterranean Sea and along the different depth ranges considered suggest that further work is needed to better parameterize the numerical options involved in river runoff representation in the Mediterranean Sea ocean model.

In particular the several tunable parameters present in the TKE vertical mixing scheme suggest that further calibration work would be needed to optimize its setup.

Chapter 5

NEMO-EBM modelling system in the Mediterranean Sea: numerical experiments and validation

5.1 The CMCC Estuary Box Model implementation for the Mediterranean Sea river outlets

The CMCC Estuary Box Model described in Section 2.2 has been implemented for 37 over 39 of the rivers listed in Table 4.1.

The rivers excluded from this modelling implementation are Lika and Trebisnjica. Lika river is excluded from the EBM implementation since its

discharge into the Adriatic Sea is mainly through karst springs along the Croatian coast (Jelić et al., 2016 [145]); Trebisnjica river is excluded since a significant part of its flow reaches the Adriatic Sea by a tunnel up to the hydro power plant of the coastal town of Dubrovnik in Croatia (Regional strategy for sustainable hydropower in the Western Balkans, 2017) [146].

As a first step, each geometrical quantity described in Section 2.2 is preliminary retrieved and used to set up the CMCC EBM on the 37 considered rivers, followed by several sensitivity experiments that will be described in the following.

The estuary width parameter (L_y) for each river is retrieved using the *Google Earth* software developed by Google Inc..

The estuary depth parameter (H) is retrieved from literature (if available) or set equal to the 30 arc-sec GEBCO bathymetric dataset value nearest to the river estuary (or to the average of the coastal GEBCO bathymetric dataset points covering the extension of the delta, in case the river outlet presents this kind of geometry), or imposed as the minimum NEMO model bathymetry (6.5m).

The estuary length parameter (L_x) is retrieved or deduced from literature, if available, or through a cluster analysis that starting from literature values has provided an attempt of the lacking values (Figure 5.1).

The cluster analysis is built using as input quantities the mean annual discharge, the estuary width and the estuary depth of the rivers. Given the peculiarity of Po, Rhone, Ebro and Nile rivers, these are excluded from the analysis.

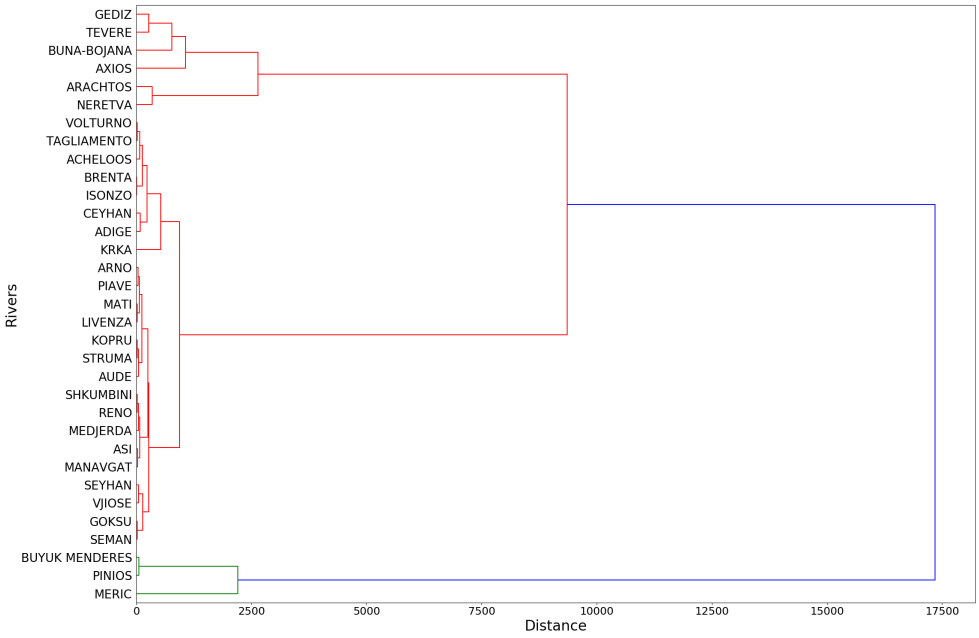

Figure 5.1: Cluster analysis for Mediterranean Sea rivers (excluding Po, Rhone, Ebro and Nile) based on mean annual discharge, estuary width and estuary depth.

The EBM input river volume flux at the estuary head (Q_{river} in Section 2.2) is provided as monthly climatological values (the same used in experiments simrs_v2, simrs_v3 and simrs_v4) at 0 PSU salinity.

The ocean-side grid box in which the ocean (NEMO model) fields are evaluated, integrated and provided to the EBM, i.e. ocean salinity and currents (see Section 2.2 for details) is set as follows: a three by three grid point box is defined in the horizontal (for large deltas the NEMO box width has been adapted to the real extension of the delta), in the vertical the box has a variable extension from the third NEMO vertical level to the deepest wet level of the box (since the ocean fields are provided to the EBM through the

lower layer).

It has to be stressed that the ocean-side fields, as well as the tidal inflow, are provided as daily fields: the tidal velocity during the flood phase (u_{tide_f} in Section 2.2), is provided to the EBM as daily average of hourly outputs of normal landward oriented velocities computed by the Oregon State University Tidal Prediction Software (OTPS, Egbert and Erofeeva (2002) [147]).

Once set up the EBM geometrical parameters, the coupling strategy which is followed to set up the NEMO-EBM modelling system consists in:

1. Run EBM sensitivity experiments at each river outlet forced by ocean data (currents and salinity) derived from different NEMO experiments (simrs_v2 and simrs_v3 described in previous sections) with prescribed river salinity and runoff values, as well using different estuary depth (H) values (derived from literature or from the GEBCO bathymetry or imposing H=6.5 m, corresponding to the minimum NEMO model bathymetry)

2. Evaluate the EBM model outputs in terms of river salinity and discharge

3. Run a NEMO experiment forced by daily river salinity and runoffs derived from the selected EBM configuration

The first set of two experiments performed focused on the impact of the choice of the NEMO model forcing experiment used to provide ocean data to the EBM, while the estuary depth for each river is the same for both the experiments and it is retrieved from literature (where available) or derived

from GEBCO bathymetry. Experiment expA_EBM uses ocean data derived from simrs_v3 experiment, while experiment expB_EBM uses ocean data from simrs_v2. This set of experiments is outlined in Table 5.1.

Table 5.1: First set of sensitivity experiments performed on the CMCC Estuary Box Model.

EBM experiment name	**Forcing experiment**	**Estuary depth** H
expA_EBM	simrs_v3	Literature or GEBCO bathymetry
expB_EBM	simrs_v2	Literature or GEBCO bathymetry

The sensitivity experiments performed showed that retrieving ocean data to be provided to the EBM from simrs_v2 or simrs_v3 generates small differences on the EBM solution (not shown), so that it has been decided to use simrs_v2 as forcing experiment for the following set of EBM sensitivity experiments, since it has provided a better skill with respect to simrs_v3, as shown in the previous chapter.

The sensitivity of the EBM solution to the estuary depth parameter (H) is evaluated by setting H=6.5 m (the minimum ocean model bathymetry) in experiment expC_EBM and comparing the EBM run results with the setup implemented for experiment expB_EBM, as summarized in Table 5.2.

Table 5.2: Second set of sensitivity experiments performed on the CMCC Estuary Box Model.

EBM experiment name	**Forcing experiment**	**Estuary depth** H
expB_EBM	simrs_v2	Literature or GEBCO bathymetry
expC_EBM	simrs_v2	NEMO model bathymetry min. depth (6.5 m)

In the following the inputs to the EBM, along with the results of the sensitivity tests on the estuary depth parameter, will be shown for the two main Mediterranean Sea rivers, the Po and the Rhone.

The river volume flux monthly climatologies provided as input to the EBM for Po and Rhone are shown in Figure 5.2.

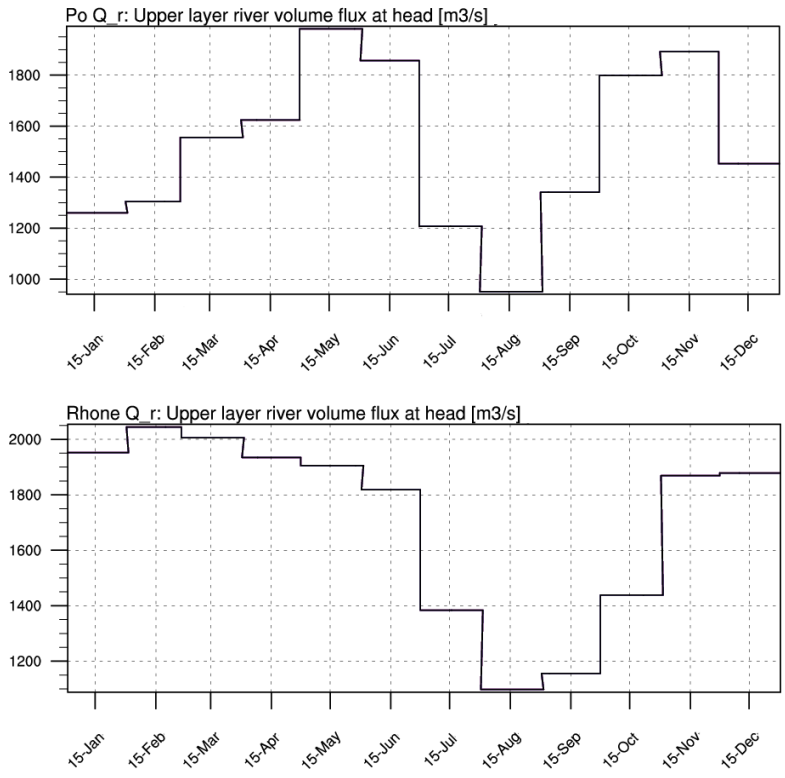

Figure 5.2: River volume flux at the estuary head for Po and Rhone rivers (m^3/s).

The ocean-side inputs and the results of the sensitivity tests expB_EBM and expC_EBM for Po and Rhone are shown in Figures from 5.3 to 5.6.

The estuary depth parameter H has shown to have a significant impact in the EBM solution: considering the Po river, H is increased from 3 m to 6.5 m from expB_EBM to expC_EBM, while for the Rhone river from 5.4 m to 6.5 m. This leads to an increased volume flux from the ocean (both from the lower layer and from the barotropic tidal flux) that produces an increased volume flux from estuary to ocean and a higher salinity at the estuary upper

layer.

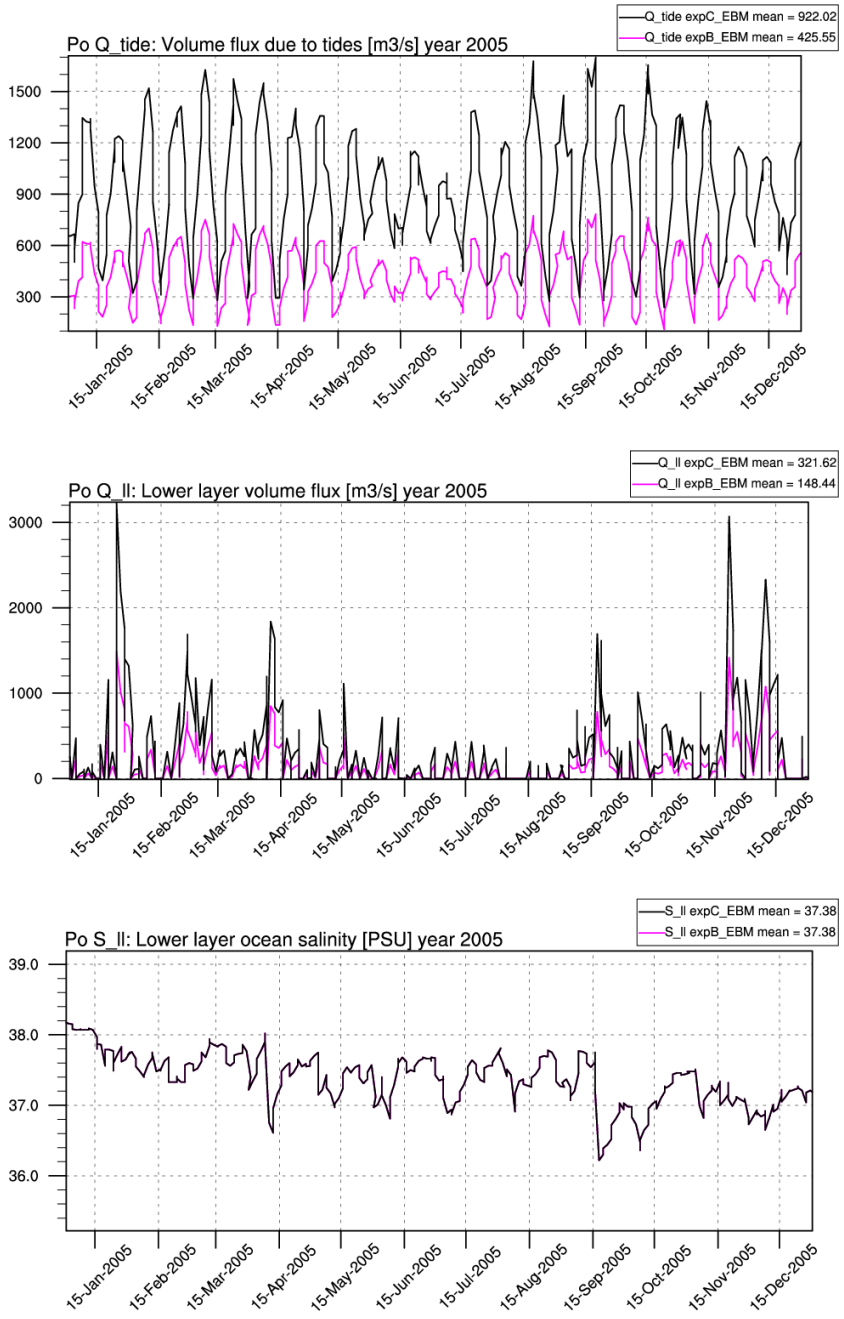

Figure 5.3: Ocean-side input fields forcing EBM for the Po river in year 2005 for experiments expB_EBM and expC_EBM. From top to bottom panel: volume flux due to tides (m^3/s), lower layer volume flux (m^3/s), lower layer ocean salinity (PSU).

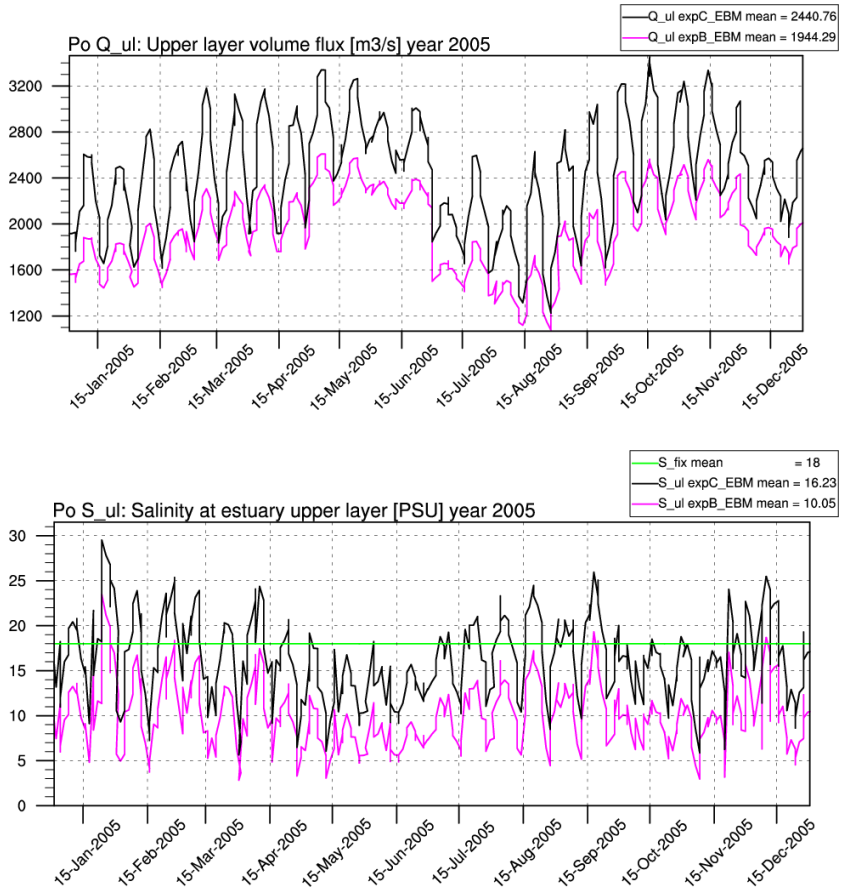

Figure 5.4: EBM output fields for Po river in year 2005 for experiments expB_EBM and expC_EBM. Top panel: upper layer volume flux (m^3/s). Bottom panel: salinity at estuary upper layer (PSU); the prescribed salinity used in experiment simrs_v2 is indicated in green.

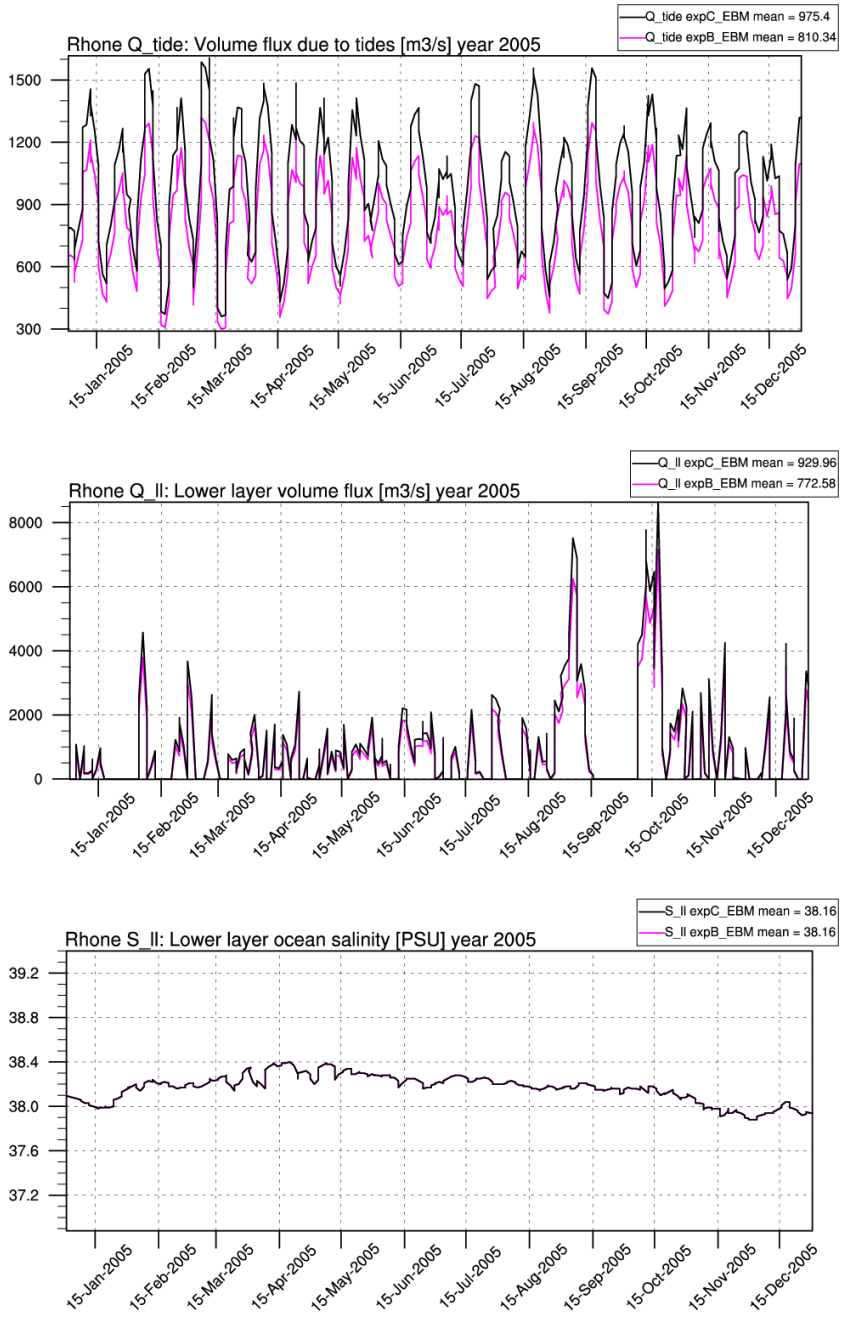

Figure 5.5: Ocean-side input fields forcing EBM for the Rhone river in year 2005 for experiments expB_EBM and expC_EBM. From top to bottom panel: volume flux due to tides (m^3/s), lower layer volume flux (m^3/s), lower layer ocean salinity (PSU).

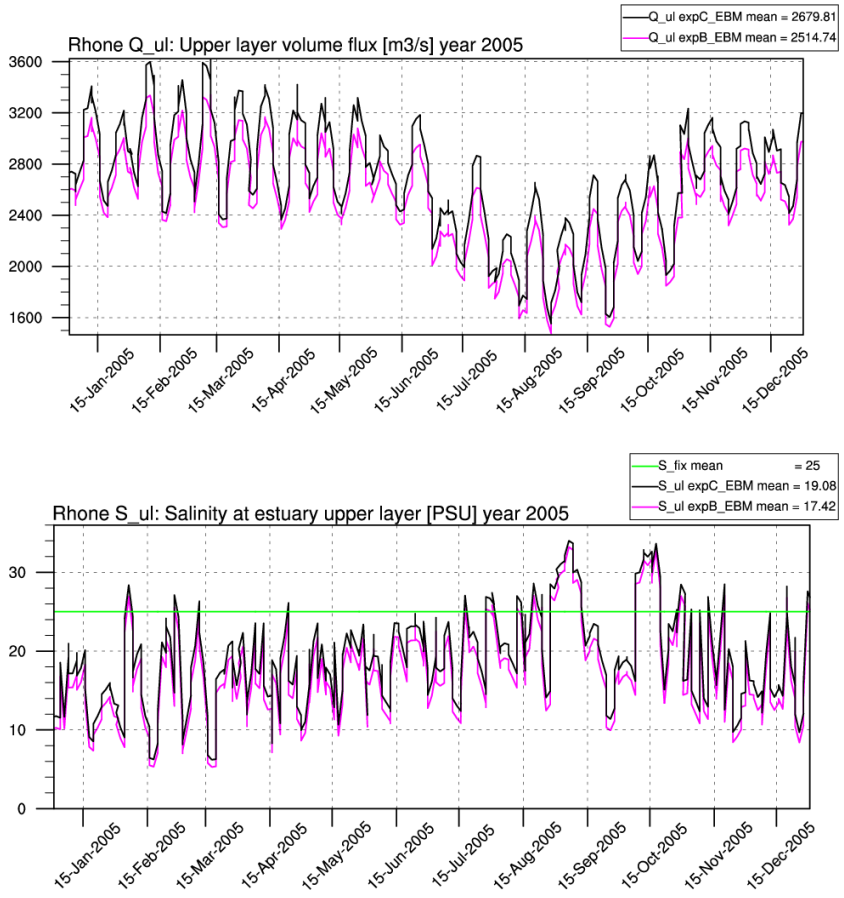

Figure 5.6: EBM output fields for Rhone river in year 2005 for experiments expB_EBM and expC_EBM. Top panel: upper layer volume flux (m^3/s). Bottom panel: salinity at estuary upper layer (PSU); the prescribed salinity used in experiment simrs_v2 is indicated in green.

The expC_EBM implementation is here chosen as the optimal EBM setup since it provides more reliable, or closer to the constant salinity values derived from previous sensitivity experiments, upper layer salinity values and moreover it is characterized by an estuary depth H equal to the minimum

depth of the NEMO model bathymetry (6.5 m) ensuring a geometrical consistency between the CMCC EBM and the NEMO model in the coupling process.

The Estuary Box Model geometrical parameters implemented for each river, estuary length (L_x) and estuary width (L_y), are listed in Table 5.3, along with the mean salinity (S_{ul}^{ebm}) and the mean outflowing volume flux through the upper layer of the CMCC EBM Q_{ul}^{ebm} over the period 2006-2010.

For estuary length (L_x) it is indicated in round brackets if retrieved or deduced from literature (literature reference), from cluster analysis (clust.), measured from Google Earth (GEarth), or from Naias data tool, 2015, HCMR (`http://naias-data.hcmr.gr/`).

Table 5.3: Estuary length (L_x) and estuary width (L_y) parameters used for the final implementation of the CMCC EBM (expC_EBM), along with mean salinity (S_{ul}^{ebm}, PSU) and the mean outflowing volume flux through the upper layer of the CMCC EBM (Q_{ul}^{ebm}, m^3/s) over the period 2006-2010.

River name	$L_x[m]$	$L_y[m]$	S_{ul}^{ebm}	Q_{ul}^{ebm}
Ebro	17785 ([124])	5000	10.41	469
Rhone	19000 ([124])	38735	18.83	2687
Po	20000 ([88])	20000	16.51	2446
Buna-Bojana	10000 ([148])	4240	7.05	683
Seman	1500 (clust.)	70	1.24	202
Vjiose	1500 (clust.)	200	1.33	184

Table 5.3 Continued: Estuary length (L_x) and estuary width (L_y) parameters used for the final implementation of the CMCC EBM (expC_EBM), along with mean salinity (S_{ul}^{ebm}, PSU) and the mean outflowing volume flux through the upper layer of the CMCC EBM (Q_{ul}^{ebm}, m^3/s) over the period 2006-2010.

Nile at Damietta	16000 ([149])	285	5.36	266
Nile at Rosetta	16125 ([150] and [151])	385	3.95	254
Aude	2850 (clust.)	160	4.78	60
Arno	25000 ([152])	215	4.89	91
Tevere	6700 ([153] and [154])	3750	17.95	285
Volturno	3000 (clust.)	360	10.27	72
Medjerda	45000 ([155] and [156])	45	1.68	59
Reno	45000 (clust.)	80	1.12	67
Adige	20000 ([157])	385	4.14	252
Brenta	11000 (clust.)	350	2.30	165
Piave	20000 ([158])	225	4.11	140
Livenza	20000 (clust.)	165	1.18	97
Tagliamento	3000 (clust.)	355	11.00	105
Isonzo	11000 ([159])	350	2.67	182
Krka	13500 ([160])	300	11.89	58

Table 5.3 Continued: Estuary length (L_x) and estuary width (L_y) parameters used for the final implementation of the CMCC EBM (expC_EBM), along with mean salinity (S_{ul}^{ebm}, PSU) and the mean outflowing volume flux through the upper layer of the CMCC EBM (Q_{ul}^{ebm}, m^3/s) over the period 2006-2010.

Neretva	10000 ([161])	2015	6.50	256
Mati	20000 (clust.)	185	2.49	101
Shkumbini	45000 (clust.)	90	2.59	54
Arachtos	28700 (GEarth)	2320	13.65	76
Acheloos	3000 ([162])	305	6.97	116
Pinios	11500 (NAIAS)	1500	12.94	69
Axios	10000 (clust.)	1500	26.48	296
Struma	2850 ([163])	120	0.75	81
Meric	10000 ([164])	1500	14.98	189
Gediz	6700 (clust.)	1500	22.39	92
Buyuk Menderes	11500 (clust.)	1500	3.90	111
Kopru	2850 (clust.)	135	6.07	86
Manavgat	1500 ([165])	70	2.17	122
Goksu	1500 (clust.)	90	0.74	204
Seyhan	1500 (clust.)	160	2.99	205

Table 5.3 Continued: Estuary length (L_x) and estuary width (L_y) parameters used for the final implementation of the CMCC EBM (expC_EBM), along with mean salinity (S_{ul}^{ebm}, PSU) and the mean outflowing volume flux through the upper layer of the CMCC EBM (Q_{ul}^{ebm}, m^3/s) over the period 2006-2010.

Ceyhan	3000 (clust.)	465	8.58	258
Asi	1500 (clust.)	55	1.29	94

5.2 Experimental design

The CMCC EBM is 1-way offline coupled with the NEMO ocean model providing daily values of salinity (S_{ul}^{ebm}) and daily values of the outflowing volume flux through the upper layer of the CMCC EBM (Q_{ul}^{ebm}).

Since CMCC EBM is not implemented for Lika and Trebisnjica rivers, for these two rivers daily discharge values are set up starting from monthly climatologies (the same used in experiment simrs_v2), while 0 PSU salinity is prescribed.

In order to assess the impact of the coupling on the thermohaline properties of the Mediterranean Sea and on its circulation structures a numerical experiment (hereafter simrs_v5) is performed, with an integration period from 2005 to 2010, considering the year 2005 as a spin-up year.

The results of the performed experiment are validated with respect to observations and compared with the results of simrs_v2, considered as the reference experiment, following the assessment analyses performed in the

previous sections.

5.3 Evaluation and validation of experimental results

5.3.1 Water fluxes

In Figure 5.7 it can be noticed that the climatological hydrologic cycle is well reproduced by both the experiments according to Mariotti et al. (2002) [127], with simrs_v5 showing lower values for upward water flux (given by E - P - R), due to the increase in the runoff (R) component, which is increased of about the 28 % with respect to simrs_v2.

The basin averaged evaporation rate does not show significant differences between simrs_v2 and simrs_v5 experiments, but differences in pattern distribution can be clearly observed, as displayed in Figure 5.8.

These differences in the area mostly impacted by river inflows could be derived by the generally lower river salinity in simrs_v5 with respect to simrs_v2, so that it can be reasonably supposed that lighter water masses are generated in simrs_v5, more sensitive to the atmospheric forcing, that can trigger a surface overcooling in Winter and a surface overwarming in Summer, leading to the evaporation rate differences described.

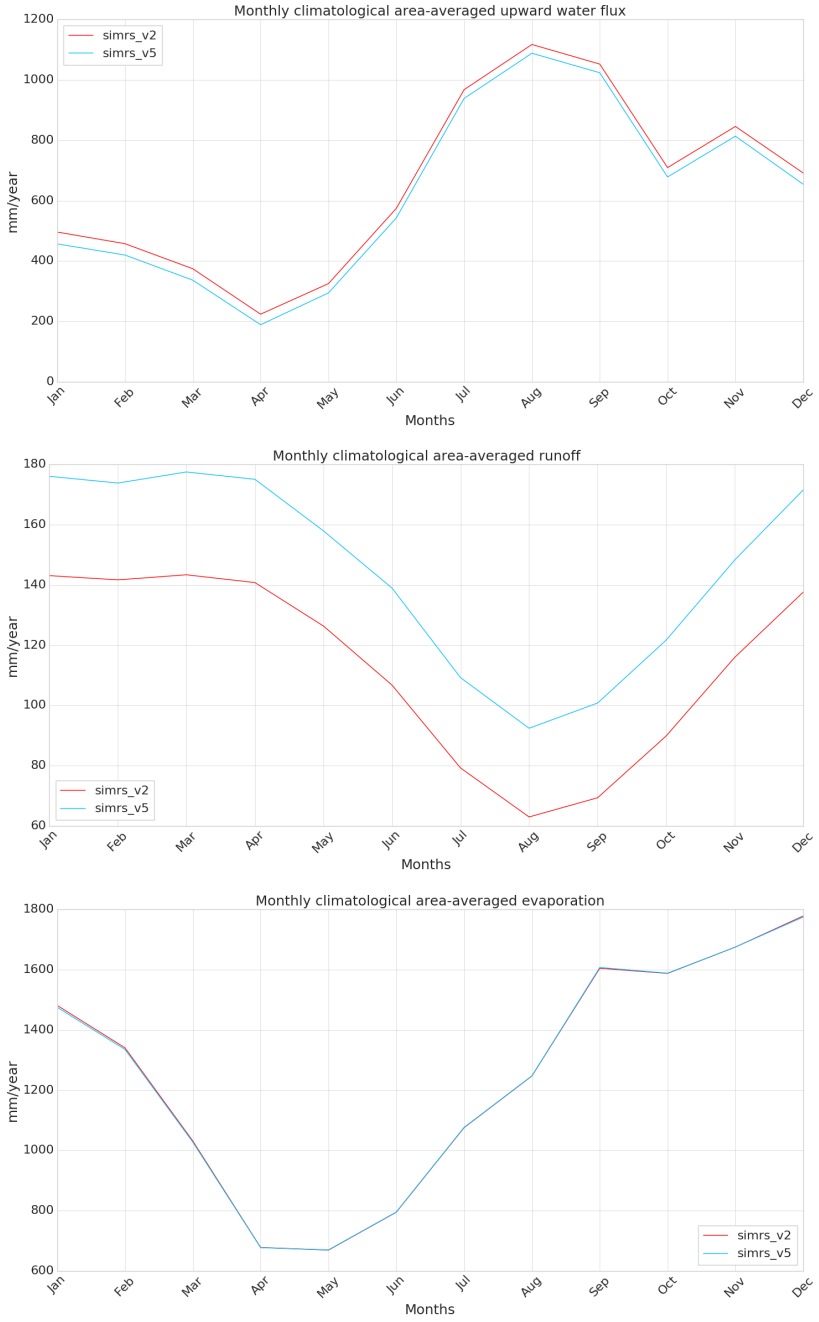

Figure 5.7: Monthly climatological area-averaged hydrologic cycle and its components for simrs_v2 and simrs_v5. From top to bottom panel: upward water flux, runoff, evaporation.

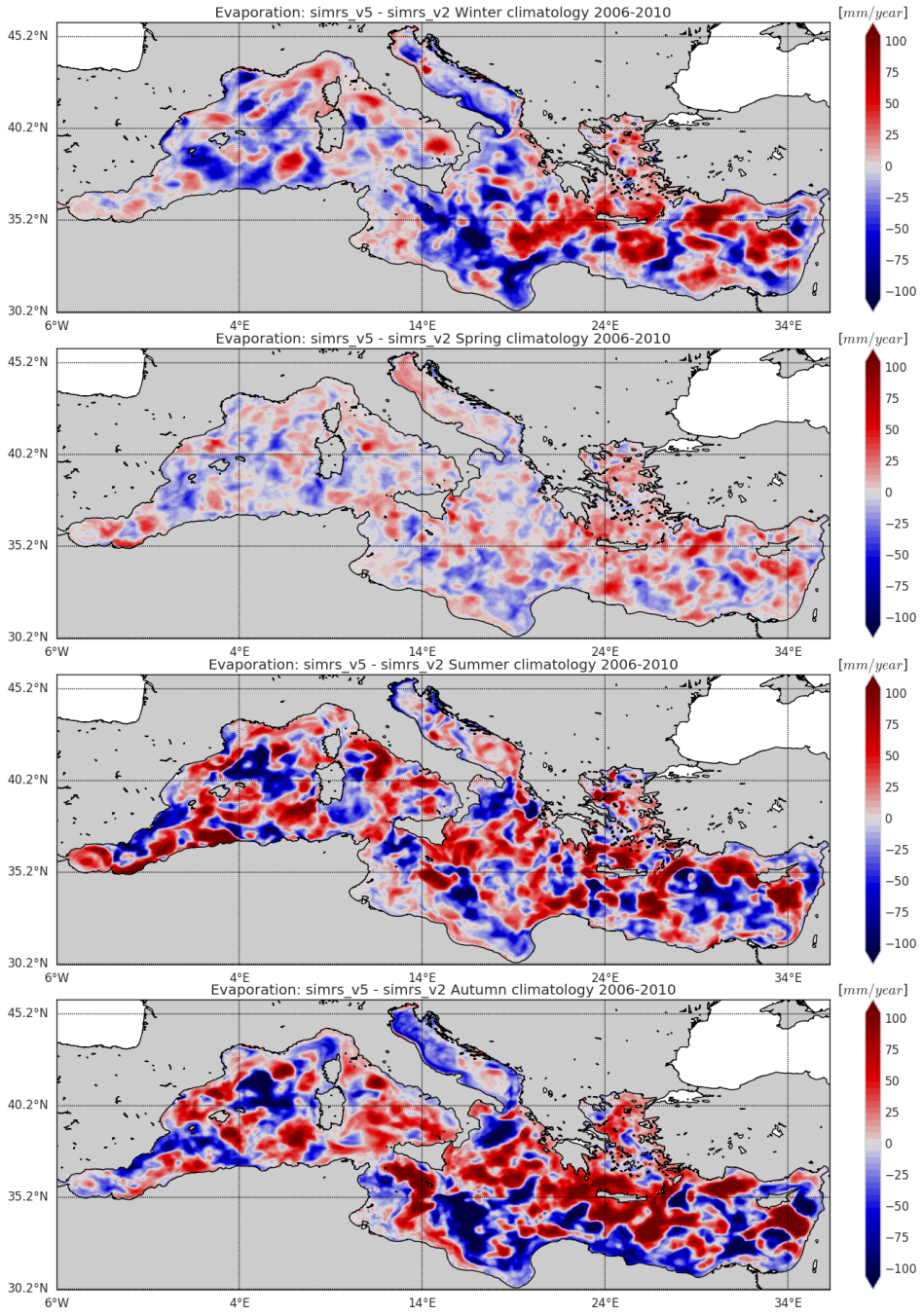

Figure 5.8: Seasonal evaporation rate differences between experiments simrs_v2 and simrs_v5. From top to bottom panel: Winter (Jan - Mar), Spring (Apr - Jun), Summer (Jul - Sep) and Autumn (Oct - Dec).

5.3.2 Temperature and salinity comparison with in situ observations

In the following, the results of simrs_v5 experiment are analyzed and compared with available in situ observations (Argo floats, XBTs and gliders), in order to assess the model skill and to evaluate how the thermohaline properties and the dynamics of the Mediterranean Sea are affected by different riverine inputs derived by the coupling with the CMCC EBM.

Figures 5.9 and 5.10 present the Mediterranean Sea mean salinity and temperature RMSE and BIAS for experiments simrs_v2 and simrs_v5 along different vertical layers. simrs_v5 shows almost the same salinity skill with respect to simrs_v2 at basin scale, while for temperature the difference between the two experiments is more significant, with simrs_v2 showing a lower RMSE with respect to simrs_v5 for the most part of the water column, due to generally lower temperature values for the depth ranges considered with respect to simrs_v5.

When considering the salinity skill at sub-regional scale (Figure 5.11), focusing on the sub-regions characterized by a large amount of riverine discharge, in the North Western Mediterranean Sea (sub-region 3 in Figure 4.7) the salinity RMSE is constantly, even though slightly, lower for simrs_v2 with respect to simrs_v5, as well as for temperature, where the only depth ranges where simrs_v5 shows better skill with respect to simrs_v2 are the 60-100 m range and the 300-600 m depth range. Differences in temperature RMSE (Table 5.12) between the two experiments are very small along the entire water column.

In the North Eastern Ionian Sea (sub-region 9 in Figure 4.7) simrs_v5 shows

a significantly lower salinity RMSE with respect to simrs_v2 in the first 60 m of the water column, while a slight worsening of the performances can be observed from 60 to 600 m depth. For what concern temperature skill, on the contrary, the simrs_v5 experiment shows worst performances with respect to simrs_v2 for the most part of the depth ranges considered.

Differences in salinity skill between the two considered experiments are smaller in Southern Adriatic Sea (sub-region 10 in Figure 4.7), even though a worsening in performances in simrs_v5 can be observed, in particular in the first 30 m of the water column, as well as for temperature skill, where the worsening in the capability of simrs_v5 with respect to simrs_v2 to reproduce the observations is extended down to 100 m depth.

The worst salinity skill for simrs_v5 is noticeable in the Northern Adriatic Sea (sub-region 11 in Figure 4.7), in particular for the first 60 m of the water column due to an excessive freshening, as observable from BIAS values; concerning temperature, higher RMSE values can be observed for simrs_v5 with respect to simrs_v2 in the depth range between 10 and 100 m, due to an excessive warming of the water column, while in the depth range between the surface and 10 m depth a good improvement in simrs_v5 with respect to simrs_v2 can be observed.

In the Central-South Levantine Sea (sub-region 15 in Figure 4.7) a constantly lower salinity RMSE along all the depth ranges considered for simrs_v5 with respect to simrs_v2 can be observed, due to a general freshening of the water column. On the contrary, an improvement in temperature skill for simrs_v5 can be observed only in the first 30 m, while similar or higher temperature RMSE values for simrs_v5 with respect to simrs_v2 characterize the

remaining portion of the water column.

In the Aegean Sea (sub-region 13 in Figure 4.7) simrs_v2 and simrs_v5 show very similar performances in reproducing salinity, even though simrs_v2 has a constant slightly lower RMSE, with the exception of the first 10 meters of the water column, where simrs_v5 provides better performances. For what concern temperature simrs_v2 provides the best results for all the depth ranges considered.

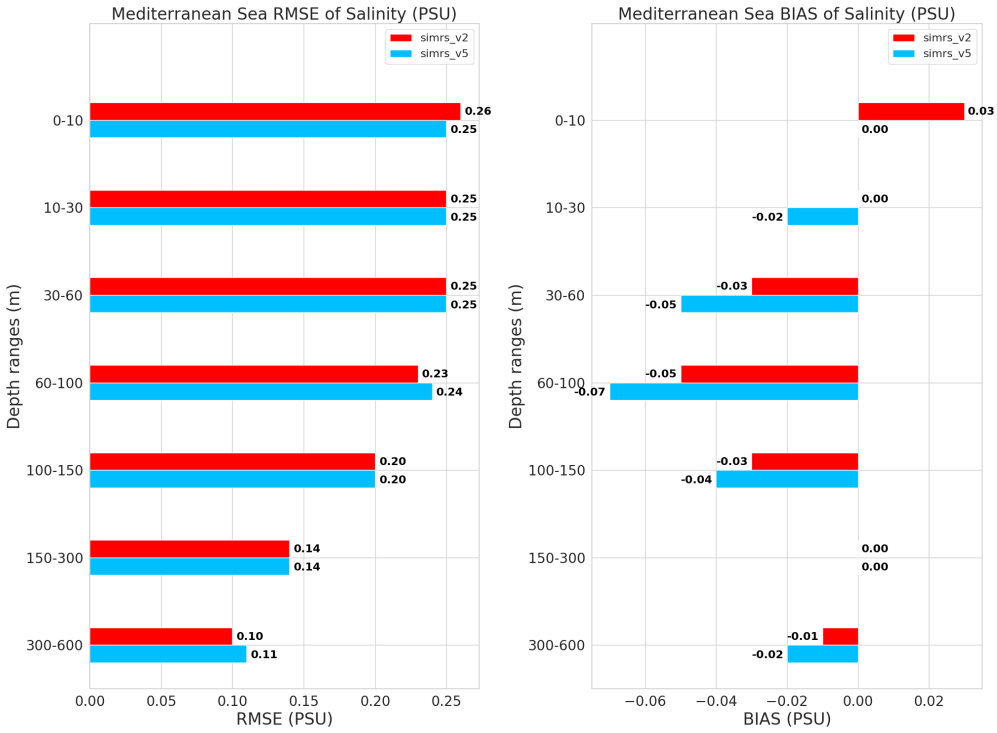

Figure 5.9: Mediterranean Sea mean RMSE and BIAS of salinity (PSU) for experiments simrs_v2 and simrs_v5.

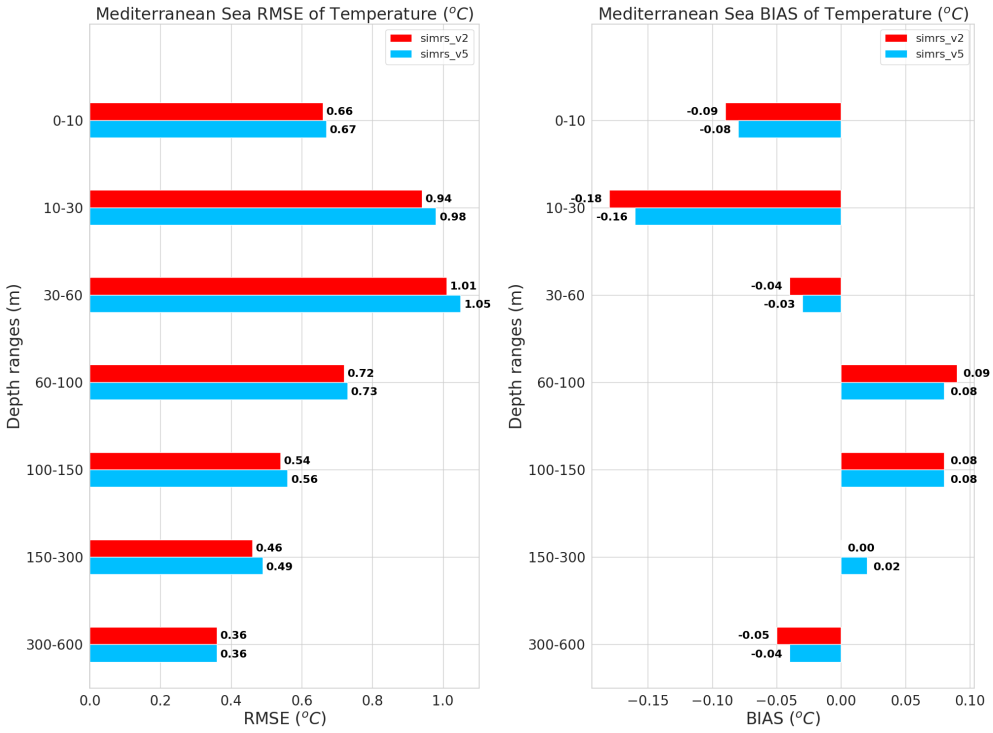

Figure 5.10: Mediterranean Sea mean RMSE and BIAS of temperature (°C) for experiments simrs_v2 and simrs_v5.

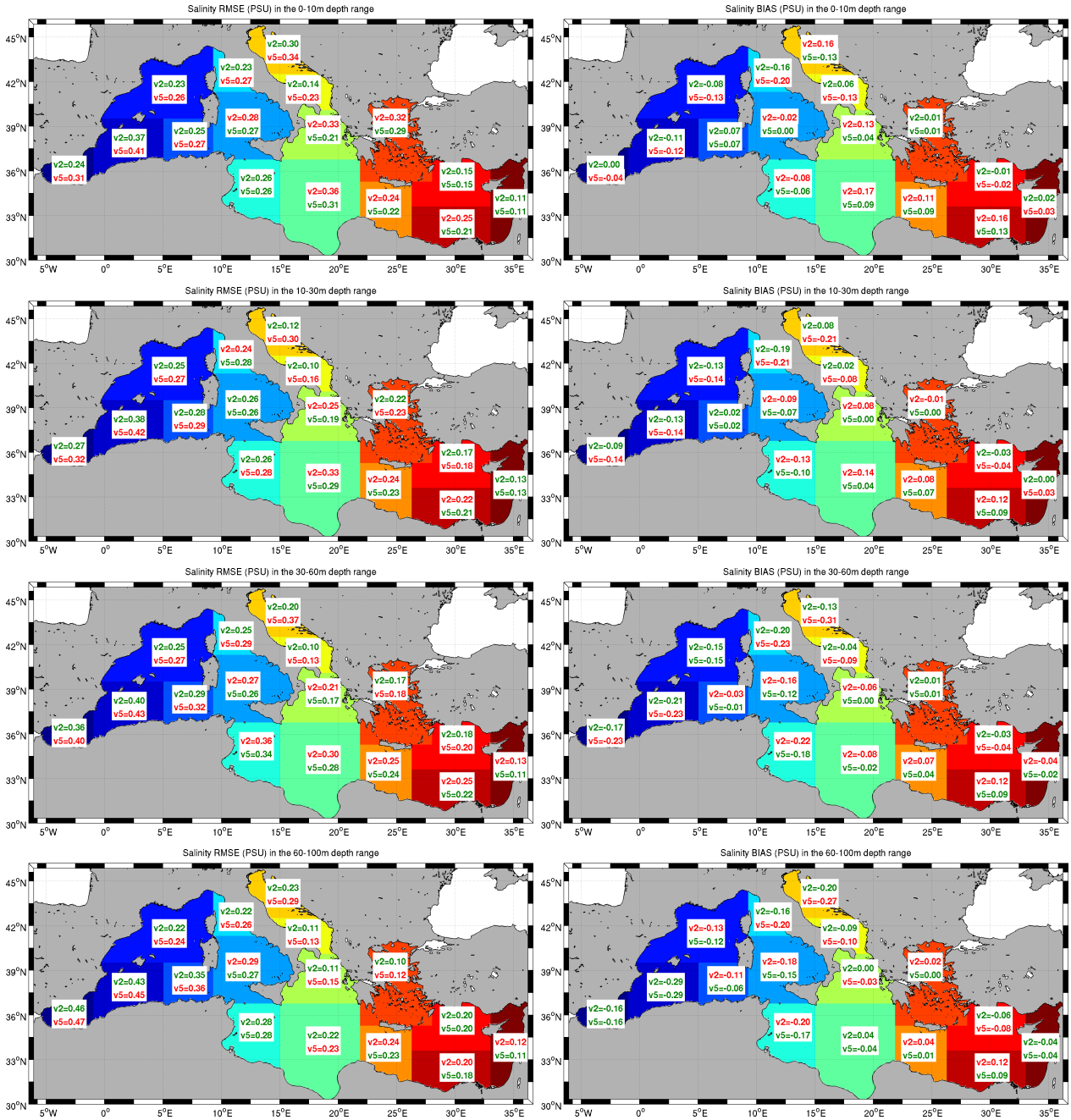

Figure 5.11: Sub-regional mean RMSE and BIAS of salinity (PSU) for experiments simrs_v2 and simrs_v5 at selected depth ranges. For each sub-region the experiment with the lowest salinity RMSE and BIAS is indicated in green, while the experiment with the highest salinity RMSE and BIAS is indicated in red.

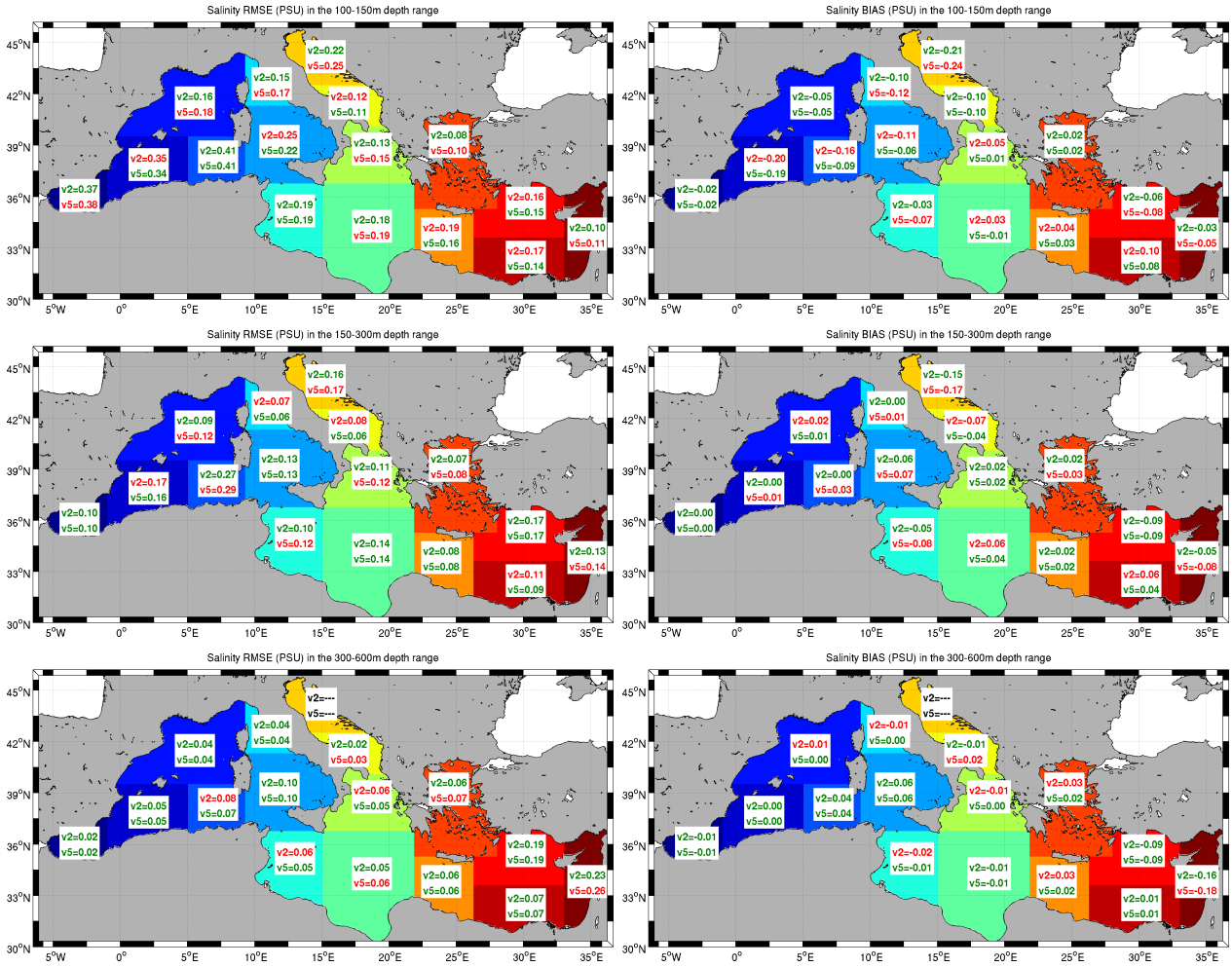

Figure 5.11: Sub-regional mean RMSE and BIAS of salinity (PSU) for experiments simrs_v2 and simrs_v5 at selected depth ranges. For each sub-region the experiment with the lowest salinity RMSE and BIAS is indicated in green, while the experiment with the highest salinity RMSE and BIAS is indicated in red (continued).

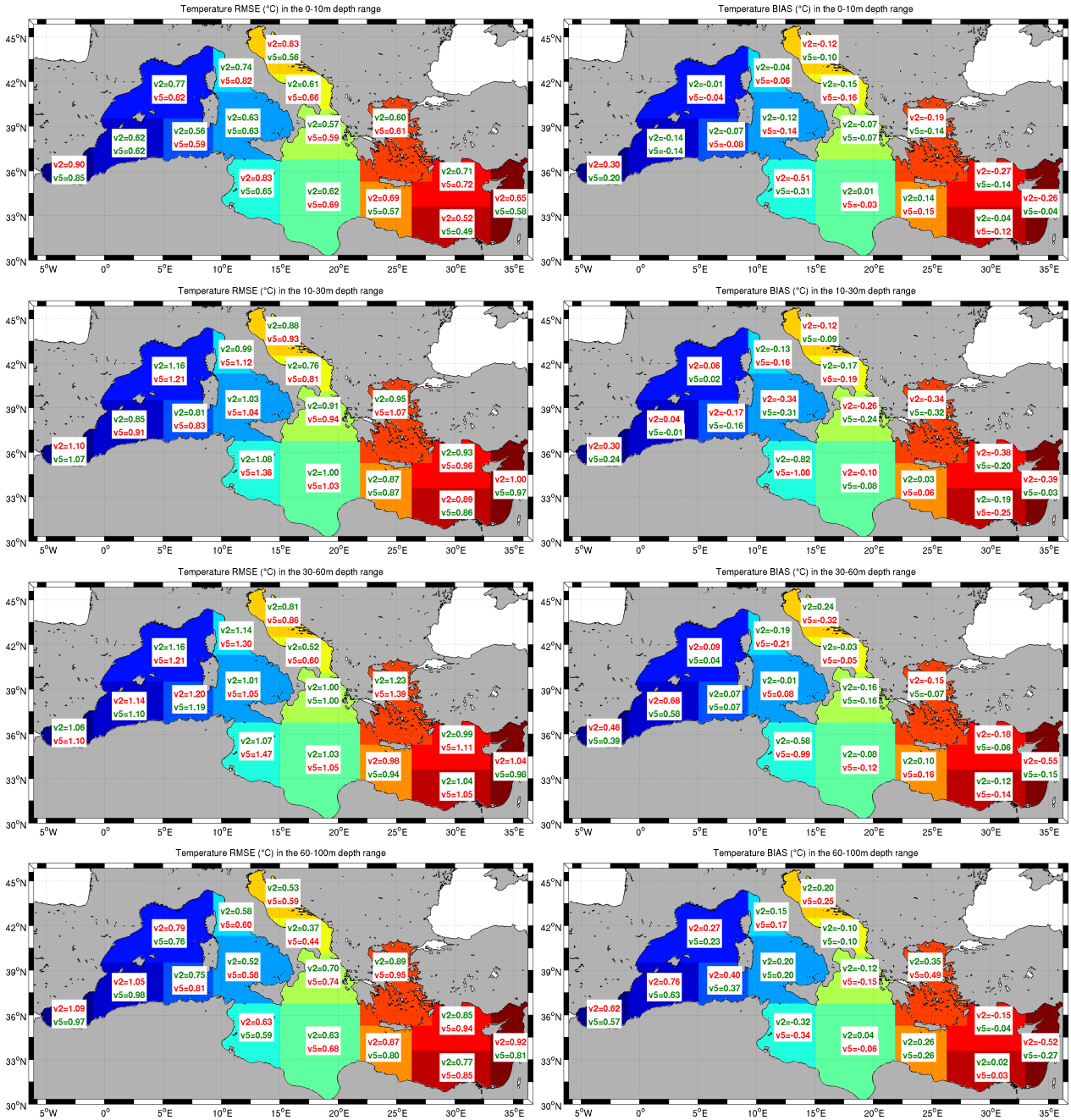

Figure 5.12: Sub-regional mean RMSE and BIAS of temperature (°C) for experiments simrs_v2 and simrs_v5 at selected depth ranges. For each sub-region the experiment with the lowest temperature RMSE and BIAS is indicated in green, while the experiment with the highest temperature RMSE and BIAS is indicated in red.

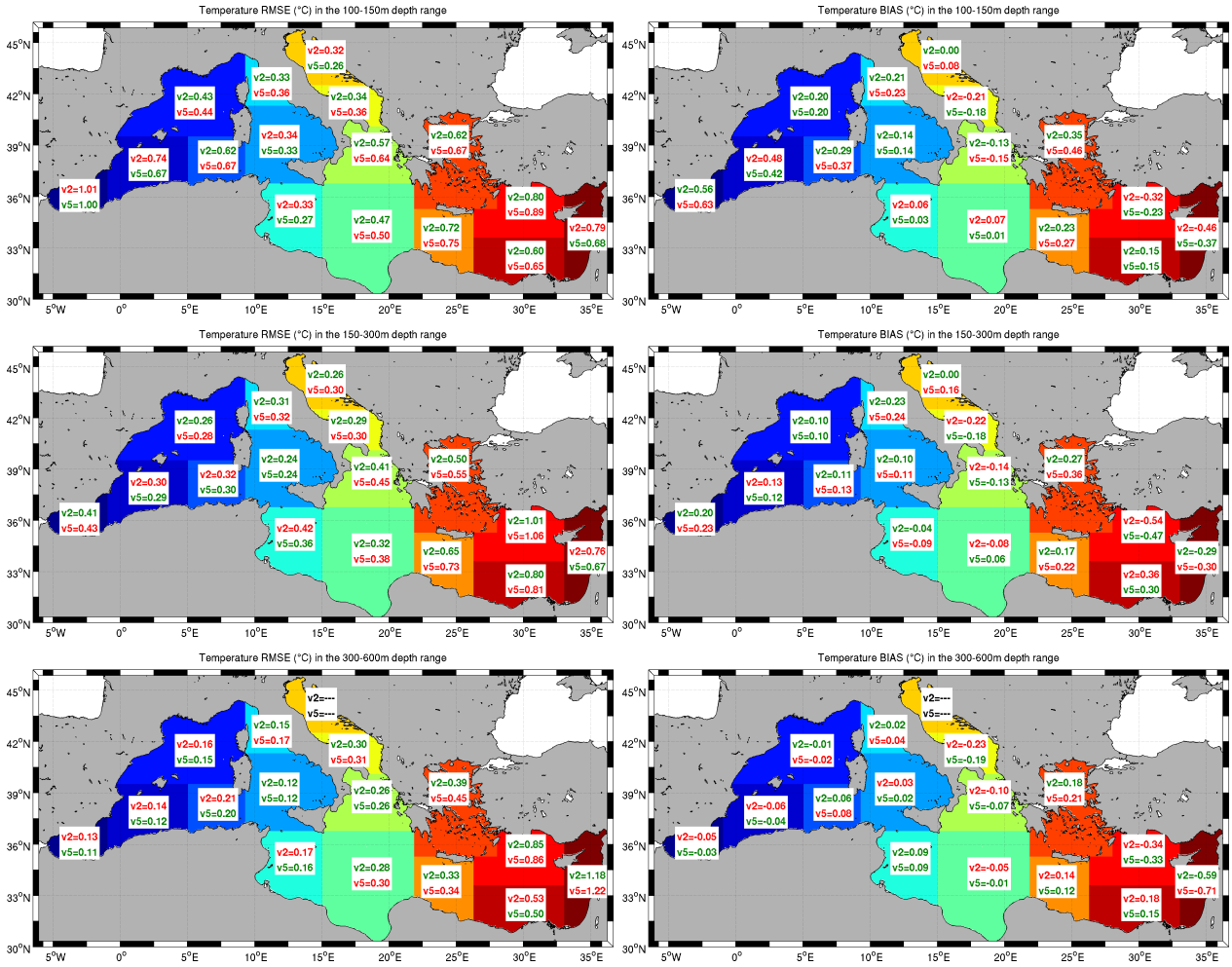

Figure 5.12: Sub-regional mean RMSE and BIAS of temperature (°C) for experiments simrs_v2 and simrs_v5 at selected depth ranges. For each sub-region the experiment with the lowest temperature RMSE and BIAS is indicated in green, while the experiment with the highest temperature RMSE and BIAS is indicated in red (continued).

5.3.3 Temperature and salinity comparison with climatological data sets and satellite data

The numerical results for temperature and salinity over the period 2006-2010 are evaluated and compared with respect to SeaDataNet V1.1 (hereafter SDN) and World Ocean Atlas 2013 version 2 (hereafter WOA) climatology data sets, along with a comparison with respect to simrs_v2.

Considering the climatological temperature and salinity profiles computed from the results of experiments simrs_v2 and simrs_v5, the largest differences can be observed in the central Mediterranean Sea (sub-regions from 5 to 11 in Figure 4.7), with differences in salinity profiles from surface down to about 200 m depth, while no significant differences can be observed for temperature profiles (Figure 5.13).

In particular, the major salinity differences can be observed in the Adriatic Sea (sub-regions 10 and 11 in Figure 4.7), while no significant differences in temperature can be detected (Figure 5.14).

The overall decrease in the coupled model salinity could derive from the lower river salinity imposed.

Except for the first 20 m of the water column, both the considered experiments underestimate the SDN and WOA climatological data sets values for the considered area.

Concerning the Southern Adriatic Sea (sub-region 10), differences between the two experiments are smaller than in the Northern Adriatic Sea area.

Experiment simrs_v2 shows at surface a better agreement with the considered climatological data sets, in particular with SDN, while both the experiments underestimate the climatological salinity profiles from about 20 m

depth down to about 200 m; at greater depths the two experiments well reproduce the climatological observations, lying in between the SDN and WOA salinity profiles.

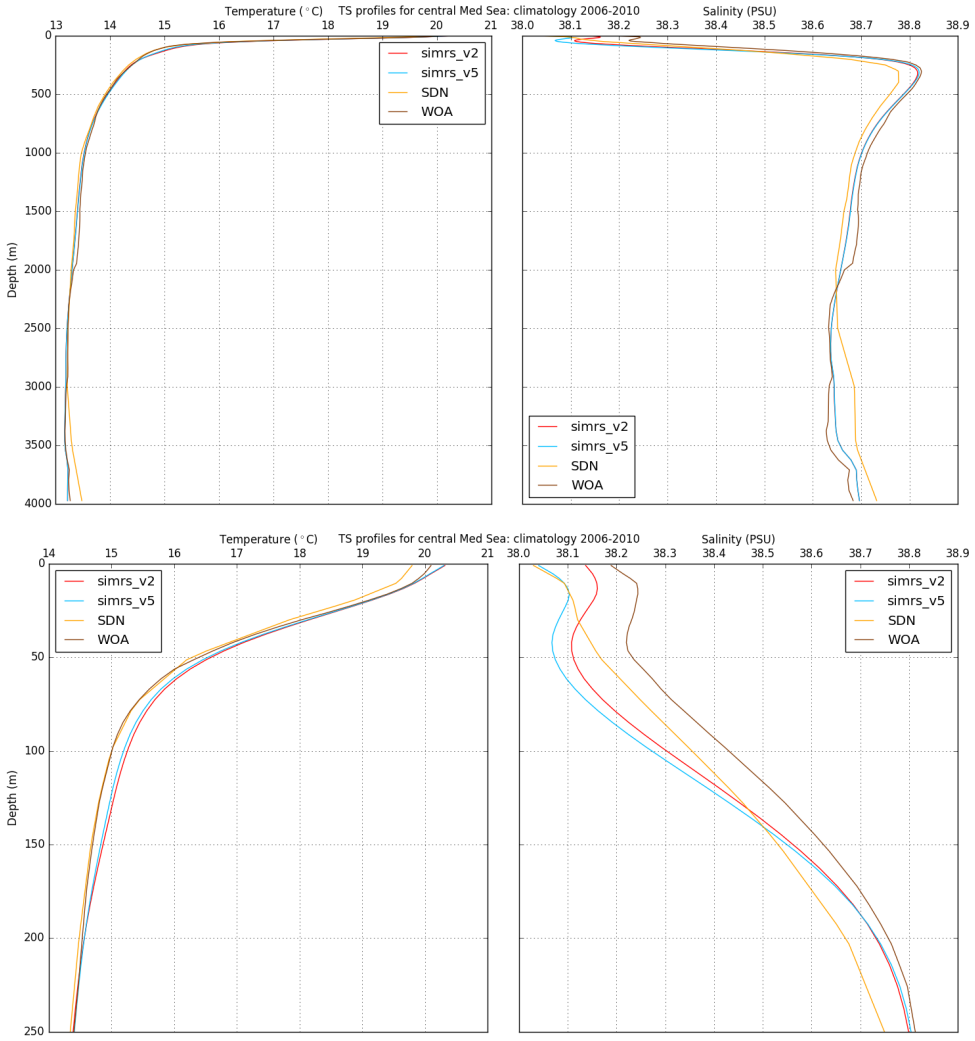

Figure 5.13: Temperature and salinity climatological profiles in central Mediterranean Sea for the whole water column (top panel) and for the depth range 0-250 m (bottom panel) over the period 2006-2010 for experiments simrs_v2, simrs_v5 and SDN and WOA climatological data sets.

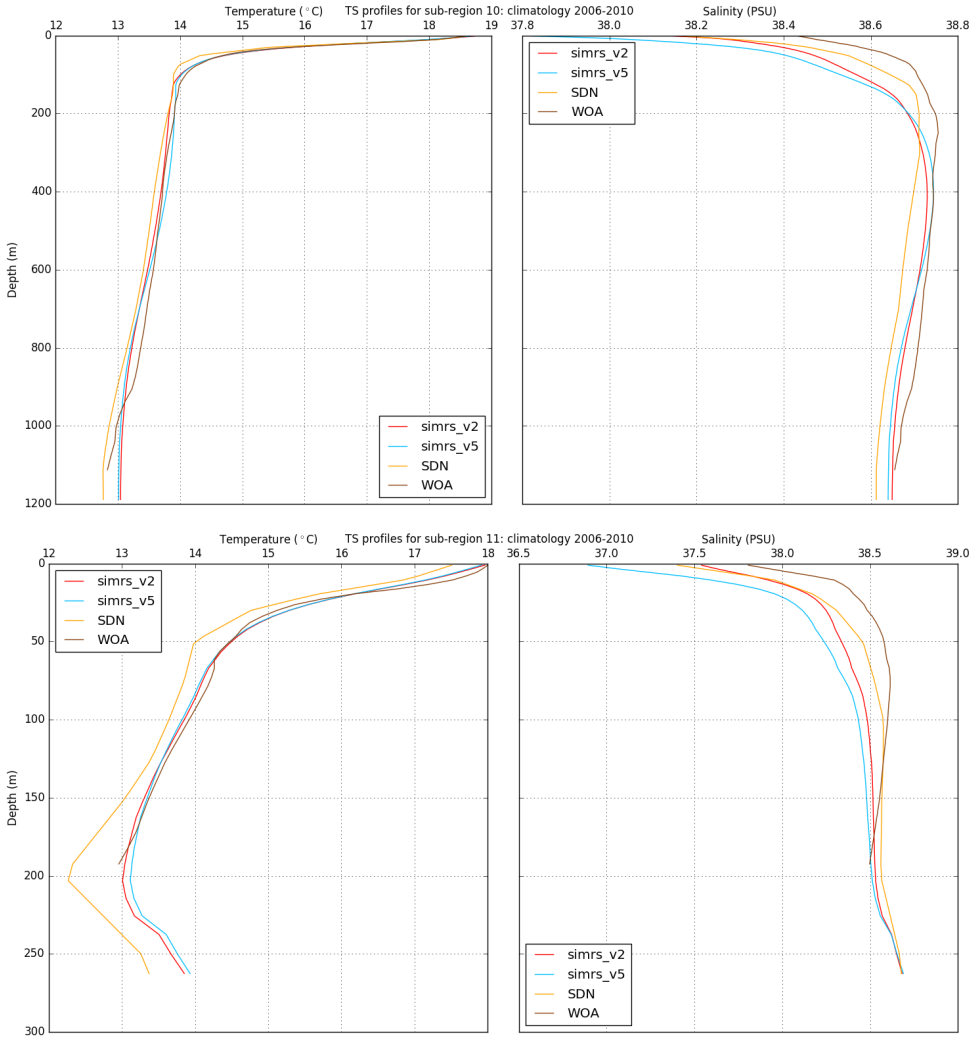

Figure 5.14: Temperature and salinity climatological profiles in sub-region 10 (top panel) and 11 (bottom panel) over the period 2006-2010 for experiments simrs_v2, simrs_v5 and SDN and WOA climatological data sets.

The surface salinity and 30 m depth temperature spatial differences between the two experiments are shown in Figure 5.15.

The main differences in surface salinity are concentrated in the Adriatic

Sea and in the North Western Mediterranean Sea. In the northernmost part of the Adriatic basin significantly lower salinity values can be observed due to the signal of Adige, Brenta, Piave, Livenza, Tagliamento and Isonzo, whose outflow salinity is lower in experiment simrs_v5.

The main difference is concentrated in the area close to the river Po delta (where simrs_v5 shows a surface salinity of about 2 PSU lower than simrs_v2), as well as along the Italian coast, where the salinity negative anomaly in simrs_v5 is spread by the Western Adriatic Coastal Current down to the Gargano Promontory, with gradually decreasing values in the southward direction.

The central part of the Adriatic basin shows lower values in simrs_v5 than in simrs_v2, even though the differences between the two experiments are smaller with respect to the western coastal areas.

A negative anomaly in simrs_v5 with respect to simrs_v2 can be observed also along the Balkan coast, in particular in correspondence of the Buna-Bojana river.

In the western part of the Mediterranean Sea basin, the lower salinity discharge from Rhone and Ebro mouths in simrs_v5 with respect to simrs_v2 generates a negative anomaly that is advected southward along the French and Spanish coast by the Liguro-Provencal-Catalan Current.

For what concern temperature, the main differences between the experiments are not located at surface, but in the upper mixed layer.

It can be observed that simrs_v5 shows higher temperature values with respect to simrs_v2 along the Po river plume, down to the area beyond the Conero Promontory, while for the remaining part of the Adriatic simrs_v5

shows generally lower temperature values with respect to simrs_v2; a strong negative temperature anomaly can be observed in correspondence of the Otranto Strait, that is spread into the North Eastern Ionian Sea, in particular off the Calabria coast.

Focusing on the eastern part of the Mediterranean Sea basin, the Aegean Sea shows higher temperature values in simrs_v5 as well as along the Asia Minor Current path.

Moving westward, in front of the Tevere river outlet simrs_v5 shows strongly higher temperature values with respect to simrs_v2.

Generally higher temperature values in simrs_v5 can be observed in correspondence of the Liguro-Provencal-Catalan Current.

The main surface salinity differences between simrs_v2 and simrs_v5 can be observed in the Adriatic Sea, and in particular during Spring (Figure 5.16), mainly due to the Po river peak discharge occurring in May, being the Po river outflow salinity lower in simrs_v5 with respect to simrs_v2.

During Summer, the Po river water spreads at the surface over the whole interior of the Northern Adriatic Sea, as a consequence of the heat input that stabilizes the water column (Orlić et al., 1992 [128]).

On the contrary, it can be noticed that during Winter and Autumn the negative anomaly is much more confined towards the Italian coast with respect to Spring and Summer.

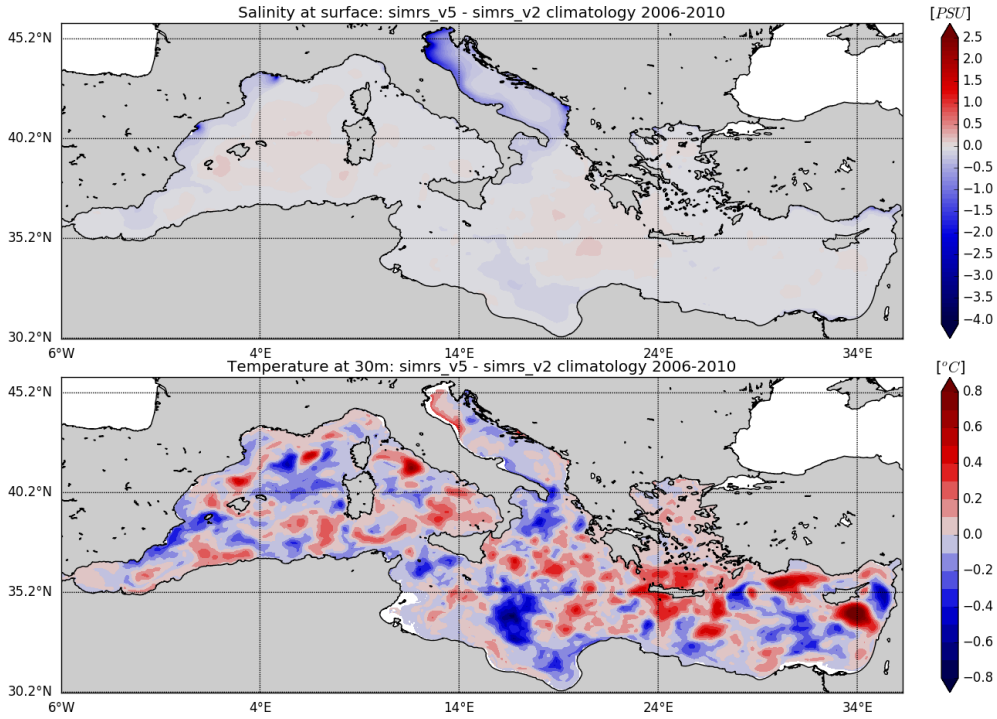

Figure 5.15: Top panel: salinity climatological differences between simrs_v2 and simrs_v5 over the period 2006-2010 at surface. Bottom panel: temperature climatological differences between simrs_v2 and simrs_v5 over the period 2006-2010 at 30 m depth.

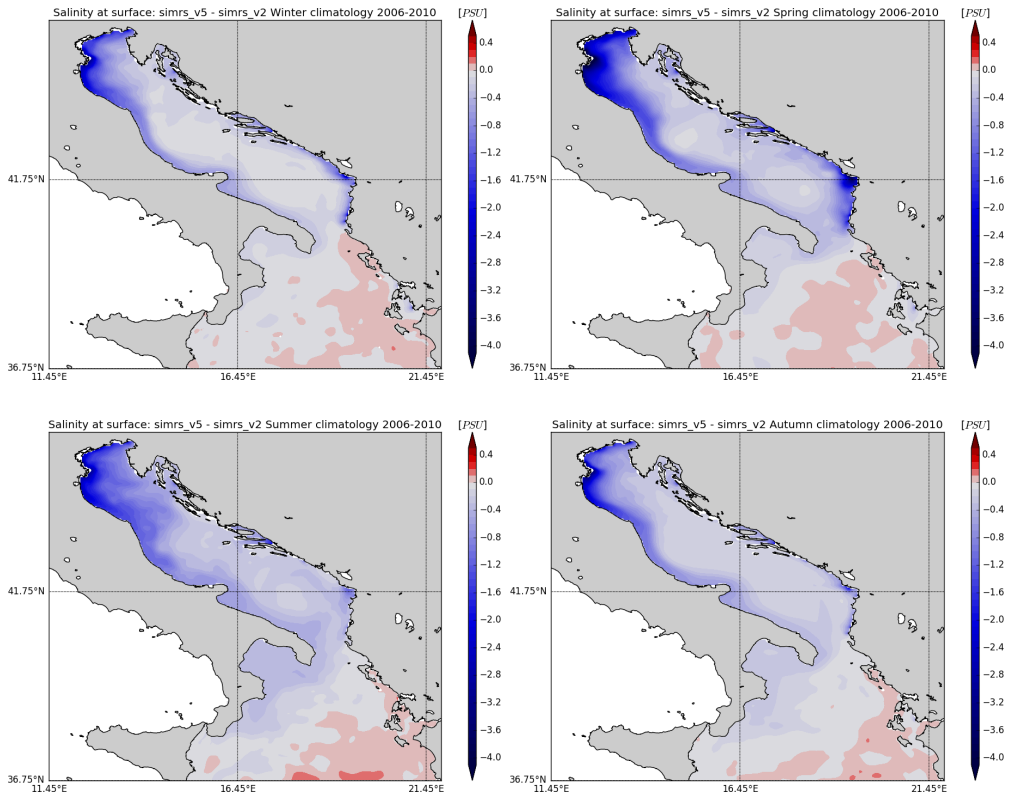

Figure 5.16: Salinity seasonal climatologies over the period 2006-2010 at surface for simrs_v5 - simrs_v2 difference. Top-left panel: Winter (Jan - Mar); top-right panel: Spring (Apr - Jun); bottom-left panel: Summer (Jul - Sep); bottom-right panel: Autumn (Oct - Dec).

The basin averaged monthly Sea Surface Temperature (SST) RMSE and BIAS of simrs_v2 and simrs_v5 with respect to satellite data show almost identical results (Table 5.4).

Observing local differences in SST RMSE and BIAS of simrs_v5 (Figure 5.17) with respect to SST from satellite data, the main differences are noticeable in February in the Northern Adriatic Sea, as well as for simrs_v2

experiment (as described in the previous chapter, Figures 4.40 and 4.41).

In general the coupled experiment shows a positive BIAS with respect to satellite data, except for the northernmost part of the Adriatic Sea, in the Ionian Sea and in the Gulf of Gabes.

The main difference with respect to simrs_v2 can be observed in the central part of the Northern Adriatic Sea, where simrs_v5 experiment shows a larger negative SST anomaly with respect to simrs_v2, reasonably due to the lower riverine outflow salinity of Po and of Adriatic rivers in simrs_v5.

As already observed for the previous experiments analyzed, this can be related to a larger freshening of the surface water masses in simrs_v5 with repect to simrs_v2, that increase the impact of the the atmospheric forcing on the sea surface, with a consequent overcooling in the area of the Northern Adriatic Sea.

As well as for simrs_v2, also in simrs_v5 the freshwater outflow from river outlets affects locally the SST, producing a negative anomaly with respect to satellite observations in the areas close to river mouths.

Table 5.4: RMSE and BIAS of SST (°C) for experiments simrs_v2 and simrs_v5 with respect to satellite data. Statistics consider the whole Mediterranean Sea basin.

Month	**SST RMSE simrs_v2**	**SST RMSE simrs_v5**	**SST BIAS simrs_v2**	**SST BIAS simrs_v5**
Jan	0.54	0.53	0.22	0.20
Feb	0.49	0.49	0.21	0.20
Mar	0.48	0.48	0.24	0.23
Apr	0.51	0.51	0.29	0.29
May	0.56	0.56	0.31	0.31
Jun	0.62	0.62	0.33	0.33
Jul	0.69	0.69	0.30	0.30
Aug	0.70	0.70	0.23	0.23
Sep	0.67	0.67	0.20	0.20
Oct	0.63	0.63	0.12	0.12
Nov	0.60	0.60	0.12	0.13
Dec	0.57	0.57	0.17	0.16

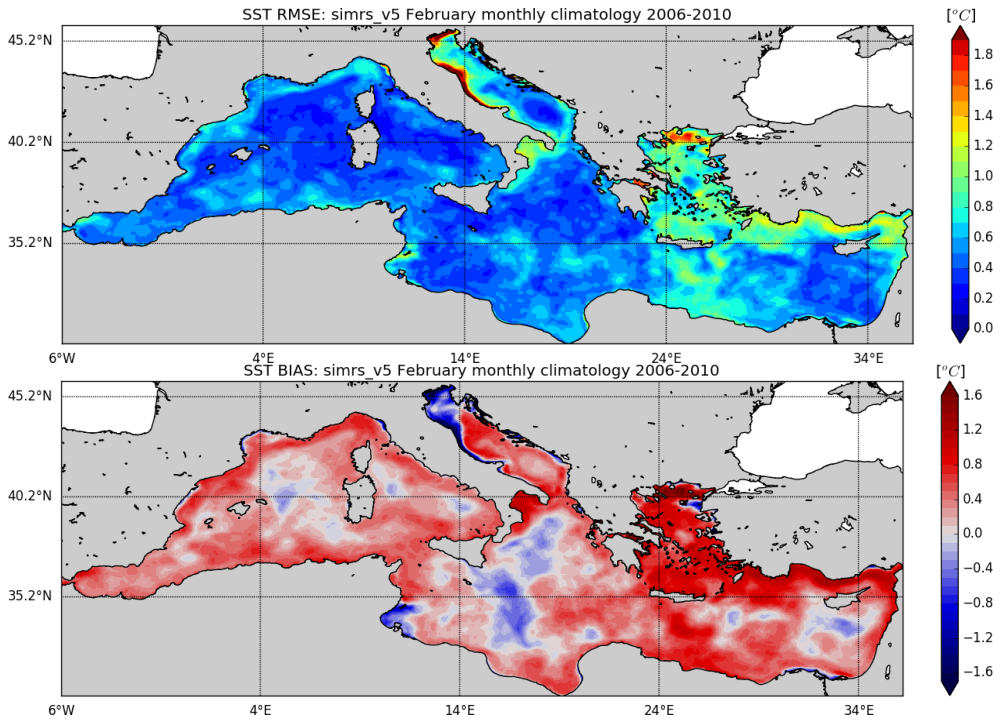

Figure 5.17: February sea surface temperature climatological RMSE (top panel) and BIAS (bottom panel).

Observing salinity daily time series averaged over the whole basin for simrs_v2 and simrs_v5 (Figure 5.18), it can be noticed that simrs_v5 shows lower salinity values with respect to simrs_v2 for all the depth ranges considered, due to the generally lower outflow salinity in experiment simrs_v5.

The major differences between the two experiments are located in the depth range between surface and 100 m depth, where the average difference is about 0.03 PSU, with simrs_v5 showing constantly lower values. It can be noticed that both the experiments show a quite strong negative trend in salinity, less pronounced for simrs_v2.

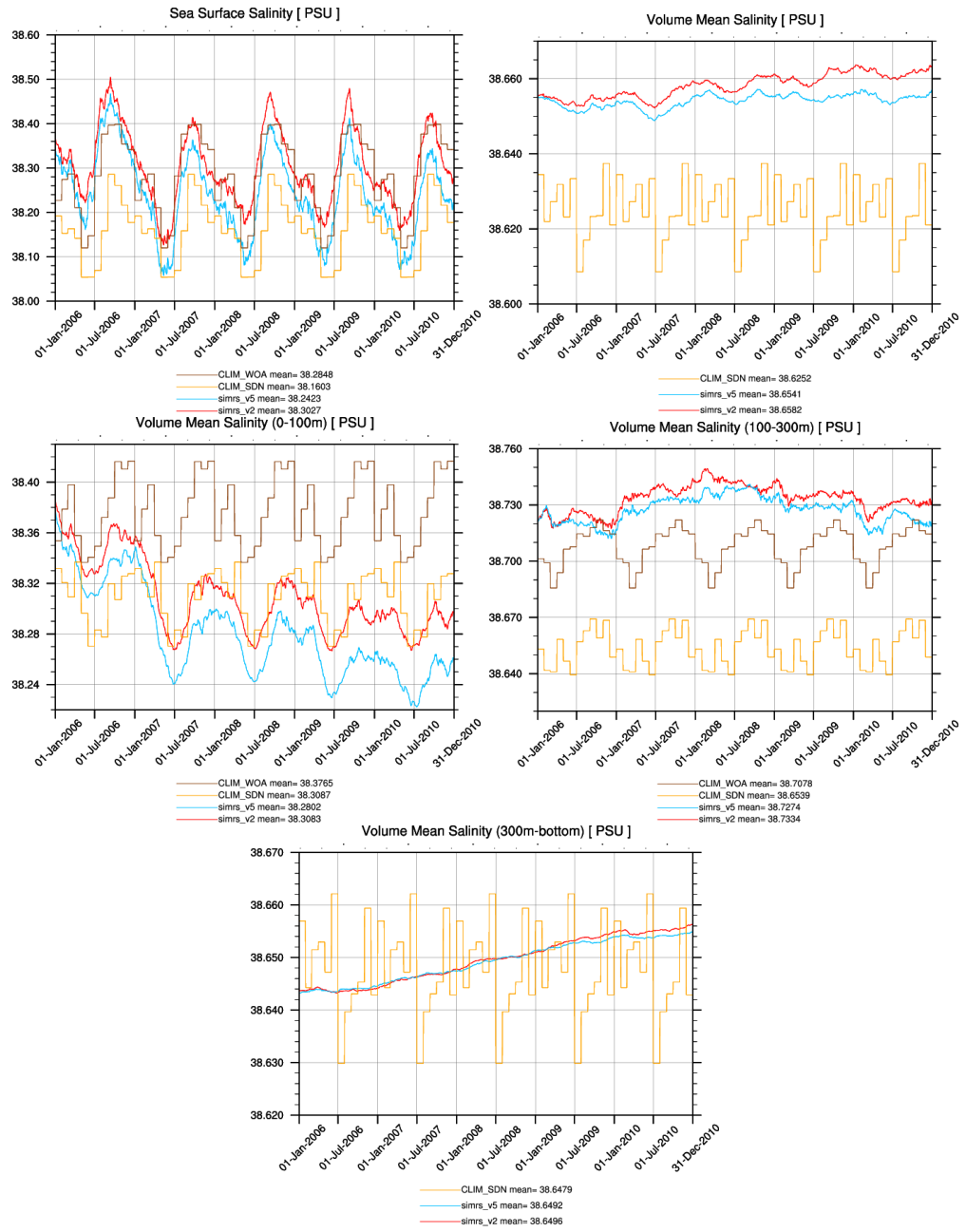

Figure 5.18: Mediterranean Sea salinity daily mean computed from numerical experiments and climatological data sets at different layers.

5.3.4 Mixed Layer Depth analysis

The main differences in Mixed Layer Depth (MLD) between the two considered experiments can be observed in Winter, and in particular in February and are located off the Gulf of Lion and in the Adriatic Sea.

In February (Figure 5.19) in the area off the Gulf of Lion simrs_v5 shows generally large deeper MLD values with respect to simrs_v2, reasonably attributable to the winter variability between the considered experiments of the Liguro-Provencal-Catalan current, while closer to the Gulf of Lion simrs_v5 shows shallower values with respect to simrs_v2. This can be attributed to the lower outflow salinity from Rhone river in simrs_v5 with respect to simrs_v2 and it is more clearly observable in December, even though the differences between the two experiments are smaller: the fingerprints of Rhone and Ebro outflow is indeed clearly observable as negative MLD anomalies in simrs_v5 with respect to simrs_v2 in the areas around the deltas of the aforementioned rivers.

In the Adriatic Sea the main differences in MLD can be observed in February, as well as for the Gulf of Lion: largely shallower values can be observed for simrs_v5 in correspondence of the South Adriatic Gyre and of the Northern Ionian Cyclonic Gyre, as well as for the Gulf of Taranto, where anyway the differences between the two experiments are smaller with respect to the aforementioned areas. Less pronounced differences can be noticed also along the Western Adriatic Coastal Current and the Eastern South-Adriatic Current paths.

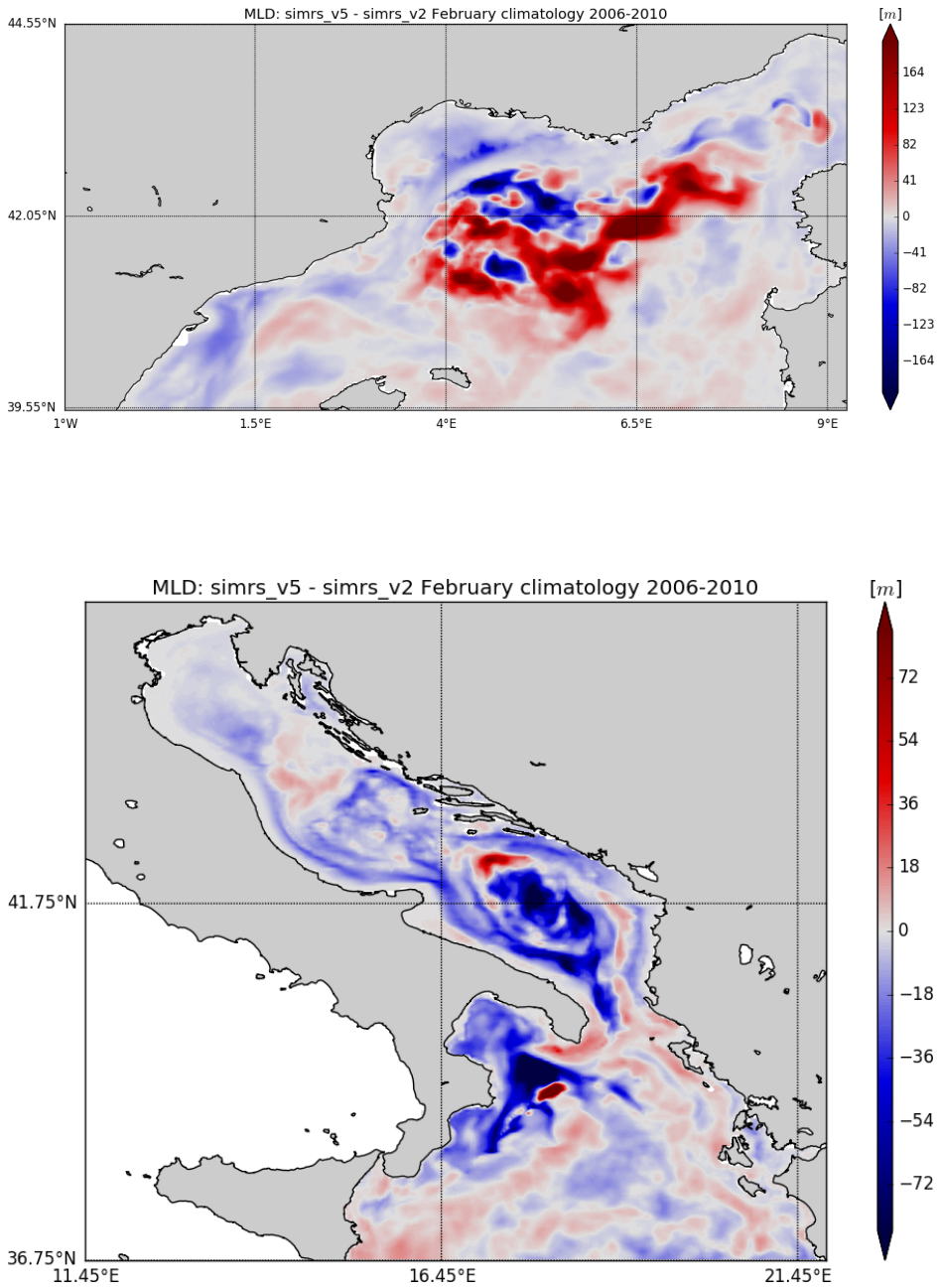

Figure 5.19: February climatological Mixed Layer Depth simrs_v5 - simrs_v2 differences over the period 2006-2010 in North Western Mediterranean Sea (top panel) and Adriatic Sea (bottom panel).

5.3.5 Currents and water volume transport at straits

The analysis of the mean circulation at 15 m depth (not shown) shows that the coupled experiment well reproduces the results from Pinardi et al. (2015) [33] as well as for the 200-300 m depth.

Surface circulation pattern shows the main differences between the two experiments during Winter and Autumn (Figure 5.20), which can be reasonably attributed to the fact that the most part of the rivers implemented have their own discharge peak during these two seasons.

Both during Winter and Autumn a clear intensification of the Western Adriatic Coastal Current and of the Eastern South-Adriatic Current can be observed in simrs_v5 with respect to simrs_v2. On the contrary, a strong weakening of the whole outer edge of the South Adriatic Gyre can be observed in Winter in simrs_v5 with respect to simrs_v2, while in Autumn the weakening appears to affect only its eastern edge.

It can be moreover noticed that in Winter an intensification of the Middle Adriatic Gyre appears in simrs_v5 with respect to simrs_v2, while in Autumn a weakening of the structure can be observed.

Another circulation structure that shows clear differences between the two experiments is the Northern Tyrrhenian Gyre, that during Winter shows a weakening in simrs_v5 with respect to simrs_v2, less pronounced in Autumn. This differences can be reasonably attributed to the differences in the outflow implementation of Tevere river, which affects the considered area.

During Winter a clear intensification of the Liguro-Provencal-Catalan Current is observable in simrs_v5 with respect to simrs_v2 and local effects of the different implementation of Rhone and Ebro rivers are noticeable, with larger

velocity amplitude values in simrs_v5 with respect to simrs_v2. A similar situation is observable also during Autumn even though the intensification of the aforementioned circulation structures in simrs_v5 appears to be smaller than in Winter.

Observing the average circulation in the 200-300 m depth layer (Figure 5.21), that well reproduce the structures identified in Pinardi et al. (2015) [33], concerning the Southern Adriatic Sea and the North Eastern Ionian Sea it can be observed that the circulation structures that show the main differences between the two experiments are the South Adriatic Gyre (in its inner core) and the current that flows along the western Calabria and Sicily coast, which both show a weakening in simrs_v5 with respect to simrs_v2.

For what concern the central and western part of the Mediterranean Sea basin, lower amplitude velocity values can be observed in correspondence of the South-Eastern Tyrrhenian Gyre in simrs_v5, while the area interested by the Gulf of Lion Gyre shows higher velocity amplitude values in simrs_v5, as well as the Liguro-Provencal-Catalan Current.

Finally, for the whole Alboran Sea, a clear weakening of the current pattern can be observed in simrs_v5 with respect to simrs_v2.

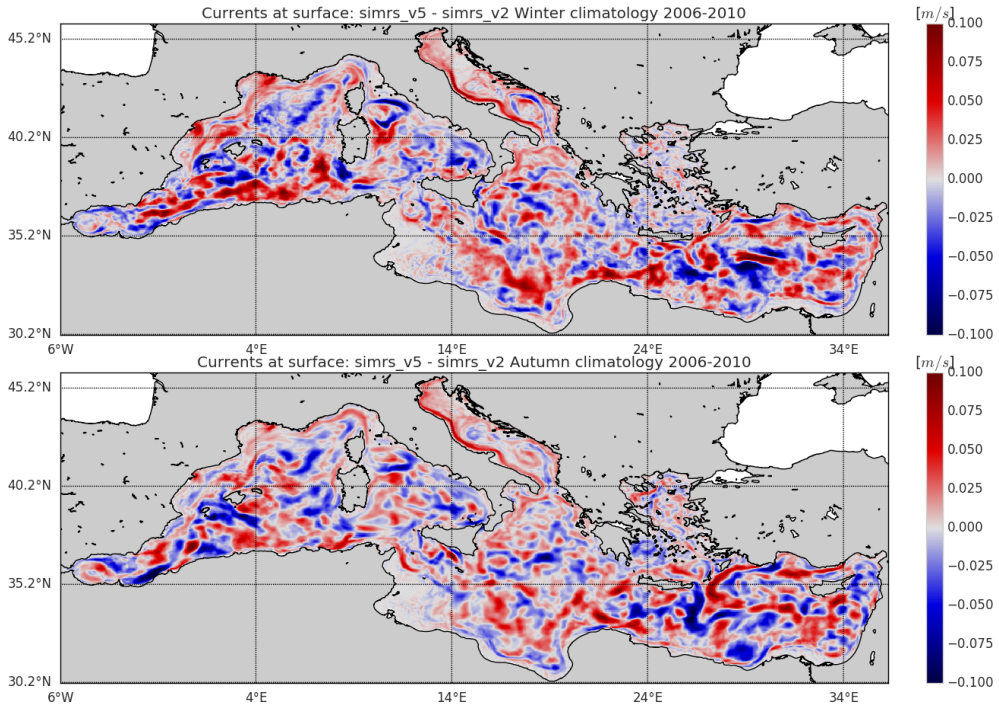

Figure 5.20: Climatological Winter (top panel) and Autumn (bottom panel) surface circulation differences between simrs_v2 and simrs_v5 over the period 2006-2010.

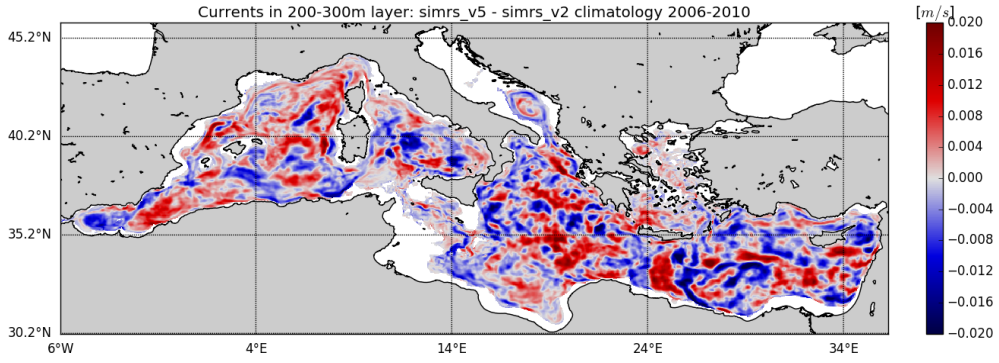

Figure 5.21: Climatological circulation average in the 200-300 m depth layer difference between simrs_v2 and simrs_v5 over the period 2006-2010.

Comparing the water volume transport through the Strait of Gibraltar (Table 5.5) simrs_v2 and simrs_v5 present similar mean net transport computed over the period 2006-2010, being both in good agreement with literature (Soto-Navarro et al., 2010 [130] and Candela (2001) [131]).

Both for eastward and westward transport through the Strait of Gibraltar the two considered experiments underestimate the values by Candela (2001) [131], while they are very close to the upper limit indicated in Soto-Navarro et al. (2010) [130].

Concerning the Strait of Otranto (Table 5.6), the net transport is the same for the two experiments, being lower with respect to the available literature (Yari et al., 2012 [132] and Astraldi et al., 1999 [133]), while the northward and southward transports are closer to the literature ones presenting lower values in the coupled experiment.

For what concern the Strait of Sicily (Table 5.7), the two considered experiments show very similar values among each other for all the components of the transport through the strait, even though small differences can be identified, being simrs_v5 the experiment showing the lowest values for all the transport components.

Table 5.5: Strait of Gibraltar water volume transport [Sv] from simrs_v2 and simrs_v5 averaged over the period 2006-2010 compared to literature values.

Gibraltar mean transport [Sv]	**simrs_v2**	**simrs_v5**	**Soto-Navarro et al., 2010**	**Candela 2001**
Net	0.043	0.040	0.038 ±0.007	0.04
Eastward	0.900	0.885	0.81 ±0.06	1.01
Westward	0.857	0.845	0.78 ±0.05	0.97

Table 5.6: Strait of Otranto water volume transport [Sv] from simrs_v2 and simrs_v5 averaged over the period 2006-2010 compared to literature values.

Otranto mean transport [Sv]	**simrs_v2**	**simrs_v5**	**Yari et al., 2012**	**Astraldi et al., 1999**
Net	-0.004	-0.005	-0.04 ±0.28	0.01
Northward	0.915	0.881	0.90 ±0.04	1.15 ±0.53
Southward	0.919	0.886	0.94 ±0.32	1.16 ±0.53

Table 5.7: Strait of Sicily water volume transport [Sv] from simrs_v2 and simrs_v5 averaged over the period 2006-2010 compared to literature values.

Sicily mean transport [Sv]	**simrs_v2**	**simrs_v5**
Net	0.105	0.092
Northward	1.940	1.873
Southward	1.835	1.781

5.3.6 Sea Surface Height comparison with satellite data

The comparison between the numerical experiments results with respect to satellite measurements highlights that the two performed experiments have almost the same SLA RMSE at basin scale, while differences between the Mediterranean Sea sub-regions can be observed (Figure 5.22).

The pattern of differences between the performed experiments (Figure 5.23) shows areas that can be reasonably directly impacted by the riverine outflow implementation: the whole Adriatic Sea shows higher Sea Surface Height (SSH) values in experiment simrs_v5 due to the generally lower mean outflow salinity of the rivers implemented in the area and to the higher discharge of Po river in simrs_v5 with respect to simrs_v2.

It can be moreover noticed that the positive SSH anomaly in simrs_v5 with respect to simrs_v2 affects also the North-Eastern part of the Ionian Sea, as a consequence of the southward spreading of Adriatic Sea waters.

A similar anomaly pattern can be identified also along the path of the Liguro-Provencal-Catalan Current, affected by Rhone and Ebro rivers discharge, as well as in the Aegean Sea.

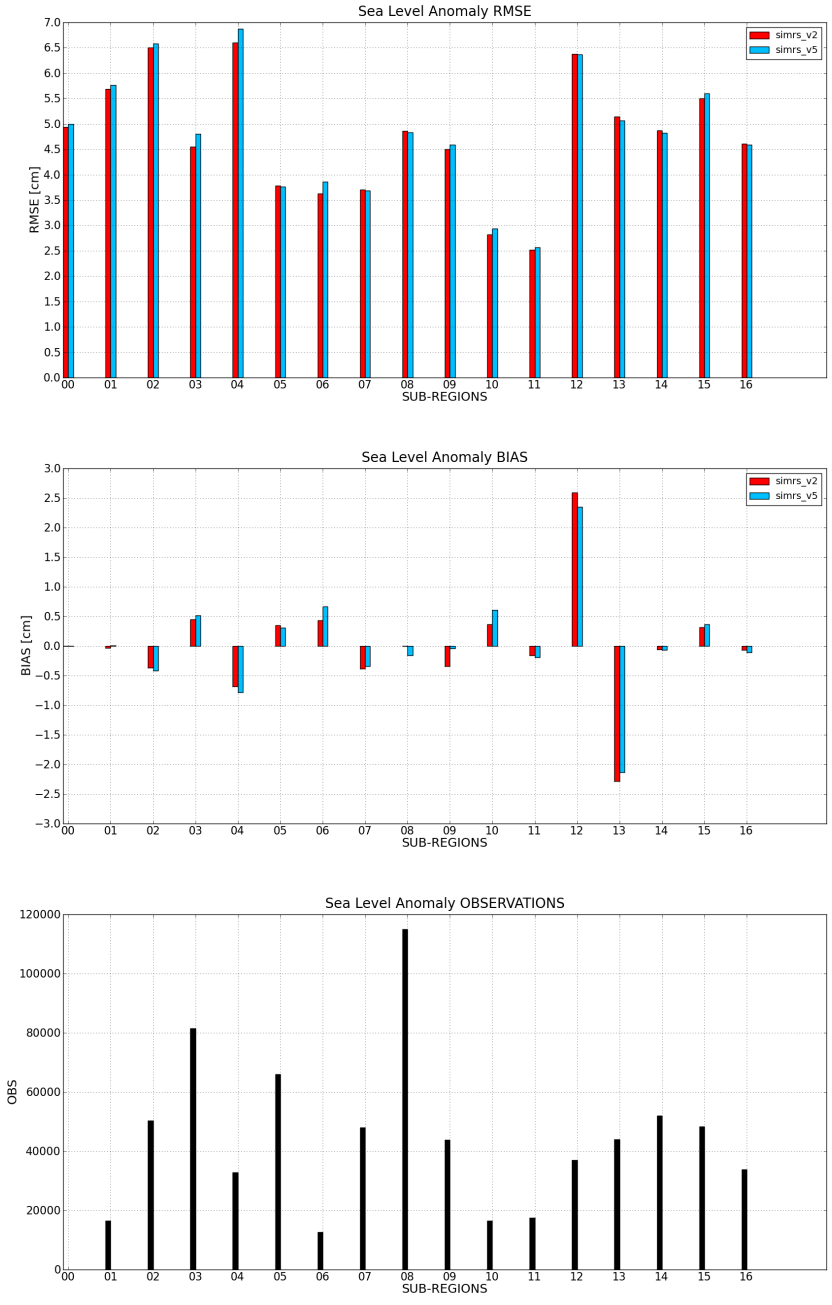

Figure 5.22: Sea Level Anomaly (cm) metrics of simrs_v2 and simrs_v5 computed over the period 2006-2010 for the Mediterranean Sea (00) and for the 16 sub-regions. From top to bottom panel: RMSE, BIAS, number of observations.

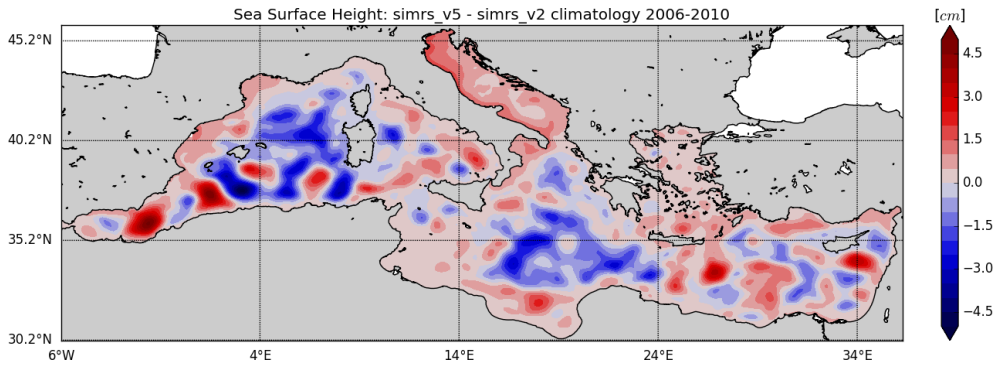

Figure 5.23: Mean SSH difference between experiments simrs_v2 and simrs_v5 over the period 2006-2010.

5.4 Summary of the chapter

In this chapter the implementation of the CMCC Estuary Box Model for the Mediterranean Sea rivers has been described.

Several sensitivity tests with different setups of the CMCC EBM have been performed, in order to define the implementation ensuring the best possible reliability of the EBM solution.

The CMCC EBM has been then implemented for the Mediterranean Sea rivers and a coupled experiment EBM-NEMO ocean model (simrs_v5) has been performed, in order to evaluate the impact of this approach on the river runoff representation and therefore on the thermohaline properties of the Mediterranean Sea.

The results of the coupled experiment have been evaluated through an assessment with in situ and satellite data, along with a comparison with the experiment ensuring the best results from previous tests, i.e. simrs_v2.

The two experiments show very similar salinity representation skills at basin scale, while simrs_v2 shows generally better performances in temperature representation in the different depth ranges considered.

The performances of the two experiments have a quite large variability among the different sub-regions of the Mediterranean Sea, but it has been noticed a worsening in the salinity representation performances in simrs_v5 with respect to simrs_v2 in the Northern Adriatic Sea, particularly evident in the depth range between the surface and 100 m depth, due to an excessive freshening of the water column.

The general freshening introduced in simrs_v5 is confirmed by the analysis of the sea surface salinity and volume mean salinity time series. In particular the surface overfreshening in the Adriatic Sea in simrs_v5 could be directly responsible for the differences in evaporation rate observed in the sub-basin for the two considered experiments, since the lighter surface water masses are more affected by the atmospheric forcing influence.

It has been observed that the injection of fresher river runoff waters in experiment simrs_v5 led to significant modifications in the deep waters formation areas of the South Adriatic Sea, with a large decrease of the Mixed Layer Depth (MLD) in correspondence of the South Adriatic Gyre during Winter.

The generally lower salinity associated to river runoff in simrs_v5 with respect to simrs_v2 affected also the Sea Surface Height (SSH) representation, in particular in the Adriatic Sea and along the Rhone river plume, where positive differences have been observed: the comparison with satellite altimetry data indicates that an overestimation of SSH is introduced by the simrs_v5

river runoff implementation in these areas.

Another effect that can be related to the surface freshening in simrs_v5 is the increase in velocity amplitude of the Western Adriatic Coastal Current (WACC) and of the portion of the Liguro-Provencal-Catalan Current (LPCC) in front of the Rhone and Ebro rivers outlets.

Chapter 6

Conclusions and future developments

The riverine input is a fundamental component of the hydrologic cycle, thus its correct representation in numerical ocean models is of crucial importance.

Since the resolution of the most part of ocean models does not allow to correctly represent the estuarine dynamics, it is necessary to parameterize these processes, along with implementing a realistic numerical setup.

The aim of this study is to analyze the impact of river runoff on the thermohaline properties and on the circulation of the Mediterranean Sea at local and basin scales.

In addition the capability of the Mediterranean Sea numerical ocean model to better reproduce the thermohaline properties of the basin through an improved implementation of the riverine outflow is investigated.

As a first step, to better represent the dynamics of the Mediterranean

Sea as a whole and of the North Aegean Sea in particular, a more realistic implementation of the mass and tracers' transports from the Marmara Sea to the North Aegean Sea through the Dardanelles Strait is achieved. The new strait configuration consists in the implementation of Lateral Open Boundary Conditions (LOBC), which is here compared to a more simplified river-like implementation.

A twin numerical experiment is performed with the purpose to assess the quality of the two configurations with respect to observations. The numerical results show that the new implementation provides an improvement in reproducing the thermohaline properties of the Aegean Sea, even though a variable skill can be observed along the water column.

The water volume transport (net, eastward and westward) through the Dardanelles Strait is well reproduced by the new implementation, being in very good agreement with literature values.

The Black Sea Waters plume structure is more realistically reproduced in the Dardanelles Strait LOBC implementation, leading to a better representation of the circulation pattern of the Aegean Sea, if compared with literature.

In terms of future developments, input fields could be possibly retrieved from a 3D numerical ocean model specifically designed to resolve the Marmara Sea dynamics and properties which would improve the representation of the Dardanelles Strait inflow into the Aegean Sea.

This would allow to reduce some approximations done in the present LOBC implementation of the Dardanelles Strait, above all the constant value of salinity prescribed to the lower layer flux, from the Mediterranean Sea to the

Marmara Sea; this would ameliorate the vertical structure of the Dardanelles Strait boundary, with a possible improvement of the thermohaline properties of the Aegean Sea.

The second goal of this work is to evaluate the riverine influence on the Mediterranean Sea ocean model, through numerical experiments characterized by different riverine setup. In particular it is evaluated the impact of:

- an increased number of river runoff sources
- a modified riverine outflow salinity, an increased mixing at river mouths and a different vertical mixing scheme
- an offline coupling with an Estuary Box Model

The increased number of river runoff sources (from 7 to 39) leads to a better representation of the total riverine discharge in the Mediterranean Sea, with values much closer to the literature ones.

It also provides, at Mediterranean Sea basin scale, a slightly better reproduction of observed salinity from the sea surface down to 60 m depth, while a small worsening is observed in the depth range from 60 m to 300 m, due to an excessive freshening of the water column. Impacts at larger depths are not detected at basin scale.

In addition, the increased number of river runoff sources provides no significant differences, at basin scale, in the temperature, along the whole water column.

On the contrary, significant impacts on the thermohaline properties is observed at sub-regional scales, with contrasting results on the capability of

the considered numerical configurations in reproducing the temperature and salinity data available from observations.

The increased riverine discharge shows also an impact on the Mixed Layer Depth (MLD), in particular in the South Adriatic Gyre, the deep water mass formation area of the Adriatic Sea, where a large number of additional rivers is implemented.

The surface circulation pattern is affected when increasing the freshwater sources in particular in the Adriatic Sea and in the North Eastern Ionian Sea structures: from a numerical point of view, the mass/volume addition due to the river runoff is added to the horizontal divergence of currents, thus increasing the diffusion term close to river mouths and hence simulating a momentum flux (Madec et al., 2017 [78]).

The large amount of riverine water introduced into the Adriatic Sea and the Aegean Sea generates an evident increase in the Sea Surface Height (SSH) of these two sub-basins.

As the river salinity is a major unknown parameter that can strongly affect the local thermohaline properties of the basin, a sensitivity experiment is performed by imposing a null salinity for all the 39 river sources implemented, comparing with numerical simulations where the river salinity is imposed larger than 0 PSU and variable from river to river.

It is observed that at basin scale the differences in salinity skill are extremely small, even though a significant reduction of surface and volume basin-averaged salinity can be noticed when a null salinity is prescribed for river runoff.

Differences are more significant for temperature, where a worsening in

reproducing the observed temperature can be noticed when imposing a null salinity at the riverine outflow.

The variability among the sub-regions is very strong, being the Adriatic Sea the area most impacted by this change, both in terms of salinity and temperature, with a worsening of the capability of the Mediterranean Sea model to correctly reproduce the observations.

The Mixed Layer Depth is strongly affected by the riverine outflow prescribed salinity, in particular in the Adriatic Sea where the Po and a large number of rivers have their own outlets as well as in correspondence of the Gulf of Lion Gyre, which is affected by the Rhone river discharge.

Differences in the circulation patterns of the aforementioned areas are also observed, in particular for the Western Adriatic Coastal Current (WACC) and for the Liguro-Provencal-Catalan Current (LPC), affected by the different parameterizations of the Po river (the WACC) as well as of the Rhone and Ebro rivers (the LPC).

In agreement with Chao and Boicourt (1986) [144] it is shown that the spreading of a lower-salinity fluid over a denser water mass generates a drop in the potential energy which is partially converted into kinetic energy, thus increasing the velocity amplitude in the proximity of river mouths. This is also observed in the present work when adding new riverine sources and it is even more evident when prescribing 0 PSU salinity at riverine outflow.

A strong impact is also observed on SSH, in particular in the Adriatic Sea, where the river null salinity further increased the SSH values.

It is observed that river discharge with null salinity also affects the Sea Surface Temperature (SST), as a consequence of the stratification induced

close to river outlets. This is confirmed by Sauvage et al. (2018) [5] where the authors show that the riverine outflow generates a freshwater barrier layer, that can isolate the underlying layers from the air-sea interaction, leaving the upper layers more exposed to the atmospheric forcing, thus triggering a stronger sensitivity of the SST.

A further experiment is carried out with the aim of assessing the impacts due to an increased vertical eddy diffusivity coefficient at river mouths, thus promoting the vertical mixing of the riverine waters with the ocean waters.

The effects of this change are much more localized and concentrated in the areas close to the river mouths with respect to the effects of the decrease in the river outflow salinity previously described.

At sub-region scale the model shows a great variability in the salinity and temperature skill, with contrasting performances from area to area and for different depth ranges.

Impacts on the MLD in the Adriatic Sea and in the Gulf of Lion are observed, as well as on the main circulation structures of the areas, even though smaller with respect to the null river salinity experiment.

Given the strong modifications of the thermohaline vertical structure introduced by river runoff in the vicinity of river outlets, which then propagate to the entire ROFI, the impact provided by a different vertical mixing scheme (TKE) in the Mediterranean Sea model is investigated.

The results of the experiment performed with the new scheme are assessed with respect to in situ and satellite observations and compared with a control experiment using a local Richardson number dependent formulation for the vertical mixing.

The two experiments show at basin scale no particular differences in the salinity skill, while the TKE experiment provides a slightly higher temperature RMSE for the entire water column.

The sub-regions most impacted by the new vertical mixing scheme adopted are the Northern Adriatic Sea and the Aegean Sea (especially): in the latter a general overestimation of both temperature and salinity in the TKE experiment can be observed, while in the Northern Adriatic Sea it provides better results for salinity in the first 30 m of the water column and better results for temperature in the first 150 m.

Minor differences between the two experiments can be observed also in the Nile and Rhone rivers outlets sub-regions, with an improvement introduced by the TKE vertical mixing scheme both in salinity and temperature for the former sub-region, while in the latter the improvement concerns only salinity.

In order to improve the riverine outflow representation including the estuarine processes that the Mediterranean Sea model cannot resolve due to its resolution and formulation, an estuary box modelling approach is tested, by implementing the CMCC Estuary Box Model (CMCC EBM) for the Mediterranean Sea rivers.

The CMCC EBM is then 1-way offline coupled with the Mediterranean Sea ocean model providing to the latter daily values of salinity and volume flux of the outflowing estuarine water.

A numerical experiment with the coupled system is performed and the results are validated against observations and compared with a control run forced by constant river salinity values.

At basin scale the coupled experiment does not show significant differences

in salinity skill, even though a reduction in surface and volume salinity values is observed, due to the generally lower riverine outflow salinity in this experiment.

Considering more local effects, the coupled configuration generally shows a worsening in the thermohaline properties representation in the areas of large riverine sources. This effect could be improved by imposing more realistic (when available) river volume flux values at the estuary head of the CMCC EBM instead of monthly climatological values.

The results of the performed experiments show that the still quite common practice in ocean modelling of imposing a prescribed null salinity for river runoff can lead to large errors in the numerical solution, while an enhancing in vertical mixing at river mouths has mostly only local effects.

The coupling of the ocean model with an Estuary Box Model appears to be a preferable approach, since it allows a physically consistent representation of the estuarine dynamics; nevertheless, in order to improve the CMCC EBM performances, and thus the coupled EBM-ocean model system skill, additional calibration of the EBM would be required, even though at the moment this is a very challenging issue due to the lack of in situ measurements at river mouths, especially for small rivers.

The setup used in the experiment with 39 rivers and outflow salinity larger than 0 PSU appears to be the most adequate, providing the best river runoff representation in the Mediterranean Sea, even though the different performances of the model among the sub-regions of the basin and along the water column need to be further investigated.

Additional improvements could be achieved by more deeply investigating

the impacts of different vertical mixing schemes such as the K-Profile Parameterization dependent vertical mixing scheme (KPP) or the most widely used Generic Length Scale scheme (GLS), which offer several choices in terms of turbulent closure parameterizations.

Since the river runoff does not affect only the vertical structure of the water column, but also the lateral mixing due to the strong modifications introduced in horizontal density gradients, it will be worth to assess the impact of a different horizontal mixing parameterization with respect to the constant mixing coefficients used in the performed experiments. In this sense the use of spatial and temporal varying horizontal turbulence coefficients, as proposed in Smagorinsky (1963) [166] formulation, would be of great interest in order to better understand if such a more sophisticated subgrid-scale parameterization is capable to better reproduce the horizontal dynamics triggered by river runoff.

Finally, regardless of the numerical solutions adopted, a possible further development in order to improve the river runoff representation in the Mediterranean Sea model would be to use higher temporal frequency runoff data (depending on data availability) instead of monthly climatologies, since this is shown to have a strong impact on the circulation and the stratification especially in coastal areas (Sauvage et al., 2018 [5]).

Bibliography

[1] Steven J Lentz and Richard Limeburner. "The Amazon River Plume during AMASSEDS: Spatial characteristics and salinity variability". In: *Journal of Geophysical Research: Oceans* 100.C2 (1995), pp. 2355–2375.

[2] John H Simpson et al. "Periodic stratification in the Rhine ROFI in the North Sea". In: *Oceanologica Acta* 16.1 (1993), pp. 23–32.

[3] Giorgia Verri et al. "River runoff influences on the Central Mediterranean overturning circulation". In: *Climate dynamics* 50.5–6 (2018), pp. 1675–1703.

[4] Boyin Huang and Vikram M Mehta. "Influences of freshwater from major rivers on global ocean circulation and temperatures in the MIT ocean general circulation model". In: *Advances in Atmospheric Sciences* 27.3 (2010), pp. 455–468.

[5] César Sauvage et al. "Impact of the representation of the freshwater river input in the Western Mediterranean Sea". In: *Ocean Modelling* 131 (2018), pp. 115–131.

[6] N Skliris, S Sofianos, and A Lascaratos. "Hydrological changes in the Mediterranean Sea in relation to changes in the freshwater budget: a numerical modelling study". In: *Journal of Marine Systems* 65.1–4 (2007), pp. 400–416.

[7] Vassiliki H Kourafalou et al. "The fate of river discharge on the continental shelf: 1. Modeling the river plume and the inner shelf coastal current". In: *Journal of Geophysical Research: Oceans* 101.C2 (1996), pp. 3415–3434.

[8] Alexander E Yankovsky and David C Chapman. "A simple theory for the fate of buoyant coastal discharges". In: *Journal of Physical oceanography* 27.7 (1997), pp. 1386–1401.

[9] Vassiliki H Kourafalou. "Process studies on the Po River plume, north Adriatic Sea". In: *Journal of Geophysical Research: Oceans* 104.C12 (1999), pp. 29963–29985.

[10] Richard W Garvine. "Penetration of buoyant coastal discharge onto the continental shelf: A numerical model experiment". In: *Journal of Physical Oceanography* 29.8 (1999), pp. 1892–1909.

[11] Rafael V Schiller and Vassiliki H Kourafalou. "Modeling river plume dynamics with the HYbrid Coordinate Ocean Model". In: *Ocean Modelling* 33.1–2 (2010), pp. 101–117.

[12] Stefan Rahmstorf. "Bifurcations of the Atlantic thermohaline circulation in response to changes in the hydrological cycle". In: *Nature* 378.6553 (1995), p. 145.

[13] Yu-heng Tseng, Frank O Bryan, and Michael M Whitney. "Impacts of the representation of riverine freshwater input in the community earth system model". In: *Ocean Modelling* 105 (2016), pp. 71–86.

[14] Qiang Sun et al. "A box model for representing estuarine physical processes in Earth system models". In: *Ocean Modelling* 112 (2017), pp. 139–153.

[15] Vassiliki H Kourafalou. "River plume development in semi–enclosed Mediterranean regions: North Adriatic Sea and northwestern Aegean Sea". In: *Journal of Marine Systems* 30.3–4 (2001), pp. 181–205.

[16] P Oddo and A Guarnieri. "A study of the hydrographic conditions in the Adriatic Sea from numerical modelling and direct observations (2000–2008)". In: *Ocean Science* 7.5 (2011), pp. 549–567.

[17] Hubert HG Savenije. *Salinity and tides in alluvial estuaries, 2nd completely revised ed.* Available at salinityandtides.com, 2012.

[18] JL Davies. "A morphogenic approach to world shorelines". In: *Zeitschrift fur Geomorphologie* 8 (1964), pp. 127–142.

[19] William E Galloway. "Process framework for describing the morphologic and stratigraphic evolution of deltaic depositional systems". In: *Society of Economic Paleontologists and Mineralogist (SEPM), Special Publication No. 31* (1975), pp. 127–156.

[20] Hansjörg Seybold, José S Andrade, and Hans J Herrmann. "Modeling river delta formation". In: *Proceedings of the National Academy of Sciences* 104.43 (2007), pp. 16804–16809.

[21] Hugo B Fischer. "Mixing and dispersion in estuaries". In: *Annual review of fluid mechanics* 8.1 (1976), pp. 107–133.

[22] Zhi-Qiang Deng, Vijay P Singh, and Lars Bengtsson. "Longitudinal dispersion coefficient in straight rivers". In: *Journal of hydraulic engineering* 127.11 (2001), pp. 919–927.

[23] JB Schijf and JC Schönfled. "Theoretical considerations on the motion of salt and fresh water". In: IAHR. 1953.

[24] RJ Uncles and JA Stephens. "Salt intrusion in the Tweed Estuary". In: *Estuarine, Coastal and Shelf Science* 43.3 (1996), pp. 271–293.

[25] HB Fischer et al. "Mixing in inland and coastal waters Academic Press". In: *New York* (1979), pp. 229–242.

[26] John Wright, Angela Colling, and Dave Park. *Waves, tides and shallow-water processes*. Vol. 4. Gulf Professional Publishing, 1999.

[27] F Verspecht et al. "Processes impacting on stratification in a region of freshwater influence: Application to Liverpool Bay". In: *Journal of Geophysical Research: Oceans* 114.C11 (2009).

[28] John H Simpson et al. "Tidal straining, density currents, and stirring in the control of estuarine stratification". In: *Estuaries* 13.2 (1990), pp. 125–132.

[29] Tom P Rippeth, Neil R Fisher, and John H Simpson. "The cycle of turbulent dissipation in the presence of tidal straining". In: *Journal of Physical Oceanography* 31.8 (2001), pp. 2458–2471.

[30] Parker MacCready and W Rockwell Geyer. "Advances in estuarine physics". In: *Annual Review of Marine Science* 2 (2010), pp. 35–58.

[31] PF Linden and JE Simpson. "Gravity-driven flows in a turbulent fluid". In: *Journal of Fluid Mechanics* 172 (1986), pp. 481–497.

[32] Malcolm E Scully, Carl Friedrichs, and John Brubaker. "Control of estuarine stratification and mixing by wind-induced straining of the estuarine density field". In: *Estuaries* 28.3 (2005), pp. 321–326.

[33] Nadia Pinardi et al. "Mediterranean Sea large-scale low-frequency ocean variability and water mass formation rates from 1987 to 2007: A retrospective analysis". In: *Progress in Oceanography* 132 (2015), pp. 318–332.

[34] Nadia Pinardi and Antonio Navarra. "Baroclinic wind adjustment processes in the Mediterranean Sea". In: *Deep Sea Research Part II: Topical Studies in Oceanography* 40.6 (1993), pp. 1299–1326.

[35] N Pinardi et al. "The physical, sedimentary and ecological structure and variability of shelf areas in the Mediterranean sea (27)". In: *The sea* 14 (2006), pp. 1243–330.

[36] Georg Wüst. "On the vertical circulation of the Mediterranean Sea". In: *Journal of Geophysical Research* 66.10 (1961), pp. 3261–3271.

[37] Marco Zavatarelli and George L Mellor. "A numerical study of the Mediterranean Sea circulation". In: *Journal of Physical Oceanography* 25.6 (1995), pp. 1384–1414.

[38] Mario Adani, Srdjan Dobricic, and Nadia Pinardi. "Quality assessment of a 1985–2007 Mediterranean Sea reanalysis". In: *Journal of Atmospheric and Oceanic Technology* 28.4 (2011), pp. 569–589.

[39] P Vélez-Belchı, Manuel Vargas-Yáñez, and Joaquín Tintoré. "Observation of a western Alborán gyre migration event". In: *Progress in Oceanography* 66.2–4 (2005), pp. 190–210.

[40] Helen M Snaith et al. "Monitoring the eastern Alborán Sea using combined altimetry and in situ data". In: *Philosophical Transactions of the Royal Society of London. Series A: Mathematical, Physical and Engineering Sciences* 361.1802 (2002), pp. 65–70.

[41] Gurvan Madec et al. "A three-dimensional numerical study of deep-water formation in the northwestern Mediterranean Sea". In: *Journal of Physical Oceanography* 21.9 (1991), pp. 1349–1371.

[42] AR Robinson et al. "The Atlantic ionian stream". In: *Journal of Marine Systems* 20.1–4 (1999), pp. 129–156.

[43] Reiner Onken et al. "Data-driven simulations of synoptic circulation and transports in the Tunisia-Sardinia-Sicily region". In: *Journal of Geophysical Research: Oceans* 108.C9 (2003).

[44] PFJ Lermusiaux and AR Robinson. "Features of dominant mesoscale variability, circulation patterns and dynamics in the Strait of Sicily". In: *Deep Sea Research Part I: Oceanographic Research Papers* 48.9 (2001), pp. 1953–1997.

[45] V Artale et al. "Seasonal variability of gyre-scale circulation in the northern Tyrrhenian Sea". In: *Journal of Geophysical Research: Oceans* 99.C7 (1994), pp. 14127–14137.

[46] Maryam Golnaraghi and Allan R Robinson. "Dynamical studies of the Eastern Mediterranean circulation". In: *Ocean processes in climate dynamics: global and mediterranean examples*. Springer, 1994, pp. 395–406.

[47] Artur Hecht, Nadia Pinardi, and Allan R Robinson. "Currents, water masses, eddies and jets in the Mediterranean Levantine Basin". In: *Journal of Physical Oceanography* 18.10 (1988), pp. 1320–1353.

[48] George Zodiatis et al. "Variability of the Cyprus warm core Eddy during the CYCLOPS project". In: *Deep Sea Research Part II: Topical Studies in Oceanography* 52.22–23 (2005), pp. 2897–2910.

[49] AR Robinson et al. "The eastern Mediterranean general circulation: features, structure and variability". In: *Dynamics of Atmospheres and Oceans* 15.3–5 (1991), pp. 215–240.

[50] Ralph F Milliff and Allan R Robinson. "Structure and dynamics of the Rhodes gyre system and dynamical interpolation for estimates of the mesoscale variability". In: *Journal of Physical Oceanography* 22.4 (1992), pp. 317–337.

[51] Antonio Artegiani et al. "The Adriatic Sea general circulation. Part II: baroclinic circulation structure". In: *Journal of physical Oceanography* 27.8 (1997), pp. 1515–1532.

[52] Dimitrios V Politikos et al. "Modeling the fate and distribution of floating litter particles in the Aegean Sea (E. Mediterranean)". In: *Frontiers in Marine Science* 4 (2017), p. 191.

[53] K Nittis and L Perivoliotis. "Circulation and hydrological characteristics of the North Aegean Sea: a contribution from real-time buoy measurements". In: *Mediterranean Marine Science* 3.1 (2002), pp. 21–32.

[54] V. H. Kourafalou and K. Barbopoulos. "High resolution simulations on the North Aegean Sea seasonal circulation". In: *Annales Geophysicae* 21.1 (2003), pp. 251–265. URL: https://hal.archives-ouvertes.fr/hal-00316978.

[55] Alex Lascaratos, Richard G Williams, and Elina Tragou. "A mixed-layer study of the formation of Levantine Intermediate Water". In: *Journal of Geophysical Research: Oceans* 98.C8 (1993), pp. 14739–14749.

[56] Entcho K Demirov and N Pinardi. "On the relationship between the water mass pathways and eddy variability in the Western Mediterranean Sea". In: *Journal of Geophysical Research: Oceans* 112.C2 (2007).

[57] N Pinardi and E Masetti. "Variability of the large scale general circulation of the Mediterranean Sea from observations and modelling: a review". In: *Palaeogeography, Palaeoclimatology, Palaeoecology* 158.3–4 (2000), pp. 153–173.

[58] Claude Millot. "Circulation in the western Mediterranean Sea". In: *Journal of Marine Systems* 20.1–4 (1999), pp. 423–442.

[59] Friedrich Schott et al. “Observations of deep convection in the Gulf of Lions, northern Mediterranean, during the winter of 1991/92”. In: *Journal of Physical Oceanography* 26.4 (1996), pp. 505–524.

[60] Claude Millot and Isabelle Taupier-Letage. “Circulation in the Mediterranean sea”. In: *The Mediterranean Sea*. Springer, 2005, pp. 29–66.

[61] L Grignon et al. “Importance of the variability of hydrographic preconditioning for deep convection in the Gulf of Lion, NW Mediterranean”. In: *Ocean Science* 6.2 (2010), pp. 573–586.

[62] S Castellari, N Pinardi, and K Leaman. “Simulation of water mass formation processes in the Mediterranean Sea: Influence of the time frequency of the atmospheric forcing”. In: *Journal of Geophysical Research: Oceans* 105.C10 (2000), pp. 24157–24181.

[63] Wolfgang Ludwig et al. “River discharges of water and nutrients to the Mediterranean and Black Sea: major drivers for ecosystem changes during past and future decades?” In: *Progress in oceanography* 80.3–4 (2009), pp. 199–217.

[64] W Ludwig, M Meybeck, and F Abousamra. “Riverine transport of water, sediments, and pollutants to the Mediterranean Sea”. In: *Medit. Action Technical Report Series* 141 (2003).

[65] DA Anati and JR Gat. “Restricted marine basins and marginal sea environments”. In: *Handbook of environmental isotope geochemistry* 3 (1989), pp. 29–73.

[66] CJ Vörösmarty, BM Fekete, and BA Tucker. "Global river discharge, 1807–1991, V. 1.1 (RivDIS)". In: *Data set. Available on-line [http://www. daac. ornl. gov] from Oak Ridge National Laboratory Distributed Active Archive Center, Oak Ridge, TN, USA* (1998).

[67] Moncef Boukthir and Bernard Barnier. "Seasonal and inter-annual variations in the surface freshwater flux in the Mediterranean Sea from the ECMWF re-analysis project". In: *Journal of Marine Systems* 24.3–4 (2000), pp. 343–354.

[68] J Margat. *Blue Plan."L'eau des Mediterraneens: situation et perspectives"*. Tech. rep. UNEP MAP Technical Report Studies, 158, Athens.(www. unepmap. org), 2004.

[69] Maria Vittoria Struglia, Annarita Mariotti, and Angelo Filograsso. "River discharge into the Mediterranean Sea: climatology and aspects of the observed variability". In: *Journal of Climate* 17.24 (2004), pp. 4740–4751.

[70] Scott W Nixon. "Replacing the Nile: are anthropogenic nutrients providing the fertility once brought to the Mediterranean by a great river?" In: *AMBIO: A journal of the human environment* 32.1 (2003), pp. 30–40.

[71] JP Bethoux and B Gentili. "The Mediterranean Sea, coastal and deep-sea signatures of climatic and environmental changes". In: *Journal of Marine Systems* 7.2–4 (1996), pp. 383–394.

[72] Marina Tonani et al. "The impact of a new high-resolution ocean model on the Met Office North-West European Shelf forecasting sys-

tem". In: *Ocean Sci. Discuss., https://doi. org/10.5194/os-2019-4, in review* (2019).

[73] Rui Xin Huang. "Real freshwater flux as a natural boundary condition for the salinity balance and thermohaline circulation forced by evaporation and precipitation". In: *Journal of Physical Oceanography* 23.11 (1993), pp. 2428–2446.

[74] Guillaume Roullet and Gurvan Madec. "Salt conservation, free surface, and varying levels: a new formulation for ocean general circulation models". In: *Journal of Geophysical Research: Oceans* 105.C10 (2000), pp. 23927–23942.

[75] Frank Bryan. "High-latitude salinity effects and interhemispheric thermohaline circulations". In: *Nature* 323.6086 (1986), pp. 301–304.

[76] Francisco J Beron-Vera, J Ochoa, and P Ripa. "A note on boundary conditions for salt and freshwater balances". In: *Ocean Modelling* 1.2–4 (1999), pp. 111–118.

[77] Bruce A Warren. "Note on the vertical velocity and diffusive salt flux induced by evaporation and precipitation". In: *Journal of physical oceanography* 39.10 (2009), pp. 2680–2682.

[78] Madec Gurvan et al. "NEMO ocean engine". Version v3.6. In: *Notes Du Pôle De Modélisation De L'institut Pierre–Simon Laplace (IPSL)* (2017). DOI: 10.5281/zenodo.3248739. URL: https://doi.org/10.5281/zenodo.3248739.

[79] David R Jackett and Trevor J Mcdougall. "Minimal adjustment of hydrographic profiles to achieve static stability". In: *Journal of Atmospheric and Oceanic Technology* 12.2 (1995), pp. 381–389.

[80] P Oddo et al. "Sensitivity of the Mediterranean sea level to atmospheric pressure and free surface elevation numerical formulation in NEMO". In: *Geoscientific Model Development* 7.6 (2014), pp. 3001–3015.

[81] Sergio Castellari, Nadia Pinardi, and Kevin Leaman. "A model study of air–sea interactions in the Mediterranean Sea". In: *Journal of Marine Systems* 18.1–3 (1998), pp. 89–114.

[82] P Oddo et al. "A nested Atlantic–Mediterranean Sea general circulation model for operational forecasting". In: *Ocean Science* 5.4 (2009), pp. 461–473.

[83] D Pettenuzzo, WG Large, and N Pinardi. "On the corrections of ERA–40 surface flux products consistent with the Mediterranean heat and water budgets and the connection between basin surface total heat flux and NAO". In: *Journal of Geophysical Research: Oceans* 115.C6 (2010).

[84] Sol Hellerman and Mel Rosenstein. "Normal monthly wind stress over the world ocean with error estimates". In: *Journal of Physical Oceanography* 13.7 (1983), pp. 1093–1104.

[85] RK Reed. "On estimating insolation over the ocean". In: *Journal of Physical Oceanography* 7.3 (1977), pp. 482–485.

[86] F Bignami et al. “Longwave radiation budget in the Mediterranean Sea”. In: *Journal of Geophysical Research: Oceans* 100.C2 (1995), pp. 2501–2514.

[87] Junsei Kondo. “Air-sea bulk transfer coefficients in diabatic conditions”. In: *Boundary-Layer Meteorology* 9.1 (1975), pp. 91–112.

[88] G. Verri N. Pinardi F. Bryan Y. Tseng G. Coppini E. Clementi. “A box model to represent estuarine dynamics in mesoscale resolution ocean models (submitted)”. In: *Ocean Modelling* (2019).

[89] E Clementi et al. “A 1/24 degree resolution Mediterranean physical analysis and forecast modeling system for the Copernicus Marine Environment Monitoring Service”. In: *Proceedings of the Eight Euro-GOOS International Conference*. 2018, pp. 275–284.

[90] Ralph Shapiro. “Linear filtering”. In: *Mathematics of computation* 29.132 (1975), pp. 1094–1097.

[91] Bram Van Leer. “Towards the ultimate conservative difference scheme. V. A second-order sequel to Godunov’s method”. In: *Journal of computational Physics* 32.1 (1979), pp. 101–136.

[92] RC Pacanowski and SGH Philander. “Parameterization of vertical mixing in numerical models of tropical oceans”. In: *Journal of Physical Oceanography* 11.11 (1981), pp. 1443–1451.

[93] A. V. Mishonov J. I. Antonov T. P. Boyer H. E. Garcia O. K. Baranova M. M. Zweng C. R. Paver J. R. Reagan D. R. Johnson M. Hamilton Locarnini R. A. and A. Mishonov Technical Ed. D. Seidov. S. Levitus

Ed. "World Ocean Atlas 2013, Volume 1: Temperature". In: *NOAA Atlas NESDIS 73* (2013).

[94] J.R. Reagan J.I. Antonov R.A. Locarnini A.V. Mishonov T.P. Boyer H.E. Garcia O.K. Baranova D.R. Johnson D.Seidov M.M. Biddle. S. Levitus Ed. A. Mishonov Technical Ed. Zweng M.M. "World Ocean Atlas 2013, Volume 2: Salinity". In: *NOAA Atlas NESDIS 73* (2013).

[95] K R Dyer. *Estuaries: A Physical Introduction, 2nd Edition s.l.* John Wiley Sons, 1997.

[96] Richard W Garvine and Michael M Whitney. "An estuarine box model of freshwater delivery to the coastal ocean for use in climate models". In: *Journal of Marine Research* 64.2 (2006), pp. 173–194.

[97] Ana E Rice et al. "Energetics in Delaware Bay: Comparison of two box models with observations". In: *Journal of Marine Research* 66.6 (2008), pp. 873–898.

[98] Robinson Hordoir et al. "Towards a parametrization of river discharges into ocean general circulation models: a closure through energy conservation". In: *Climate dynamics* 31.7–8 (2008), pp. 891–908.

[99] M Herzfeld. "Methods for freshwater riverine input into regional ocean models". In: *Ocean Modelling* 90 (2015), pp. 1–15.

[100] NS Banas et al. "Dynamics of Willapa Bay, Washington: A highly unsteady, partially mixed estuary". In: *Journal of Physical Oceanography* 34.11 (2004), pp. 2413–2427.

[101] B Buongiorno Nardelli et al. "High and Ultra-High resolution processing of satellite Sea Surface Temperature data over Southern European Seas in the framework of MyOcean project". In: *Remote Sensing of Environment* 129 (2013), pp. 1–16.

[102] A Pisano et al. "The new Mediterranean optimally interpolated pathfinder AVHRR SST Dataset (1982–2012)". In: *Remote Sensing of Environment* 176 (2016), pp. 107–116.

[103] Durrieu De Madron X Houpert L Testor P. *Gridded climatology of the Mixed Layer (Depth and Temperature), the bottom of the Seasonal Thermocline (Depth and Temperature), and the upper–ocean Heat Storage Rate for the Mediterrean Sea*. 2015. DOI: /10.17882/46532. URL: https://www.seanoe.org/data/00354/46532/.

[104] Ewa Jarosz et al. "Observations on the characteristics of the exchange flow in the Dardanelles Strait". In: *Journal of Geophysical Research: Oceans* 117.C11 (2012).

[105] LP Røed and CK Cooper. "Open boundary conditions in numerical ocean models". In: *Advanced physical oceanographic numerical modelling*. Springer, 1986, pp. 411–436.

[106] Patrick Marchesiello, James C McWilliams, and Alexander Shchepetkin. "Open boundary conditions for long-term integration of regional oceanic models". In: *Ocean modelling* 3.1–2 (2001), pp. 1–20.

[107] P Oddo and N Pinardi. "Lateral open boundary conditions for nested limited area models: a scale selective approach". In: *Ocean modelling* 20.2 (2008), pp. 134–156.

[108] V Maderich, Yu Ilyin, and E Lemeshko. “Seasonal and interannual variability of the water exchange in the Turkish Straits System estimated by modelling”. In: *Mediterranean Marine Science* 16.2 (2015), pp. 444–459.

[109] RA Flather. “A tidal model of the north–west European continental shelf”. In: *Mem. Soc. R. Sci. Liege.* 10 (1976), pp. 141–164.

[110] I Orlanski. “A simple boundary condition for unbounded hyperbolic flows”. In: *Journal of computational physics* 21.3 (1976), pp. 251–269.

[111] S Tuğrul, T Beşiktepe, and I Salihoğlu. “Nutrient exchange fluxes between the Aegean and Black Seas through the Marmara Sea”. In: *Mediterranean Marine Science* 3.1 (2002), pp. 33–42.

[112] Şükrü T Beşiktepe et al. “The circulation and hydrography of the Marmara Sea”. In: *Progress in Oceanography* 34.4 (1994), pp. 285–334.

[113] Emin Özsoy and Ümit Ünlüata. “Oceanography of the Black Sea: a review of some recent results”. In: *Earth-Science Reviews* 42.4 (1997), pp. 231–272.

[114] Ü Ünlülata et al. “On the physical oceanography of the Turkish Straits”. In: *The physical oceanography of sea straits*. Springer, 1990, pp. 25–60.

[115] MA Latif et al. “Observations of the Mediterranean inflow into the Black Sea”. In: *Deep Sea Research Part A. Oceanographic Research Papers* 38 (1991), S711–S723.

[116] Ewa Jarosz et al. “Observed volume fluxes and mixing in the Dardanelles Strait”. In: *Journal of Geophysical Research: Oceans* 118.10 (2013), pp. 5007–5021.

[117] N Skliris et al. “Satellite–derived variability of the Aegean Sea ecohydrodynamics”. In: *Continental Shelf Research* 30.5 (2010), pp. 403–418.

[118] Donald B Olson et al. “Aegean surface circulation from a satellite–tracked drifter array”. In: *Journal of Physical Oceanography* 37.7 (2007), pp. 1898–1917.

[119] Wolfgang Roether et al. “Recent changes in eastern Mediterranean deep waters”. In: *Science* 271.5247 (1996), pp. 333–335.

[120] Balazs M Fekete, Charles J Vörösmarty, and Wolfgang Grabs. *Global, composite runoff fields based on observed river discharge and simulated water balances*. 1999.

[121] Simona Simoncelli et al. “Coastal rapid environmental assessment in the Northern Adriatic Sea”. In: *Dynamics of atmospheres and oceans* 52.1–2 (2011), pp. 250–283.

[122] Fabio Raicich. “On the fresh balance of the Adriatic Sea”. In: *Journal of Marine Systems* 9.3–4 (1996), pp. 305–319.

[123] E Demiraj et al. “Implications of climate change for the Albanian Coast”. In: *MAP technical reports series* 98 (1996).

[124] Carles Ibañez, Didier Pont, and Narcís Prat. “Characterization of the Ebre and Rhone estuaries: A basis for defining and classifying

salt-wedge estuaries". In: *Limnology and Oceanography* 42.1 (1997), pp. 89–101.

[125] A Provini, G Crosa, and R Marchetti. "Nutrient export from the Po and Adige river basins over the last 20 years". In: *Marine Coastal Eutrophication*. Elsevier, 1992, pp. 291–313.

[126] Waleed Hamza et al. "The 3D physical-biological model study in the Egyptian Mediterranean coastal sea". In: *Aquatic Ecology* 37.3 (2003), pp. 307–324.

[127] Annarita Mariotti et al. "The hydrological cycle in the Mediterranean region and implications for the water budget of the Mediterranean Sea". In: *Journal of climate* 15.13 (2002), pp. 1674–1690.

[128] Mirko Orlić, Miroslav Gačić, and Paul E LaViolette. "The currents and circulation of the Adriatic Sea". In: *Oceanologica acta* 15.2 (1992), p. 109.

[129] Pascal Conan and Claude Millot. "Variability of the northern current off Marseilles, Western Mediterranean Sea: from February to June 1992". In: *Oceanologica acta* 18.2 (1995), pp. 193–205.

[130] Javier Soto-Navarro et al. "Estimation of the Atlantic inflow through the Strait of Gibraltar from climatological and in situ data". In: *Journal of Geophysical Research: Oceans* 115.C10 (2010).

[131] Julio Candela. ".7 Mediterranean water and global circulation". In: *International Geophysics*. Vol. 77. Elsevier, 2001, pp. 419–XLVIII.

[132] Sadegh Yari et al. “Direct estimate of water, heat, and salt transport through the Strait of Otranto”. In: *Journal of Geophysical Research: Oceans* 117.C9 (2012).

[133] M Astraldi et al. “The role of straits and channels in understanding the characteristics of Mediterranean circulation”. In: *Progress in oceanography* 44.1–3 (1999), pp. 65–108.

[134] DJ Webb. “A comparison of sea surface temperatures in the Equatorial Pacific Nino regions with results from two early runs of the NEMO 1/12° Ocean Model”. In: *National Oceanography Centre Research and Consultancy Report* 55 (2016).

[135] EW Blockley et al. “Recent development of the Met Office operational ocean forecasting system: an overview and assessment of the new Global FOAM forecasts”. In: *Geoscientific Model Development* 7.6 (2014), pp. 2613–2638.

[136] Verena Haid, Doroteaciro Iovino, and Simona Masina. “Impacts of freshwater changes on Antarctic sea ice in an eddy-permitting sea-ice-ocean model”. In: *The Cryosphere* 11.3 (2017).

[137] AP Megann et al. “GO 5.0: The joint NERC-Met Office NEMO global ocean model for use in coupled and forced applications”. In: *Geotechnical Model Development* 7.3 (2014), pp. 1069–1092.

[138] Rachid Benshila et al. “The upper Bay of Bengal salinity structure in a high-resolution model”. In: *Ocean Modelling* 74 (2014), pp. 36–52.

[139] Philippe Gaspar, Yves Grégoris, and Jean-Michel Lefevre. "A simple eddy kinetic energy model for simulations of the oceanic vertical mixing: Tests at station Papa and Long-Term Upper Ocean Study site". In: *Journal of Geophysical Research: Oceans* 95.C9 (1990), pp. 16179–16193.

[140] G Reffray, R Bourdalle-Badie, and C Calone. "Modelling turbulent vertical mixing sensitivity using a 1-D version of NEMO." In: *Geoscientific Model Development* 8.1 (2015).

[141] D Calvert and J Siddorn. "Revised vertical mixing parameters for the UK community standard configuration of the global NEMO ocean model". In: *Met Office Hadley Centre Technical Note* 95 (2013). URL: https://digital.nmla.metoffice.gov.uk/IO_151d75b9-6deb-43ec-935c-696937721cae/.

[142] AN Kolmogorov. "Incompressible fluid turbulent motion equations". In: *Izv. Akad. Nauk SSSR, Ser. Fiz* 6 (1942), pp. 56–58.

[143] Peter D Craig and Michael L Banner. "Modeling wave-enhanced turbulence in the ocean surface layer". In: *Journal of Physical Oceanography* 24.12 (1994), pp. 2546–2559.

[144] Chao Shenn-Yu and Boicourt William C. "Onset of estuarine plumes". In: *Journal of Physical Oceanography* 16.12 (1986), pp. 2137–2149.

[145] DuŠan Jelić, Ivan Špelić, and Petar Žutinić. "Introduced species community over-dominates endemic ichthyofauna of High Lika Plateau (Central Croatia) over a 100 year period". In: *Acta Zoologica Academiae Scientiarum Hungaricae* 62.2 (2016), pp. 191–216.

[146] *Regional strategy for sustainable hydropower in the Western Balkans. Background Report No. 5. Transboundary considerations. Final Draft 5*. Tech. rep. IPA 2011-WBIF-Infrastructure Project Facility. Technical Assistance 3. EuropeAid/131160/C/SER/MULTI/3C, 2017.

[147] Gary D Egbert and Svetlana Y Erofeeva. "Efficient inverse modeling of barotropic ocean tides". In: *Journal of Atmospheric and Oceanic Technology* 19.2 (2002), pp. 183–204.

[148] *Integrated Resources Management Plan (IRMP) for the Buna/Bojana Area*. Tech. rep. GWP-Med, PAP/RAC, UNESCO-IHP. Paris, France, 2015.

[149] M.S.M. EL-Bady and H.I. Metwally. "Evaluation of water quality of the surface water of the Damietta Nile Branch, Damietta Governorate, Egypt". In: *International Journal of ChemTech Research* 9.5 (2016), pp. 119–134.

[150] MAR Abdel-Moati. "Iodine speciation in the Nile River estuary". In: *Marine Chemistry* 65.3–4 (1999), pp. 211–225.

[151] Masayoshi Satoh and Samir Aboulroos. *Irrigated agriculture in Egypt: past, present and future*. Springer, 2017.

[152] P Giani et al. "Studio sulla presenza di acqua di mare nel tratto terminale del Fiume Arno con metodologie chimico-isotopiche". In: *Atti della SocietaToscana di Scienze Naturali, Memorie Serie A* (2000), pp. 53–60.

[153] G Capelli and R Mazza. "Intrusione salina nel delta del Fiume Tevere". In: *Evoluzione Del Fenomeno Nei Primi Anni Del Terzo Millennio. La Geologia Di Roma: Dal Centro Storico Alla Periferia e Seconda Parte e Memorie Descrittive Della Carta Geologica d'Italia* 80 (2008).

[154] MV Mikhailova et al. "Intrusion of seawater into the River Part of the Tiber Mouth". In: *Water Resources* 26.6 (1999), pp. 679–686.

[155] Selma Etteieb, Semia Cherif, and Jamila Tarhouni. "Hydrochemical assessment of water quality for irrigation: a case study of the Medjerda River in Tunisia". In: *Applied Water Science* 7.1 (2017), pp. 469–480.

[156] Slimani Noura, Bejaoui Mustapha, and Boumaiza Moncef. "Taxonomic diversity and benthic community structures of watersheds of Medjerda and Joumine (North east of Tunisia)". In: *Inter Res J Earth Sci* 3 (2015), pp. 24–30.

[157] *I bacini idrografici in provincia di Venezia*. Tech. rep. Agenzia Regionale per la Prevenzione e Protezione Ambientale del Veneto, 2012.

[158] L Tosi et al. *Intrusione salina. In: Atlante geologico della Provincia di Venezia*. Provincia di Venezia, 2011.

[159] Stefano Covelli et al. "Behaviour of Hg species in a microtidal deltaic system: the Isonzo River mouth (northern Adriatic Sea)". In: *Science of the total environment* 368.1 (2006), pp. 210–223.

[160] *The Krka River basin management plan*. Tech. rep. URL: `https://www.unece.org/fileadmin/DAM/env/water/meetings/Sarajevo_`

workshop/presentations/session4/Adriatic_Sea_group/Krka.pdf.

[161] Roko Andričević. *ADRICOSM – NERES Project: Task 2-1: Evaluation of the extension of the salt water intrusion*. Tech. rep. UNIVERSITY OF SPLIT, FACULTY OF CIVIL ENGINEERING and ARCHITECTURE CENTER FOR ENVIRONMENTAL RESEARCH.

[162] N Th Fourniotis. "A proposal for impact evaluation of the diversion of the Acheloos River, on the acheloos estuary in western Greece". In: *International Journal of Engineering Science and Technology* 4.4 (2012), pp. 1792–1802.

[163] Kiriaki Haralambidou, Georgios Sylaios, and Vassilios A Tsihrintzis. "Salt-wedge propagation in a Mediterranean micro-tidal river mouth". In: *Estuarine, Coastal and Shelf Science* 90.4 (2010), pp. 174–184.

[164] Maria Tzortziou et al. "Colored dissolved organic matter dynamics and anthropogenic influences in a major transboundary river and its coastal wetland". In: *Limnology and oceanography* 60.4 (2015), pp. 1222–1240.

[165] Ömer ERDOĞAN, Nezire Lerzan ÇİÇEK, and Ömer Osman ERTAN. "Manavgat Nehri Nehirağzı Bölgesi Fitoplanktonunun Mevsimsel Dağılımı". In: *Süleyman Demirel Üniversitesi Eğirdir Su Ürünleri Fakültesi Dergisi* 8.1 (2012), pp. 9–21.

[166] Joseph Smagorinsky. "General circulation experiments with the primitive equations: I. The basic experiment". In: *Monthly weather review* 91.3 (1963), pp. 99–164.